The attenuation of sweep events within the turbulent boundary layer over a flat plate using a micro-cavity array

Anton Silvestri

School of Mechanical Engineering

The University of Adelaide

South Australia, 5005

Australia

A thesis submitted in fulfilment of the requirements for the degree of Ph.D. in Mechanical Engineering

5 October 2018

Abstract

For most aeronautical applications skin friction drag is a significant issue for efficient operation. It is estimated that 49% of the total drag an aircraft experiences is due to skin friction drag and a small reduction of 5% would currently result in an annual saving of $3.3 billion US dollars. The large Reynolds number at which aerospace applications typically operate results in a turbulent boundary layer, which causes a large increase in shear stresses and a subsequent increase in skin friction drag. The key culprits for the large shear stresses are the turbulent boundary layer structures that form once the boundary layer transitions from the initial laminar state, the most influential of which are the coherent structures. These structures pump fluid into (sweep) and away (ejection) from the near wall region and generate the shear stresses. Hence the aim of this research is to manipulate the turbulent boundary layer to reduce the effect of the aforementioned coherent structures. Specific attention has been applied to the passive application of a micro-cavity array as a potential control technique to attenuate the coherent structures. The micro-cavity array consists of a cavity arranged flush with the surface, underneath of which is a backing cavity similar to the design of a Helmholtz resonator. As a passive control technique, this device aims to have the advantages of an easy implementation and the absence of an external power source, with targeted control of the coherent structures commonly achieved by active systems. The micro-cavity array aims to capture and dampen the sweep events, therefore reducing the strength of both the ejection and sweep events due to their high dependence on one another. As such the present work

assesses the ability of an array of micro-cavities to reduce the turbulent properties of a fully developed boundary layer.

Previous results from the flow excited Helmholtz resonator and a two-dimensional square cavity on a flat plate have confirmed the potential of the micro-cavity array. Both techniques achieved successful control of the boundary layer and attenuation of the coherent structures. However these applications had limitations at higher Reynolds numbers and as a result a smaller device such as the micro-cavity is proposed and forms the basis of this thesis. Being of smaller size, the shear layer is hypothesised not to break apart while traversing the small orifices of the micro-cavity, which occurs for the larger flow excited Helmholtz resonator and results in an adverse pressure gradient and an undesirable increase in the disturbances and viscous drag in the boundary layer.

To investigate the potential of the proposed micro-cavity array, the device has been thoroughly examined experimentally at a range of Reynolds numbers ($1195 < Re_\theta < 3771$). Experiments were predominately focused on identifying the potential of the micro-cavity, whilst evaluating the impact of the orifice distribution along the cavity array and the effect of other geometric parameters, including the length of the cavity array and the backing volume. Measurements were made using a single hot-wire and a constant temperature hot-wire anemometry system downstream of the cavity arrays, with all results being compared against canonical boundary layer profiles to record the effect of the micro-cavity array. These experiments demonstrated the success of the micro-cavity array in controlling the turbulent boundary layer and identified the mechanism causing the recorded attenuation of the boundary layer.

The results showed that the optimal orifice diameter must be equal to a value of approximately 60 times the viscous length scale. This resulted in a maximum reduction in the turbulence and sweep intensities of 13% and 14%, respectively. The results demonstrated that for a cavity orifice diameter less than 20 times the viscous length scale, the sweep events are restricted and no events are captured by the array. Additionally, if the diameter of the orifice exceeds 145 times the viscous length scale, separation of the shear layer was observed, causing an increase in the turbulence energy production in the near wall region. The volume of the backing cavity was also shown to be a very important characteristic in the design of the micro-cavity array, while the orifice length of the cavity array had negligible effect in modifying the reduction of the turbulent energy by the cavity array. The maximum reduction in turbulence generation occurred when the backing volume was as large as possible, which reduced the reactive impedance of the micro-cavity device. However, the sweep intensity reduction reached a limiting value as the volume increased. The reduction in turbulent energy was also shown to occur irrespective of whether the individual cavity arrays shared a common backing volume or had individual backing volumes. Consequently a strongly supported finding is that the cavity array weakens the sweep intensity of the captured sweep events by damping the energy of the events through the friction losses in the cavity array and also in the large volume of the backing cavity. This results in a reduction in the strength of the bursting events responsible for the shear stresses in the near wall region.

The body of work presented here is only the beginning of the development of the knowledge required for this area of work. The results of this study demonstrate an improved understanding of the micro-cavity array as a potential flow control device for the turbulent boundary layer in the future and as such requires further investigation.

Contents

Declaration

I, Anton Silvestri, certify that this work contains no material which has been accepted for the award of any other degree or diploma in my name, in any university or other tertiary institution and, to the best of my knowledge and belief, contains no material previously published or written by another person, except where due reference has been made in the text. In addition, I certify that no part of this work will, in the future, be used in a submission in my name, for any other degree or diploma in any university or other tertiary institution without the prior approval of the University of Adelaide and where applicable, any partner institution responsible for the joint-award of this degree.

I acknowledge that copyright of published works contained within this thesis resides with the copyright holder(s) of those works.

I also give permission for the digital version of my thesis to be made available on the web, via the University's digital research repository, the Library Search and also through web search engines, unless permission has been granted by the University to restrict access for a period of time.

I acknowledge the support I have received for my research through the provision of an Australian Government Research Training Program Scholarship.

Signed: … ……… Date: ……………………………………… 5 October 2018

Acknowledgments

To begin I would like to thank my supportive Ph.D. supervisors A/Prof Maziar Arjomandi, Prof Ben Cazzolato, Prof Anthony Zander and Dr Rey Chin. Your insightful supervision over the past three years has given me the resources to achieve this Ph.D. Despite your extremely busy schedules I am tremendously grateful for the time you have given me and giving up your weekends and time with your family to read my work whilst giving insightful feedback. I am extremely appreciative of all your efforts and look forward to working with you all in the future.

I would also like to thank my mentor and friend Dr Farzin Ghanadi. It is by no means a simple task to start a Ph.D. but it becomes a lot easier with the guidance of someone like Farzin. I will always remember the early times of my Ph.D. when we would meet twice a week to discuss, what now seems like the most fundamental of Fluid Mechanics and our very early problems regarding the hotwire anemometry system. I can honestly say without your help my Ph.D. would not be where it is today. I am extremely grateful for all the time you have given me and am looking forward to the next step of our professional relationship.

Nomenclature

$B(\sigma)$ = probability density function of streamwise velocity

c_f = skin friction coefficient

d = cavity diameter (mm)

D = backing cavity depth (mm)

f = frequency (Hz)

f_b = bursting frequency (Hz)

H = shape factor

k = variable-interval time-averaging (VITA) threshold

K_x = streamwise wavenumber

Re_x = Reynolds number based on streamwise distance

Re_{u_τ} = Reynolds number based on friction velocity

Re_θ = Reynolds number based on momentum thickness

t = time (s)

T_{av} = averaging duration (s)

T_W = window length (s)

Tu = turbulence intensity

L = orifice length (mm)

u = streamwise flow velocity (m/s)

u_τ = friction velocity (m/s)

$\hat{u}$ = local mean of the streamwise velocity (m/s)

v = wall-normal flow velocity (m/s)

w = spanwise flow velocity (m/s)

V = volume of backing cavity (m³)

Var = variance

x = indicates x-distance (streamwise) (m)

y = indicates y- distance (wall-normal direction) (m)

z = indicates z- distance (spanwise) (m)

Symbols

σ = standard deviation

λ_x = streamwise wavelength (m)

ρ = density of air (kg/m³)

δ = boundary layer thickness (mm)

δ^+ = displacement thickness (mm)

θ = momentum thickness (mm)

Ψ = pre-multiplied energy spectrum

ν = kinematic viscosity (m/s^2)

Superscripts

+ = denotes viscous time scale ($\frac{\nu}{u_\tau^2}$) or viscous length scale (ν/u_τ)

Chapter 1

Introduction

1.1 Background

Turbulent boundary layers consist of three-dimensional instabilities which interact with the wall resulting in an increase in the shear stresses and skin friction drag. As such skin friction drag is a significant problem for many applications, particularly in aerospace systems such as aircraft and helicopters, due to the large operational Reynolds number and the unavoidable transition into turbulence. It is estimated 49% of the total drag on an aircraft is due to skin friction and viscous drag (Gad-el-Hak, 1994; Marec, 2000; Abbas et al., 2017) as shown in Fig. 1.1. Consequently reducing the skin friction drag component of drag has become of utmost importance in recent times to mitigate the sharp rise in the cost of fossil fuels. The global fuel bill of the airline industry is estimated to be US$130 billion in 2017, and accounts for almost 20% of the total operating expenses of an aircraft (International Air Transport Association, 2017). This cost is expected to increase in the future with the rising price of crude oil and as such a 20% increase in the global cost of the air transport industry is expected in 2018 from the previous value in 2017 (International Air Transport Association, 2017). As such, a reduction in the amount of fuel

required is of utmost importance and would result in a tremendous annual saving. This can be achieved by a reduction in the skin friction drag an aircraft experiences. It is estimated a small reduction of 5% alone would result in an annual saving of US$3.3 billion (International Air Transport Association, 2017). Furthermore, the reduction of the skin friction drag component can also have significant advantages in other fields, including mixing in internal combustion engines and a reduction in pumping power for pipelines (Gad-el-Hak, 2000; Kasagi et al. 2009).
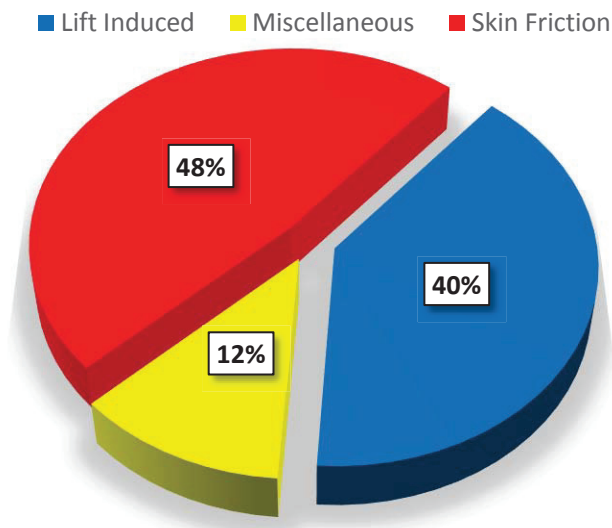
Fig 1.1 Outline of drag types for a typical aircraft based on data from Marec (2000).

The near wall coherent structures, consisting of streamwise longitudinal vortices, are considered by many to play an important role in the skin friction generated by the turbulent boundary layer (Guo et al., 2010; Whalley, 2011; Ghanadi, 2015). These vortices pump fluid into (sweep) and away (ejection) from the near wall region. At a pipe Reynolds number of approximately 11,000, ejection events generate approximately 70% of the total stresses in the inner wall region, while sweep events account for the remaining 30% (Kim et al., 1971; Offen and Kline, 1975, Whalley, 2011). Consequently these coherent

structures are very important during turbulence generation (Corino and Brodkey; 1969, Wallace et al., 1972; Guo et al., 2010). Furthermore these events have been shown to be highly dependent on one another and together are known as the bursting cycle. Consequently modifying one of these structures will have a significant effect on the other as well as the bursting cycle itself. Therefore, many researchers have attempted to target these structures to reduce turbulence generation within the boundary layer and reduce the shear stresses and the resulting skin friction drag.

One of the most successful passive turbulence reduction techniques is the streamwise riblet (Walsh, 1983; Choi, 1987, 1989; Greidanus et al., 2015; Benschop and Breugem, 2017). Streamwise riblets are small grooves spaced in the spanwise direction, approximately equal in size to the turbulent structures and aligned with the flow direction. It was shown that they can successfully reduce the skin friction drag by up to 8% (Walsh, 1983). Choi (1987) demonstrated that riblets act as small fences and restrict the streamwise vortices that form the legs of the hairpin vortical structure. By acting as a fence, the growth of the streamwise vortices in the spanwise direction can be prohibited. Furthermore, instead of using riblets Choi and Fujisawa (1993) demonstrated a similar effect could be achieved by using a two-dimensional square cavity on a flat plate. They showed a net drag reduction in the order of one percent could be achieved by using a single cavity.

Techniques other than riblets have been proposed for boundary layer control. A flow excited Helmholtz resonator was used by Ghanadi (2015) to provide a jet of suction and ejection to target the ejection and sweep events, respectively. This resulted in an 11% reduction in sweep intensity and a 5% reduction in the sweep duration within the

logarithmic region of the boundary layer ($y^+ > 35$). At higher flow velocities (U>15m/s) it was found that the resonator did not significantly change the structure of the sweep events. This was attributed to the increased Reynolds number and its amplification of the generation of the turbulent events. The shear layer breaks up more violently across the orifice gap and essentially increases the viscous drag more than the reduction from the sweep events being attenuated.

Comparable to the absorption of sweep events, Maa (1998) utilised the idea of a submillimetre micro-perforated panel to absorb sound. He found the most important parameter in his investigation was the perforate constant, which was proportional to the ratio of the perforation radius to viscous boundary layer thickness. This technique has shown tremendous potential for wide-band absorption and it has since been hypothesised that a similar device could dampen and weaken the sweep events in the boundary layer. The potential of this device was first revealed by the Helmholtz resonator. The resonator was found to have a small impact on the sweep events reducing their intensity and duration by 5% and 8% respectively without the activation of the Helmholtz mode (Ghanadi, 2015). It was suggested that the reduction in the intensity and duration of the sweep events was achieved by allowing the sweep event to partially or completely enter the orifice of the resonator. Consequently, some of the energy associated with the high speed events was absorbed and dampened by the surface area of the neck of the Helmholtz resonator.

As an extension to Maa's (1998) and Ghanadi's (2015) work, a similar device is considered. Hence the objective for this research is the successful implementation of micro-cavities for the purpose of an alternative method for boundary layer control. It is hypothesised

that a micro-cavity targets the flow travelling at normal incidence towards the wall commonly associated with sweep events in a similar way micro-perforated panels absorb sound by dissipating flow through the orifice. During the inrush of the sweep events towards the wall the structure is broken up when it enters a single orifice in the cavity array as shown by Ghanadi's (2015) work. This results in the next ejection event being delayed as no sweep event is present to push the slower moving fluid away from the wall (ejection event). It is hypothesised the cavity array will weaken the structure of the captured sweep events by damping the energy of the events through the friction losses in the neck of the orifice and the large volume of the backing cavity below the array itself. In the present study the flow features of the turbulent boundary layer will be considered after the control of the boundary layer using the micro cavity. This will consequently be used to provide an insight into the performance of the cavity array in attenuating the turbulent structures.

1.2 Aim and objectives

The main aim of the research presented in this thesis is to investigate the potential of a cavity array to control the coherent structures in a turbulent boundary layer. Consequently the objectives of the research are defined as the following:

- *Characterise the turbulent boundary layer and experimentally investigate how the cavity manipulates the boundary layer.* This will be achieved by first developing a fully transitioned turbulent boundary layer using artificial tripping techniques. This will be coupled with the design and implementation of a constant temperature hot-wire anemometer system to accurately measure the flow features of the turbulent boundary with and without the cavity array present.

- *Experimentally Parameterise the configuration and distribution of orifices required to effectively control the boundary layer across the flat plate.* This will be completed using the constant temperature hot-wire anemometer system to accurately measure the flow features of the turbulent boundary. The design, manufacture and implementation of a flat plate setup with an interchangeable micro-cavity array plate will be investigated to identify the key parameters for the control of the turbulent boundary layer.

- *Determine the optimal geometric arrangement for the micro-cavities as a boundary layer control device and the method in which the micro-cavities achieve boundary layer control.* Upon identifying the key parameters for the micro-cavity array the parameters will be optimised to increase the effectiveness of the cavity array in controlling the turbulent boundary layer. This will be followed by analyses of the mechanism for the attenuation of captured sweep events, which will build upon the previous objectives.

1.3 Thesis outline

The sequence of chapters reflects the chronology of the knowledge gained throughout the timeline of the research. The current chapter provides the overview and introduction to the research. This is followed by Chapter 2 which provides an extensive literature review on established techniques and the fundamental knowledge which were used to commence the research into utilising the micro-cavity array as a potential boundary layer control technique. The main body of the thesis, Chapter 3 through to Chapter 6, contains the research that establishes the micro-cavity array as a successful turbulent boundary layer control technique. Four manuscripts which have come as a direct result of this work

are included in these chapters, all of which are published in peer reviewed journals. The final chapter of this thesis presents conclusions drawn from the research and future recommendations on where the research could further its findings. In the following pages the content, scope and influence of each chapter is further discussed.

Chapter 2 of this thesis is a literature review in which the structures of the turbulent boundary layer and their effect on increasing the skin friction drag in the near wall region is discussed and reviewed. This is coupled with an extensive literature review of previous control techniques where the advantages and disadvantages of such techniques have been critically analysed. This review has been used to identify the shortcomings of previous techniques to illustrate how the potential use of a micro-cavity array can overcome limitations experienced by other control techniques. The chapter identifies the research gaps and how they can be addressed by the current work.

The main body of the thesis begins in Chapter 3, which commences by investigating the turbulent boundary layer and the higher statistics for generating a naturally developed turbulent boundary layer are quantified. The chapter consists of the first of four journal papers and is used as an initial benchmark for the flat plate test section and constant temperature hot-wire anemometry system. The chapter provides an insight into the effect of the investigated trip techniques on the induced transition of a laminar boundary layer into turbulence. The results demonstrate that to produce a natural turbulent boundary layer using a 2D protuberance, the height of the trip must be less than the undisturbed boundary layer thickness.

Chapter 4 presents a detailed experimental evaluation of the micro-cavity array as a potential boundary layer control device. The key purpose of this chapter is to analyse the

effect of the micro-cavity array on the boundary layer. In this chapter the surface geometries of the array are modified to develop a relationship with boundary layer control and parameterise the number and distribution of devices required to effectively control the boundary layer across the flat plate. The work is significant as the cavity array is shown to have a substantial effect on the coherent structures. The cavity array is shown to reduce the intensity of the sweep events in the near wall region, where the geometry of the orifices is found to have a significant effect on the net reduction.

In Chapter 5 the cavity array for boundary layer control is further explored. Building upon the findings in the previous chapter, an additional experimental analysis is used to determine the optimal arrangement for the micro-cavities to achieve maximum boundary layer control. The sensitivity of the internal geometry of the cavity array is evaluated, specifically the volume of the backing cavity below the array itself, as well as the length of the orifice neck. The results suggest a larger reduction in turbulence intensity, sweep intensity and energy spectrum can be achieved with a larger backing volume. However changing the length of the orifice is shown to be negligible in modifying the boundary layer.

Chapter 6 analyses the mechanism by which the micro-cavity array achieves attenuation of captured sweep events and builds upon the previous two chapters. A single cavity array is analysed experimentally with two different backing cavity arrangements; one with a common backing cavity for all orifices and another utilising a cell-like design to prohibit the captured flows interacting. Results from this chapter reveal that the cavity array weakens captured sweep events by damping the energy of the events through the friction losses in the orifices of the cavity array and also in the large volume of the backing cavity

below the array itself. From the experimental results this chapter achieves its intended objective of investigating the method by which the micro-cavities achieve boundary layer control, as well as providing additional data to solidify the relationship between the turbulence energy reduction and the backing volume of the cavity array.

The final chapter documents the conclusions made from the research in this thesis. While the research covered in this thesis has taken a significant step forward in developing the micro-cavity array as a potential boundary layer control device, subsequent work is required before the cavity array can be used in real life applications. Consequently additional research is required and key recommendations are made at the end of this chapter for the future of this area of research.

1.4 Publications arising from this thesis

Journal papers

Silvestri, A, Ghanadi, F, Arjomandi, M, Cazzolato, BS, Zander, AC, 2017a, *'Attenuation of sweep events in a turbulent boundary layer using micro-cavities', Experiments in Fluids, vol. 58, no. 5, pp. 58.*

Silvestri, A, Ghanadi, F, Arjomandi, M, Cazzolato, BS, Zander, AC, 2017b, *'The application of different tripping techniques to determine the characteristics of the turbulent boundary layer over a flat plate', ASME Journal of Fluid Engineering, vol. 140, no. 1, pp. 011204.*

Silvestri, A, Ghanadi, F, Arjomandi, M, Chin, R, Cazzolato, BS, Zander, AC, 2017c, *'Attenuation of turbulence by the passive control of sweep events in a turbulent boundary layer using micro-cavities', Physics of Fluids,* vol. 29, pp. 115102.

Silvestri, A, Ghanadi, F, Arjomandi, M, Cazzolato, BS, Zander, AC, Chin, R, 2017d, *'Mechanism of sweep event attenuation using micro-cavities in a turbulent boundary layer', Physics of Fluids,* vol. 30, Issue. 4, pp. 055108.

Refereed conference papers

Silvestri, A, Ghanadi, F, Arjomandi, M, Cazzolato, BS, Zander, AC, 2016, *'Control of the turbulent boundary layer by the application of a cavity array', 20th Australasian Fluid Mechanics Conference*, Perth, Australia, 5-8 December.

Silvestri, A, Ghanadi, F, Arjomandi, M, Cazzolato, BS, Zander, AC, 2017e*, 'The effect of the backing cavity on the control of the turbulent boundary layer by the application of a cavity array', 10th International Symposium on Turbulence and Shear Flow Phenomena*, Chicago, IL, USA, 6-9 July.

1.5 Format

This thesis has been submitted as a portfolio of publications arising from the research and is compliant with the formatting requirements of The University of Adelaide. The printed and online version of this thesis are identical, where the online version of this thesis is available as a PDF.

1.6 References

Abbas, A, Bugeda, G, Ferrer, E, Fu, S, Periaux, J, Pons-Prats, J, Valero, E, Zheng, Y, 2017, '*Drag reduction via turbulent boundary layer flow control', Science China Technological Sciences*, vol. 60, no. 9, pp. 1281-1290.

Benschop, HOG, Breugem, WP, 2017*, 'Drag reduction by herringbone riblet texture in direct numerical simulations of turbulent channel flow', Journal of Turbulence,* vol. 18, no. 8, pp. 717-759.

Chang, K, Constantinescu, G, Park, SO, 2006, '*Analysis of the flow and mass transfer processes for the incompressible flow past an open cavity with a laminar and a fully turbulent incoming boundary layer', Journal of Fluid Mechanics*, vol. 561, pp. 113-145.

Choi, KS, 1987*, 'On physical mechanism of turbulent drag reduction using riblets', Transport Phenomena in Turbulent flows*, pp. 185-198, New York, USA.

Choi, KS, 1989, *'Near-wall structure of a turbulent boundary layer with riblets'*, *Journal of Fluid Mechanics*, vol. 208, pp. 417-458.

Choi, KS, Fujisawa, N, 1993, *'Possibility of drag reduction using d-type roughness'*, Applied Scientific Research, vol. 50, pp. 315-324.

Corino, ER, Brodkey, RS, 1969, *'A visual investigation of the wall region in turbulent flow', Journal of Fluid Mechanics*, vol. 37, part. 1, pp. 1-30.

Gad-el-Hak, M, 1994, *'Interactive control of turbulent boundary layers - A futuristic overview', AIAA Journal,* vol. 32, no. 9, pp. 1753-1765.

Gad-el-Hak, M, 2000, *'Flow Control: Passive active and reactive flow management', Canbridge University Press.*

Ghanadi, F, 2015, *'Application of a Helmholtz resonator excited by grazing flow for manipulation of a turbulent boundary layer', PhD thesis,* School of Mechanical Engineering, University of Adelaide, Australia.

Greidanus, AJ, Delfos, R, Tokgoz, S, Westerweel, J, 2017, *'Turbulent Taylor–Couette flow over riblets: drag reduction and the effect of bulk fluid rotation', Experiments in Fluids, vol. 56, pp. 107.*

Guo, H, Boridulin, VI, Kachanov, YS, Pan, C, Wang, JJ, Lian, QX, Wang, SF, 2010*, 'Nature of sweep and ejection events in transitional and turbulent boundary layers', Journal of Turbulence,* vol. 11, no. 34, pp. 1-51.

International Air Transport Assocation, 2017, *'IATA Fact Sheet – Fuel (June update)'*, viewed 6 November 2017, https://www.iata.org/pressroom/facts_figures/fact_sheets/Documents/fact-sheet-fuel.pdf.

Kasagi, N, Suzuki, Y, Fukagata, K, 2009, *'Microelectromechanical systems-based feedback control of turbulence for skin friction reduction', Annual Review of Fluid Mechanics*, vol. 41, pp. 231-251.

Kim, HT, Kline, SJ, Reynolds, WC, 1971*, 'The production of turbulence near a smooth wall in a turbulent boundary layer', Journal of Fluid Mechanics*, vol. 50, part. 1, pp. 133-160.

Maa, DY, 1998, *'Potential of microperforated panel absorber', Journal of the Acoustical Society of America*, vol. 104, no. 5, pp. 2861- 2866.

Marec, J, 2000, *'Drag reduction: a major task for research', European Drag Reduction Conference*, Potsdam, Germany, 19-21 June.

Offen, GR, Kline, SJ, 1975, *'A proposed model of the bursting process in turbulent boundary layers', Journal of Fluid Mechanics*, vol. 70, part. 2, pp. 209-228.

Wallace, JM, Eckelmann, H, Brodkey, RS, 1972, *'The wall region in turbulent shear flow', Journal of Fluid Mechanics*, vol. 54, pp. 39-48.

Walsh, MJ, 1983*, 'Riblets as a viscous drag reduction technique', AIAA Journal,* vol. 21, no. 4, pp. 485-486.

Whalley, RD, 2011, *'Turbulent boundary-layer control with DBD plasma actuators using spanwise travelling-wave technique', PhD Thesis,* The University of Nottingham, England, UK.

Chapter 2

Literature Review

In this chapter an overview of fundamental research on turbulent boundary layers and previous attempts at controlling the boundary layer will be presented. The chapter begins by characterising and reviewing the turbulent boundary layer literature and the coherent structures which are responsible for the increased shear stresses in the near wall region. Following on from this, Section 2.2 investigates the techniques implemented for boundary layer control. This is subsequently followed by Section 2.3 in which the history of using micro-cavity arrays to control the instabilities in the turbulent boundary layer is discussed. Section 2.4 reviews experimental techniques that are commonly used to measure the statistics of the boundary layer, while the chapter concludes with Section 2.5, which provides a summary of the literature review and the overall objectives of this thesis.

2.1 Turbulent boundary layer

The turbulent boundary layer consists of coherent structures which dominate the events in the near wall region of the boundary layer. These events, which are usually subdivided into the categories of sweep and ejection events, amplify the generation of turbulent energy. These three dimensional instabilities have been shown to be responsible for the large shear stresses and skin friction drag in the turbulent boundary layer (Kline et al.,

1967; Offen and Kline, 1975; Robinson, 1991). Implementing a technique to control these events for boundary layer control has been considered by many researchers (Lockerby, 2001; Whalley, 2011; Ghanadi, 2015), however, a firm understanding of the turbulent boundary layer and its structure must be obtained before developing such a technique.

2.1.1 Near-wall region

Initial research into the near-wall region and the dominant structures was first undertaken by Kline et al. (1967). Using the hydrogen bubble technique to visualise the near-wall region of the boundary layer, Kline et al. (1967) showed a distinctive streaky structure shown in Fig. 2.1. From these findings Kline et al. (1967) were able to determine the structure of the boundary layer as three-dimensional, which had previously been believed to be two dimensional. Furthermore it was shown the streaky structure is capable of traversing 100 viscous units in the spanwise direction ($z^+ = 100$) and up to 50 viscous units away from the wall ($y^+ = 100$), after which the streak terminates violently by bursting into the outer region of the boundary layer, a process which dominates the energy transfer from the near-wall region to the outer boundary layer.

While Kline et al. (1967) were successful in portraying the ejection of low speed fluid away from the wall known as ejection events, they were not able to capture the sweep events that also form a critical part of the structures in the near-wall region of the boundary layer. This was later achieved by Corino and Brodkey (1969) who not only verified the findings of Kline et al. (1967) but also introduced the notion of sweep events in the turbulent boundary layer. Using Particle Image Velocimetry (PIV), Corino and Brodkey (1969) were able to show the near wall region itself had two distinct areas of high and low speed fluids, which is represented in Fig. 2.2. The high speed fluid was shown to move the

decelerated region away from the wall, which causes the ejection of low speed fluid away from the wall. The streak then quickly becomes unstable and begins to break apart (Kim et al., 1971). This is followed by the inrush of high speed fluid as described by Corino and Brodkey (1969) which causes the next low speed streak ejection. The significance of these two events was instantly recognised and by using flow visualisation Corino and Brodkey (1969) reported that 70% of the total production of Reynolds stress in the near wall region comes from the ejection event, while the remainder is contributed to the sweep event. This three stage cycle was also shown to repeat and was subsequently termed 'bursting' (Kim et al., 1971). This was further confirmed by Offen and Kline (1975) and a definitive regenerative cycle of the sweep and ejection events and near-wall turbulence generation was conceived.
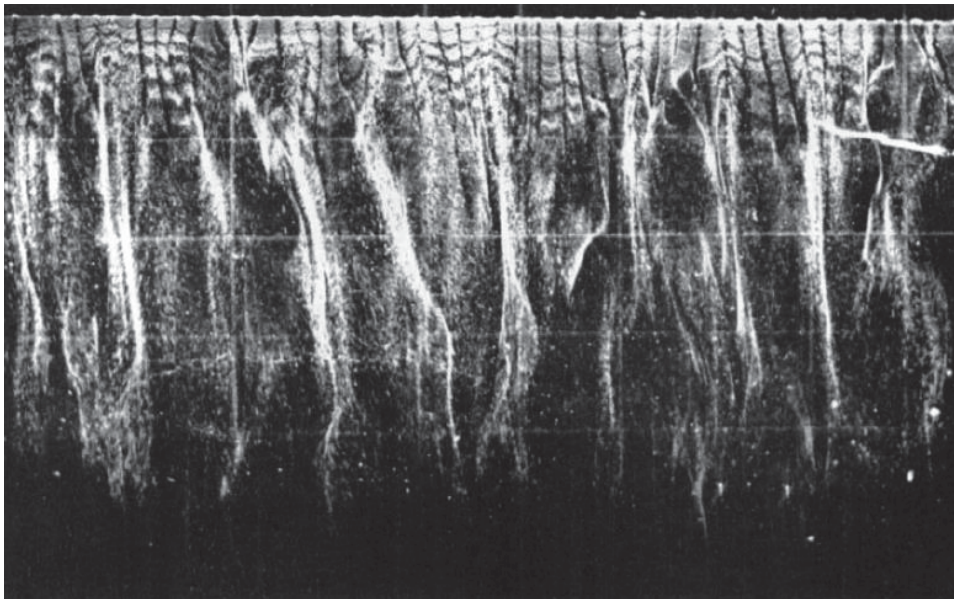
Fig. 2.1 Near-wall streaky structure of a turbulent boundary layer at $y^+ = 4.5$ visualised using hydrogen bubble technique. In this picture the wire is located parallel to the plate and normal to the direction of flow, which is moving from top of the image to bottom (Kline et al. 1967).
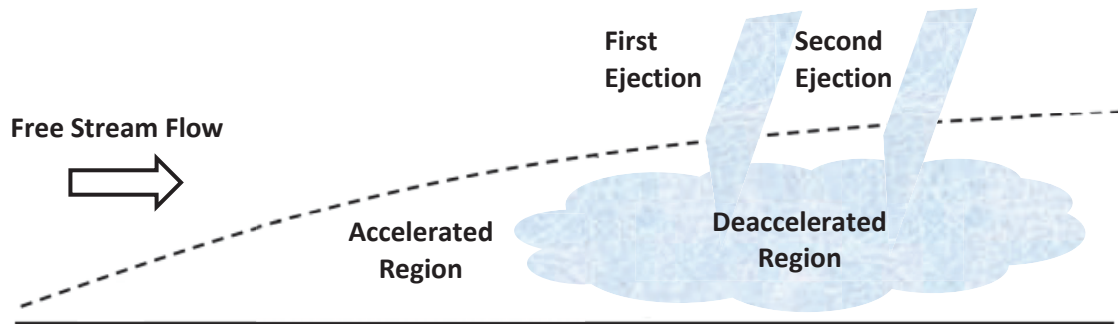
Fig. 2.2 Near-wall structure showing the low and high speed flow along with ejection events.

Continuing the research of Kline et al. (1967) and Corino and Brodkey (1969), Wallace et al. (1972) and Lu and Wilmarth (1973) showed there were two additional types of events that can take place in the near-wall regions. A four quadrant system was introduced to distinguish between the four possible events (Lu and Wilmarth, 1973) and given the notation Q1, Q2, Q3 and Q4 as shown in Table 2.1. Ejection and sweep events were labelled as Q2 and Q4 events, respectively, and were shown to generate approximately 70% of the total stresses each, equating to a total 140% of the total stresses in the near wall region at a pipe Reynolds number of approximately 11,000 (Corino and Brodkey, 1969; Kim et al., 1971; Wallace et al., 1972; Offen and Kline, 1975). Furthermore the size of the structures were shown to be highly dependent on the Reynolds number, where an increased Reynolds number would effectively reduce the size of the structure (Robinson, 1991). The newly discovered events (Q1 and Q3) were shown to account for the 40% discrepancy due to their negative contribution to the total Reynolds stresses.

Table 2.1: Reynolds stress contributions (Whalley, 2011).

Quadrant	Sign of u	Sign of v	Sign of −uv	Type of motion
Q1	+	+	-	Outward Interaction
Q2	-	+	+	Ejection
Q3	-	-	-	Inward Interaction
Q4	+	-	+	Sweep

The techniques used to measure the properties of the coherent structures in the near-wall region are also of significant importance. When quantifying the coherent structures many techniques have been used, one of which is the Variable Interval Time Averaging (VITA) technique for detection of the changes in the turbulent boundary layer associated with coherent structures. The technique was initially applied by Blackwelder and Kaplan (1976) for studying the near wall region and detecting the sweep and ejection events. The events are monitored by calculating the VITA of the streamwise velocity fluctuations according to the definition

$$\hat{u}(t, T_W) = \lim_{t \to \infty} \frac{1}{t} \int_0^t u^2(t)\, dt,$$

$$(2.1)$$

where T_W, is the interval used for the time averaging and is selected to be of the order of the time scale between bursts. This value (T_W) is used to assign small windows, which scan the fluctuating velocity at each point and within which the local variance of the signal is calculated using

$$\text{Var}(t, T_W) = \hat{u}^2(t, T_W) - [\hat{u}(t, T_W)]^2.$$

$$(2.2)$$

The variance of the entire signal is defined as

$$\text{Var}(t) = \lim_{t \to \infty} \frac{1}{t} \int_0^t u^2(t)\, dt.$$

<div align="right">(2.3)</div>

If the value of the local variance, $\text{Var}(t, T_W)$ is greater than the variance of the entire signal $k\text{Var}(t)$, where k is a threshold value, a sweep or ejection event is considered to have occurred. Whalley (2011) defined the detection function, $D(t)$, to distinguish between the different events, where

$$D(t) = \begin{cases} 1 & \text{Var}(t, T_W) > k\text{Var}(t) & \dfrac{du}{dt} > 0 \ (\text{sweep event}) \\ 0 & \text{Var}(t, T_W) < k\text{Var}(t) & (\text{no event}) \\ -1 & \text{Var}(t, T_W) > k\text{Var}(t) & \dfrac{du}{dt} < 0 \ (\text{ejection event}) \end{cases}$$

<div align="right">(2.4)</div>

The number of detected events is strongly dependent on the selected threshold value, k. The averaged VITA events can reveal the intensity and duration of the coherent structures. These are important as they determine the characteristics of the coherent structures and their effect on the boundary layer. The intensity of the events is calculated based on the peak-to-peak value of the streamwise velocity of the events. The duration on the other hand is calculated from the time separation of the peaks in each VITA analysis as shown in Fig. 2.3. Increased duration or intensity of the events reveals an increase in the turbulence energy production.
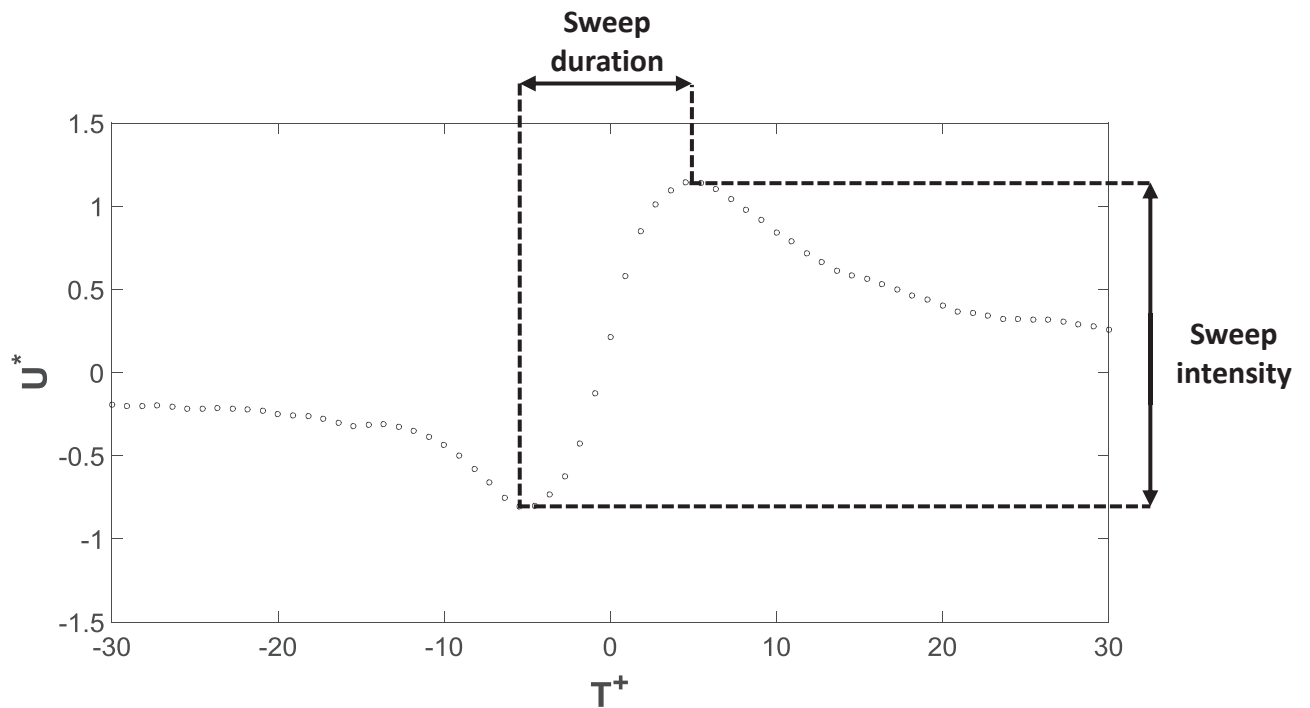
Fig. 2.3 Average VITA sweep events at $Re_\theta = 1927$ demonstrating the difference between sweep intensity and duration.

2.1.2 Outer region

The outer region of the turbulent boundary layer also has a part to play in the events seen close to the wall (Falco, 1977). The structure of the turbulent boundary layer in the outer region can be clearly seen using experimental techniques. One such example is presented in Fig. 2.4 using fluorescent dye in a water tunnel performed by Gad-el-Hak and Bandyopadhyay (1994). The visible bulges cause the boundary layer to be re-energised by continually entraining fluid from the free stream into the boundary layer. Falco (1977) initially hypothesised these turbulent bulges moving towards the wall could be responsible for the inrush of fluid towards the wall during a sweep event as part of a bursting cycle.
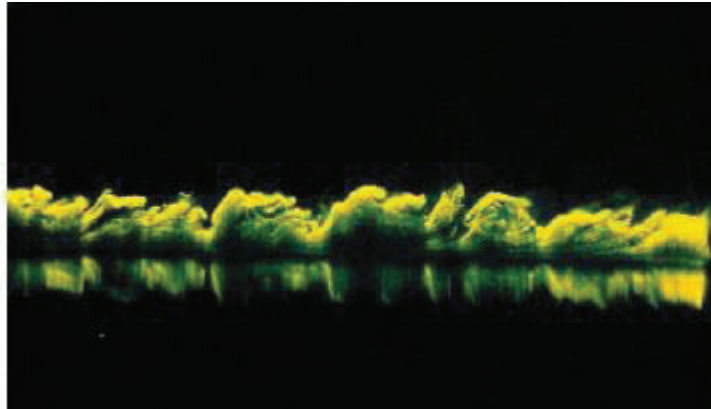
Fig. 2.4 Flow visualisation of a turbulent boundary layer, $Re_\theta = 725$ (Gad-el-Hak and Bandyopadhyay, 1994).

The vortical structures that exist in the outer region of the boundary layer also have an impact on the turbulent events observed in the near wall region. The most common of which is the hairpin vortex proposed by Theodorsen (1952). Head and Bandyopadhyay (1981) and Robinson (1991) identified the three main components of this vortex structure, which are the legs, neck and head. The legs of the hairpin vortex have been shown to be responsible for the generation of quasi-streamwise vortices. The legs of the hairpin vortex stay attached to the wall (Perry and Marusic 1995) as illustrated in Fig. 2.5. Consequently the hairpin legs are elongated and as a result form quasi-streamwise vortices, which are closely linked to the near-wall low speed streaks which occur during ejection events (Robinson, 1991).

Robinson (1991) hypothesised the streamwise vortices move low speed fluid in the near wall region away from the wall on the upwash of the legs of the hairpin, giving the appearance of streaks documented in previous investigations (Kline et al., 1967; Corino and Brodkey, 1969). The sweep events that occur in the near wall region have also been proposed to be due to the downwash of the quasi-streamwise vortices. During the

downwash of the hairpin leg, flow from the free stream is entrained and pushed towards

the wall causing the inrush of high speed fluid into the near wall region. Consequently

targeting such structures can have significant effects on the sweep and ejection events.
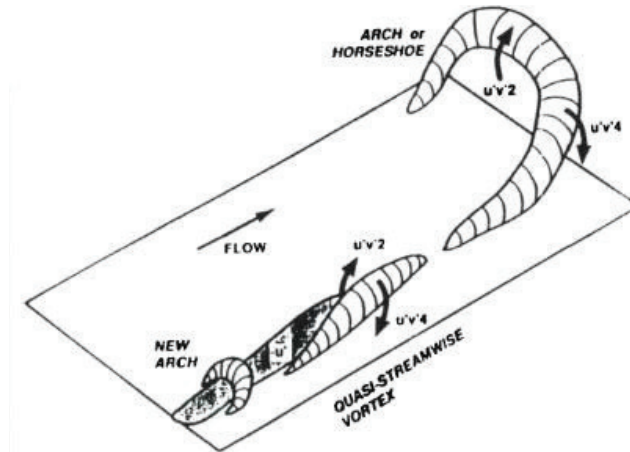
Fig. 2.5 Conceptual model of the relationship between quasi-streamwise vortices and

hairpin vortex structures (horseshoe) (Adrian et al., 2000).

As the coherent events are responsible for the Reynolds stress and resultant shear

stresses in the near-wall region many researchers have aimed to control these structures

to reduce the skin friction drag. Consequently many drag reduction techniques have been

implemented to achieve this via the manipulation of the bursting process by directly

targeting the coherent structures or through the quasi-streamwise vortices. Such

techniques are discussed in the next section of this chapter, where their shortcomings

and advantages will be discussed.

2.2 Turbulent boundary layer control

Controlling the turbulent boundary layer has been a major focus for many researchers

over the years. An extensive amount of time and resources has been devoted to

developing a successful technique to suppress the instabilities in the boundary layer responsible for skin friction drag. Generally these control techniques can be subdivided into two categories; passive and active control techniques. Active systems require an external power source and as a result have the advantage of greater drag reduction capability due to the potential implementation of feedback systems. However, this comes at a cost of complicated implementation which is undesirable in aerospace applications. Passive control techniques are generally more favourable for this reason as the absence of need of a power source means passive techniques are relatively easily implemented, at the expense of limited control. The following section summarises current turbulent boundary layer control techniques, whilst outlining the advantages and limitations associated with such techniques.

2.2.1   Riblets

One of the most successful passive techniques for control of the turbulent boundary layer is the streamwise riblet (Walsh, 1983; Choi, 1987, 1989, Greidanus et al., 2015; Benschop and Breugem, 2017). Streamwise riblets are small longitudinal grooves which are aligned in the flow direction (Fig. 2.6). They are passive devices and as such have an extremely simple implementation. Riblets act as small fences and restrict the quasi-streamwise vortices which form part of the legs of the hairpin vortical structure. The fencing of the streamwise vortices inhibits their growth in the spanwise direction which causes the downwash cycle to be reduced significantly and as a result the sweep events occur prematurely with a reduced duration and intensity (Choi et al., 1993; Tardu et al., 1993). The corresponding reduction was revealed to be a function of the height of the individual grooves (h) and the spacing between each of the grooves (s). Walsh (1983) demonstrated

that at an approximate height of $15l^+$ a maximum drag reduction of 8% could be achieved. Subsequent research by Garcia-Mayoral and Jimenez (2011) also revealed that when the spacing between each of the grooves became too large ($s^+ > 30$) a detrimental effect on the turbulent eddies would occur, resulting in an increased interaction of the high-speed flow and wetted surface with an increase in the skin friction drag, a finding further supported by Benschop and Breugem (2017).
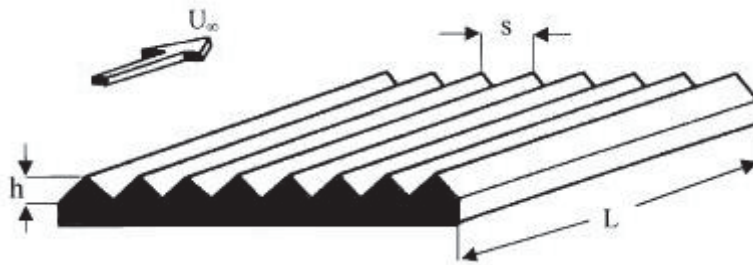
Fig. 2.6 Schemetic of riblets (Choi *et al.,* 1993).

In addition to fencing off the streamwise vortices, the riblets have also been shown to inhibit the fluctuations in the cross flow. Smaller fluctuations in the cross flow provide a more uniform flow and a decrease in momentum transfer from the boundary layer into the free stream (Luchini et al., 1991; Bechert et al., 1997). Bechert et al. (1997) investigated this method in further depth by using slits with longitudinal blade ribs (Fig. 2.7). While the slits in the surface did not contribute to the boundary layer control in their investigation, it was shown how perforated surfaces for boundary layer control could be implemented for minimal parasitic drag. Bechert et al. (1997) achieved a 9.9% reduction in skin friction drag, which was an improvement on the maximum drag reduction reported in other literature (Walsh, 1983; Walsh and Lindemann, 1984).
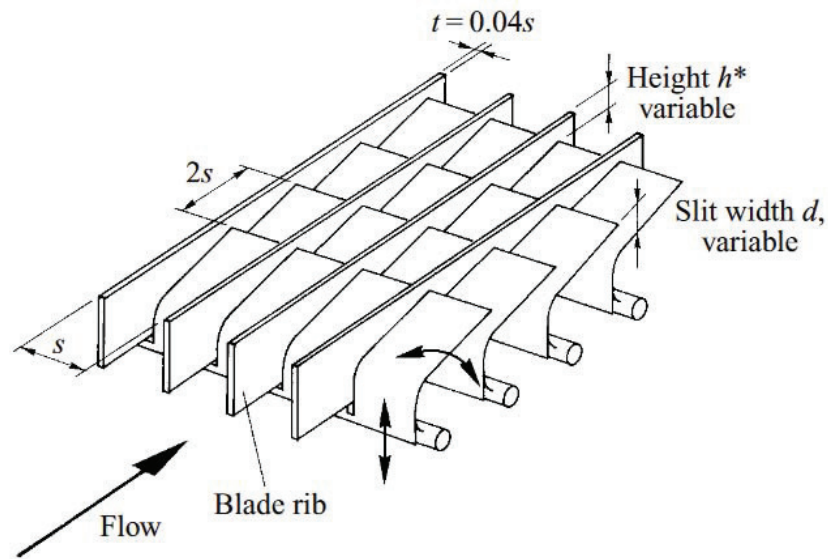
Fig. 2.7 Schemetic of riblets with slits and longitudinal ribs (Bechert et al., 1997).

As successful as riblets are, there are still numerous potential drawbacks with their application. Firstly, the angle of the riblets is detrimental for their success, as due to boundary layer separation, riblets can increase the turbulence events when their yaw angle is greater than 30 degrees (Choi, 1989; Choi, 1993) or if the geometry is not selected correctly (Garcia-Mayoral and Jimenez, 2011; Benschop and Breugem, 2017). Furthermore the manufacture and maintenance of riblets over structures in real applications, such as an aircraft, is a major issue and consequently it is often an impractical choice to reduce the skin friction drag commercially.

2.2.2 Spanwise travelling wave

Utilising spanwise excitation to create travelling waves is another technique that has been investigated to modify the streamwise vortices and reduce the effect of skin friction drag. The spanwise travelling wave creates synthetic streamwise vorticity to modify the naturally occurring quasi-streamiwse vortices to reduce the coherent structures and

viscous drag in the near wall region (Du et al., 2002; Choi et al., 2011; Li et al., 2014; Wong et al., 2015). This is illustrated in the flow visualisation by Choi et al. (2011) shown in Fig. 2.8. This wave is produced using an unsteady force in the viscous sublayer which is strongest at the surface and decays exponentially as it moves away from the wall (Du and Karniadakis, 2000).
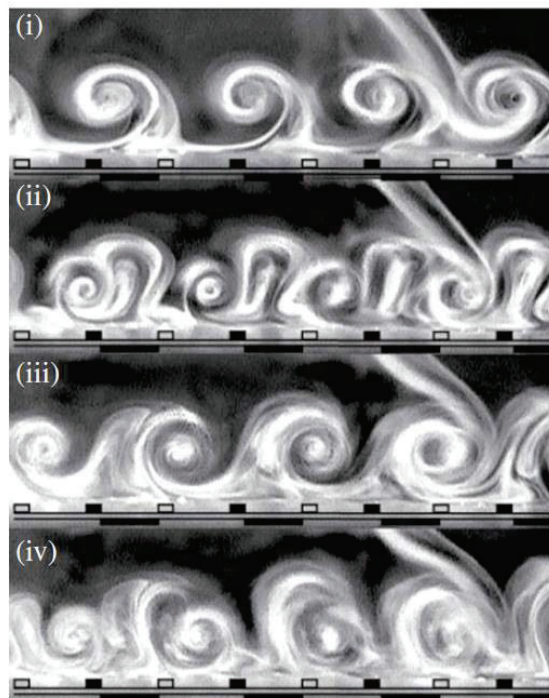
Fig. 2.8 Flow visualisation of the application of the spanwise travelling wave technique, i) and iii) no control, ii) and iv) control through the use of forced plasma oscillation (Choi et al., 2011).

The unsteady force used to generate the artificial vortices can be achieved multiple ways, but most commonly by using electrodes (Whalley, 2011) or magnets (Weier et al., 2001). When the force is applied to the fluid it curls the flow to create artificial vortices which interact with the existing streamwise vortices (Du and Karniadakis, 2000). The generated vortices reorganise the near wall region by spacing the low speed streaks more evenly

across the surface, which leads to a reduction in the skin friction drag, and as shown in Fig. 2.9 the high speed streaks are eliminated during the rearrangement process (Dhanak and Si, 1999; Du and Karniadakis, 2000; Du et al., 2002; Pan and Choi, 2004; Whalley, 2011).
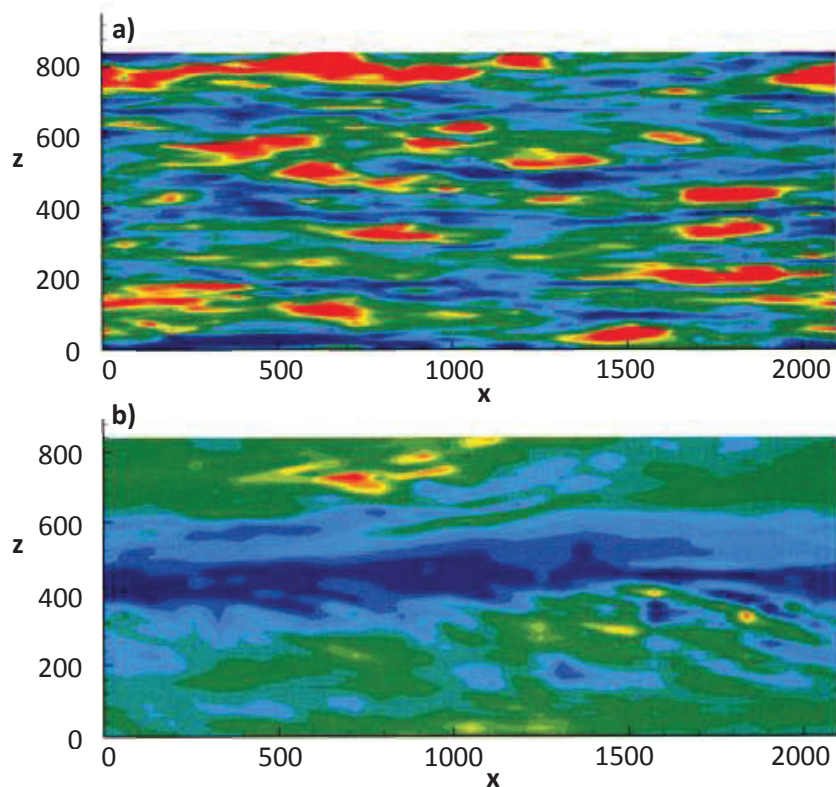
Fig. 2.9 Instantaneous flow visualisation of the wall streaks; a) no control, b) travelling wave excitation, where red regions denote high speed and blue regions denote low speed (Du and Karniadakis, 2000).

Dielectric barrier discharge (DBD) plasma actuactors have been successful in generating the travelling waves for turbulent boundary layer control as shown by Jukes et al. (2006), Choi et al. (2011), Whalley and Choi (2014) and Mahfoze and Laizet (2017). The plasma actuator is a completely electrical device and as such has no mechanical moving parts, which generates a Lorentz force by the movement of charged particles inside the electric

field. For flow control purposes a plasma actuator is composed of two electrodes with a dielectric layer between them. One of the electrodes is embedded below the dielectric layer and surface, while the other is placed within the flow and boundary layer itself. When a large AC voltage is applied to the electrodes, ionization of the surrounding air occurs at the top electrode, which causes the appearance of plasma at the surface. This is used to induce a jet of fluid and resulting artificial vortices at the surface. While this technique has yet to be used in practical applications, the device has been shown to reduce skin friction drag by 33%-45% (Whalley and Choi, 2014; Mahfoze and Laizet, 2017). Furthermore, the intensity and duration of sweep events were shown to be reduced by up to 10% and 50% respectively at low Reynolds numbers (Jukes et al., 2006; Choi et al., 2011; Whalley and Choi, 2014), while Mahfoze and Laizet (2017) reported even larger values.

The reduction in the duration and intensity of the sweep event is typically measured using the Variable Interval Time Averaging (VITA) technique previously discussed in Section 2.1. Fig. 2.10 clearly shows the reduction achieved using the DBD plasma actuator to create the spanwise travelling wave, which is estimated to be a 20% and 35% reduction in the intensity and duration, respectively.

While the spanwise travelling wave technique has shown significant impact on the boundary layer, a substantial issue still surrounds the application of this technique in practice. The external power required to induce the oscillation of the travelling wave is a drawback for the technique. It was estimated by Quadrio and Ricco (2004) that the power saved due to the reduction in skin friction drag was magnitudes lower than the power required to run the spanwise oscillation technique, which has similar power requirements

to the spanwise travelling wave technique. Coupled with the fact that the device is extremely difficult to install on current aerospace applications at large Reynolds numbers, this technique remains infeasible to reduce skin friction drag on aircraft.
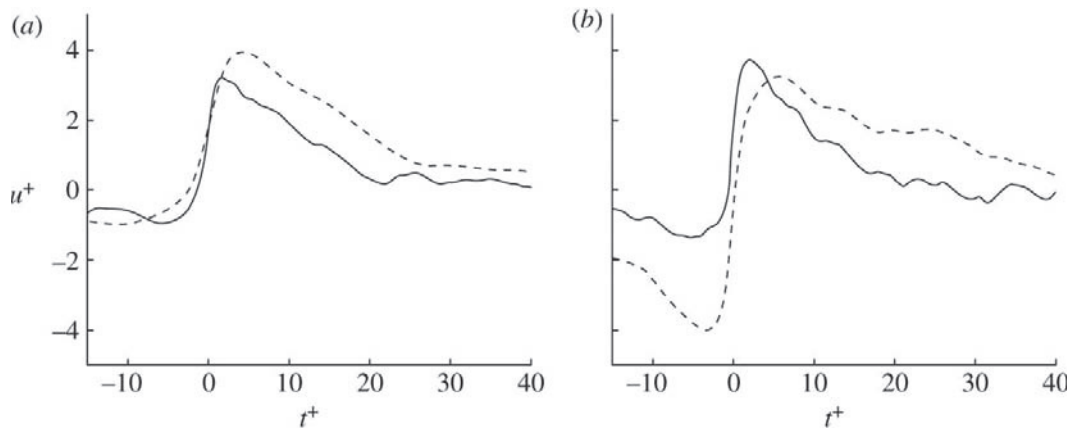
Fig. 2.10 VITA-detected sweep events with spanwise travelling wave at a) $y^+ = 5$ and b) $y^+ = 20$. Dashed line is the canonical data, while the solid line is the spanwise oscillation (Choi et al., 2011).

2.2.3   Selective suction/ blowing and the synthetic jet

While several techniques have been successful in controlling the coherent events by targeting the structures which influence the outer region, there are numerous techniques which have attempted to target the coherent events themselves. One such method is an active control technique which utilises blowing and suction on the sweep and ejection events respectively. This technique has been successful in reducing the skin friction drag as well as postponement of the transition of the boundary layer into turbulence (Gad-el-Hak, 2000; Lockerby, 2001, 2005; Atik et al., 2005; Segawa et al., 2007; Spinosa and Zhong, 2017). Small amounts of suction are applied to the low speed streaks to bring them closer to the wall, while the ejection of fluid is used to push the high speed events away from the near-wall region, as shown in Fig. 2.11. This causes the velocity difference between

low and high speed regions to be reduced and as such reduces the intensity of the bursting events and delays the bursting process.
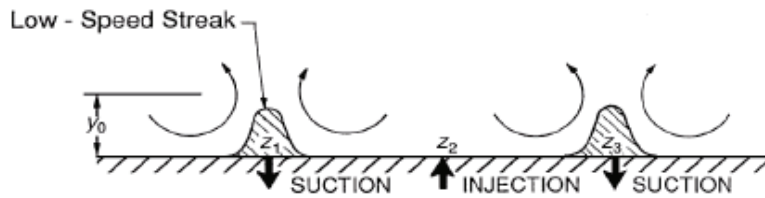
Fig. 2.11 Schematic of selective suction (z_1 and z_3) and injection (z_2) being applied at low and high speed fluid locations (Gad-el-Hak and Blackwelder, 1989).

Gad-el-Hak and Blackwelder (1989) first showed the successful implementation of this technique. They introduced artificial bursts upstream of their implemented control device using small suction holes and utilised selective suction to remove a portion of the low speed flow in the near wall region. This causes the velocity difference to be reduced drastically and a reduction in the bursting cycle occurs as shown in Fig. 2.12.
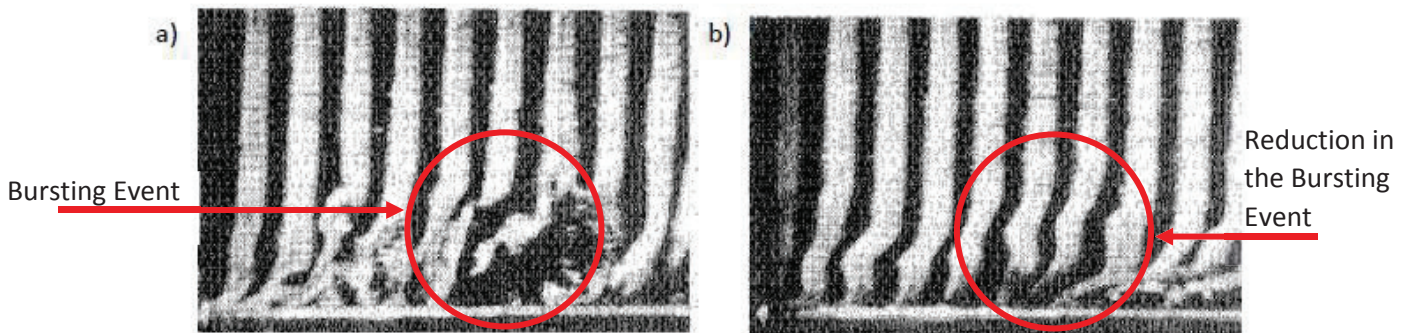
Fig. 2.12 The effect of selective suction on near-wall coherent structures: a) No control, b) Selective suction (Gad-el-Hak and Blackwelder, 1989).

Building upon the initial research into selective suction and ejection the synthetic jet was researched by Jacobs et al. (1993) and James et al. (1994). The design utilised a synthetic jet design at the micro scale ($l_{orifice} < 1$mm) in which a diaphragm is set in a cavity and

driven by a piezo electric element at its resonance frequency. With an open neck and orifice, fluid is drawn in and out of the cavity during the oscillation of the diaphragm. During the outflow cycle, vortex rings are generated at the orifice and travel away from the synthetic jet (Smith and Glezer, 1998) causing the high speed sweep events to be pushed away from the wall. During the inflow cycle, fluid is drawn into the cavity of the synthetic jet, which does not affect the vortex ring produced during the outflow cycle, yet allows the low speed ejection events to be brought closer to the wall. The design is highly desirable in turbulent flow control due to its self-contained nature with no external fluid source since the grazing flow is used to drive the jet.

Synthetic jets have had significant success in reducing the drag in the turbulent boundary layer. Most noticeable is the work by Choi and Kim (1994), Lockerby (2001), Rathnasingham and Breuer (2003) and Kang et al. (2008) to name a few. Rathnasingham and Breuer (2003) used a series of synthetic jets to reduce the mean wall shear stress by 7% and reduce the bursting frequency by up to 23% as shown in Fig. 2.13. While extremely successful, Rathnasignham and Breuer (2003) reported one of the biggest difficulties with their work was implementing their control laws to determine which areas to target in the boundary layer, an issue that plagues all active control techniques.

While the flow control capabilities of synthetic jets are clearly evident, the devices have another problem in regards to targeted control. The synthetic jet has an orifice diameter at the micro-scale, however, in comparison coherent structures have a much smaller scale ($l\_orifice$ < 100μm) in flight conditions. Consequently, for a synthetic jet to be applicable for flight conditions, the driving frequency would need to be approximately 4-20MHz and magnitudes smaller in size than the device investigated by Rathnasignham and Breuer

(2003) (Lockerby, 2001). One such device that can be used at this range is the micro-electromechanical systems actuator or MEMS-actuators for short. Lockerby (2001) investigated a MEMS scale synthetic jet actuator using direct numerical simulation (DNS). Lockerby (2001) was able to demonstrate success in manipulating the boundary layer structures using multiple DNS investigations. However, he could only achieve localised control of each individual streak and as such recommended distributed control via many devices was the best way to break down the streaks in the future. This would however be extremely expensive using MEMS actuators at this point in time. Nevertheless Lockerby outlined potential geometry details for such a device as illustrated in the Table 2.2.
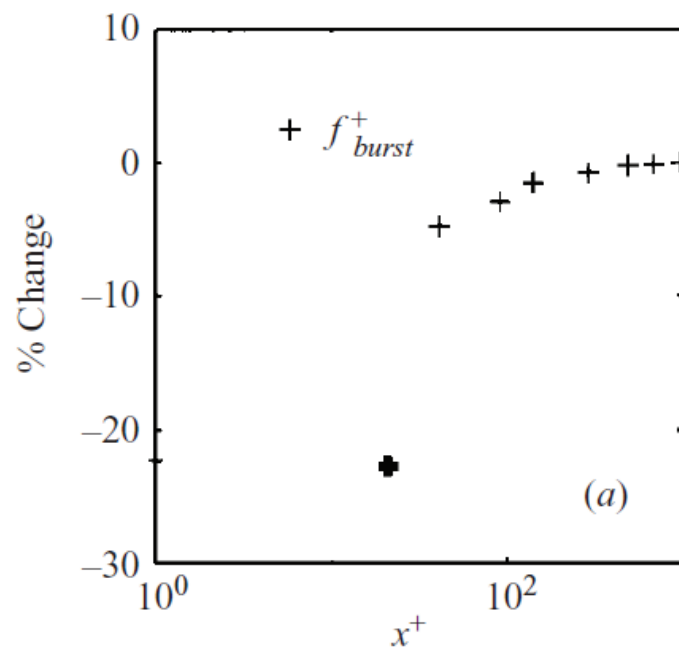
Fig. 2.13 Percentage reduction in bursting frequency with streamwise distance from the centre of the actuator (Rathnasingham and Breuer, 2003).

Table 2.2: Required characteristics of the successful implementation of a synthetic jet for targeted control at flight conditions ($u = 300m/s$). Data from Kline et al. (1967), Blackwelder and Eckelmann (1979), Blackwelder and Haritonidis (1983), Lockerby (2001).

Characteristic of the synthetic jet	Approximate Value scaled with viscous length scale	Approximate value in flight conditions
Orifice diameter (Lockerby, 2001)	$d^+ = 40$	$d = 60 \ \mu m$
Streamwise spacing (Blackwelder and Eckelmann, 1979)	$x^+ = 1000$	$x = 1500 \ \mu m$
Spanwise spacing (Kline et al. 1967)	$z^+ = 100$	$z = 150 \ \mu m$
Driving Frequency (Blackwelder and Haritonidis, 1983)	$f^+ = 0.04$	$f = 240 \ kHz$

While the synthetic jet technique has shown significant potential, the drawbacks make such a device untenable for real life applications. Like many active control techniques the device is extremely difficult to implement, control, manufacture and install on current aerospace applications due to the size of the coherent structures at large Reynolds numbers. Consequently this creates a significant issue that cannot be overcome by the technology at this stage.

2.2.4 Helmholtz resonator

As a variant to synthetic jets, the Helmholtz resonator has also been considered as a possible passive alternative to achieve targeted control of the turbulent boundary layer (Ghanadi et al., 2013, 2014a &b, 2015). While limited research has been conducted on the potential control of the boundary layer using a Helmholtz resonator, Ghanadi et al. (2014b &c, 2015) achieved a significant reduction in the turbulent energy production using the passive device. Unlike the synthetic jet the Helmholtz resonator utilises the resonance of the Helmholtz mode to achieve localised suction and ejection at the orifice. This is achieved when the breakdown of the shear layer occurs as it travels across the opening of the resonator (De Metz and Farabee, 1977; Nelson et al., 1981, 1983; Flynn and Panton, 1990; Ghanadi, 2015). The resulting quasi-periodic vortices travel to the trailing edge of the orifice and cause pressure waves to propagate back towards the leading edge and into the neck and cavity of the Helmholtz resonator. This pressure wave oscillation in the neck and cavity, coupled with the existing fluid, causes a mass and spring-like oscillation to occur, resulting in small oscillations of the suction and injection to occur at the orifice as illustrated in Fig. 2.14.
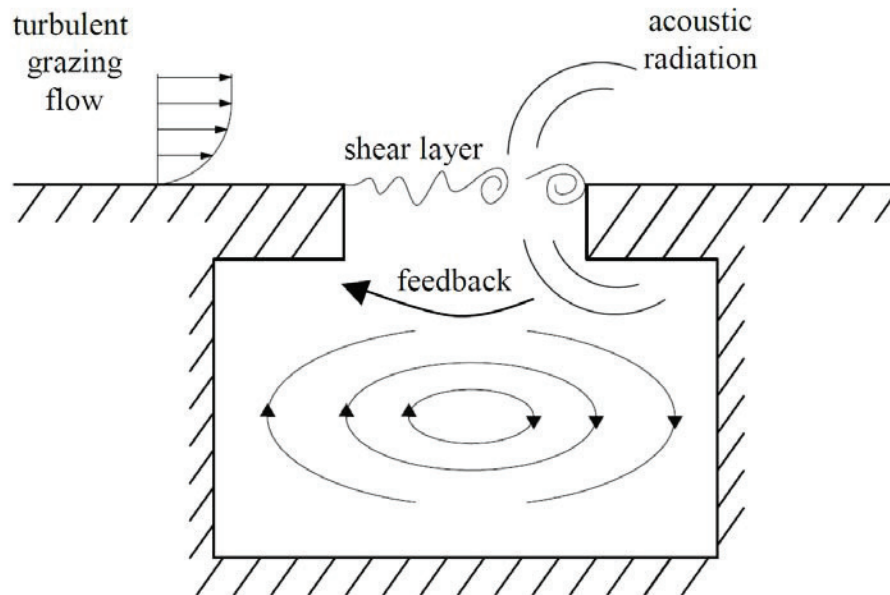
Fig. 2.14 Flow behaviour inside and outside a cylindrical Helmholtz resonator with a

turbulent boundary layer grazing flow (Ghanadi, 2015).

The activation of the Helmholtz resonator results in a passive method for targeted suction

and ejection control of the near wall structures. This was first illustrated by Ghanadi et al.

(2014b, 2014c, 2015) who utilised Computational Fluid Dynamics (CFD) and experimental

techniques to analyse four configurations of the resonator. At low Reynolds numbers the

resonator achieved a 12% (LES investigation) and 16% (experimental investigation)

reduction in turbulence intensity as shown in Fig. 2.15. Furthermore, 11% and 8%

reductions in sweep intensity and duration were also achieved using the Helmholtz

resonator (Ghanadi, 2015).
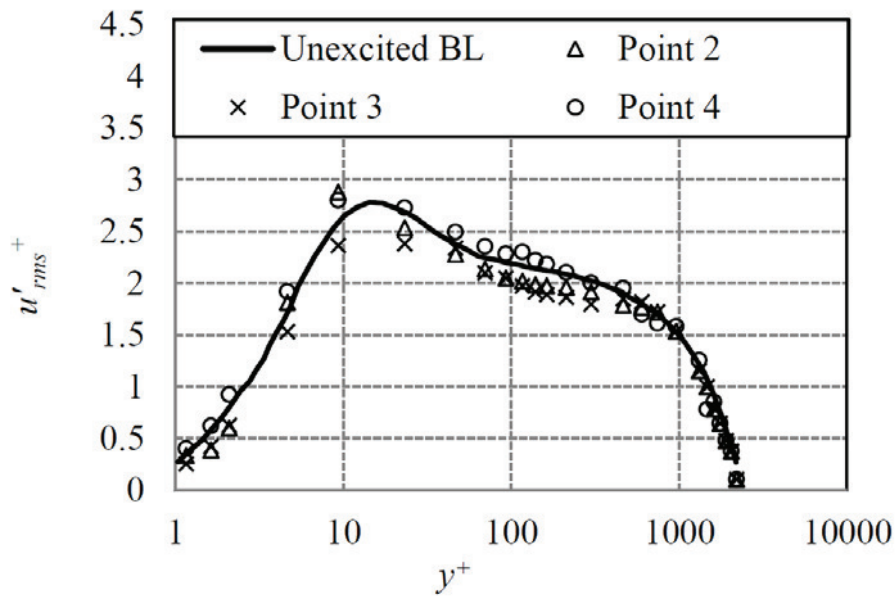
Fig. 2.15 Turbulence intensity profiles with and without the Helmholtz resonator at

$Re_\tau = 936$ (Ghanadi et al., 2015). (Point 2) $x^+ = .5$, (Point 3) $x^+ = 1$, (Point 4) $x^+ = 2$.

While the Helmholtz resonator was successful in disrupting the coherent structures, only

two resonators out of the four were capable of achieving reduction in the production of

turbulent energy. Theses resonators had a 5mm orifice diameter and a 5mm neck length

(HR2), and had a 10mm orifice diameter and a 15mm neck length (HR4), as shown in Fig.

2.16.

The reduction in sweep intensity and duration achieved by the Helmholtz mode however

was identified to be achieved irrespective of the activation of the Helmholtz mode. When

the Helmholtz mode was activated (Fig. 2.17), 11% and 8% reductions in sweep intensity

and duration were achieved. Yet the Helmholtz resonator was also shown to reduce the

intensity and duration of sweep events by 5% and 8% in the absence of targeted suction

and ejection in the near wall region due to the activation of the Helmholtz mode.
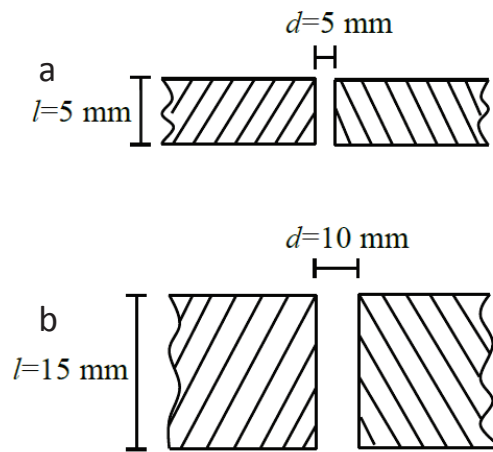
Fig. 2.16 Neck details of the two cylindrical Helmholtz resonators which were found to be effective in controlling the boundary layer. a) HR2, b) HR4 (Ghanadi et al., 2015).

The limitations of the Helmholtz resonator were explained by Ghanadi et al. (2015), the most prominent of which was the negligible effect on the boundary layer by the resonator once the Reynolds number increased. Lockerby (2011) and Ghanadi (2015) discussed this phenomenon where the orifice of the control device needs to be of similar size to the structures the device is trying to eliminate or suppress. For the case of the Helmholtz resonator the smallest dimension of the orifice studied by Ghanadi (2015) was 5mm, in comparison to the size of the coherent structures (<5mm) which were expected to be much smaller as the Reynolds number increased. As such the structures become so small at higher Reynolds numbers that the Helmholtz resonator is no longer able to supress a single event without influencing the bulk flow at the same time, resulting in instances where the device increased the intensity of the sweep events in the near wall region (Ghanadi et al., 2015; Ghanadi, 2015). However, similar to the synthetic jet discussed in Section 2.2.3, this drawback is due to the sizing of the device and not the mechanism. While a tiny Helmholtz resonator could be implemented for flight scale boundary layer control a simpler solution might be more viable as identified by Ghanadi et al. (2013,

2014a & b, 2015) who demonstrated that the resonator was capable of attenuation of the sweep event irrespective of the activation of the Helmholtz mode.
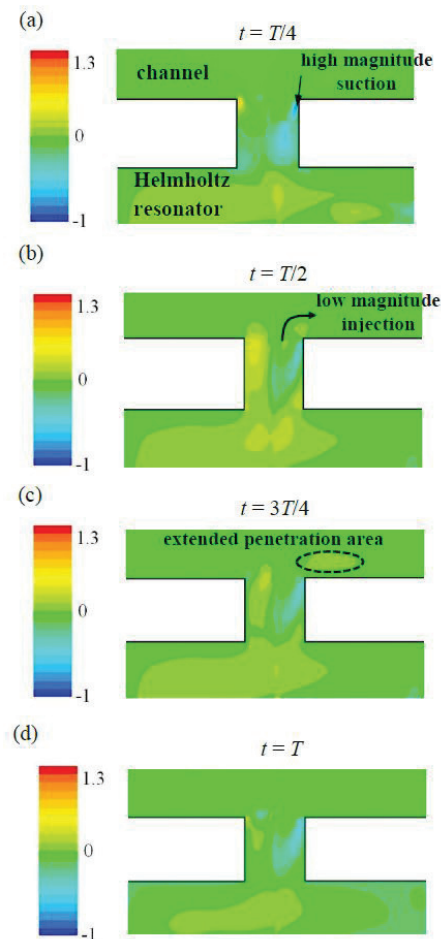
Fig. 2.17 Instantaneous normal to the wall velocity over the orifice of HR2 at $Re_\tau = 936$

(Ghanadi et al., 2015).

2.2.5 Micro-cavity array

While techniques have shown success during the execution of Computational Fluid Dynamics or experimental investigations, a successful technique has yet to be implemented in practice. An interesting concept, which forms the basis of this research, is the potential of an array of micro-cavities as a control device to attenuate the coherent

structures in the near wall region, as shown in Fig. 2.18. Such a device would naturally have the positive benefits of other passive techniques, such as easy implementation and no external power source.

Orifice length (l^+) Cavity array orifice locations

Variable backing cavity V^+

Movable Backing face
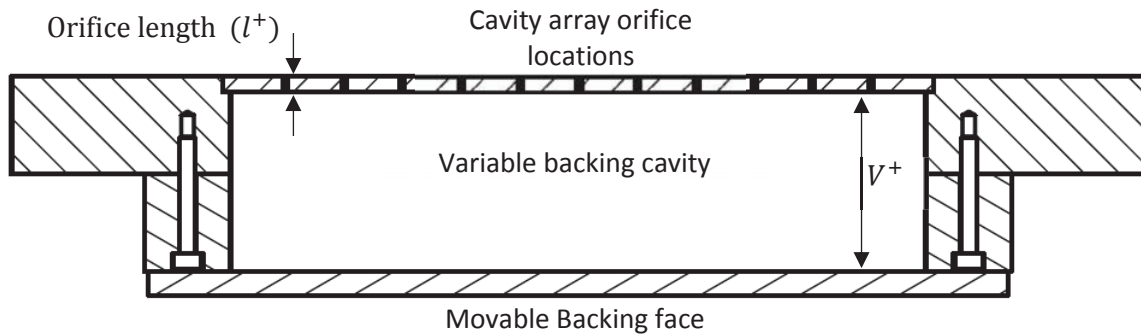
Fig. 2.18 Schematic of the proposed micro-cavity array technique.

The potential of this device for controlling the turbulent boundary layer was inspired by the Helmholtz resonator where it was found to have an impact on the sweep events away from the wall in the logarithmic region, reducing their intensity and duration by 5% and 8% respectively without the activation of the Helmholtz mode (Ghanadi, 2015). Further, Ghanadi (2015) also showed a 12% reduction in the turbulence intensity using the Helmholtz resonator without the activation of the Helmholtz mode. As such it can be concluded that the Helmholtz resonator was able to passively attenuate the sweep events and reduce the turbulent energy in the boundary layer. Consequently, some of the energy associated with the high speed events was absorbed and dampened by the Helmholtz resonator, which may have occurred by allowing the sweep event to partially or completely enter the orifice of the resonator and effectively reducing the Helmholtz resonator to a perforated plate with a single cavity.

However this is not the first time perforated plates have been considered for flow control purposes. Maa (1998) utilised the idea of a submillimetre micro-perforated panel to absorb sound. He found the most important parameter in his investigation was the perforate constant, which was proportional to the ratio of the perforation radius to viscous boundary layer thickness. As such the perforate constant was shown to dictate the structure of the micro-perforated panel and its frequency characteristics. The cavities of the micro-perforated panel were separated by a predetermined distance. This value was found to be much larger than the perforation radius, which was determined by the perforate constant. Ultimately, however, the distance between perforations was designed to be small in comparison to the wavelength of the impinging sound wave. This technique was shown to have tremendous potential for wide-band absorption for up to 3 or 4 octaves (Maa, 1998). The similarities between sound waves and the turbulent boundary layer structures have led to the possibility of the micro-perforated device being used for boundary layer control. As an extension to Maa's (1998) work, it has been hypothesised by the author to utilise a micro-perforated device to provide absorption in the near wall region of the boundary layer. Such a device may potentially capture the sweep structures as they move towards the wall and thus modify the bursting cycle which is responsible for the shear stress and viscous drag in the inner wall region. This application will consequently target the fluctuating component of velocity normal to the wall, as shown in Fig. 2.19, an approach which is yet to be reported in the available literature.
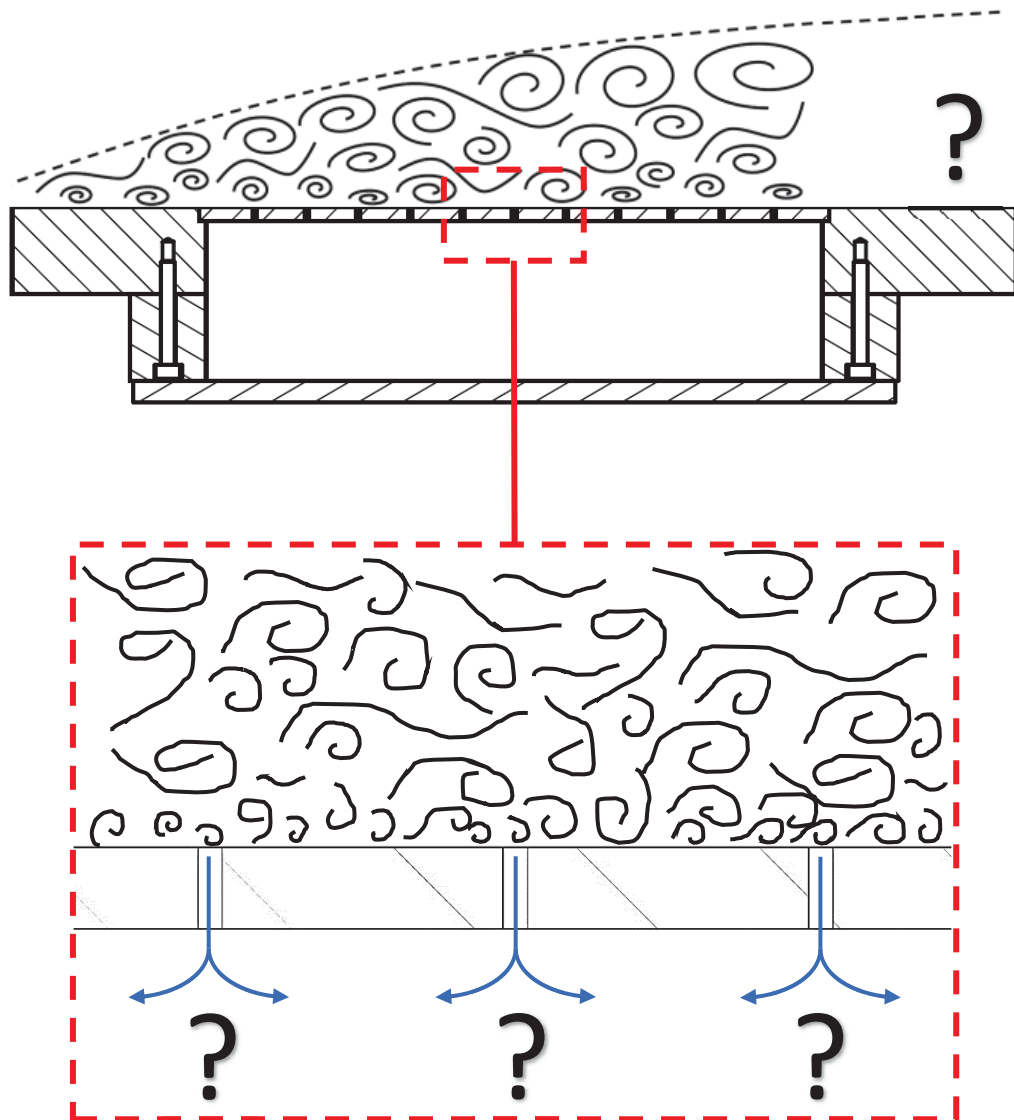
Fig. 2.19 Illustration depicting the proposed mechanism of the attenuation of sweep events.

Choi and Fujisawa (1993) used a two-dimensional square cavity on a flat plate to reduce the skin friction drag and control the turbulent boundary layer. Choi and Fujisawa (1993) showed a net drag reduction of the order of one percent (Fig. 2.20) could be achieved by

using a single cavity, which reduced the skin friction over the cavity and lasted for x/d=100

lengths. The single square cavity was shown to absorb and reorganise the incoming

turbulence and thereby modify the near wall turbulence structure of the boundary layer.

Choi and Fujisawa (1993) also demonstrated a significant reduction in the frequency of

burst like structures near the cavity, which produced mean velocity and turbulence

intensity profiles remarkably similar to the drag-reducing riblet surfaces (Choi, 1989).

While the skin friction reduction was only 1%, this was achieved using only a single square

cavity and as per the recommendations by Lockerby (2001), a distributed control of many

devices would likely increase the achieved reduction.
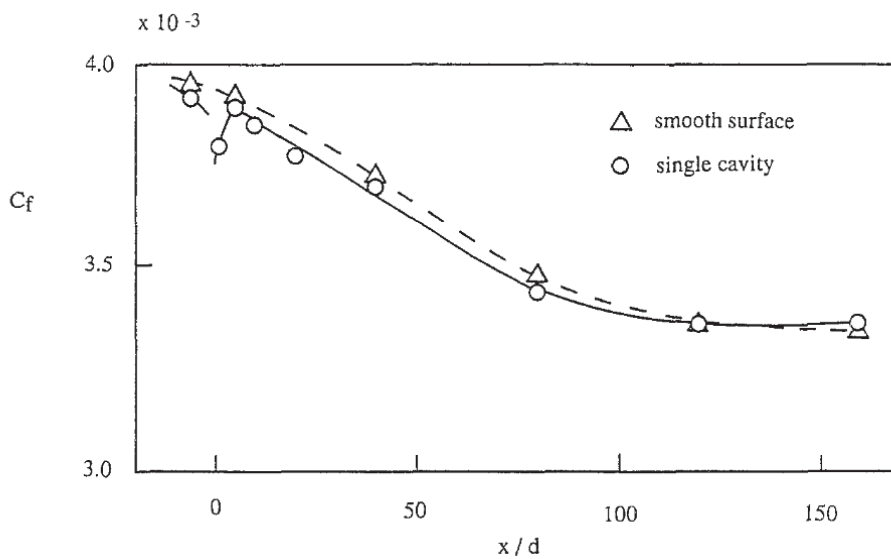
Fig. 2.20 Skin-friction coefficient downstream of a square cavity (Choi and Fujisawa,

1993).

As such the cavity array could provide targeted passive control of sweep events. However

for such a device to be successful in its implementation the cavity array would need to be

designed with a very small orifice diameter to ensure the streamwise and spanwise

velocity profile would remain undisturbed, something not considered by Choi and Fujisawa (1993). This would prevent the shear layer from breaking apart while traversing the small orifice of the cavity, thereby avoiding an adverse pressure gradient and a consequent increase in the disturbances and viscous drag in the boundary layer (Chang et al., 2006). If the spanwise and streamwise velocity are found to be undisturbed, then the only component of velocity which would be affected would be that normal to the wall flow, the direction associated with ejection (positive, away from the wall) and sweep (negative, towards the wall) events. While limited investigations have been made on cavities in turbulent flow, Sarohia (1977) found the critical length of the orifice of a cavity such that the shear layer does not break apart for laminar flow conditions to be $\left(\frac{d}{\delta_0}\right) \times$

$\left(Re_{\delta_0}\right)^{\frac{1}{2}} < 0.29 \times 10^3$, where δ_0 is the shear layer thickness. This was further supported by Chang et al. (2006) who showed the shear layer was more prone to breaking apart in high turbulence flow, but their numerical models illustrated an area close to the leading edge of the cavity where the streamwise velocity profile did not significantly change as the flow traversed the cavity.

For turbulent boundary layer control, the dimensions of the array must be similar to the size of the targeted coherent structures. This was first considered by Maa (1998) when implementing the micro-perforated panel for noise control and was revealed to be dependent on the viscous length scale. As such a similar method can be applied to determine the geometric parameters of a device for attenuation of the turbulent structures. This has been studied extensively by Lockerby (2001), who recommends that the orifice diameter is 40 times the viscous length scale. Blackwelder and Haritonidis (1983) determined the spanwise spacing of the coherent structures are 100 times the

viscous length scale. In addition, literature states that the length of coherent structures can be up to 10 times the spanwise spacing ($x^+ = 1000$) (Blackwelder and Eckelmann, 1979), which gives a very specific design criteria for such a device and developed, in the current work as shown in Fig. 2.21.
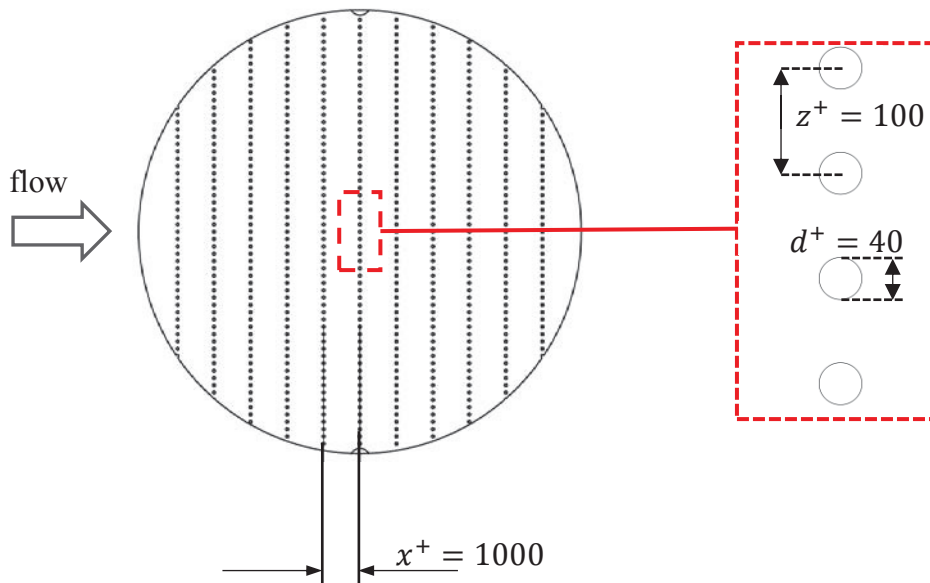
Fig. 2.21 Schematic of the developed design criteria for cavity array dimensions.

Successful implementation of micro-cavities as an alternative method for boundary layer control has yet to be achieved. While the device has shown to be successful in wide-band sound absorption, little effort has been made to develop a similar device for boundary layer control. While the Helmholtz resonator investigated by Ghanadi et al. (2015) and the two-dimensional square cavity investigated by Choi and Fujisawa (1993) have shown promising results, the potential of a cavity array in controlling the boundary layer remains a significant gap in the literature.

2.3 Experimental techniques

To investigate the turbulent boundary layer an appropriate experimental technique must be used. The first experimental technique investigated in this literature review is Particle Image Velocimetry (PIV), a technique employed by many researchers to visualise the flow as well as extract quantitative measurements of complex instantaneous velocity fields (Raffel et al., 2013). This technique has been quite successful in showing the streamwise boundary layer statistics as well as the coherent motions which the cavity array is employed to target (Hutchins et al., 2005; Carlier and Stanislas, 2005; Li et al., 2006) an example of which is shown in Fig. 2.22.
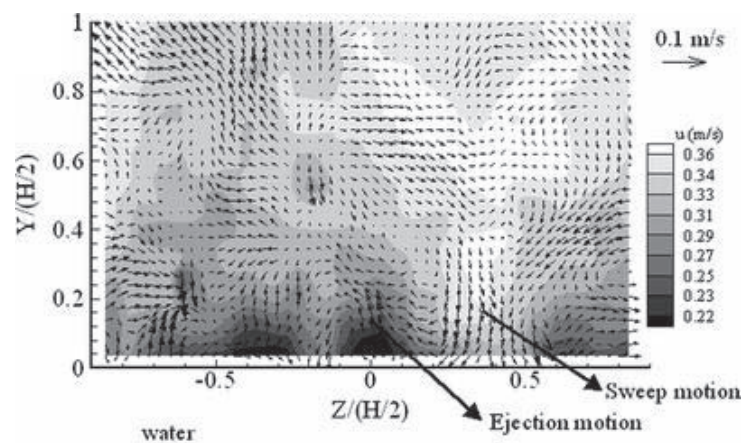
Fig. 2.22 Example of measured velocity contour map in a y-z plane for water to visualise the coherent motions using particle image velocimetry (Li et al., 2006).

The experimental set-up of PIV systems consists of several sub-systems as shown in Fig. 2.23, the most important of which are the tracer particles which are added to the flow to visualise the flow field. These particles are subsequently illuminated in a plane using a laser sheet which are then recorded frame by frame to form a sequence of images. The

PIV recordings are consequently evaluated using a sophisticated post-processing tool to handle the large amount of data collected (Raffel et al., 2013; Leknys et al., 2017).
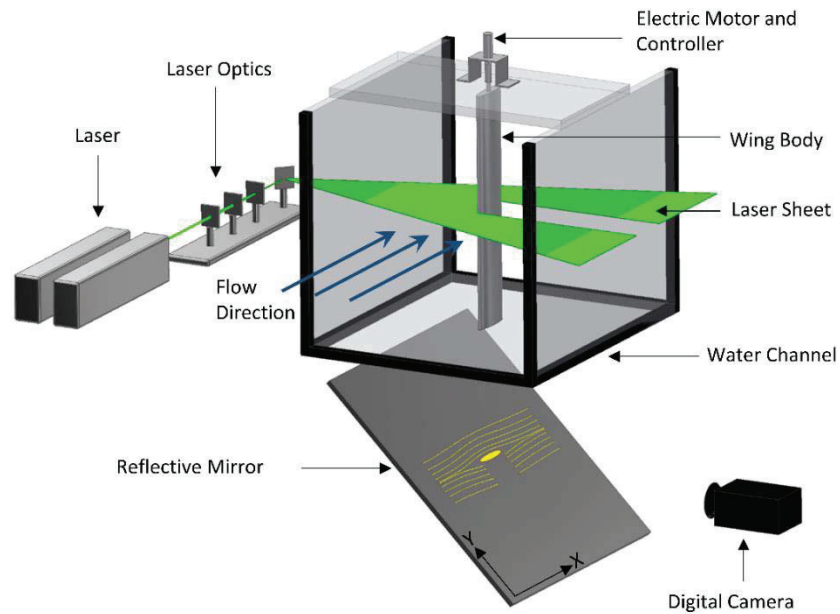
Fig. 2.23 Schematic of a conventional particle image velocimetry setup (Leknys et al., 2018).

To visualise coherent structures a sufficiently small particle size must be selected for operation in wind or water tunnels. While this can be quite simple in water tunnels due to the increased size of the coherent structures arising from the increased viscosity of the fluid, wind tunnels can be quite challenging. In addition, an interrogation window small enough to provide high spatial resolution and an appropriate laser to achieve a sufficient temporal resolution must be considered (Santiago et al., 1998; Adrian and Westerweel, 2011; Raffel et al., 2013; Westerweel et al., 2013) to visualise the small coherent structures must also be present. To visualise the coherent structures at flight scale the PIV interrogation window would be required to be no more than the spanwise spacing ($x^+ = 1000$) (Blackwelder and Eckelmann, 1979), which is estimated to be approximately

1.5mm (Lockerby, 2001). In addition the camera and laser would require a temporal resolution no larger than the average bursting frequency, estimated at $f = 260\text{kHz}$ (Lockerby, 2001).

Another experimental technique used for measuring the boundary layer is the constant temperature hot-wire anemometer. Hot-wire anemometry is a very accurate method for measuring the velocity of the boundary layer as well as the small fluctuations due to the turbulent structures. The hot-wire utilises the principle of electrical resistance through a very thin wire attached to two or more prongs. The voltage across the wire non-linearly increases as the boundary layer passes over the probe and effectively cools down the hot-wire. A faster velocity results in a greater rate of cooling and consequently a larger voltage to maintain the same amount of temperature across the wire. This relationship between voltage and velocity is accurately calibrated using a series of data points, allowing for very quick and precise flow velocity measurements. The basic relation between voltage and velocity for a wire placed normal to the flow was first suggested by King (1914). However, an increased polynomial order has been shown to provide greater accuracy during calibration (Hansen, 2012).

The spatial resolution of the hot-wire has been analysed by many researchers over the years, beginning with Ligrani and Bradshaw (1987a, 1987b), which was followed extensively by many studies at high Reynolds numbers (Hutchins et al., 2009; Monkewitz et al., 2010; Chin et al., 2011; Smits et al., 2011). While the spatial resolution is highly dependent on the characteristic length of the wire between the prongs of the probes, this only becomes a potential problem at very high Reynolds numbers, where the friction velocity is significantly increased causing a reduction in the turbulent structure. The

temporal resolution on the other hand has received less attention (Ashok et al., 2012; Hutchins et al., 2015). The hot-wire was shown to have sufficient temporal resolution at low to mid-range Reynolds numbers, where some dispute into the resolution of the probes at high Reynolds numbers. This issue was extensively reviewed by Hutchins et al. (2015), who developed a method to predict the errors arising from hot-wire measurement responses, which can be corrected at extreme cases.

Due to its versatility and ability to provide highly resolved flow measurements many have used the hot-wire anemometer to measure the near wall region of the boundary layer. This includes: Dróżdż and Elsner (2016) who performed very accurate variable interval time averaging (VITA) analysis of the coherent structure using a hot-wire anemometer; Chandran et al. (2016) to measure two-dimensional energy spectra; Abbassi et al. (2017) who used hot-wire anemometry to produce detailed streamwise velocity and turbulence intensity profiles very close to the wall ($y^+ < 10$); and countless others (de Silva et al., 2017; Chandran et al., 2017; Baidya et al., 2017).

2.4 Conclusion of literature review and research objectives

Numerous techniques for controlling the turbulent boundary layer and reducing the impact of viscous drag have been reviewed and analysed in this chapter. As discussed, the aforementioned techniques have succeeded in achieving their goals in laboratory experiments. Bechert et al. (1997) achieved a 9.9% reduction in skin friction drag using the passive riblets technique, whilst active control methods where capable of achieving a skin friction drag reduction up to 45% (Whalley and Choi, 2014; Mahfoze and Laizet, 2017) using the travelling wave technique. However, the implementation of such techniques in real applications are difficult due to the numerous drawbacks identified. Such drawbacks

include the large energy consumption associated with the active techniques outlined in this chapter, which includes the spanwise travelling wave and the synthetic jet. These devices suffer from the implications of a complicated manufacture and installation into existing aerospace technologies such as aircraft. Passive techniques also suffer several drawbacks. This includes having negligible effect on the boundary layer outside of the optimal operating conditions, where in some cases the boundary layer instabilities are increased. Furthermore the manufacture of such devices becomes extremely difficult at the required scale for flight.

The literature in this chapter shows the need for a device to be implemented to control the turbulent boundary layer. One potential technique for turbulent boundary layer control which has received little attention is the cavity array. The application of a cavity array for such a purpose has yet to be investigated by the fluid mechanics community. As such the gaps of the research are extensive and need to be achieved before such a device can be deemed successful and able to be used in real life applications. This can be completed by first identifying the effect of the key geometric parameters on the ability of the device to attenuate the coherent structures. While the literature review presented in this chapter has resulted in developed design criteria for the cavity array dimensions, they have yet to be validated. Furthermore, there are numerous other key components of the cavity array which remain unknown and form a significant part of the research.

Therefore, in the present thesis, boundary layer control using the micro-cavity array will be considered. The technique will be developed and investigated experimentally within a turbulent boundary layer using hot-wire anemometry. As such this thesis has the following objectives:

- *Characterise the turbulent boundary layer and experimentally investigate how the cavity manipulates the boundary layer.* The application of a cavity array for turbulent boundary layer control has yet to be investigated by the fluid mechanics community. As such a significant gap exists concerning the possibility of using a cavity array for this purpose. Furthermore details of the turbulent boundary layer which are deemed important for turbulent boundary layer control (variable interval time averaging (VITA) sweep profiles, pre-multiplied energy spectrum, etc.) are not readily available in the literature. Consequently characterisation of the boundary layer must also be completed.

- *Experimentally parameterise the configuration and distribution of orifices required to effectively control the boundary layer across the flat plate.* As a significant research gap exists for the cavity array being used for boundary layer control many design variables are unknown for the array. As such the configuration and distribution of the array to achieve boundary layer control must be determined during the project. These values can then be optimised for more efficient control of the turbulent boundary layer.

- *Determine the optimal geometric arrangement for the micro-cavities as a boundary layer control device and identify the method by which which the micro-cavities achieve boundary layer control.* The mechanism for the attenuation of captured sweep events will also be resolved during the project. This task must be completed within the the project as it allows for the optimal geometric arrangement to be developed. Furthermore, it gives a definitive understanding of the mechanism in which the array controls the boundary layer.

2.5 References

Abbassi, MR, Baars, WJ, Hutchins, N, Marusic, I, 2017, *'Skin-friction drag reduction in a high-Reynolds-number turbulent boundary layer via real-time control of large-scale structures', International Journal of Heat and Fluid Flow*, vol. 67, part B, pp. 30-41.

Adrian, RJ, Meinhart, CD, Tomkins, CD, 2000, *'Vortex organisation in the outer region of the turbulent boundary layer', Journal of Fluid Mechanics,* vol. 422, pp. 1-54.

Adrian, RJ, Westerweel, J, 2011, '*Particle Image Velocimetry'*, ed. 1, Cambridge, Cambridge University Press*.*

Ashok, A, Bailey, SCC, Hultmark, M, Smits, AJ, 2015, *'Hot-wire spatial resolution effects in measurements of grid-generated turbulence', Experiments in Fluids, vol. 53, no. 6, pp. 1713-1722.*

Atik, H, Kim, CY, Van Dommelen, LL, Walker, JDA, 2005, *'Boundary-layer separation control on a thin airfoil using local suction', Journal of Fluid Mechanics,* vol. 535, pp. 415-443.

Baidya, R, Philip, J, Hutchins, N, Monty, JP, Marusic, I, 2017, *'Distance-from-the-wall scaling of turbulent motions in wall-bounded flows', Physics of Fluids*, vol. 29, no. 2, pp. 020712.

Bechert, DW, Bruse, M, Hage, W, Van Der Hoeven, JGT, Hoppe G, 1997, '*Experiments on drag reducing surfaces and their optimization with an adjustable geometry', Journal of Fluid Mechanics,* vol. 338, pp. 59-87.

Benschop, HOG, Breugem, WP, 2017*, 'Drag reduction by herringbone riblet texture in direct numerical simulations of turbulent channel flow', Journal of Turbulence,* vol. 18, no. 8, pp. 717-759.

Blackwelder, RF, Kaplan, RE, 1976, '*On the wall structure of the turbulent boundary layer', Journal of Fluid Mechanics,* vol. 76, part 1, pp. 89-112.

Blackwelder, RF, Eckelmann, H, 1979, *'Streamwise vortices associated with the bursting phenomenon', Journal of Fluid Mechanics,* vol. 94, pp. 577-594.

Blackwelder, R, Haritonidis, J, 1983, *'Scaling of the bursting frequency in turbulent boundary layers', Journal of Fluid Mechanics*, vol. 132, no. 1, pp. 87-103.

Carlier, J, Stanislas, M, 2005, *'Experimental study of eddy structures in a turbulent boundary layer using particle image velocimetry', Journal of Fluid Mechanics*, vol. 535, pp. 143-188.

Chandran, D, Baidya, R, Monty, JP, Marusic, I, 2016, *'Measurement of two-dimensional energy spectra in a turbulent boundary layer', 20th Australasian Fluid Mechanics Conference*, Perth, Australia, 5-8 December.

Chandran, D, Baidya, R, Monty, JP, Marusic, I, 2017, *'Two-dimensional energy spectra in high-Reynolds-number turbulent boundary layers', Journal of Fluid Mechanics*, vol. 826, R1.

Chang, K, Constantinescu, G, Park, SO, 2006, *'Analysis of the flow and mass transfer processes for the incompressible flow past an open cavity with a laminar and a fully turbulent incoming boundary layer', Journal of Fluid Mechanics,* vol. 561, pp. 113-145.

Chin CC, Hutchins N, Ooi A, Marusic I, 2011, *'Spatial resolution correction for hot-wire anemometry in wall turbulence', Experiments in Fluids, vol. 50, pp. 1443-1453.*

Choi, H, Moin, P, Kim, J, 1993, *'Direct numerical simulation of turbulent flow over riblets', Journal of Fluid Mechanics*, vol. 255, no. 1, pp. 503-539.

Choi, H, Kim, J, 1994, *'Active turbulence control for drag reduction in wall-bounded flows', Journal of Fluid Mechanics*, vol. 262, pp. 75-110.

Choi, KS, 1987, *'On physical mechanism of turbulent drag reduction using riblets', Transport Phenomena in Turbulent flows*, pp. 185-198, New York, USA.

Choi, KS, 1989, *'Near-wall structure of a turbulent boundary layer with riblets', Journal of Fluid Mechanics,* vol. 208, pp. 417-458.

Choi, KS, Fujisawa, N, 1993, *'Possibility of drag reduction using d-type roughness', Applied Scientific Research*, vol. 50, pp. 315-324.

Choi, KS, Jukes, T, Whalley, R, 2011, '*Turbulent boundary-layer control with plasma actuators', Philosophical Transactions of the Royal Society A,* vol. 369, pp. 1443-1458.

Corino, ER, Brodkey, RS, 1969, *'A visual investigation of the wall region in turbulent flow', Journal of Fluid Mechanics*, vol. 37, part. 1, pp. 1-30.

De Metz, FC, Farabee, TM, 1977, '*Laminar and turbulent shear flow induced cavity resonance', AIAA paper*, AIAA 77- 1293, New York, USA.

de Silva, CM, Krug, D, Lohse, D, Marusic, I 2017, *'Universality of the energy-containing structures in wall-bounded turbulence', Journal of Fluid Mechanics,* vol. 823, pp. 498-510.

Dhanak, MR, Si, C, 1999, *'On reduction of turbulent wall friction through spanwise oscillations', Journal of Fluid Mechanics,* vol. 383, pp. 175-195.

Dróżdż, A, Elsner, W, 2016, '*Analysis of vortices generation process in turbulent boundary subjected to pressure gradient', Progress in Wall Turbulence 2, ERCOFTAC Series*, vol. 23, Springer, Cham.

Du, Y, Karniadakis, GE, 2000, *'Supressing wall turbulence by means of a transverse travelling wave', Science*, vol. 288, pp. 1230–1234.

Du, Y, Symeonidis, Y, Karniadakis, GE, 2002, *'Drag reduction in wall-bounded turbulence via a transverse travelling wave', Journal of Fluid Mechanics*, vol. 457, pp. 1–34.

Falco, R, 1977, *'Coherent motions in the outer region of turbulent boundary layers', Physics of Fluids,* vol. 20, pp. 124-132.

Flynn, KP, Panton, RL, 1990, '*The interaction of Helmholtz resonators in a row when excited by a turbulent boundary layer', Journal of the Acoustical Society of America*, vol. 87, no. 4, pp. 1482-1488.

Gad-el-Hak, M, Blackwelder, RF, 1989, *'Selective suction for controlling bursting events in a boundary layer', AIAA Journal,* vol. 27, no. 3, pp. 308-314.

Gad-el-Hak, M, Bandyopadhyay, P, 1994*, 'Reynolds number effects in wall-bounded turbulent flows', Applied Mechanics Reviews,* vol. 47, pp. 307-365.

Gad-el-Hak, M, 2000, *'Flow Control: passive active and reactive flow management'*, ed. 1, Cambridge, Cambridge University Press.

García-Mayoral, R, Jiménez, J, 2011, *'Drag reduction by riblets'*, *Philosophical Transactions of the Royal Society A: Mathematical, Physical and Engineering Sciences*, vol. 369, pp. 1412-1427.

Ghanadi, F, Arjomandi, M, Cazzolato, BS, Zander, AC, 2013, *'Numerical simulation of grazing flow over a self-excited Helmholtz resonator', Engineering Letters*, vol. 21, no 3, pp. 137-142.

Ghanadi, F, Arjomandi, M, Cazzolato, BS, Zander, AC, 2014a, *'Understanding of the flow behaviour on a Helmholtz resonator excited by grazing flow', International Journal of Computational Fluid Dynamics*, vol. 28, no. 5, pp. 219–231.

Ghanadi, F, Arjomandi, M, Cazzolato, BS, Zander, AC, 2014b, *'Interaction of a flow-excited Helmholtz resonator with a grazing turbulent boundary layer', Experimental Thermal and Fluid Science*, vol. 58, pp. 80-92.

Ghanadi, F, Arjomandi, M, Cazzolato, BS, Zander, AC, 2015*, 'Analysis of the turbulent boundary layer in the vicinity of a self-excited cylindrical Helmholtz resonator', Journal of Turbulence,* vol. 16, pp. 705-728.

Ghanadi, F, 2015, *'Application of a Helmholtz resonator excited by grazing flow for manipulation of a turbulent boundary layer'*, *PhD thesis*, School of Mechanical Engineering, University of Adelaide, Australia.

Greidanus, AJ, Delfos, R, Tokgoz, S, Westerweel, J, 2017, *'Turbulent Taylor–Couette flow over riblets: drag reduction and the effect of bulk fluid rotation', Experiments in Fluids, vol. 56, pp. 107.*

Hansen, KL, 2012, *'Effect of leading edge tubercles on airfoil performance'*, *PhD thesis*, School of Mechanical Engineering, University of Adelaide, Australia.

Head, MR, Bandyopadhyay, P, 1981, '*New aspects of turbulent boundary-layer structure', Journal of Fluid Mechanics*, vol. 107, pp. 297-338.

Hutchins, N, Hambleton, WT, Marusic, I, 2005, '*Inclined cross-stream stereo particle image velocimetry measurements in turbulent boundary layers', Journal of Fluid Mechanics*, vol. 541, pp. 21-54.

Hutchins N, Nickels TB, Marusic I, Chong MS, 2009, '*Hot-wire spatial resolution issues in wall-bounded turbulence', Journal of Fluid Mechanics*, vol. 635, pp. 103-136.

Hutchins, N, Monty, JP, Hultmark, M, Smits, AJ, 2015, '*A direct measure of the frequency response of hot-wire anemometers: temporal resolution issues in wall-bounded turbulence', Experiments in Fluids, vol. 56, pp. 18.*

Jacobs, JW, James, RD, Glezer, A, Ratliff, CT, 1993, '*Turbulent jets induced by surface actuators', AIAA 2nd Shear Flow Conference,* Orlando, FL, USA, 6 – 9 July.

James, RD, Jacobs, JW, Glezer, A, 1994, '*Experimental investigation of a turbulent jet produced by an oscillating surface actuator', Appl. Mech*, vol. 47, no. 6, part. 2, pp. 127‑131.

Jukes, TN, Choi, KS, Johnson, GA, Scott, SJ, 2006, '*Turbulent drag reduction by surface plasma through spanwise flow oscillation', 3rd AIAA Flow Contorl Conference*, Paper No. AIAA-2006-3693, California, USA.

Kang, YD, Choi, KS, Chun, HH, 2008, '*Direct intervention of hairpin structures for turbulent boundary-layer control', Physics of Fluids*, vol. 20, no. 10, pp. 1-13.

Kim, HT, Kline, SJ, Reynolds, WC, 1971, '*The production of turbulence near a smooth wall in a turbulent boundary layer', Journal of Fluid Mechanics,* vol. 50, part. 1, pp. 133-160.

King, LV, 1914, '*On the convection of heat from small cylinders in a stream of fluid: Determination of the convection constants of small platinum wires with application to hot-wire anemometry', Philosophical Transactions of the Royal Society A: Mathematical, Physical and Engineering Sciences*, vol. 214, pp. 373–432.

Kline, SJ, Reynolds, WC, Schraub, FA, Runstadler, PW, 1967, '*The structure of turbulent boundary layers', Journal of Fluid Mechanics,* vol. 30, part 4, pp. 741-773.

Li, YP, Wong, CW, Li, YZ, Zhang, BF, Zhou, Y, 2014, *'Drag reduction of a turbulent boundary layer using plasma actuators ', 19th Australasian Fluid Mechanics Conference*, Melbourne, Australia, 8-11 December.

Ligrani, PM, Bradshaw, P, 1987a, *'Subminiature hot-wire sensors: Development and Use', Journal of Physics E: Scientific Instruments*, vol. 20, no. 3, pp. 323-332.

Ligrani, PM, Bradshaw, P, 1987b, *'Spatial resolution and measurement of turbulence in the viscous sublayer using subminiature hot-wire probes', Experiments in Fluids*, vol. 5, no. 6, pp. 407-417.

Leknys, RR, Arjomandi, M, Kelso, RM, Birzer, CH, 2017, *'Dynamic stall flow structure and forces on symmetrical airfoils at high angles of attack and rotation rates', Proceedings of the Institution of Mechanical Engineers, Part G: Journal of Aerospace Engineering,* vol. 232, no. 6, pp. 1171-1185.

Leknys, RR, Arjomandi, M, Kelso, RM, Birzer, CH, 2018, *'Dynamic Stall Flow Structure and Forces on Symmetrical Airfoils at High Angles of Attack and Rotation Rates', accepted by ASME Journal of Fluids Engineering.*

Li, FC, Kawaguchi, Y, Hishida, K, Oshima, M, 2006, *'Investigation of turbulence structures in a drag-reduced turbulent channel flow with surfactant additive by stereoscopic particle image velocimetry', Experiments in Fluids,* vol. 40, no. 2, pp. 218-230.

Lockerby, DA, 2001, *'Numerical simulation of boundary-layer control using MEMS actuation', PhD thesis*, The University of Warwick, England, UK.

Lockerby, DA, Carpenter, PW, Davies, C, 2005, *'Control of sublayer streaks using microjet actuators', AIAA Journal,* vol. 43, no. 9, pp. 1878-1886.

Lu, SS, Willmarth, WW, 1973, *'Measurements of the structure of the Reynolds stress in a turbulent boundary layer', Journal of Fluid Mechanics,* vol. 60, pp. 481-511.

Luchini, P, Manzo, F, Pozzi, A, 1991, *'Resistance of a grooved surface to parallel flow and cross flow', Journal of Fluid Mechanics,* vol. 228, pp. 87-109.

Maa, DY, 1998, *'Potential of microperforated panel absorber', Journal of the Acoustical Society of America*, vol. 104, no. 5, pp. 2861- 2866.

Mahfoze, O, Laizet, S, 2017, *'Skin-friction drag reduction in a channel flow with streamwise-aligned plasma actuators', International Journal of Heat and Fluid Flow*, vol. 66, pp. 83-94.

Monkewitz PA, Duncan RD, Nagib HM, 2010, *'Correcting hot-wire measurements of stream-wise turbulence intensity in boundary layers', Physics of Fluids*, vol. 22, pp. 091701.

Nelson, PA, Halliwell, NA, Doak, PE, 1981, '*Fluid dynamics of a flow excited resonance, part I: Experiment', Journal of Sound and Vibration*, vol. 78, no. 1, pp. 15-38.

Nelson, PA, Halliwell, NA, Doak, PE, 1981, '*Fluid dynamics of a flow excited resonance, part* II: Flow acoustic interaction', *Journal of Sound and Vibration*, vol. 91, no. 3, pp. 375-402.

Offen, GR, Kline, SJ, 1975, *'A proposed model of the bursting process in turbulent boundary layers', Journal of Fluid Mechanics*, vol. 70, part. 2, pp. 209-228.

Pang, J, Choi, KS, 2004, '*Turbulent drag reduction by Lorentz force oscillation', Physics of Fluids*, vol. 16, pp. 35-38.

Perry, AE, Marusic, I, 1995, *'A wall-wake model for the turbulence structure of boundary layers. Part 1. Extension of the attached eddy hypothesis', Journal of Fluid Mechanics,* vol. 298, pp. 361-388.

Quadrio, M, Ricco, P, 2004, *'Critical assessment of turbulent drag reduction through spanwise wall oscillations', Journal of Fluid Mechanics*, vol. 521, part. 2, pp. 251-271.

Raffel, M, Eillert, CE, Wereley, S, Kompenhans, J, 2007, *'Particle Image Velocimetry: A Practical Guide',* ed. 2, Springer-Verlag Berlin Heidelberg.

Rathnasingham, R, Breuer, K, 2003, '*Active control of turbulent boundary layers', Journal of Fluid Mechanics*, vol. 495, pp. 209–233.

Robinson, SK, 1991, *'Coherent motions in the turbulent boundary layer', Annual Review of Fluid Mechanics*, vol. 23, pp. 601-639.

Santiago, JG, Wereley, ST, Meinhart, CD, Beebe, DJ, Adrian, RJ, 1998, *'A particle image velocimetry system for microfluidics', Experiments in Fluids,* vol. 25, no. 4, pp. 316-319.

Sarohia, V, 1977, *'Experimental investigation of oscillations in flows over shallow cavities', AIAA Journal,* vol. 15, no. 7, pp. 984-991.

Segawa, T, Mizunuma, H, Murakami, K, Yoshida, H, 2007, *'Turbulent drag reduction by means of alternating suction and blowing jets', Fluid Dynamics Research*, vol. 39, no. 7, pp. 552-568.

Smith, BL, Glezer, A, 1998, *'The formation and evolution of synthetic jets', Physics of Fluids*, vol. 10, pp. 2281–2297.

Smits AJ, Monty JP, Hultmark M, Bailey SC, Hutchins N, Marusic I, 2011, *'Spatial resolution correction for wall-bounded turbulence measurements'*, *Journal of Fluid Mechanics*, vol. 676, pp. 41-53.

Spinosa, E, Zhong, S, 2017, *'Reduction of Skin Friction Drag in a Turbulent Boundary Layer Using Circular Synthetic Jets', 55th American Institute of Aeronautics and Astronautics Aerospace Sciences Meeting*, Grapevine, Texas, USA, 9-13 January.

Tardu, S, Truong, T, Tanguay, B, 1993, *'Bursting and structure of the turbulence in an internal flow manipulated by riblets', Applied Scientific Research*, vol. 50, no. 3, pp. 189-213.

Theodorsen, T, 1952, '*Mechanisms of turbulence', 2nd Mid-Western Conference of Fluid Dynamics*, Ohio State University, Columbus, Ohio, USA, March 17-19.

Wallace, JM, Eckelmann, H, Brodkey, RS, 1972, *'The wall region in turbulent shear flow', Journal of Fluid Mechanics*, vol. 54, pp. 39-48.

Walsh, MJ, 1983, *'Riblets as a viscous drag reduction technique', AIAA Journal,* vol. 21, no. 4, pp. 485-486.

Walsh, MJ, Lindemann, AM, 1984, '*Optimization and application of riblets for turbulent drag reduction', AIAA 22nd Aerospace Science Meeting*, Reno, Nevada, USA, January 9-12.

Weier, T, Fey, U, Gerbeth, G, Mutschke, G, Lielausis, O, Platacis, E, 2001, *'Boundary layer control by means of wall parallel Lorentz Forces ', Magnetohydrodynamics*, vol. 37, no. 1-2, pp. 177-186.

Westerweel, J, Elsinga, GE, Adrian, RJ, 2013, *'Particle image velocimetry for complex and turbulent flows', Annual Review of Fluid Mechanics*, vol. 45, pp. 409-436.

Whalley, RD, 2011, *'Turbulent boundary-layer control with DBD plasma actuators using spanwise travelling-wave technique', PhD thesis,* The University of Nottingham, England, UK.

Whalley, RD, Choi, KS, 2014, *'Turbulent boundary-layer control with plasma spanwise travelling waves', Physics of Fluids,* vol. 55, pp. 1796.

Wong, CW, Zhou, Y, Li, Y, Li, Y, 2015, *'Active drag reduction in a turbulent boundary layer based on plasma-actuator-generated streamwise vortices', 9th International Symposium on Turbulence and Shear Flow Phenomena*, Melbourne, Vic, Australia, 30-3 June/ July.

Chapter 3

Characterisation of the turbulent boundary layer

3.1   Paper 1: The application of different tripping techniques to determine the characteristics of the turbulent boundary layer over a flat plate

An understanding of the turbulent boundary layer is an essential requirement in the process of controlling the structures that exist in the near wall region. The first task of which is to determine where transition into a turbulent boundary layer occurs and identify the turbulence statistics of an uncontrolled boundary layer. While previous literature has quantified the boundary layer statistics, a more detailed evaluation is required, as a gap exists when considering the effect of induced turbulence on the sweep events and other high order statistics of the boundary layer. Consequently this chapter presents a thorough analysis of several tripping techniques used to induce a naturally fully developed turbulent boundary layer and its effect on the boundary layer statistics. Such techniques investigated included circular rods, steps and different types of sandpaper. During this analysis the hot-wire anemometry technique was used to measure experimentally the velocity over a flat plate in a wind tunnel at a variety of locations and Reynolds numbers.

The results successfully demonstrated that to produce a natural turbulent boundary layer using a 2D protuberance, the height of the trip must be less than the undisturbed boundary layer thickness. Using such a trip was shown to reduce the development length of the turbulent boundary layer by approximately 50%, which held true for all Reynolds numbers investigated in this chapter ($1.2 \times 10^5 < Re_x < 1.5 \times 10^6$). A larger trip was shown to cause a large regeneration region far away from the trip or a large separation region close to the leading edge of the trip. This resulted in elevated levels of turbulence (turbulence intensity, sweep intensity and pre-multiplied energy spectrum) and should thus be avoided when performing experiments requiring a natural turbulent boundary layer.

The findings from this chapter are applied in all future experimental evaluations in this thesis. The subsequent chapters utilise the results to ensure a fully turbulent boundary layer during testing to evaluate the effect of the micro-cavity array on the sweep events in the near wall region of the boundary layer.

This chapter has been published as:

Silvestri, A, Ghanadi, F, Arjomandi, M, Cazzolato, BS, Zander, AC, 2017, *'The application of different tripping techniques to determine the characteristics of the turbulent boundary layer over a flat plate', ASME Journal of Fluid Engineering, vol. 140, no. 1, pp. 011204.*

Statement of Authorship

Title of Paper	The application of different tripping techniques to determine the characteristics of the turbulent boundary layer over a flat plate
Publication Status	☑ Published ☐ Accepted for Publication ☐ Submitted for Publication ☐ Unpublished and Unsubmitted work written in manuscript style
Publication Details	Silvestri, A, Ghanadi, F, Arjomandi, M, Cazzolato, BS, Zander, AC, 2017, 'The application of different tripping techniques to determine the characteristics of the turbulent boundary layer over a flat plate', ASME Journal of Fluid Engineering, vol. 140, no. 1, pp. 011204.

Principal Author

Name of Principal Author (Candidate)	Anton Silvestri		
Contribution to the Paper	Performed data analysis and interpretation, wrote manuscript and acted as corresponding author.		
Overall percentage (%)	70		
Certification:	This paper reports on original research I conducted during the period of my Higher Degree by Research candidature and is not subject to any obligations or contractual agreements with a third party that would constrain its inclusion in this thesis. I am the primary author of this paper.		
Signature		Date	15/06/18

Co-Author Contributions

Name of Co-Author	Farzin Ghanadi		
Contribution to the Paper	Supervised the development of the research and contributed in academic discussion and the review process of submitted manuscripts.		
Signature		Date	15/06/18

Name of Co-Author	Maziar Arjomandi		
Contribution to the Paper	Supervised the development of the research and contributed in academic discussion and the review process of submitted manuscripts.		
Signature		Date	15/06/18

Name of Co-Author	Benjamin Cazzolato		
Contribution to the Paper	Supervised the development of the research and contributed in academic discussion and the review process of submitted manuscripts.		
Signature		Date	15/06/18

Name of Co-Author	Anthony Zander		
Contribution to the Paper	Supervised the development of the research and contributed in academic discussion and the review process of submitted manuscripts.		
Signature		Date	15/06/18

Anton Silvestri
School of Mechanical Engineering,
University of Adelaide,
Adelaide, South Australia 5005, Australia
e-mail: anton.silvestri@adelaide.edu.au

Farzin Ghanadi
School of Mechanical Engineering,
University of Adelaide,
Adelaide, South Australia 5005, Australia
e-mail: farzin.ghanadi@adelaide.edu.au

Maziar Arjomandi
School of Mechanical Engineering,
University of Adelaide,
Adelaide, South Australia 5005, Australia
e-mail: maziar.arjomandi@adelaide.edu.au

Benjamin Cazzolato
School of Mechanical Engineering,
University of Adelaide,
Adelaide, South Australia 5005, Australia
e-mail: benjamin.cazzolato@adelaide.edu.au

Anthony Zander
School of Mechanical Engineering,
University of Adelaide,
Adelaide, South Australia 5005, Australia
e-mail: anthony.zander@adelaide.edu.au

The Application of Different Tripping Techniques to Determine the Characteristics of the Turbulent Boundary Layer Over a Flat Plate

In the present study, the optimal two-dimensional (2D) tripping technique for inducing a naturally fully developed turbulent boundary layer in wind tunnels has been investigated. Various tripping techniques were tested, including wires of different diameters and changes in roughness. Experimental measurements were taken on a flat plate in a wind tunnel at a number of locations along the flat plate and at a variety of flow speeds using hot-wire anemometry to measure the boundary layer resulting from each tripping method. The results have demonstrated that to produce a natural turbulent boundary layer using a 2D protuberance, the height of the trip must be less than the undisturbed boundary layer thickness. Using such a trip was shown to reduce the development length of the turbulent boundary layer by approximately 50%. This was shown to hold true for all Reynolds numbers investigated ($Re_x = 1.2 \times 10^5 - 1.5 \times 10^6$). The present study provides an insight into the effect of the investigated trip techniques on the induced transition of a laminar boundary layer into turbulence. [DOI: 10.1115/1.4037675]

1 Introduction

The structure of any turbulent flow dictates the production, transport, and dissipation of turbulent kinetic energy. In a fully developed turbulent boundary layer, turbulence production is mainly concentrated within the near wall region. Consequently, this region is known to be the greatest contributor to the Reynolds stress experienced in the boundary layer [1]. Wind tunnel testing is extensively used for experimental testing, and due to different constraints such as the tunnel or model size and the characteristics of the flow, the turbulence production is not achieved properly in some cases. It has been shown that when the laminar boundary layer is subjected to a local disturbance, the flow will respond by transitioning into turbulence further upstream than the natural location [2], thus a smaller test section can be used. Therefore, a wide range of passive and active tripping techniques has been used by researchers to stimulate the flow into a fully developed turbulent regime [3–6]. The motivation of this study is to explore the characteristics of various tripping techniques to identify the optimal technique for inducing transition in the boundary layer.

The most commonly used techniques have been passive in nature and two-dimensional (2D), due to their simplicity and ease of implementation, and consequently form the scope of this investigation. The simplest means of inducing turbulence is to use roughness strips to artificially induce the transition of turbulence. This technique uses small distributed roughness elements to promote transition and the growth of Tollmien–Schlichting waves [7], which are known to be a main factor in the transition of the

laminar boundary layer into turbulence. This technique can be applied to the model in different ways. One such method is to apply a premade sample strip very close to the leading edge of the model [8,9] to promote the growth of the Tollmien–Schlichting waves earlier than occurring naturally. It has been shown in previous experiments that the level of turbulence can be significantly increased due to the large turbulent energy production near the roughness strip [10]. Locations well downstream of the change in roughness were shown to have reached a second self-preserving state. Roughness strips have been shown to produce fully developed turbulent boundary layers at lower Reynolds numbers quite effectively (as low as $Re_\theta = 465$). However, as demonstrated by Putrell et al. [11], this has been shown to be highly dependent on the roughness size and its relationship with the boundary layer.

In contrast to the distribution of roughness particles, a single roughness element is also frequently used. The roughness element could be in the form of different geometric shapes including circular or rectangular cross section wires. Boundary layer tripping using this technique can be divided into two subcategories: 2D protuberances (wires and steps) and three-dimensional (3D) protuberances (ball bearings and trip dots). Research into two-dimensional protuberances and their interaction with the boundary layer [12,13] have focused on the difference between straight edge protuberances, which are steps in cross flow, and smooth edge protuberances, which are circular cross section wires in cross flow [9,13]. With both of these techniques, a closed vortex is formed at the trailing edge of the protuberance [2,13]. The straight edge protuberance (step) results were shown to be independent of the freestream velocity and the vortex formed at all flow speeds. The smooth surface (circular wire), on the other hand, was able to produce a closed vortex downstream only if a critical velocity was met. The performance of smooth edge protuberances also has a
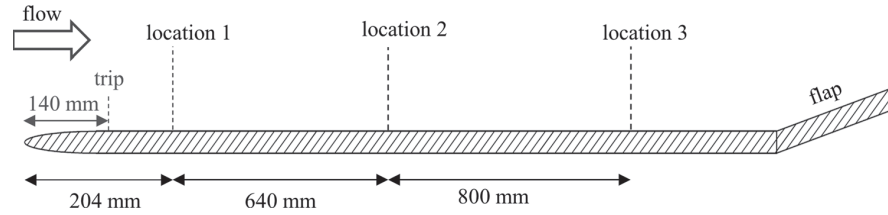
Fig. 1 Schematic of the experimental arrangement

strong dependence on the diameter of the wire being used. In subsonic flow, the transition location moves upstream to be very close to the trip wire itself. A minimum distance of ten wire diameters downstream of the trip is required to ensure fully turbulent flow has been achieved [14].

These particular methods have been shown to be quite effective at inducing turbulence at both low and high Reynolds numbers [9,15,16]. However, it has the drawback of negatively affecting the boundary layer if the size of the trip has been incorrectly selected [17]. Several studies investigated tripping using 2D protuberances [9,15,18,19]. Elsinga and Westerweel [19] investigated a zigzag boundary layer trip using particle image velocimetry. While this method is clearly unique in comparison to the standard wire trip commonly used, its roughness height was shown to be reduced in comparison to the standard trips discussed previously. However, no discussion was given to the development and recovery length.

Recent research on 3D protuberances has also demonstrated their ability to act as a successful mechanism [20–22]. An analytical model was developed to demonstrate the effect of 3D protuberances on the boundary layer [23] and was studied more recently by Bernardini et al. [20]. A hemisphere was used for the trip model in this investigation and the 3D structure had a vorticity concentration that would occur near the stagnation point, causing a streamwise component of vorticity to be induced. It was documented that the difference between the results for 2D and 3D protuberances is the vorticity component of the fluid, which only occurs in the direction normal to the wall and only changes due to viscous diffusion in the 2D case.

Consequently in the current study, the main focus was to investigate easily accessible tripping techniques including wires of different diameters and changes in roughness using different grades of sandpaper. While 3D protuberances have been shown to be successful in inducing transition, the authors recognize such tripping techniques are difficult to access in comparison to 2D protrusions, such as sandpaper and rods. Consequently, they fall outside the scope of the research presented. Each tripping technique was investigated at a variety of Reynolds numbers and multiple locations downstream from the initial trip location. The purpose of the present research is to evaluate different techniques and identify which technique is optimal in inducing turbulence representative of a naturally fully developed boundary layer. Optimal in this investigation is defined as the shortest development length to reach a naturally fully developed boundary layer. In Secs. 3–9, the characteristics of the tripping mechanisms will be discussed and detail into the experimental method will be provided. This is followed by a discussion on the results to provide an insight into the capabilities of different tripping mechanisms and determine which technique was optimal at inducing turbulence.

2 Experimental Procedure

All the experiments were performed in the "KC" closed-return type wind tunnel located at the University of Adelaide, Adelaide, Australia, which can be operated up to a maximum velocity of 30 m/s with low level turbulence intensity, approximately 0.53%. The test section is rectangular with a cross section of

500 mm × 500 mm and 2000 mm in length. A horizontal 2000 mm long flat plate, as shown in Fig. 1, was positioned inside the tunnel such that it spanned the whole width of the test section. The finite thickness of the flat plate leads to bluff body separation effects, therefore to minimize any possible flow separation, a super-elliptical leading edge of a nominal major radius of 114 mm was attached to the flat plate. A 125 mm long circulation flap was also mounted downstream of the plate to minimize any circulation developed over the plate and to ensure that the stagnation point is on the measurement side of the plate. The flap could also be adjusted as appropriate to balance the pressure gradient along the working section, which was selected to be a zero pressure gradient in this investigation. This was done to eliminate the effects of favorable and adverse pressure gradients, as discussed by Shin and Song [24,25]. The velocity profile of the wind tunnel is assumed to be 2D due to the zero pressure gradient and low turbulence intensity. The boundary layer investigated in the study was tripped by a variety of different mechanisms placed near the leading edge.

This research focuses on the near wall regions, as approximately half of the total turbulence production occurs within this small region. Therefore, a hot-wire anemometer was used downstream of the boundary layer trips to characterize the changes in the turbulent structures within the boundary layer regions. This was done at three locations downstream from the initial trip at two different Reynolds numbers. The streamwise velocity measurements were made with a TSI IFA 300 CTA system, using a single platinum-plated tungsten wire of 5 μm in diameter and 1.25 mm in length, which was operated with an over-heat ratio of 1.8 and an operating temperature around 230 °C, which provided sufficient sensitivity to measure the velocity fluctuations with minimum thermal effects. The repeatability of each measurement was also verified three times and the data were sampled at 10 kHz for 10 s. This equates to a viscous-scaled sample interval of $1.4 < \Delta t^+ < 2.4$, which exceeds the minimum timescale for energetic turbulent fluctuations ($t^+ \approx 3$) [26].

3 Characteristics of Tripping Techniques

To investigate the effect that tripping has on inducing turbulence in the boundary later, a total of five different methods have been considered at two freestream velocities, namely, 9.3 m/s and 13.5 m/s, as shown in Table 1. Two wires with circular cross

Table 1 Summary of the tripping methods used

Type of trip	Dimensions/roughness grit
3 mm diameter rod	3mm 3 mm
5 mm diameter rod	5mm 5 mm
5 mm step	5mm 5 mm
Fine sandpaper	58.5 μm
Rough sandpaper	269 μm

Paper 1: The application of different tripping techniques to determine the characteristics of the turbulent boundary layer over a flat plate

section and one rectangular wire acted as a step in the flow. Wires of different diameters and cross sections were selected initially for investigation, as the effect of the wire dimension was believed to be a key parameter in determining the success of this trip technique. The selected wires ranged between 3 mm and 5 mm in size to investigate the effect of trips, with both larger and smaller sizes than the undisturbed boundary layer thickness. An investigation into the effect of a change of roughness on the boundary layer also followed. This was achieved by using strips of sandpaper placed near the leading edge. The two sandpapers selected had roughness grits of 58.5 μm and 269 μm, respectively, and were of equal width (60 mm).

4 Hot-Wire Measurements

A single hot-wire probe was used throughout the experiments to determine the velocity in the streamwise direction. The hot-wire probe was initially calibrated using a Baratron pressure sensor, which has high accuracy when measuring the mean flow (0.5%). As the relationship between the hot-wire's voltage and the flow's velocity is not linear, this step was of significant importance and a total of 20 wind tunnel velocities ranging from 0 m/s to 25 m/s were selected. A polynomial curve fit was then applied to the calibration data, where a fifth-order polynomial fit was shown to produce the greatest curve fit. This calibration was performed multiple times over the testing period to improve the accuracy of the results and account for changes in the ambient temperature ($\pm 1.5 \,^\circ$C).

Voltage measurements were then converted into velocity using the coefficients determined from the fifth-order polynomial fit found during the calibration of the hot-wire probe. Testing was conducted over a period of 3 days, and during this time, the ambient temperature of the wind tunnel varied by $\pm 1.5 \,^\circ$C from the average ambient temperature. This was shown to have a small error on the freestream velocity, where the maximum fluctuation in freestream velocity was found to be 2.8% at the highest Reynolds number tested. Velocity data were taken at a single streamwise/spanwise location. The spanwise location of the hot-wire probe during this investigation was the midpoint of the wind tunnel and a total of 48 measurements were taken to accurately quantify the boundary layer. The boundary layer probe used had a slight offset between the bottom of the probe and the location of the hot-wire. This was used to ensure that the hot-wire did not touch the wall and damage the sensitive sensor. This distance was known (.13 mm) and was used to accurately determine the distance the probe was from the wall at all times.

To ensure that the measurements recorded by the hot-wire anemometry system were accurate, a comparison with previous published data has been conducted. As shown in Fig. 2(*a*), the nondimensional mean velocity profile at $Re_\theta = 1927$, location 2, has been compared against the results obtained by Marusic and Kunkel [27] and Schlatter and Orlu [28], where the Reynolds number based on momentum thickness is given by $Re_\theta = u\theta/\nu$. A maximum error of 5% occurs at the points closest to the flat plate ($y^+ < 30$); however, this small variation is deemed negligible as the key focus of this paper is the logarithmic region of the boundary layer ($30 < y^+ < 200$), where a maximum error of approximately 2.5% is present. While the Reynolds numbers investigated by Marusic and Kunkel [27] and Schlatter and Orlu [28], $Re_\theta = 2220$ and $Re_\theta = 3064$, respectively, are not the same as the values examined in this paper, the logarithmic and viscous subregions are shown to be comparable irrespective of Reynolds number as discussed by Marusic and Hutchins [29]. Furthermore, if the thickness of the boundary layer at location 1 is investigated, a clear laminar profile is found. This boundary layer is shown to have a thickness of 3.1 mm (Fig. 2(*b*)), while the Blassius solution for an ideal laminar boundary layer has a 3 mm idealized boundary layer thickness. Consequently, the authors are extremely confident of the initial boundary layer being a laminar profile. The boundary layer thickness was also found to be between 2 mm
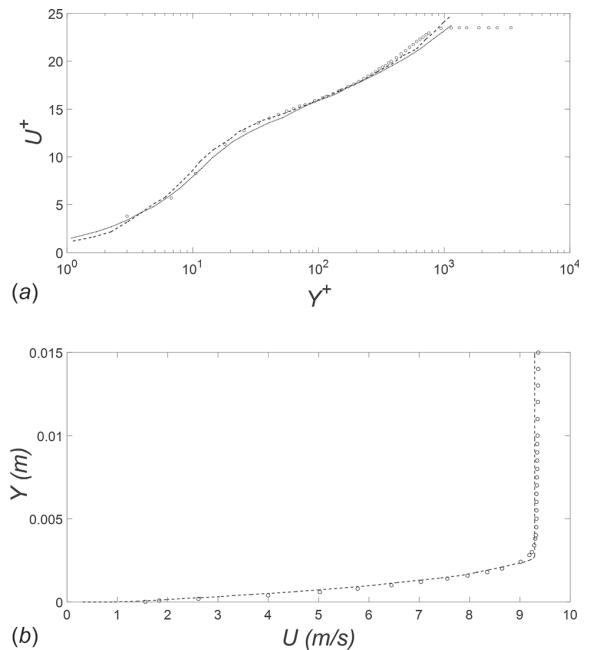

(*a*)

(*b*)

Fig. 2 (*a*) Error analysis of the turbulent velocity profile of the boundary layer at $Re_\theta = 1927$: (o) experimental results, (..) results obtained by Marusic and Kunkel [27], and (--) results obtained by Schlatter and Orlu [28] and (*b*) error analysis of the laminar velocity profile of the boundary layer at $Re_\theta = 1927$: (o) experimental data and (--) Blassius solution

and 2.4 mm at the trip location for each Reynolds number investigated.

The data collected from the hot-wire probes were also nondimensionlized for comparison with the no trip boundary layers investigated. This was done by using the friction velocity (u_τ) of each boundary layer (tripped and untripped cases), which was calculated using the log law expression defined by Clauser [30] as, $U^+ = 5.6 \, \log_{10} y^+ + 4.9$. This was done via an iterative process, which used a varying value for the friction velocity to curve fit the logarithmic region of the experimental data with the log law expression defined by Clauser [30] and demonstrated by Kendall and Koochesfahani [31]. This method was performed in favor of using the near-wall gradient due to the increased number of hot-wire measurements obtained in the logarithmic region. The results were shown to provide accurate estimates with a maximum error of 2%. This was repeated for all the boundary layers investigated resulting in a unique friction velocity value for each boundary layer investigated.

5 Characteristics of the Turbulent Boundary Layer

The investigation commenced by initially characterizing the streamwise and turbulence intensity profiles of the boundary layer. These two particular statistics were initially considered due to their significance and simple indication of whether a boundary layer was turbulent. The mean velocity profiles and turbulence intensities at location 1 for two different Reynolds numbers of $Re_x = 1.2 \times 10^5$ ($U_\infty = 9.3$ m/s) and $Re_x = 1.8 \times 10^5$ ($U_\infty = 13.5$ m/s) were investigated. It is important to note that both these Reynolds number are below the critical transition Reynolds number ($Re_x = 3 \times 10^5$). The results for $Re_x = 1.2 \times 10^5$ have been plotted against a fully naturally developed turbulent boundary layer by Marusic and Kunkel [27] and Schlatter and Orlu [28] for comparison in Fig. 3. The data from each location and flow speed have been grouped together by using a Reynolds number based on development length to associate at
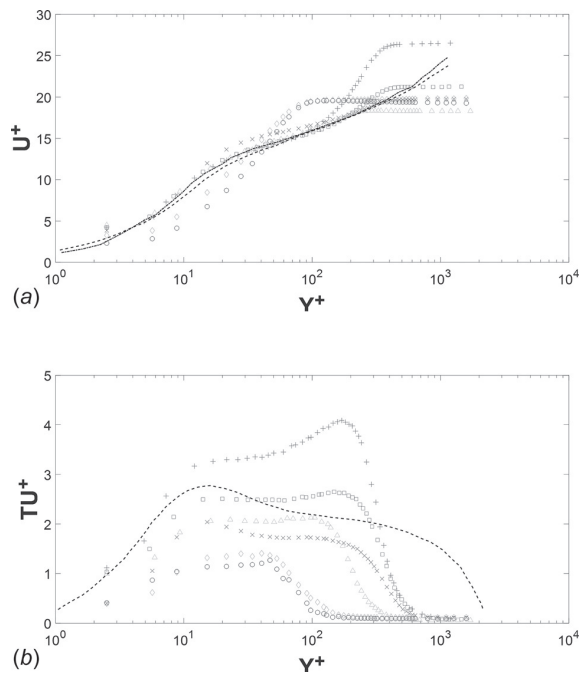
Fig. 3 (a) Mean velocity (U^+) profile and (b) turbulence intensity (TU^+) profile at $Re_x = 1.2 \times 10^5$, location 1: (o) no trip, (+) 5 mm trip, (x) 3 mm trip, ($\diamond$) fine sandpaper, ($\square$) 5 mm step, ($\triangle$) rough sandpaper, (--) Marusic and Kunkel [27] data, and (-.-) Schlatter and Orlu [28] data

Fig. 4 Mean velocity (U^+) profile at location 2 for (a) $Re_x = 5.3 \times 10^5$ and (b) $Re_x = 7.5 \times 10^5$: (o) no trip, (+) 5 mm trip, (x) 3 mm trip, ($\diamond$) Fine sandpaper, ($\square$) 5 mm step, ($\triangle$) rough sandpaper, (--) Marusic and Kunkel [27] data, and (-.-) Schlatter and Orlu [28] data

what location and speed the boundary layer was measured. This value, however, was not used for nondimensionalization. As can be seen in Fig. 3(a), the results obtained do not match the published data. The boundary layer thickness was shown to be equal to that of a laminar boundary layer for the no trip and fine sandpaper ($\delta = 3.1$ mm) as discussed previously, while the other tripping techniques (5 mm diameter rod and 5 mm step) increased the thickness of the boundary layer fivefold. This is due to the fact that at location 1, the boundary layer investigated here was still transitioning into full turbulence when each of the fine/rough sandpaper and 3 mm diameter trips was used. Moreover, the hot-wire probe was located in a separation region caused by the larger sized 5 mm diameter and 5 mm step trips. The turbulent intensity results also show that none of the trips is able to induce a fully turbulent boundary layer. While the larger trips cause the boundary layer to appear highly turbulent at location 1, exhibiting a very energetic outer region (Fig. 3(b)), it is not representative of a naturally developed turbulent boundary layer. Similar results were recorded by Marusic et al. [9] for the outer region when using 6 mm and 10 mm threaded rods at low Reynolds numbers. The findings from Ref. [9] suggest the over-stimulated trips introduce large-scale disturbances into the boundary layer, which agrees closely with the findings of this study.

Gibson [14] stated that a minimum distance of ten wire diameters is required to ensure that fully turbulent flow has been achieved. Research by Goldstein et al. [32] suggested the separation region occurs within a maximum value of 13 times the step height ($l = 13 h_{step}$), while Moore [33] found a much more conservative maximum value of 22 times ($l = 22 h_{step}$). In the present study, the first probe is located at a length corresponding to approximately 13 diameters ($l = 13 d$), downstream of the larger 5 mm diameter trips. However, from the results presented, it is clear that transition has not occurred. Increasing the Reynolds number also appears to have no effect on the results such that none of the trips investigated can induce a fully developed turbulent boundary layer at location 1.
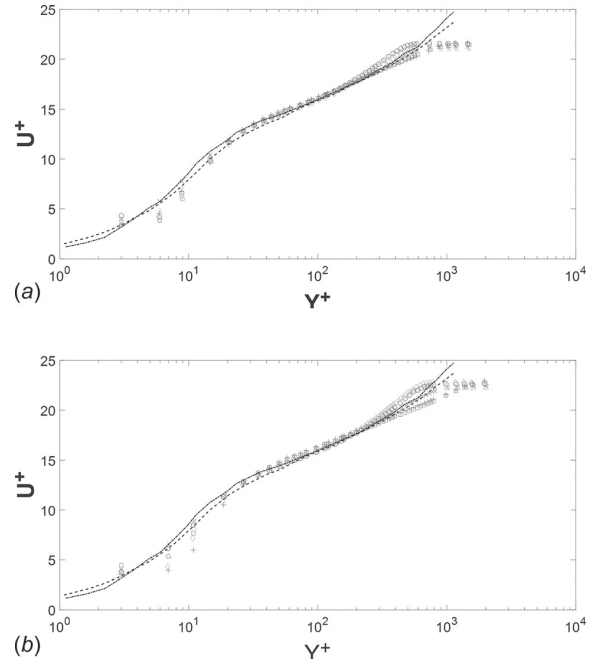
The flow farther downstream of the trips has been investigated to determine the effect development length and Reynolds number have on the performance of the trip techniques. As can be seen in Fig. 4(a), previously published data matches very closely with the results obtained up to the top of the logarithmic region, with a maximum error of 2.9% when comparing the boundary layer generated by the 3 mm wire and the published data. The boundary layer thickness was shown to be equal for all the trips investigated. The results indicate that the boundary layer is completely turbulent at location 2, independent of the trip technique and Reynolds number, which was changed by varying the flow speeds (Fig. 4(b)). This is to be expected as the Reynolds number at this location is above the critical Reynolds number for transition. The interesting aspect to note at this location is the turbulence intensity profiles shown in Fig. 5. While each technique appears to have produced a near identical streamwise profile, the same cannot be said about the turbulence intensity profile, where the peak value and shape change depending on which technique is used. At these Reynolds numbers, it is shown that the finer sandpaper and 3 mm diameter trip produce a boundary layer that is quite similar to the no trip data. This is shown at both Reynolds numbers for the streamwise and turbulence intensity profiles.

As shown in Fig. 6(a), a fully developed turbulent boundary layer can be seen at location 3 which is independent of tripping technique. The turbulence intensity profile shown in Fig. 6(b) shows similar trends between different tripping techniques. This result demonstrates that a natural turbulent boundary layer has been achieved at this location and indicates at that the larger Reynolds number investigated that sufficiently far downstream of the trip, a fully turbulent boundary layer is generated, independently of the tripping mechanism.

The shape factor is another parameter that can be considered to further distinguish the boundary layer. As marked in Fig. 7, a roughly uniform shape factor is achieved at a Reynolds number above approximately $Re_x = 5 \times 10^5$. As can be seen in Table 2, above this value the shape factor, $H = 1.3$–1.4, which reveals that the boundary layer can be considered to be turbulent as discussed
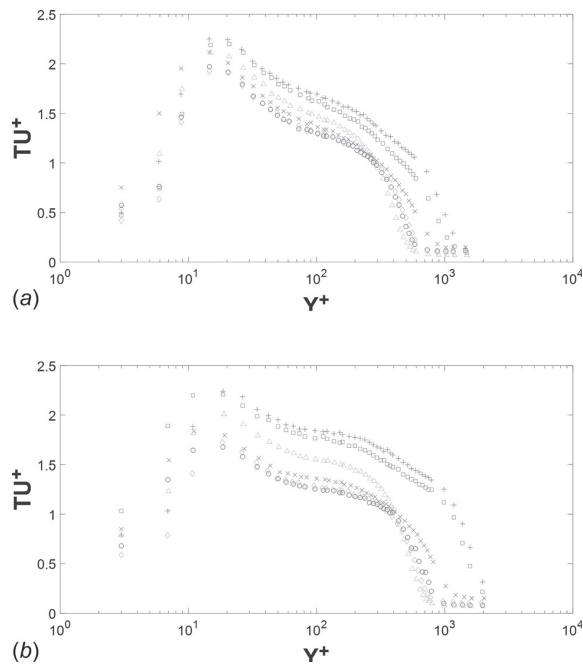
66

Paper 1: The application of different tripping techniques to determine
the characteristics of the turbulent boundary layer over a flat plate

(a)

(b)

Fig. 5 Turbulence (TU^+) intensity at location 2 for (a) $Re_x = 5.3{\times}10^5$ and (b) $Re_x = 7.5{\times}10^5$: (o) no trip, (+) 5 mm trip, (x) 3 mm trip, ($\diamond$) fine sandpaper, ($\square$) 5 mm step, and (Δ) rough sandpaper

by Ng and Spalding [34]. This also corresponds with the results observed at location 2. This shape factor value was shown to not be achieved at location 1, which indicates the turbulent boundary layer had not been achieved at this point.
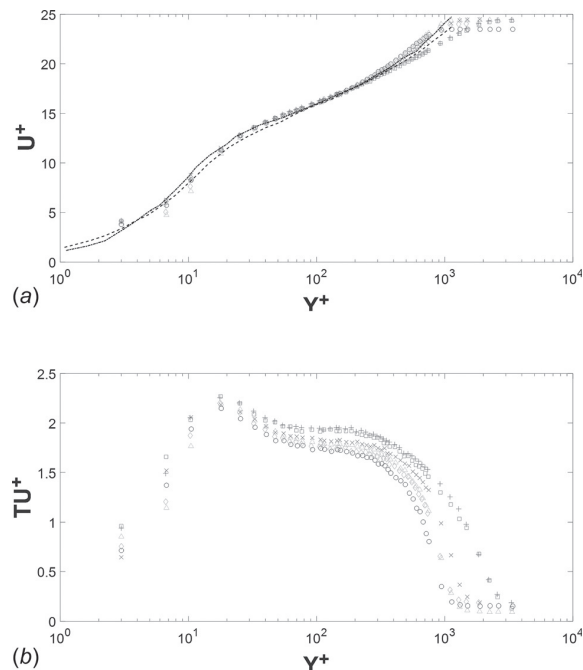

(a)

(b)

Fig. 6 (a) Mean velocity (TU^+) profile and (b) turbulence intensity profile at $Re_x = 1.5{\times}10^6$, location 3: (o) no trip, (+) 5 mm trip, (x) 3 mm trip, ($\diamond$) fine sandpaper, ($\square$) 5 mm step, (Δ) rough sandpaper, (--) Marusic and Kunkel [27] data, and (-.-) Schlatter and Orlu [28] data
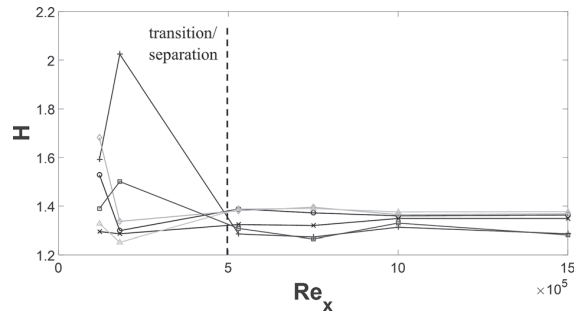
Fig. 7 Shape factor, H, versus Reynolds number: (o) no trip, (+) 5 mm trip, (x) 3 mm trip, ($\diamond$) fine sandpaper, ($\square$) 5 mm step, and (Δ) rough sandpaper

To verify the successful development of the zero pressure gradient turbulent boundary layer, the experimental results including the friction coefficient of all nontrip cases have been compared with the canonical data from Ref. [35] in Fig. 8. The friction coefficient of the boundary layer is given by $C_f = 2/U^{+2}$, and the Reynolds number based on momentum thickness is given by $Re_\theta = u\theta/\nu$. The data are shown to be very similar to the results provided by Sillero et al. [35] and can be used to verify whether a zero pressure gradient turbulent boundary layer is achieved.

In Secs. 6–9 of this paper, the higher statistics of the boundary layer will be investigated including coherent structures, probability density functions (PDFs), and power spectral density results to provide more detail on the effectiveness of each tripping mechanism.

6 Quantifying the Coherent Structures

In this study, the variable interval time averaging (VITA) technique has been used to detect the changes in the turbulent boundary layer associated with coherent structures. The technique, applied first by Blackwelder and Kaplan [36] for studying the near wall region, detects the sweep and ejection events where by the velocity rapidly changes. This is monitored by calculating the VITA of the streamwise velocity fluctuations according to the definition

$$\hat{u}(t, T_W) = \frac{1}{T_W} \int_{t-T_w/2}^{t+T_w/2} u(s)ds \tag{1}$$

where T_W is the interval used for the time averaging and is selected to be of the order of the time scale, which is typically chosen to be $T_W^+ = 10$, as selected by Blackwelder and Kaplan [36]. This value is used to assign small windows, which scan the fluctuating velocity at each point and calculates the local variance of the signal using

$$\mathrm{Var}(t, T_W) = \hat{u}^2(t, T_W) - [\hat{u}(t, T_W)]^2 \tag{2}$$

The variance of the entire signal is defined as

$$\mathrm{Var}(t) = \lim_{t\to\infty} \frac{1}{t} \int_0^t u^2(t)dt \tag{3}$$

If the value of the local variance, $\mathrm{Var}(t, T_W)$ is greater than the variance of the entire signal $k\mathrm{Var}(t)$, where k is a threshold value, a sweep or ejection event is considered to have occurred. Whalley [17] defined the detection function, $D(t)$, to differentiate between the different events, where

$$D(t) = \begin{cases} 1 & \mathrm{Var}(t, T_W) > k\mathrm{Var}(t) & \frac{\partial u}{\partial t} > 0 \ (\text{sweep event}) \\ 0 & \mathrm{Var}(t, T_W) < k\mathrm{Var}(t) & (\text{no event}) \\ -1 & \mathrm{Var}(t, T_W) > k\mathrm{Var}(t) & \frac{\partial u}{\partial t} < 0 \ (\text{ejection event}) \end{cases}$$

$$\tag{4}$$

Table 2   Summary of the calculated shape factor for a range of Reynolds numbers and trip types

R_x	Shape factor (H)					
	No trip	5 mm rod	3 mm rod	Fine sandpaper	5 mm square step	Rough sandpaper
1.2×10^5	1.529	1.592	1.295	1.682	1.390	1.328
1.8×10^5	1.299	2.024	1.286	1.337	1.501	1.252
5.3×10^5	1.388	1.285	1.324	1.381	1.308	1.388
7.5×10^5	1.372	1.273	1.320	1.395	1.265	1.390
1.0×10^6	1.360	1.313	1.349	1.365	1.330	1.376
1.5×10^6	1.363	1.286	1.349	1.368	1.281	1.377

A sweep event is expected to have a positive $\partial u/\partial t$ since the event is approaching the wall and consequently its streamwise velocity increases. The opposite happens for ejection events, where a negative $\partial u/\partial t$ occurs as the detected event moves away from the wall.

The number of detected events is strongly dependent on the selected threshold value, k. In this study, the value of k was set to 1.2 as discussed by Whalley [17]. In Figs. 9 and 10, the fluctuating u-component, the local variance, and the detection function can be seen for several of the tripping techniques investigated. In Fig. 9, for the 5 mm rod trip, a total of five sweep events were detected in the short window, while six ejection events were found. In Fig. 10, the 5 mm step trip, four sweep events, and three ejection

events were detected in the small window shown. Figure 11 shows the individual and ensemble-averaged VITA events for the 5 mm diameter rod trip at $\mathrm{Re}_x = 1.5 \times 10^6$. In this figure, the ensemble average is shown as a dashed bold line, while the individual VITA events are shown by the lines in different shades of gray. In total, 636 sweep events were detected and have been ensemble-averaged. While the detection method will most certainly report a small amount of false sweep and ejection events, an ensemble average at the end of the VITA analysis significantly mitigates the impact of the false events. Consequently, it has been shown by Adrian et al. [37], Choi et al. [38], Whalley [17], and Ghanadi et al. [5] to have a very successful rate of detecting coherent events.

Table 3 contains the total sweep and ejection events over the entire signal for the other trips over each location. The numbers of coherent structures are deemed important when understanding the
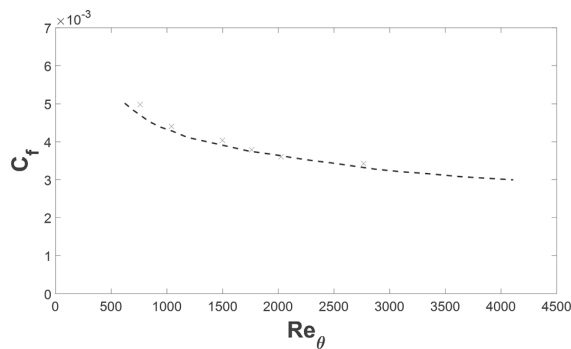
Fig. 8   Friction coefficient, C_f, versus Reynolds number based on momentum thickness. (x) Experimental data for the no trip data at all locations and (--) Sillero et al. [35] data.

Fig. 10   VITA detection at location 3 at $Y^+ \approx 15$ for the 5 mm diameter step trip, at $\mathrm{Re}_x = 1.0 \times 10^6$: (a) streamwise velocity fluctuations, (b) local variance, and (c) detector function

Fig. 9   VITA detection at location 3 at $Y^+ \approx 15$ for the 5 mm diameter rod trip, at $\mathrm{Re}_x = 1.0 \times 10^6$: (a) streamwise velocity fluctuations, (b) local variance, and (c) detector function

Fig. 11   VITA events at location 3 at $Y^+ \approx 15$ for the 5 mm diameter rod trip, at $\mathrm{Re}_x = 1.5 \times 10^6$, for sweep events, where (--) is the ensemble average VITA sweep event

68

Paper 1: The application of different tripping techniques to determine the characteristics of the turbulent boundary layer over a flat plate

Table 3 Summary of the sweep and ejection events detected using the VITA technique

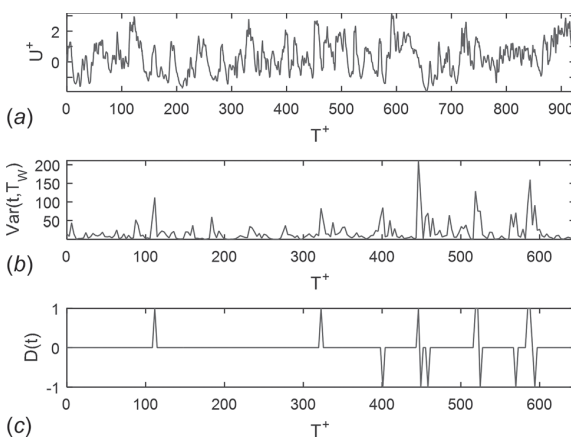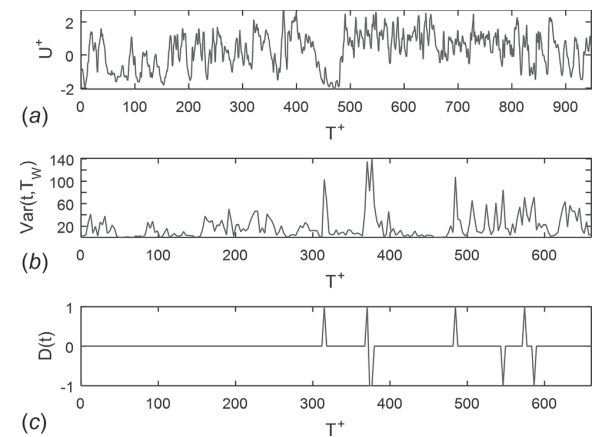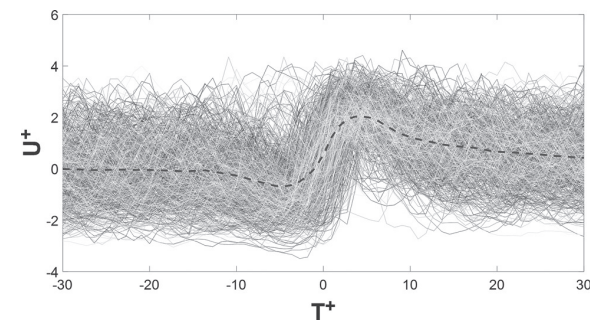|		Location 1		Location 2		Location 3	
		$R_x = 1.2 \times 10^5$	$R_x = 1.8 \times 10^5$	$R_x = 5.3 \times 10^5$	$R_x = 7.5 \times 10^5$	$R_x = 1.0 \times 10^6$	$R_x = 1.5 \times 10^6$
No trip	Sweep	553	920	106	239	535	779
	Ejection	505	863	28	67	248	583
5 mm rod	Sweep	864	1281	566	746	475	636
	Ejection	785	1282	198	524	191	441
3 mm rod	Sweep	1014	1311	129	199	479	703
	Ejection	689	1298	18	62	151	495
Fine sandpaper	Sweep	776	1497	130	252	516	706
	Ejection	769	1538	25	66	176	471
5 mm step	Sweep	906	1194	599	654	411	656
	Ejection	783	1265	236	469	107	441
Rough sandpaper	Sweep	596	1618	300	772	149	384
	Ejection	511	1698	95	499	25	192

turbulent boundary layer, as they are the main source of natural turbulence production in the near wall region [39].

The large number of sweep and ejection events observed at location 1 relative to locations 2 and 3 supports the hypothesis that the boundary layer at this location cannot be considered fully turbulent. Since the VITA technique is only used for fully developed turbulent flow, using the technique in a laminar/transition boundary layer results in the technique becoming unreliable, as shown in Table 3.

The results at location 2 indicate that several of the trips have not significantly changed the flow from the boundary layer with no trip. Both the 3 mm trip and fine sandpaper values are shown to be very similar to the naturally developed boundary layer, which is a positive sign as these boundary layers were shown to be all fully turbulent in Sec. 5. The rough sandpaper (295% increase) and both 5 mm trips (570% for the rod and 620% for the step) indicate a large increase in the coherent structures detected at a Reynolds number of 5.3×10^5 and this was also supported at a Reynolds number of 7.5×10^5 (415% for the sandpaper, 415% for the rod, and 400% for the step). This would indicate that these boundary layer trips have not produced a boundary layer which is representative of a naturally developed turbulent boundary layer. Such a large increase in the detected events would suggest that even at location 2, the larger trips (both 5 mm trips and the course sandpaper) are in a region of flow where the boundary layer is being affected by the upstream wake from the separation layer.

Location 3 can be seen to show a completely turbulent boundary layer at both Reynolds numbers and each trip techniques investigated. While there are some variations in the number of detected events for each tripping technique, no consistent pattern can be determined and the measured response is based on the time at which the instantaneous velocity was measured. This supports the conclusion from Sec. 5 where all the boundary layer and turbulence intensity profiles were identical and no clear differences could be determined between the various tripping techniques. This results in a turbulent boundary layer which represents a naturally developed boundary layer irrespective of the Reynolds number and tripping technique at this particular development length.

The averaged VITA events can also reveal the intensity and duration of the coherent structures. These are important as they determine the characteristics of the coherent structures and their effect on the boundary layer. The intensity of the events is calculated based on the peak-to-peak value of the streamwise velocity of the events. The duration, on the other hand, is calculated from the time separation of the peaks in each VITA analysis. Increasing the duration/intensity of the events reveals an increase in the turbulence energy production. The VITA analysis for the boundary layer will focus on the sweep events, as sweep events are the major contributor to turbulent skin friction [40].

The following predominantly focuses on the results obtained at locations 2 and 3 because the results from location 1 have already been shown to be not representative of the desired naturally developed turbulent boundary layer. The results at location 2 showed increased intensity of the sweep events for the 3 mm diameter trip (8.5%) and the rough sandpaper (4%) at a Reynolds number of $Re_x = 5.3 \times 10^5$ (Fig. 12). This reveals that the strength of the coherent structures has been increased by these trips. Increasing the Reynolds number to $Re_x = 7.5 \times 10^5$ only affects the downstream flow properties for the 3 mm trip, such that the sweep event intensity is increased by 9.5% (Fig. 13). These values are quite small and as the 3 mm trip did not affect the duration of the sweep events, the trip can be seen to mimic the naturally developed turbulent boundary layer. An interesting observation can be seen when considering the sweep duration of the larger trips (both 5 mm trips and the rough sandpaper). At both Reynolds numbers investigated, it was shown that the 5 mm diameter trip, the 5 mm step, and the rough sandpaper reduced the duration of the sweep events. The reduction in the events was found to be 10.6% at a Reynolds number of $Re_x = 5.3 \times 10^5$ and 33% at a Reynolds number of $Re_x = 7.5 \times 10^5$. This demonstrates that the downstream flow resulting from these trips is not representative of the natural turbulent boundary layer. The VITA profile is significantly different from the no trip case and coupled with the number of detected events discussed previously, a noticeable difference exists between the natural turbulent boundary layer and the one obtained from these particular trip techniques. This is quite interesting as it supports the previous observation that the boundary layer has been changed significantly by the larger trips, as indicated by the sweep events, something which was not identifiable from the streamwise velocity profile.
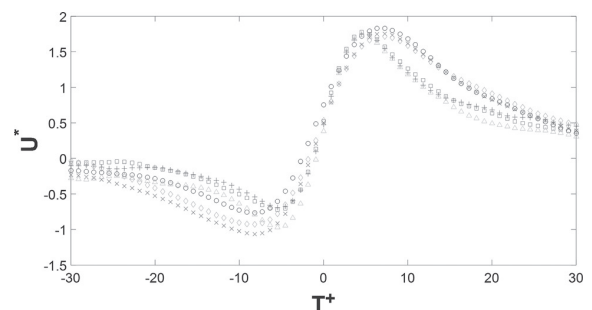

Fig. 12 Average VITA sweep events at $Re_x = 5.3 \times 10^5$, location 2: (o) no trip, (+) 5 mm trip, (x) 3 mm trip, ($\diamond$) fine sandpaper, ($\square$) 5 mm step, and (Δ) rough sandpaper

69

Fig. 13   Average VITA sweep events at $Re_x = 7.5 \times 10^5$, location 2: (o) no trip, (+) 5 mm trip, (x) 3 mm trip, ($\diamond$) fine sandpaper, ($\square$) 5 mm step, and (Δ) rough sandpaper

Fig. 15   Average VITA sweep events at $Re_x = 1.5 \times 10^6$, location 3: (o) no trip, (+) 5 mm trip, (x) 3 mm trip, ($\diamond$) fine sandpaper, ($\square$) 5 mm step, and (Δ) rough sandpaper
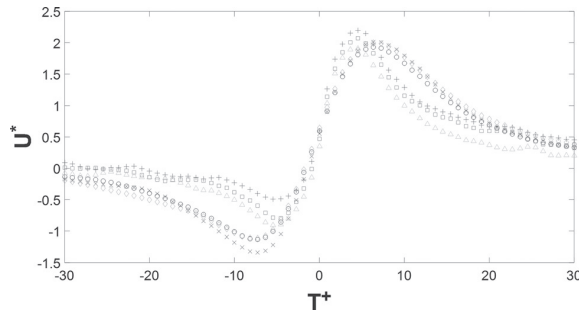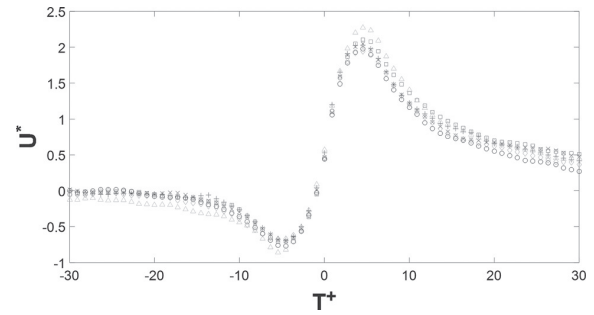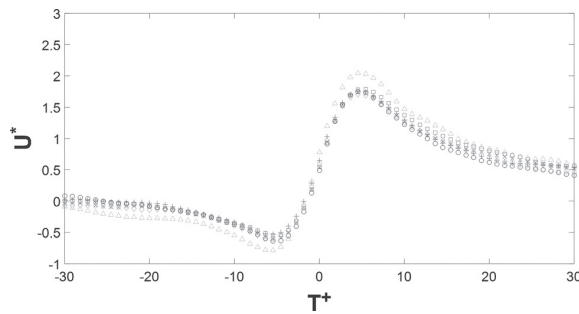

Fig. 14   Average VITA sweep events at $Re_x = 1.0 \times 10^6$, location 3: (o) no trip, (+) 5 mm trip, (x) 3 mm trip, ($\diamond$) fine sandpaper, ($\square$) 5 mm step, and (Δ) rough sandpaper

The averaged sweep events observed at location 3 show that at this development length, all the boundary layers converged to values which resembled the naturally developed boundary layer. At a Reynolds number of $Re_x = 1.0 \times 10^6$, it was shown that the intensity and the duration of sweep events downstream of all the trips were identical, except for rough sandpaper, which experienced an increased intensity and duration by 18% and 20%, respectively (Fig. 14). Increasing the Reynolds number to $Re_x = 1.5 \times 10^6$, the intensity and duration of the sweep events were increased by 12.7% and 10%, respectively, for the rough sandpaper (Fig. 15). However, when investigating the VITA profiles, these changes do not appear to be significantly different from the VITA results for the other trips at this location. Consequently, these results can be used to conclude that at location 3 and at larger Reynolds number, downstream of the trip a fully turbulent boundary layer is generated independently of the trip type.

7   Energy Spectra and Probability Density Function

The energy spectra at three different wall distances of $y^+ = 15$, 50, and 150 have been investigated. These locations have been selected to gather spectra over the first 150 wall lengths of the boundary layer where the majority of the turbulence energy is produced. The energy spectrum is able to provide information on the turbulence intensity, where the area under each curve is the equivalent of the turbulence intensity squared. The results at location 1 have been ignored for this part of the paper because as established previously, no trip technique was successful in inducing transition at this location.

As shown in Fig. 16, at location 2 when $Re_x = 5.3 \times 10^5$, a much higher energy spectrum occurs within the near wall region at $y^+ < 15$. The no trip, 3 mm trip, and fine sandpaper had near identical energy spectra, while the 5 mm rod, course sandpaper, and 5 mm step all increased the energy spectrum. This increase

occurred across the entire wavelength range, representing an increase in small-scale turbulence eddies and large-scale turbulence eddies due to the trips, aligning well with the results from Marusic et al. [9]. It is thought that this increase in the eddy structures is a result of the recovery from the over excitement of the larger trips. The recovery from these large trips has over stimulated the boundary layer and introduced large-scale disturbances and increased the turbulent regime. This was shown to occur across the entire boundary layer, as demonstrated in Fig. 16(a) ($y^+ = 15$), Fig. 16(b) ($y^+ = 50$), and Fig. 16(c) ($y^+ = 150$). Furthermore, this effect also occurs at larger Reynolds numbers and indicates that this over stimulated zone is present irrespective of the selected Reynolds number.

The values of the energy spectra at location 3 demonstrated that the boundary layer developed into a naturally turbulent boundary layer independent of the trip mechanism and Reynolds number.

The PDF was also investigated to provide information on the skewness and kurtosis of the data obtained. Skewness is the measure of symmetry, while kurtosis is the measure of whether the data are peaked or flat. Figure 17 shows the PDF at $y^+ = 15$ and 50 at $Re_x = 1.5 \times 10^6$, at location 3. The probability density functions were shown to have little dependence on the location and Reynolds number and had a very similar appearance at the other locations and Reynolds numbers. Consequently, this statistic was unable to provide any additional information to demonstrate which trip technique was the most effective at producing a naturally turbulent boundary layer. However, all the PDFs were shown to have a large positive skewness (large positive tail with a value of 0.855) as shown in Figs. 17(a) and 17(b), which is expected for turbulent boundary layers [17,41].

8   Discussion

At low Reynolds number below the critical value ($Re_{x,Crit} = 3 \times 10^5$), the results were shown to be inconclusive for determining which trip technique was the most effective at inducing a natural turbulent boundary layer, as such the no trip scenario remained laminar. All of the trips investigated were shown to not induce the boundary layer into turbulence. However, taking this into account, several comments can still be made on the effectiveness of the techniques used.

At location 2, the Reynolds number was well above the critical transition value. Consequently, we can directly compare the tripped boundary layers with the naturally developed turbulent boundary layer. While the streamwise profile of each technique appeared similar (Fig. 4), this was shown to not be the case on further inspection (Figs. 5, 12, 13, and 16). Once the higher statistics of the boundary layer were analyzed, it became evident that certain techniques had over stimulated the flow and several of the boundary layers were still in recovery from their upstream trips.

At the most downstream location, location 3, all the trips were shown to produce results identical to the naturally acquired
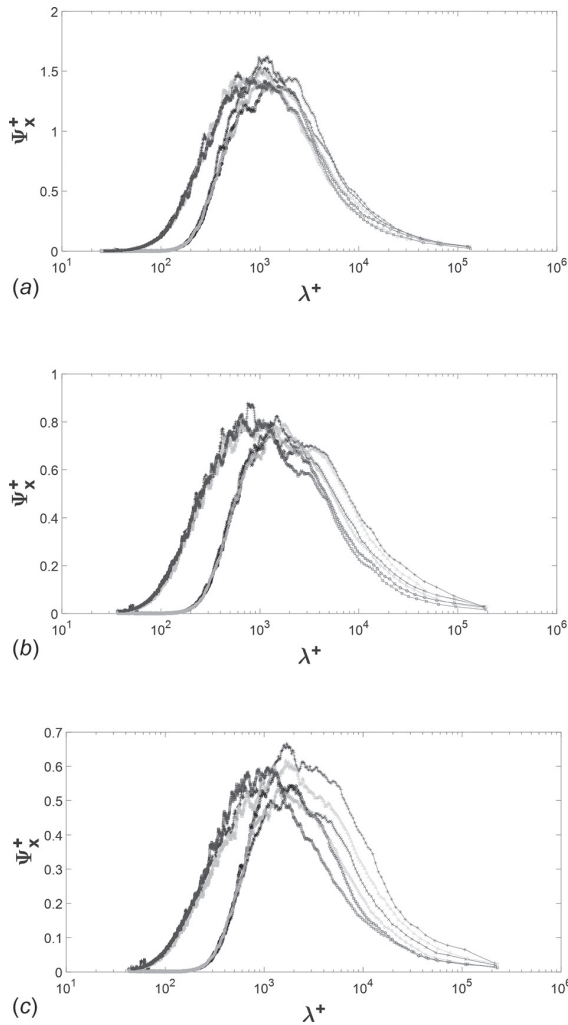
(a)

(b)

(c)

Fig. 16 Average energy spectra at Re$_x$ = 5.3×10^5: (a) y^+ = 15, (b) y^+ = 50, and (c) y^+ = 150, location 2: (o) no trip, (+) 5 mm trip, (x) 3 mm trip, ($\diamond$) fine sandpaper, ($\square$) 5 mm step, and (Δ) rough sandpaper

(a)

(b)

Fig. 17 Probability density function at Re$_x$ = 1.5×10^6: (a) y^+ = 50 and (b) y^+ = 50, location 3: (o) no trip, (+) 5 mm trip, (x) 3 mm trip, ($\diamond$) fine sandpaper, ($\square$) 5 mm step, and (Δ) rough sandpaper

boundary layer in the absence of a trip. This location was shown to be so far downstream that the development length and Reynolds number were large enough to acquire a naturally turbulent boundary layer [27,28] irrespective of the trip mechanism or Reynolds number. This paper will now focus on each individual trip technique.

The fine sandpaper, with a grit size of 58.5 μm, was shown to have no effect on the boundary layer at all of the Reynolds numbers considered. At location 1 (low Reynolds number), both the streamwise and turbulence intensity profiles demonstrated no significant change from the natural boundary layer, and consequently, this particular trip was not capable of stimulating the boundary layer at all. Even when the flow characteristics for this trip were examined at the other locations and the higher statistics of the boundary layer were determined, no difference could be found between the boundary layer generated from this particular trip and the natural boundary layer obtained with no trip. Consequently, this trip technique was shown to be ineffective.

The 5 mm rod and 5 mm step were also shown to be ineffective for inducing turbulence. Unlike the fine sandpaper, these two trip techniques over stimulated the boundary layer. While the boundary layer is certainly not laminar at the Reynolds number below
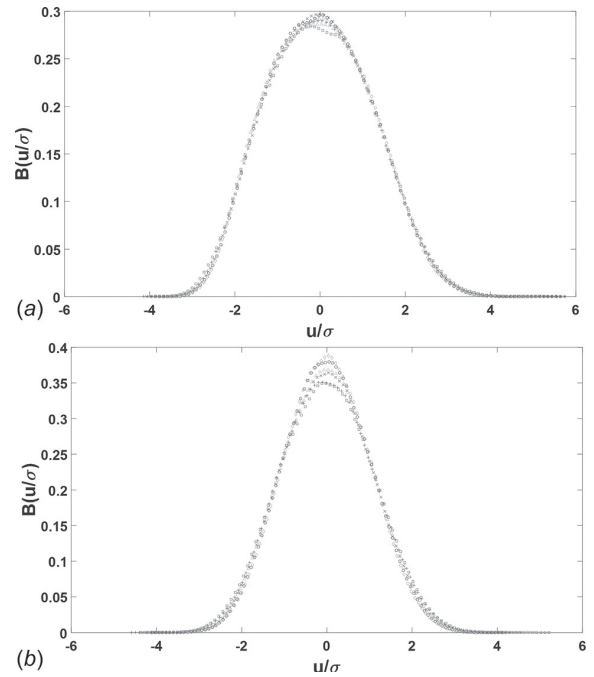
the critical value, it does not appear to be turbulent either. After closer inspection of the turbulence intensity and other statistics, it is clear that these two trips were too large for the boundary layer, and consequently, a separation region has occurred in the flow due to these objects. As reported by Marusic et al. [9], using an overstimulated trip introduces large-scale disturbances into the boundary layer. The disturbances predominantly reside in the outer region of the boundary layer and are believed to be a direct result of the shedding of the wake region behind the larger trips. Unfortunately, the inability of these trips to induce turbulence becomes even more evident at location 2. At location 2, these trips were shown to be more ineffective for inducing turbulence in comparison to the method of using no trip. These larger trips showed a heightened level of coherent structures, smaller eddies, and a larger overall turbulence intensity. As discussed previously, these particular trips have overstimulated the flow, and consequently, a larger recovery length is required. This recovery length appears to be significantly larger than the natural development length of a turbulent boundary layer, and consequently, an increased length is required for a natural turbulent boundary layer to be induced. At location 3, it was shown that recovery had been achieved and a natural turbulent boundary layer was achieved from these particular trips.

The coarse sandpaper, with a grit size of 269 μm, was shown to have a similar effect on the boundary layer to the larger 2D protuberances mentioned previously. At location 1, both the streamwise and turbulence intensity profiles demonstrated significant change from the natural boundary layer, however, they did not represent the profiles of a naturally turbulent boundary layer. This was demonstrated mainly in the turbulence intensity profile and the maximum value of the profile, which represents the location of the coherent structures, which are located at a distance from the wall greater than would be expected. As we start to investigate the other locations, we begin to notice similar trends to the boundary layers generated by the large 5 mm trips. Once again, we see a region at location 2, which has an increase in its turbulence

measures, irrespective of Reynolds number. This indicates a boundary layer which is still recovering from its upstream disturbance. It was shown that complete recovery was achieved at location 3.

The final trip that will be discussed in this section is the 3 mm trip. This trip was shown to be the most promising as shown by the results gathered at each location. Although the 3 mm trip was unable to induce complete turbulence at location 1, the results indicate a positive response in comparison to the other trip techniques. First, the streamwise profile and turbulence intensity were changed significantly by the trip. However unlike the other trips where the turbulence intensity was changed into an irregular pattern, the 3 mm trip demonstrated a shape which mimics a naturally developed turbulent boundary layer. Consequently while the trip was not successful in inducing turbulence, it clearly had a positive effect in comparison to the other investigated trips, where the maximum difference with the published data from Marusic and Kunkel [27] was 14.27%, the smallest value of all the trips investigated. Furthermore, the boundary layer statistics at locations 2 and 3 were identical in comparison to the natural turbulent boundary layer. Therefore unlike the other trips investigated in this paper, the 3 mm trip did not have an excessive regeneration length and did not have an adverse effect on the results at location 2. This was shown to be irrespective of Reynolds number.

Consequently, the effectiveness of the 2D protuberances was notable across the three locations. The 3 mm rod had a ratio of $3d = 4\delta$ to the boundary layer thickness, while the 5 mm step and rod had a ratio of $5d = 4\delta$ to the boundary layer thickness. This would suggest that a trip with a smaller dimension than the boundary layer thickness, but of comparable size, has the greater effect for artificially generating a turbulent boundary layer at low Reynolds number. Even at the larger flow speed investigated here, the 3 mm trip was shown to be the most reliable trip with its boundary layer thickness ratio being reduced to $3d = 5\delta$ due to the larger Reynolds number increasing the boundary layer thickness. Consequently, the 3 mm diameter trip appears to be the most successful trip in producing a turbulent boundary layer in a shorter distance than required for a naturally occurring boundary layer for both of the Reynolds numbers tested. This would suggest that when using a trip to induce boundary layer transition, a trip of diameter comparable to the boundary layer thickness is recommended, however, it must be smaller than the boundary layer thickness.

To support this observation, additional data were collected at a location between locations 1 and 2 to determine the effect of the 3 mm trip on the development of a turbulent boundary layer. This location corresponds to 350 mm downstream of the leading edge (approximately 150 mm downstream of the trip location) and was evaluated at Reynolds numbers corresponding to $Re_x = 2.2 \times 10^5$ and $Re_x = 3.1 \times 10^5$. Figures 18(a) and 18(b) depict the streamwise velocity profiles of the natural boundary layer and the 3 mm tripped boundary layer at this location corresponding to these Reynolds numbers. It can be seen clearly that the 3 mm tripped boundary layer resembles the published data from Refs. [27] and [28], while the untripped naturally developed boundary layer is yet to achieve turbulence.

A maximum difference of 6% was recorded in the velocity $U+$ when comparing the boundary layer generated by the 3 mm wire and the published data for the naturally developed turbulent boundary layer. The turbulence intensity profile at this location between locations 1 and 2 also shows that the boundary layer has been induced into turbulence by the 3 mm diameter wire.

Figure 19(a) demonstrates a profile which is identical to the profile achieved at location 2 previously. The no trip profile once again fails to resemble the naturally developed turbulent boundary layer profile and provides similar results to the conclusions drawn from the streamwise profiles. Increasing the Reynolds number (Fig. 19(b)) has no impact on the effectiveness of the 3 mm trip and the profile remains unchanged between the two Reynolds number values investigated.
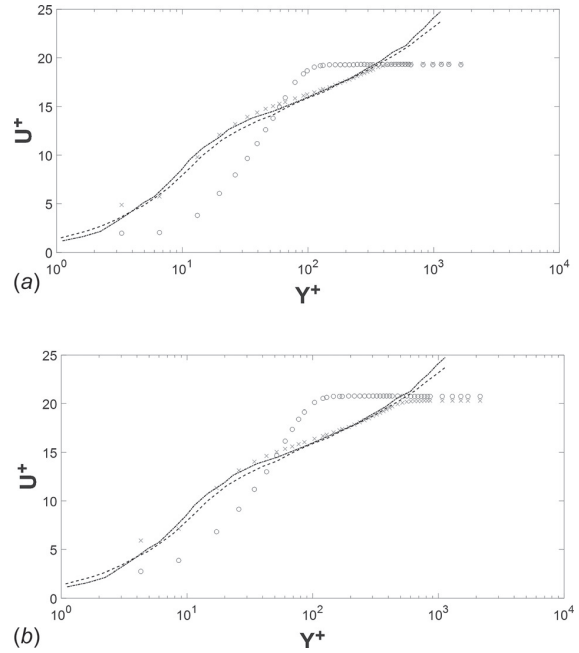
Fig. 18 Mean velocity profile for (a) $Re_x = 2.2 \times 10^5$ and (b) $Re_x = 3.1 \times 10^5$: (o) no trip, (x) 3 mm trip, (--) Marusic and Kunkel [27] data, and (-.-) Schlatter and Orlu [28] data

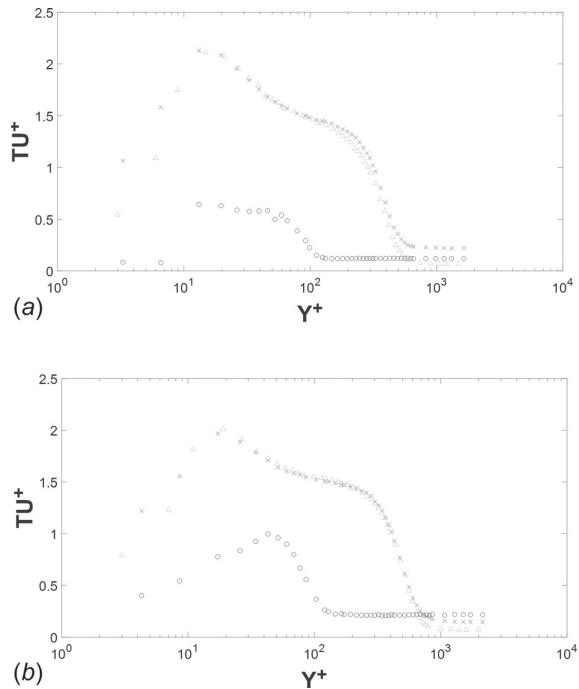**Fig. 19** Turbulence intensity for (a) $Re_x = 2.2 \times 10^5$ and (b) $Re_x = 3.1 \times 10^5$: (o) no trip, (x) 3 mm trip, and (Δ) 3 mm trip at location 2

9 Summary and Conclusion

The structure of any turbulent flow dictates the production of turbulence in the boundary layer. Forcing a boundary layer from a laminar state into a turbulent state via boundary layer tripping is

commonly used to fix the point of transition, to prevent laminar separation bubbles from occurring, and to reduce the drag of bluff bodies at certain Reynolds numbers. This forcing can be performed through various means: passive roughness elements attached to the wall such as sandpaper or 2D protuberances such as circular wires and steps. In this study, the main tripping techniques investigated were wires of different diameters and changes in roughness. Each tripping technique was investigated at a variety of Reynolds numbers and multiple locations downstream of the trip location. The characteristics of the tripping mechanisms were analyzed using hot-wire anemometry and the results were used to calculate the streamwise boundary layer profile, the properties of the coherent structures, the energy spectrum, and other statistics.

When implementing a trip mechanism in the flow, a scale close to the undisturbed boundary layer thickness is suggested. For experiments requiring a natural turbulent boundary layer, a trip of characteristic dimensions less than the undisturbed boundary layer thickness is recommended. This was shown to be true at all of the Reynolds numbers investigated here. A larger trip was shown to cause a large regeneration region far away from the trip or a large separation region close to the leading edge and should thus be avoided.

The conclusions drawn here are based on the results of measurements at three locations downstream of the trip, which were chosen to give a broad study of potential wind tunnel arrangements. Future work intends to focus more intently on the region between $\mathrm{Re}_x = 1.8 \times 10^5$ and $\mathrm{Re}_x = 5.3 \times 10^5$ where transition occurred. This region was explored for the tripping techniques which showed promise for inducing turbulence, but not for the remaining techniques which showed negative effects at the three measurement locations. Future work could further include 3D protuberance techniques and other trip geometries used by other researchers. The results presented here, however, are only the beginning of the development of the knowledge required for this area of work.

Nomenclature

$B(\sigma)$ = probability density function of streamwise velocity
d = trip diameter/size (mm)
H = shape factor
k = VITA threshold
K = wavenumber
Re_x = Reynolds number based on streamwise distance
Re_{u_τ} = Reynolds number based on friction velocity
Re_θ = Reynolds number based on momentum thickness
t = time (s)
T_{av} = averaging duration (s)
T_W = window length (s)
Tu = turbulence intensity
u = streamwise flow velocity (m/s)
u_τ = friction velocity (m/s)
Var = variance
x = indicates x-direction (streamwise) (m)
y = indicates y-direction (wall-normal direction) (m)
z = indicates z-direction (spanwise) (m)

Symbols

δ = boundary layer thickness (mm)
δ^+ = displacement thickness (mm)
θ = momentum thickness (mm)
λ = wavelength
ν = kinematic viscosity (m/s^2)
σ = standard deviation

Superscript

$+$ = denotes time scale (ν/u_τ^2) or length scale (ν/u_τ)

References

[1] Panton, R. L., 2001, "Overview of the Self-Sustaining Mechanisms of Wall Turbulence," Prog. Aerosp. Sci., 37(4), pp. 341–383.
[2] Braslow, A., Hicks, R., and Harris, R., 1966, "Use of Grit-Type Boundary-Layer-Transition Trips on Wind-Tunnel Models," NASA Langley Research Center, Cleveland, OH, Technical Report No. NASA-TN-D-3579.
[3] Rathnasingham, R., and Breuer, S., 2003, "Active Control of Turbulent Boundary Layers," J. Fluid Mech., 495(1), pp. 209–233.
[4] Schlatter, P., and Orlu, R., 2012, "Turbulent Boundary Layers at Moderate Reynolds Numbers. Inflow Length and Tripping Effects," J. Fluid Mech., 710, pp. 5–34.
[5] Ghanadi, F., Arjomandi, M., Cazzolato, B. S., and Zander, A. C., 2015, "Analysis of the Turbulent Boundary Layer in the Vicinity of a Self-Excited Cylindrical Helmholtz Resonator," J. Turbul., 16(8), pp. 705–728.
[6] Zhou, W., Rao, Y., and Hui, H., 2015, "An Experimental Investigation on the Characteristics of Turbulent Boundary Layer Flows Over a Dimpled Surface," ASME J. Fluids Eng., 138(2), p. 021204.
[7] Morkovin, M. V., 1990, "On Roughness-Induced Transtion: Facts, Views, and Speculations," Instability and Transition (ICASE/NASA LARC Series, Vol. 1), M. Y. Hussaini and R. G. Voigt, eds., Springer, Berlin, pp. 281–295.
[8] Chan, Y. Y., 1988, "Comparison of Boundary Layer Trips of Disk and Grit Types on Airfoil Performance at Transonic Speeds," National Aeronautical Establishment, Ottawa, ON, Canada, Technical Report No. 29908.
[9] Marusic, I., Chauhan, K. A., Kulandaivelu, V., and Hutchins, N., 2015, "Evolution of Zero-Pressure-Gradient Boundary Layers From Different Tripping Conditions," J. Fluid Mech., 783, pp. 379–411.
[10] Antonia, R. A., and Luxton, R. E., 1971, "The Response of a Turbulent Boundary Layer to a Step Change in Surface Roughness Part 1: Smooth to Rough," J. Fluid Mech., 48(4), pp. 721–761.
[11] Putrell, L. P., Klebanoff, P. S., and Buckley, F. T., 1981, "Turbulent Boundary Layer at Low Reynolds Number," Phys. Fluids, 24(5), pp. 802–811.
[12] Erm, L. P., and Joubert, P. N., 1991, "Low-Reynolds-Number Turbulent Boundary Layers," J. Fluid Mech., 230, pp. 1–44.
[13] Slangen, R. A. C. M., 2009, "Experimental Investigation of Artificial Boundary Layer Transition," M.Sc. thesis, Delft University of Technology, Delft, The Netherlands.
[14] Gibson, B. A., 2012, "Laminar Flow Control of a Flat Plate Boundary Layer Using Dielectric Barrier Discharge Plasma," Ph.D. thesis, University of Adelaide, Adelaide, Australia.
[15] Schroder, A., Geisler, R., Elsinga, G. E., Scarano, F., and Dierksheide, U., 2008, "Investigation of a Turbulent Spot and a Tripped Turbulent Boundary Layer Flow Using Time-Resolved Tomographic PIV," Exp. Fluids, 44(2), pp. 305–316.
[16] de Silva, C. M., Gnanamanickam, E. P., Atkinson, C., Buchmann, N. A., Hutchins, N., Soria, J., and Marusic, I., 2014, "High Spatial Range Velocity Measurements in a High Reynolds Number Turbulent Boundary Layer," Phys. Fluids, 26(2), p. 025117.
[17] Whalley, R. D., 2011, "Turbulent Boundary-Layer Control With DBD Plasma Actuators Using Spanwise Travelling-Wave Technique," Ph.D. thesis, The University of Nottingham, Nottingham, UK.
[18] Rona, A., and Soueid, H., 2010, "Boundary Layer Trips for Low Reynolds Number Wind Tunnel Tests," AIAA Paper No. 2010-399.
[19] Elsinga, G. E., and Westerweel, J., 2012, "Tomographic-PIV Measurement of the Flow Around a Zigzag Boundary Layer Trip," Exp. Fluids, 52(4), pp. 865–876.
[20] Bernardini, M., Pirozzoli, S., Orlandi, P., and Lele, S. K., 2014, "Parameterization of Boundary-Layer Transition Induced by Isolated Roughness Elements," AIAA J., 52(10), pp. 2261–2269.
[21] Doolittle, C. J., Drews, S. D., and Goldstein, D. B., 2014, "Near-Field Flow Structures About Subcritical Surface Roughness," Phys. Fluids, 26(12), p. 124106.
[22] Loiseau, J. C., Cherubini, S., Robinet, J. C., and Leriche, E., 2015, "Influence of the Shape on the Roughness-Induced Transition," Instability and Control of Massively Separated Flows (Fluid Mechanics and Its Applications, Vol. 107), Springer, Berlin.
[23] Sedney, R., 1969, "A Review of the Effects of Steady, Three-Dimensional Perturbations in Laminar Boundary Layer," Research Institute for Advanced Study, Baltimore, MD, Report No. TR 71-24.
[24] Shin, J. H., and Seung, J. S., 2014, "Pressure Gradient Effects on Smooth and Rough Surface Turbulent Boundary Layers—Part I: Favourable Pressure Gradient," ASME J. Fluids Eng., 137(1), p. 011203.
[25] Shin, J. H., and Seung, J. S., 2014, "Pressure Gradient Effects on Smooth and Rough Surface Turbulent Boundary Layers—Part II: Adverse Pressure Gradient," ASME J. Fluids Eng., 137(1), p. 011204.
[26] Hutchins, N., Nickels, T. B., Marusic, I., and Chong, M. S., 2009, "Hot-Wire Spatial Resolution Issues in Wall-Bounded Turbulence," J. Fluid Mech., 635, pp. 103–136.
[27] Marusic, I., and Kunkel, G. J., 2003, "Streamwise Turbulence Intensity Formulation for Flat-Plate Boundary layers," Phys. Fluids, 15(8), pp. 2461–2464.
[28] Schlatter, P., and Orlu, R., 2010, "Assessment of Direct Numerical Simulation Data of Turbulent Boundary Layers," J. Fluid Mech., 659, pp. 116–126.
[29] Marusic, I., and Hutchins, N., 2008, "Study of the Log-Layer Structure in Wall Turbulence Over a Very Large Range of Reynolds Number," Flow, Turbul. Combust., 81(1–2), pp. 115–130.
[30] Clauser, F. H., 1954, "The Turbulent Boundary Layer," Adv. Appl. Mech., 4, pp. 1–51.

[31] Kendall, A., and Koochesfahani, M., 2006, "A Method for Estimating Wall Friction in Turbulent Boundary Layer," AIAA Paper No. 2006-3834.

[32] Goldstein, R. J., Eriksen, V. L., Olson, R. M., and Eckert, E. R. G., 1970, "Laminar Separation Reattachment and Transition of the Flow Over a Downstream-Facing Step," ASME J. Basic Eng., **92**(4), pp. 732–739.

[33] Moore, T. W. F., 1960, "Some Experiments on the Reattachment of a Laminar Boundary Layer Separating From a Rearward Facing Step on a Flat Plate Aerofoil," J. R. Aeronaut. Soc., **64**(599), pp. 668–672.

[34] Ng, K. H., and Spalding, D. B., 1972, "Turbulence Model for Boundary Layers Near Walls," Phys. Fluids, **15**(1), pp. 20–30.

[35] Sillero, J. A., Jimenez, J., and Mozer, R. D., 2013, "One-Point Statistics for Turbulent Wall-Bounded Flows at Reynolds Numbers up to $\delta^+ \approx 2000$," Phys. Fluids, **25**(10), p. 105102.

[36] Blackwelder, R. F., and Kaplan, R. E., 1976, "On the Wall Structure of the Turbulent Boundary Layer," J. Fluid Mech., **76**(1), pp. 89–112.

[37] Adrian, R. J., Meinhart, C. D., and Tomkins, C. D., 2000, "Vortex Organization in the Outer Region of the Turbulent Boundary Layer," J. Fluid Mech., **422**, pp. 1–54.

[38] Choi, K. S., Jukes, T., and Whalley, R., 2011, "Turbulent Boundary-Layer Control With Plasma Actuators," Philos. Trans. R. Soc. A, **369**(1940), pp. 1443–1458.

[39] Robinson, S. K., 1991, "Coherent Motions in the Turbulent Boundary Layer," Annu. Rev. Fluid Mech., **23**(1), pp. 601–639.

[40] Orlandi, P., and Jimenez, J., 1993, "On the Generation of Turbulent Wall Friction," Phys. Fluids, **6**(2), pp. 634–641.

[41] Kim, J., Moin, P., and Moser, R., 1987, "Turbulence Statistics in Fully Developed Channel Flow at Low Reynolds Number," J. Fluid Mech., **177**, pp. 133–166.

74

Chapter 4

The impact of the distribution and sizing of the orifices on boundary layer control

4.1 Paper 2: Attenuation of sweep events in a turbulent boundary layer using micro-cavities

In this chapter a preliminary investigation is conducted into the capability of the micro-cavities as a technique to control the boundary layer. As discussed in the previous chapters a significant gap exists concerning the possibility of using a cavity array for this purpose. This chapter determines the feasibility of the technique, whilst investigating several key parameters of the manufacture of the cavity array. This includes the streamwise and spanwise spacing, as well as the diameter of the orifices. Experimental measurements of the flow over an array of applied micro-cavities are analysed and the results are reported.

The results show that the turbulent energy production within a fully developed turbulent boundary layer is reduced using a flushed-surface cavity array and that the geometry

affects this reduction. The cavity arrays were shown to manipulate the sweep events in the boundary layer by capturing and damping their duration and intensity. The size of the holes in the cavity array were selected to be comparable with the dimensions of the expected coherent structures, based on the friction velocity and the known spacing and sizing of the sweep events.

The velocity was measured using hotwire anemometry in a wind tunnel at a range of Reynolds numbers. These results show that when the orifice diameter is 60 times the viscous length scale a maximum reduction in the turbulence and sweep intensities of 13% and 14% could be achieved, respectively. Furthermore the results also demonstrate that when the cavity orifice diameter was less than 20 times the viscous length scale, the sweep events were not captured by the array. In addition, if the diameter of the orifice exceeded 145 times the viscous length scale then separation of the shear layer occurred causing a smaller reduction in the turbulence and sweep intensities.

Evidence from this chapter shows that the boundary layer can be controlled using the micro-cavity array and the following chapters further evaluate the technique. In Chapter 5 the internal geometry of the cavity array and its effect on the control of the turbulent boundary layer is investigated.

This chapter has been published as:

Silvestri, A, Ghanadi, F, Arjomandi, M, Cazzolato, BS, Zander, AC, 2017, *'Attenuation of sweep events in a turbulent boundary layer using micro-cavities', Experiments in Fluids, vol. 58, no. 5, pp. 58.*

Statement of Authorship

Title of Paper	Attenuation of sweep events in a turbulent boundary layer using micro-cavities
Publication Status	☑ Published ☐ Accepted for Publication ☐ Submitted for Publication ☐ Unpublished and Unsubmitted work written in manuscript style
Publication Details	Silvestri, A, Ghanadi, F, Arjomandi, M, Cazzolato, BS, Zander, AC, 2017, 'Attenuation of sweep events in a turbulent boundary layer using micro-cavities', Experiments in Fluids, vol. 58, no. 5, pp. 58.

Principal Author

Name of Principal Author (Candidate)	Anton Silvestri		
Contribution to the Paper	Performed data analysis and interpretation, wrote manuscript and acted as corresponding author.		
Overall percentage (%)	70		
Certification:	This paper reports on original research I conducted during the period of my Higher Degree by Research candidature and is not subject to any obligations or contractual agreements with a third party that would constrain its inclusion in this thesis. I am the primary author of this paper.		
Signature		Date	15/06/18

Co-Author Contributions

Name of Co-Author	Farzin Ghanadi
Contribution to the Paper	Supervised the development of the research and contributed in academic discussion and the review process of submitted manuscripts.
Signature	Date 15/06/18

Name of Co-Author	Maziar Arjomandi
Contribution to the Paper	Supervised the development of the research and contributed in academic discussion and the review process of submitted manuscripts.
Signature	Date 15/06/18

Name of Co-Author	Benjamin Cazzolato
Contribution to the Paper	Supervised the development of the research and contributed in academic discussion and the review process of submitted manuscripts.
Signature	Date 15/06/18

Name of Co-Author	Anthony Zander
Contribution to the Paper	Supervised the development of the research and contributed in academic discussion and the review process of submitted manuscripts.
Signature	Date 15/06/18

CrossMark

RESEARCH ARTICLE

Attenuation of sweep events in a turbulent boundary layer using micro-cavities

Anton Silvestri[1] · Farzin Ghanadi[1] · Maziar Arjomandi[1] · Benjamin Cazzolato[1] · Anthony Zander[1]

Abstract In the present study, the turbulent energy production within a fully developed turbulent boundary layer has been reduced using a variety of flushed-surface cavity arrays with different geometries embedded within a flat plate. The cavity arrays manipulate the sweep events in the boundary layer by capturing and damping their duration and intensity. The size of the holes in the cavity array was selected to be comparable with the dimensions of the expected coherent structures, based on the friction velocity and the known spacing and sizing of the sweep events. The velocity fluctuations within the turbulent boundary layer were measured using hot-wire anemometry in a wind tunnel for a range of Reynolds numbers. The results show that when the orifice diameter is equal to a value of 60 times the viscous length scale there is a maximum reduction in the turbulence and sweep intensities of 13 and 14%, respectively. The results also demonstrated that for a cavity orifice diameter less than 20 times the viscous length scale, the sweep events are restricted and no events are captured by the array. Furthermore, if the diameter of the orifice exceeds 145 times the viscous length scale, separation of the shear layer occurs, causing an increase in the turbulence energy production in the near-wall region.

List of symbols

$B(\sigma)$	Probability density function of streamwise velocity
c_f	Skin friction coefficient
d	Cavity diameter (mm)
H	Shape factor
k	Variable-interval time-averaging (VITA) threshold
Re_x	Reynolds number based on streamwise distance
Re_{u_τ}	Reynolds number based on friction velocity
Re_θ	Reynolds number based on momentum thickness
t	Time (s)
T_{av}	Averaging duration (s)
T_W	Window length (s)
Tu	Turbulence intensity
u	Streamwise flow velocity (m/s)
u_τ	Friction velocity (m/s)
Var	Variance
x	Indicates x-direction (streamwise) (m)
y	Indicates y-direction (wall-normal direction) (m)
z	Indicates z-direction (spanwise) (m)

Symbols

σ	Standard deviation
δ	Boundary layer thickness (mm)
δ^+	Displacement thickness (mm)
θ	Momentum thickness (mm)
ν	Kinematic viscosity (m/s^2)

Superscripts

$+$	Denotes viscous time scale $\left(\frac{\nu}{u_\tau^2}\right)$ or viscous length scale $\left(\frac{\nu}{u_\tau}\right)$

✉ Anton Silvestri
anton.silvestri@adelaide.edu.au

Farzin Ghanadi
farzin.ghanadi@adelaide.edu.au

Maziar Arjomandi
maziar.arjomandi@adelaide.edu.au

Benjamin Cazzolato
benjamin.cazzolato@adelaide.edu.au

Anthony Zander
anthony.zander@adelaide.edu.au

[1] School of Mechanical Engineering, University of Adelaide, Adelaide, South Australia 5005, Australia

⧉ Springer

1 Introduction

Coherent structures consisting of streamwise longitudinal vortices are considered by many to be an important part of the boundary layer. These vortices pump fluid into (sweep) and away (ejection) from the near-wall region. It has been shown that both ejection (Q2) and sweep events (Q4) generate approximately 70% of the total stresses each, equating to a 140% of the total stresses in the near-wall region at a pipe Reynolds number of approximately 11000 (Offen and Kline 1975; Kim et al. 1971; Corino and Brodkey 1969; Wallace et al. 1972). The discrepancy was due to the negative contribution of the total Reynolds stresses from the Q1 (outward interaction) and Q3 (wallward interaction) events. Furthermore, these events have been shown to be highly dependent on one another and consequently modifying one of these structures will have a significant effect on the other. Therefore, most studies target these vortices for a reduction in turbulence generation within the turbulent boundary layer. For example, the travelling wave and oscillating wall methods are shown to manipulate the streamwise vortices generated in the boundary layer. The oscillating wall techniques have been successful in reducing the skin friction drag by 45% (Choi and Graham 1998) and the sweep intensity and duration has been reduced by 35% using the travelling wave (Choi et al. 2011). The synthetic jet is another technique that has found great success at the micro-scale ($d < 10$ mm) by utilising a diaphragm set in a cavity and driven by a piezo-electric element excited at the element's resonant frequency. With an open neck and orifice, fluid is drawn in and out of the cavity during the oscillation of the diaphragm. During the outflow cycle vortex rings are generated at the orifice and travel away from the synthetic jet (Smith and Glezer 1998). During the inflow cycle fluid is drawn into the cavity of the synthetic jet, which does not affect the vortex ring produced during the outflow cycle as it has moved sufficiently far away from the orifice. The design is highly desirable in turbulent flow control due to its self-contained nature with no external fluid source as the grazing flow is used to drive the jet. If timed correctly the ejection process from the synthetic jet targets fast moving fluid (sweep events), which is moved away from the wall. The inflow stage is used to bring the slow moving fluid (ejection events) closer to the wall. Research from Lockerby (2001) has shown this to be successful in disrupting both events. However, passive control techniques are generally more favourable then active ones in real applications due to the absence of a power source and their relative ease of implementation.

Similar to the previously discussed active techniques, different areas of the boundary layer are also targeted by certain passive techniques. One of the most successful passive turbulence reduction techniques is the streamwise riblet (Walsh 1983; Choi 1987, 1989). Streamwise riblets are small grooves spaced in the spanwise direction, approximately equal in size to the boundary layer, aligned in the flow direction. It was shown that they can successfully reduce the skin friction drag by up to 8% (Walsh 1983). Choi (1987) demonstrated that riblets act as small fences and restrict the streamwise vortices that form the legs of the hairpin vortical structure. By acting as a fence, the growth of the streamwise vortices in the spanwise direction can be prohibited. Furthermore, Choi and Fujisawa (1993) demonstrated a similar effect on the turbulence structure to the drag-reducing riblets surface could be achieved by using a two-dimensional square cavity on a flat plate. Choi and Fujisawa (1993) showed a net drag reduction of the order of 1% could be achieved by using the single cavity, which reduced the skin friction over the cavity and lasted for $\frac{x}{d} = 100$ lengths.

Congruent to the synthetic jet, a flow excited Helmholtz resonator was used by Ghanadi (2014) to provide a jet of suction and ejection to target the ejection and sweep events, respectively. However, unlike the synthetic jet, the device is completely passive and its driving mechanism is provided by the grazing flow as opposed to a piezo-electric element. The results showed that when the orifice diameter was 5 mm, the resonator was excited by the grazing flow causing local suction and ejection to occur. This resulted in an 11% reduction in sweep intensity and a 5% reduction in the sweep duration within the logarithmic region of the boundary layer ($y^+ < 35$). However, when the orifice length was 10 mm the resonator could not be activated by the grazing flow and was effectively a simple cavity in cross-flow (Ghanadi 2014). Nevertheless, this resonator was found to have a small impact on the sweep events away from the wall in the logarithmic region and reduced their intensity and duration by 5 and 8%, respectively. From these results it appears that the reduction in the intensity and duration of the sweep events was achieved by allowing the sweep event to partially or completely enter the orifice of the resonator. Consequently, some of the energy associated with the high-speed events will be absorbed and dampened by the surface area of the cavity. At higher flow velocities it was found that the resonator did not significantly change the structure of the sweep events. This was attributed to the increased Reynolds number and its amplification of the generation of the turbulent events. The shear layer would break up more violently across the orifice gap and essentially increase the viscous drag more than the reduction from the sweep events being attenuated. By using a cavity with a small orifice it is expected that the shear layer would be unaffected by crossing the small opening. This would allow the cavity to be used as a drag-reduction device for higher Reynolds number flow as well as low-speed flow.

Comparable to the absorption of sweep events, Maa (1998) utilised the idea of a sub-millimetre micro-perforated panel to absorb sound. He found the most important parameter in his investigation is the perforate constant, which is proportional to the ratio of the perforation radius to viscous boundary layer thickness. This technique was found to have tremendous potential for wide-band absorption. As an extension to Maa's (1998) work it has been hypothesised that a similar device could have absorption qualities with regard to the sweep events occurring in the turbulent boundary layer and consequently the parameters to be investigated in this paper are the plate orifice size and its spatial relationship to the sweep events. Such a device is envisioned to dampen the coherent structures and disrupt the bursting cycle, which is responsible for the shear stress and viscous drag in the inner wall region. The application of boundary layer control will target the fluctuating component of velocity normal to the wall. If the cavity were to be designed with a very small orifice diameter of $d^+ < 150$ (in this study $d < 3$ mm), the streamwise and spanwise velocity profile would be undisturbed. The shear layer would not break apart while traversing the small gap, which usually occurs in larger cavities resulting in an adverse pressure gradient and an increase in the disturbances and viscous drag in the boundary layer (Chang et al. 2006). If the spanwise and streamwise velocity is found to be undisturbed, then the only component of velocity which would be affected would be that normal to the wall flow. This direction is often associated with ejection (positive, away from the wall) and sweep (negative, towards the wall) events. While limited investigations have been made on cavities in turbulent flow, Sarohia (1977) found a critical length of the orifice of a cavity where the shear layer does not break apart for laminar flow conditions. Chang et al. (2006) also commented on the shear layer being more prone to breaking apart in high turbulence flow, but their numerical models illustrated an area close to the

leading edge of the cavity where the streamwise velocity profile did not significantly change as the flow traversed the cavity.

A successful implementation of micro-cavities for the purpose of an alternative method for boundary layer control has yet to be achieved and forms the key motivation of this study. The present work assesses the ability of an array of micro-cavities to reduce the turbulent properties of a fully developed boundary layer of varying Reynolds numbers ($1195 \leq Re_\theta \leq 3771$). In the subsequent sections the characteristics of the cavity array will be discussed and detail into the experimental setup will be presented. A discussion of the results will be provided and an insight into the performance of the cavities in reducing the turbulent structures will be provided.

2 Experimental procedure

All experiments were performed in a closed-return type wind tunnel located at the University of Adelaide, which can be operated up to a maximum velocity of 30 m/s with low turbulence intensity (ranging between 0.4 and 1%). The test section is rectangular with a cross section of 500 mm × 500 mm and 2000 mm in length. A horizontal 2000 mm long flat plate, as shown in Fig. 1, was positioned inside the tunnel such that it spanned the whole width of the test section. The finite thickness of the flat plate leads to bluff body separation effects. Therefore to minimise any possible flow separation a super-elliptical leading edge of a nominal major radius of 114 mm was attached to the flat plate. A 125 mm long circulation flap was also mounted downstream of the plate to minimise any circulation developed over the plate and to ensure that the stagnation point was on the measurement side of the plate. The flap could also be adjusted as appropriate to balance the pressure gradient along the working section, which was selected to be a zero pressure gradient for these experiments. The boundary

Fig. 1 Schematic of the experimental arrangement
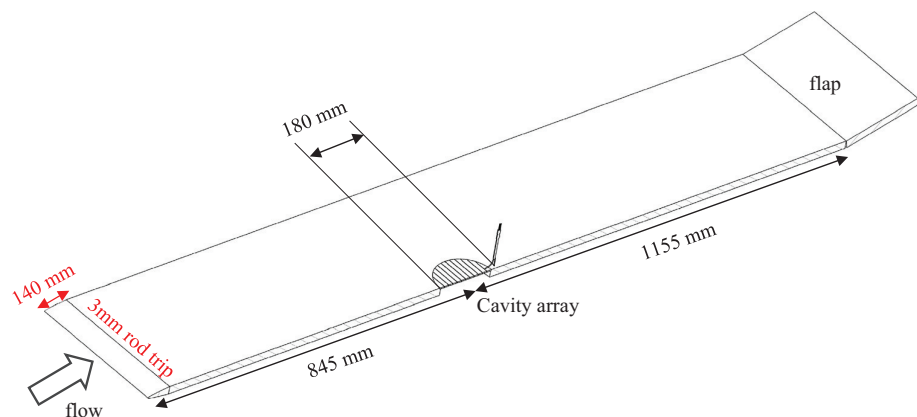
layer investigated in the study was tripped by a 3 mm rod located 140 mm downstream of the leading edge as advised by Silvestri et al. (2017). This was done to ensure a fully turbulent boundary layer was achieved.

This research focuses on the near-wall regions, as approximately half of the total turbulence production occurs within this small region (Robinson 1991). A hot-wire anemometer was used downstream of the boundary layer trip to characterise the changes in the turbulent structures within the boundary layer regions from the cavity array located 845 mm downstream of the leading edge. The experimental measurements were taken at a length selected to ensure a fully turbulent boundary layer was developed. This was done 180 mm downstream from the leading edge of the cavity array at a variety of Reynolds numbers and cavity dimensions. The streamwise velocity measurements were made with an IFA 300 CTA system, using a single platinum-plated tungsten wire of 5 µm in diameter and 1.25 mm in length, which was operated with an over-heat ratio of 1.8 and an operating temperature around 230 °C, which provided sufficient sensitivity to measure the velocity fluctuations with minimum thermal effects. The repeatability of each measurement was also verified three times and the data were sampled at 10 kHz for 10 s. This equates to a viscous-scaled sample interval of $.19 < \Delta t^+ < .24$, which exceeds the minimum viscous timescale investigated in this paper. Furthermore the sampling frequency is approximately 50 times the frequency of the coherent structures investigated, therefore aliasing is not believed to be an issue.

To investigate the effect of the cavity array geometry on reducing the turbulence energy production three different arrays were manufactured and tested (Fig. 2). The first array (cavity array 1) was designed based on the friction velocity value equal to $u_\tau = 0.5$ m/s, a value obtained previously by Silvestri et al. (2017) for a Reynolds number approximately equal to $Re_\theta = 1927$, where $Re_\theta = \frac{u\theta}{v}$. Using this friction velocity value the spanwise spacing and the approximate orifice diameter were calculated based on the method specified by Lockerby (2001), which states that the orifice diameter to be 40 times the viscous length scale and the spanwise spacing to be 100 times the viscous length scale. This resulted in a cavity array comprising 1.2 mm diameter holes and a spanwise spacing of 3 mm. Two additional arrays (cavity arrays 2 and 3) were designed with different holes and spacing dimensions based on alternative friction velocities. Using the method specified by Lockerby (2001) for friction velocity values equal to $u_\tau = 0.375$ m/s and $u_\tau = 0.24$ m/s, cavity arrays with 1.8 and 2.5 mm diameter holes, with spanwise spacing of 4.5 and 6 mm, respectively, were designed. All three cavity array plates were manufactured using a 3D printer located at the University of Adelaide with a constant streamwise spacing of 15 mm and constant thickness of 4 mm. Literature states that the length of coherent structures can be up to 10 times the spanwise spacing (Blackwelder and Eckelmann 1979). Consequently, 15 mm falls well below this value no matter which plate the authors tested. All cavity arrays were aligned perpendicular with the flow. To ensure dimensional accuracy, magnified images of the individual cavities were captured using a microscope. These images (Fig. 3) demonstrate small variance from the nominal values reported; however, such variance would be expected irrespective of which manufacturing technique was selected due to the small orifice diameters.
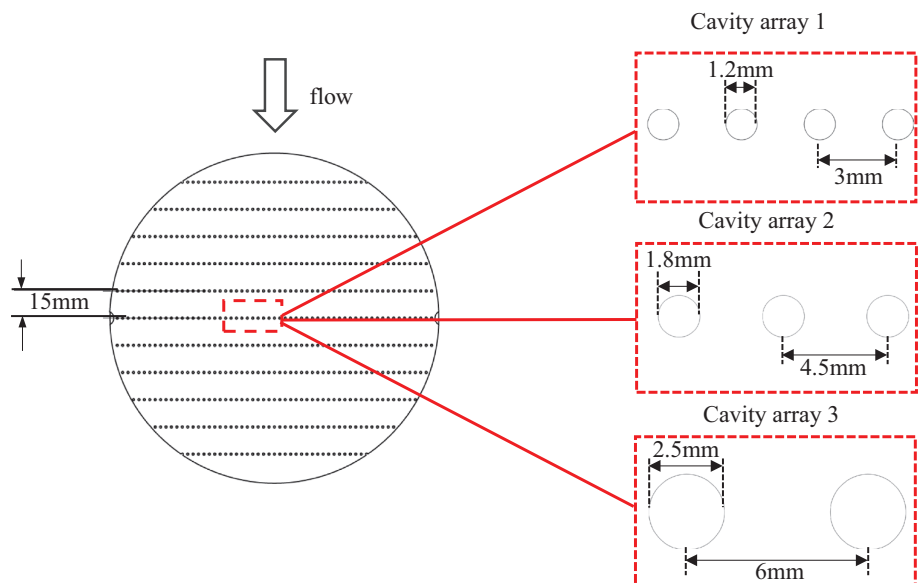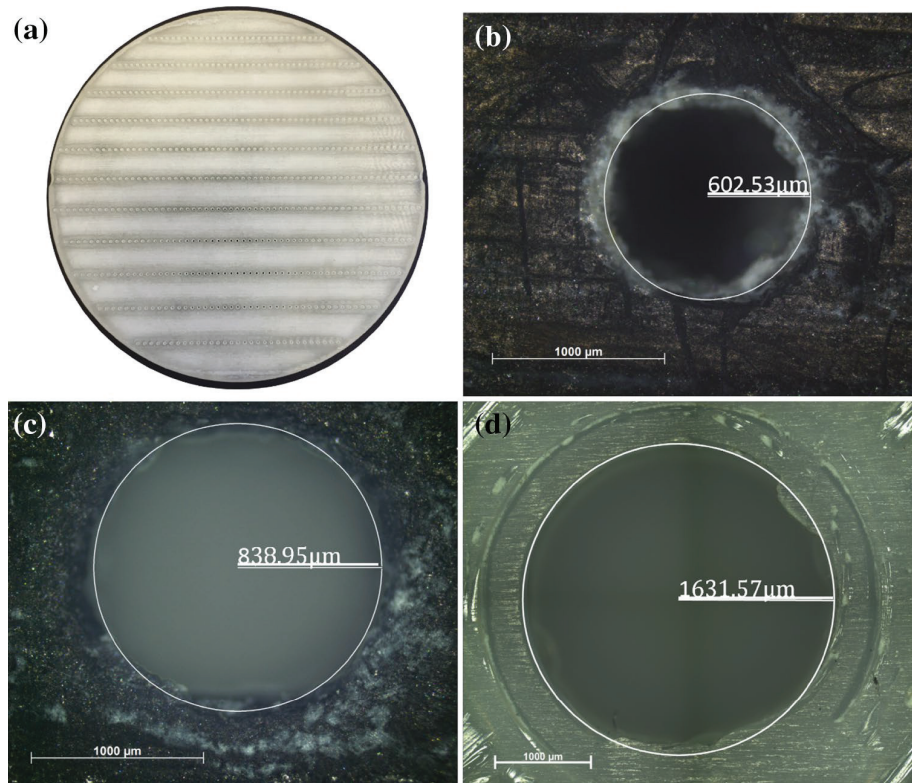

Fig. 2 Schematic of cavity arrays

Fig. 3 a Picture of cavity array 1; **b** microscope picture of cavity array 1; **c** microscope picture of cavity array 2; **d** microscope picture of cavity array 3

3 Hot-wire measurements

A single hot-wire probe was used throughout the experiments to determine the velocity fluctuations in the streamwise direction. The hot-wire probe was initially calibrated using a Baratron pressure sensor, which has high accuracy when measuring the mean flow. As the relationship between the hot-wire's voltage and the flow's velocity is not linear, this step was of significant importance and a total of 20 wind tunnel velocities ranging from 0–25 m/s were selected. A polynomial curve fit was then applied to the calibration data, where a 5th order polynomial fit was shown to produce the greatest curve fit. This calibration was performed multiple times over the testing period to improve the accuracy of the results and account for changes in the ambient temperature.

Voltage measurements were then converted into velocity using the coefficients determined from the 5th order polynomial fit found during the calibration of the hot-wire probe. Testing was conducted over a period of 4 days and during this time the ambient temperature of the wind tunnel varied by ± 2 °C from the average ambient temperature. This was shown to have a small error on the free stream velocity, where the maximum fluctuation in free stream velocity was found to be 1.8% at the

highest Reynolds number tested. Velocity data were taken at a single streamwise/spanwise location. This location was selected to be 180 mm from the leading edge of the cavity array, which resulted in the hot-wire probe taking data 5 mm behind the last row in the cavity array. The spanwise location of the hot-wire probe during this investigation was the midpoint of the cavity array and a total of 48 measurements were taken to accurately quantify the boundary layer. The boundary layer probe used had a slight offset between the bottom of the probe and the location of the hot-wire. This distance was known and was used to accurately determine the distance of the probe from the wall at all times.

To ensure the measurements recorded by the hot-wire anemometry system were accurate, an error analysis has also been conducted. As shown in Fig. 4, the non-dimensional mean velocity profile at $Re_\theta = 3771$ was compared against the results obtained by Marusic and Kunkel (2003) and Ghanadi et al. (2015). A maximum error of 15% occurs at the points closest to the flat plate ($y^+ < 30$); however, this small variation is deemed negligible as the key focus of this paper is the logarithmic region of the boundary layer ($30 < y^+ < 200$), where the turbulence reduction occurs and a maximum error of approximately 4.5% is present. In comparison to the published results of Ghanadi et al.
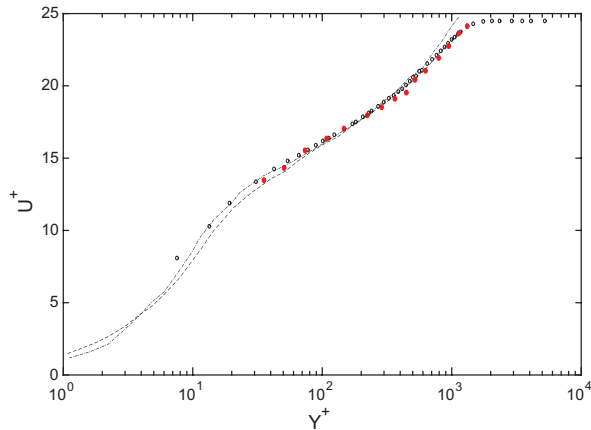
Fig. 4 Error analysis of the mean velocity profile of the boundary layer at $Re_\theta = 3771$. *Black circles* experimental results, *long dash* results obtained by Marusic and Kunkel (2003), *hyphen with dots* DNS results obtained by Schlatter and Orlu (2010), *red circles* experimental data obtained by Ghanadi et al. (2015) at $Re_\theta = 3920$

(2015) which has a Reynolds number much closer to the boundary layer investigated, the maximum error was shown to be only 2.7%.

The data collected from the hot-wire probes were also non-dimensionlised for comparison with the no-control boundary layers investigated. This was done by using the friction velocity (u_τ) and viscous length scale $\left(\frac{\nu}{u_\tau}\right)$ to normalise the hot-wire data. To do this the friction velocity (u_τ) of each boundary layer was calculated using the log law expression defined by Clauser (1954) as $U^+ = 5.6 \log_{10}(Y^+) + 4.9$. This was done via an iterative process which used a varying value for the friction velocity to curve fit the logarithmic region of the experimental data with the log law expression defined by Clauser (1954) as
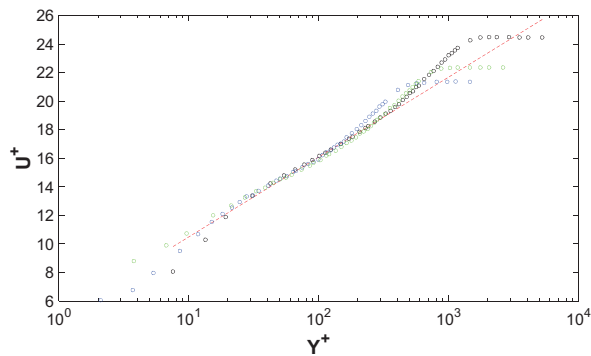
shown in Fig. 5 and demonstrated by Kendall and Kooches-fahani (2006). This method was performed in favour of using the near-wall gradient due to the increased number of hot-wire measurements obtained in the logarithmic region. The results were shown to provide accurate estimates with a maximum error of 2%. This was repeated for all the boundary layers investigated as shown by the continuity of the logarithmic region in Fig. 5, resulting in a unique friction velocity value for each boundary layer.

4 Effects of the cavity array on the velocity and turbulence intensity profiles

The effect of the cavity array on the turbulent boundary layer was first studied at a Reynolds number of $Re_\theta = 1927$. Throughout this paper the canonical friction velocity was used to scale all the data. Figure 6 shows the streamwise profile of the boundary layer immediately downstream of the cavity arrays and the corresponding unaltered turbulent boundary layer for comparison. The three cavity arrays investigated appear to shift the viscous and logarithmic subregion ($y^+ < 200$) upwards, while not changing the overall boundary layer thickness. This can be seen to make the boundary layer shallower for the control cases and consequently giving the boundary layer a more laminar appearance. This can be seen to cause a drag reduction from previous work (Savins and Seyer 1977; Patterson et al. 1977; Hooshmand et al. 1983) where an upward shift of the logarithmic region results in a decreased friction velocity or skin friction coefficient.

This reduction is also clearly evident in Fig. 7, which shows the turbulence intensity of the same boundary layers investigated. Cavity arrays 1, 2 and 3 are shown to provide a substantial turbulence intensity reduction of up to 13% within the logarithmic region $15 < y^+ < 200$. This

Fig. 5 a Streamwise boundary layer profile at $Re_\theta = 3771$. *Red line* log law expression defined by Clauser (1954), *blue circles* experimental results at $Re_\theta = 1195$, *green circles* experimental results at $Re_\theta = 1927$, *black circles* experimental results at $Re_\theta = 3771$
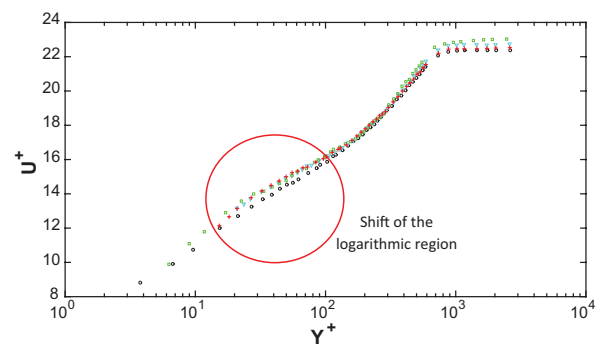

Fig. 6 Mean velocity profile at $Re_\theta = 1927$. *Black circles* no control, *blue triangles* cavity array 1, *green squares* cavity array 2 and *plus symbols* cavity array 3

Fig. 7 Turbulence intensity profile at $Re_\theta = 1927$. *Black circles* no control, *blue triangles* cavity array 1, *green squares* cavity array 2, *plus symbols* cavity array 3

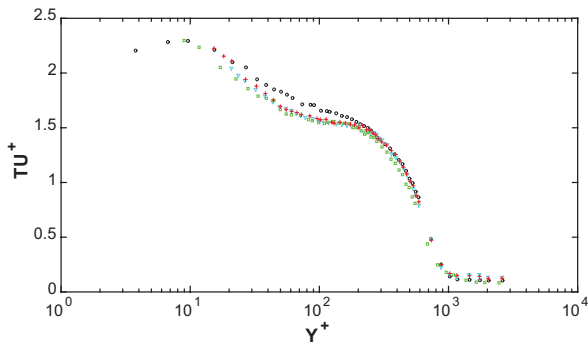**Table 1** Summary of Reynolds number and boundary layer parameters

Re_X	$\left(Re_x = \frac{ux}{\nu}\right)$	1.69×10^5	5.30×10^5	1.18×10^6
$Re_{\delta+}$	$\left(Re_{\delta+} = \frac{u\delta^+}{\nu}\right)$	1601	2521	4913
Re_θ	$\left(Re_\theta = \frac{u\theta}{\nu}\right)$	1195	1927	3771
Friction velocity (u_τ)		0.24 m/s	0.50 m/s	0.92 m/s
Viscous length scale $\frac{\nu}{u_\tau}$		6.25×10^{-5} m	3.00×10^{-5} m	1.63×10^{-5} m

is quite curious as while cavity array 1 has been specifically designed with dimensions to correspond to the size of the coherent structures at this Reynolds number, cavity arrays 2 and 3 have dimensions substantially larger than the expected sizes of the structures. However, all three cavity arrays provide a similar reduction in turbulence intensity. Consequently, the design guidelines described by Lockerby (2001) may not apply in this application.

To understand the effect of the Reynolds number on the effectiveness of the cavity arrays in reducing the turbulence energy production, two additional Reynolds numbers were studied. The details of the flow characteristics investigated can be found in Table 1. The streamwise profile in Fig. 8a shows that when the Reynolds number is reduced to $Re_\theta = 1195$, the boundary layer is not affected significantly by the cavity arrays. While the boundary layer has the logarithmic subregion shift upwards similar to $Re_\theta = 1927$, the change is much more subtle. At a larger Reynolds number of $Re_\theta = 3771$, as shown in Fig. 8b, a response similar to that measured at a Reynolds number of $Re_\theta = 1927$ occurs. Once again this can be seen to cause a drag reduction from previous work (Savins and Seyer 1977; Patterson et al. 1977; Hooshmand et al. 1983), where an upward shift of the logarithmic region results in a decreased friction velocity or skin friction coefficient.

The turbulence intensity profiles downstream of cavity arrays 1, 2 and 3 can be seen in Fig. 9 and may be used to provide a better understanding of the effect of the Reynolds number on the effectiveness of the arrays in reducing the turbulence energy production. As shown in Fig. 9a, cavity array 1 produces no recognisable effect (less than 0.5%) on the boundary layer at a Reynolds number of $Re_\theta = 1195$, whilst cavity arrays 2 and 3 produce maximum reduction values of 9 and 10% of the turbulence intensity, respectively, at a distance of $Y^+ = 50$. At a higher Reynolds number of $Re_\theta = 3771$ all cavity arrays produce a turbulence intensity reduction. A maximum turbulence intensity reduction of 10% at $y^+ = 100$ is achieved by all cavities; however, cavity array 1 produces a reduction over a much larger range ($20 < y^+ < 500$) in comparison to cavity array 2 ($30 < y^+ < 500$) and cavity array 3 ($40 < y^+ < 300$). This result indicates that at higher flow speeds ($Re_\theta > 3771$)
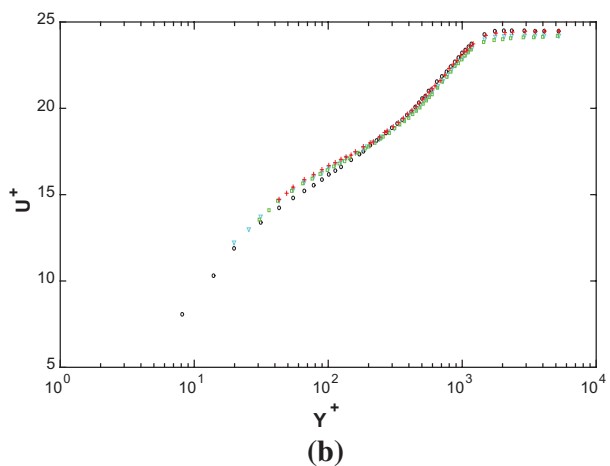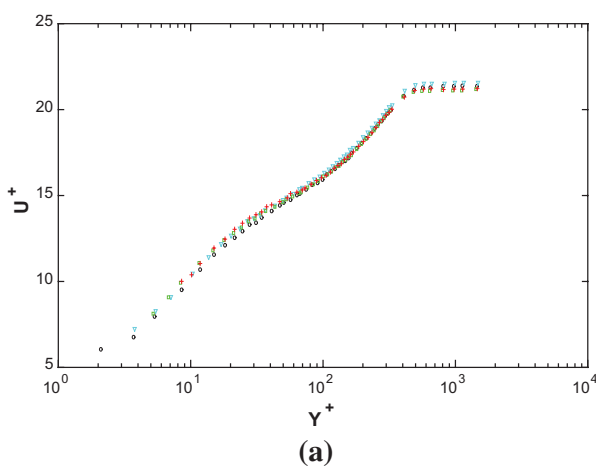

(a)

(b)

Fig. 8 Mean velocity profile at **a** $Re_\theta = 1195$, **b** $Re_\theta = 3771$. *Black circles* no control, *blue triangles* cavity array 1, *green squares* cavity array 2, *plus symbols* cavity array 3
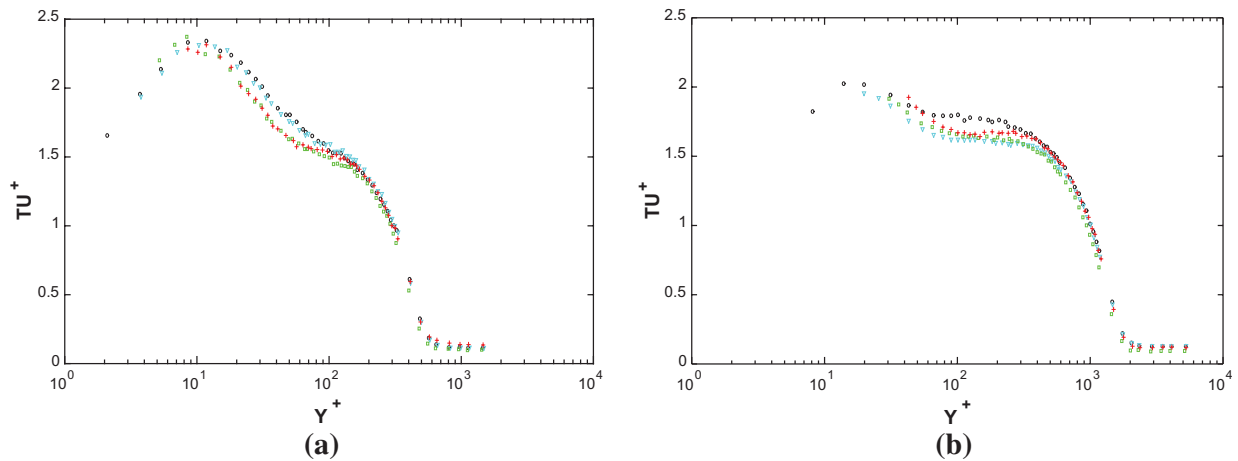
⧽ Springer

Fig. 9 Turbulence intensity profile at **a** $Re_\theta = 1195$, **b** $Re_\theta = 3771$. *Black circles* no control, *blue triangles* cavity array 1, *green squares* cavity array 2, *plus symbols* cavity array 3

cavity array 1 ($d^+ = 80$) is most successful in reducing the turbulence energy production. Furthermore, cavity array 3 is shown to cause a slight increase in turbulence intensity very close to the wall ($y^+ < 20$), which is thought to be due to the shear layer breaking apart across the larger hole diameters ($d^+ = 145$) found in this cavity array. Such a reaction would cause an increase in turbulence energy production and is deemed undesirable.

In the following sections the higher statistics of the boundary layer will be investigated including coherent structures, probability density functions (PDFs) and power spectral density (PSD) results to analyse the effect of the cavity arrays on reducing the turbulence energy production.

5 Effects of the cavity array on the coherent structures

In this study, the variable interval time-averaging (VITA) technique is used for detection of the changes in the turbulent boundary layer associated with coherent structures. The technique was initially applied by Blackwelder and Kaplan (1976) for studying the near-wall region and detecting the sweep and ejection events. The VITA analysis for the current boundary layer analysis will focus on the sweep events, since these are the major contributors to turbulent skin friction (Orlandi and Jimenez 1993). The sweep events are monitored by calculating the VITA of the streamwise velocity fluctuations according to the definition

$$\hat{u}(t, T_W) = \frac{1}{T_W} \int_{t-T_W/2}^{t+T_W/2} u(s)\,\mathrm{d}s, \tag{1}$$

where T_W is the interval used for the time averaging and is selected to be of the order of the time scale, which is typically chosen to be $T_W^+ = 10$, as selected by Blackwelder and Kaplan (1976). This value is used to assign small windows, which scan the fluctuating velocity at each point and within which the local variance of the signal is calculated using

$$\mathrm{Var}(t, T_W) = \hat{u}^2(t, T_W) - [\hat{u}(t, T_W)]^2. \tag{2}$$

The variance of the entire signal is defined as

$$\mathrm{Var}(t) = \lim_{t \to \infty} \frac{1}{t} \int_0^t u^2(t)\,\mathrm{d}t. \tag{3}$$

If the value of the local variance, $\mathrm{Var}(t, T_W)$ is greater than the variance of the entire signal $k\,\mathrm{Var}(t)$, where k is a threshold value, a sweep or ejection event is considered to have occurred. Whalley (2011) defined the detection function, $D(t)$, to differentiate between the different events, where

$$D(t) = \begin{cases} 1 & \mathrm{Var}(t, T_W) > k\mathrm{Var}(t) \ \frac{\mathrm{d}u}{\mathrm{d}t} > 0 \ (\text{sweep event}) \\ 0 & \mathrm{Var}(t, T_W) < k\mathrm{Var}(t) \ (\text{no event}) \\ -1 & \mathrm{Var}(t, T_W) > k\mathrm{Var}(t) \ \frac{\mathrm{d}u}{\mathrm{d}t} < 0 \ (\text{ejection event}). \end{cases} \tag{4}$$

The number of detected events is strongly dependent on the selected threshold value, k. In this study, the value of k was set to 1.2 as proposed by Whalley (2011). The averaged VITA events can also reveal the intensity and duration of the coherent structures. These are important as they determine the characteristics of the coherent structures and their effect on the boundary layer. The intensity of the events is calculated based on the peak-to-peak value of the

streamwise velocity of the events. The duration on the other hand is calculated from the time separation of the peaks in each VITA analysis. Increased duration or intensity of the events reveals an increase in the turbulence energy production. Throughout the investigation a total of 100–600 ensembles were used in each VITA analysis depending on which Reynolds number was examined. This occurred at a $Y^+ = 100$ for all cases investigated.

The results at $Re_\theta = 1927$ show a reduction in the intensity and duration of the sweep events downstream of all the cavity arrays investigated. Figure 10 demonstrates a 9% reduction in intensity arising from cavity arrays 1 and 3. Cavity array 2 on the other hand provided a 14% reduction in sweep intensity. The duration of $T^+ = 10$, however, is not affected significantly for any of the arrangements. Cavity arrays 1 and 3 provide similar results, which is quite surprising as cavity array 1 ($d^+ < 40$) was specifically designed for flow at $Re_\theta = 1927$, while cavity array 3 ($d^+ < 80$) had larger parameters (designed for $u_\tau = 0.24$ m/s) in comparison to the sweep events in the boundary layer. Furthermore, cavity array 2 ($d^+ < 60$) provides the largest reduction in sweep intensity of all the cavity arrays investigated. Consequently, the design guidelines described by Lockerby (2001) may not be accurate in this application, as identified earlier.

At a Reynolds number of $Re_\theta = 1195$, cavity array 3 was shown to have a greater effect in reducing the duration and intensity of the sweep events. Figure 11 demonstrates a reduction in intensity of 10.5% when using cavity array 3 ($d^+ < 40$), while the duration is unchanged. A notable difference occurs when using cavity array 1 ($d^+ < 20$), where no change occurs with regard to sweep intensity and duration, and cavity array 2 ($d^+ < 30$), where a 7% reduction in sweep intensity occurs. This result is expected as the larger holes ($d^+ = 40$) are aligned to the size of the sweep events experienced at the lower Reynolds numbers and demonstrates that the diameter and spacing of the holes are important parameters in turbulence reduction.
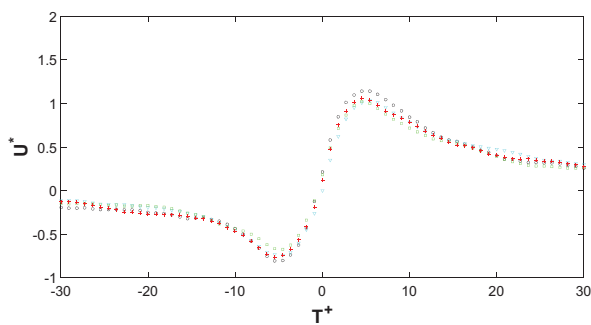

Fig. 11 Average VITA sweep events at $Re_\theta = 1195$ at $Y^+ = 100$. *Black circles* no control, *blue triangles* cavity array 1, *green squares* cavity array 2, *plus symbols* cavity array 3

At $Re_\theta = 3771$ cavity array 1 was shown to have a greater effect in reducing the duration and intensity of the sweep events in comparison to cavity arrays 2 and 3. Figure 12 shows a maximum reduction in intensity of 10.5% when using cavity array 1, whilst the reduction that occurs when using cavity arrays 2 and 3 differs as the intensity was reduced by only 9 and 2%, respectively. This reduction is expected once again as the smaller holes ($d^+ = 70$) are aligned to sizes of the sweep events experienced at the higher Reynolds numbers. Cavity array 2 is also shown to provide a substantial reduction, at $Re_\theta = 3771$ in addition to the reduction values experienced at the other Reynolds numbers investigated (7 and 14%). Cavity array 3 is shown to provide a reduction much smaller than the values documented at the lower Reynolds numbers (10.5 and 9%). This could be caused by the breaking up of the shear layer of the orifice. The larger Reynolds number has caused the shear layer to break apart more violently, which results in an increase in turbulence energy. This would effectively mitigate any reduction achieved by absorbing the sweep events and consequently decreases the overall turbulence reduction.

Fig. 10 Average VITA sweep events at $Re_\theta = 1927$ at $Y^+ = 100$. *Black circles* no control, *blue triangles* cavity array 1, *green squares* cavity array 2, *plus symbols* cavity array 3
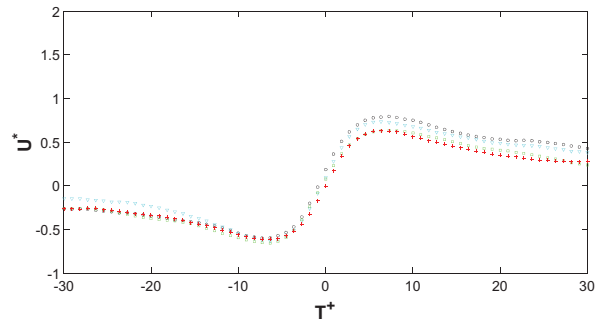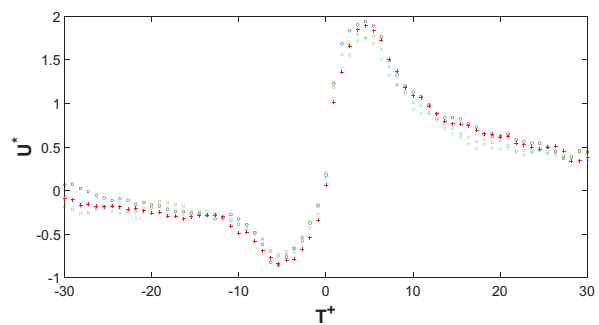

Fig. 12 Average VITA sweep events at $Re_\theta = 3771$ at $Y^+ = 100$. *Black circles* no control, *blue triangles* cavity array 1, *green squares* cavity array 2, *plus symbols* cavity array 3

6 Energy spectra and probability density function

The energy spectrum is able to provide information on the turbulence intensity, where the area under each curve is equivalent to the turbulence intensity squared. The energy spectra at the three different flow speeds have also been investigated. The locations have all been selected to be below $y^+ = 200$, as it is expected that the majority of the turbulence energy is produced in this region. Each energy spectrum was shown to have a peak at approximately 2–2.5 kHz. This peak is associated with the electronic noise from the instrumentation including the IFA 300 CTA system. As shown in Fig. 13, the energy spectra at $Re_\theta = 1927$ shows a small reduction of up to 2 dB for all of the cavity arrays. The decrease is shown to be most profound in the low-frequency range ($f < 100$ Hz), representing a decrease in the large-scale turbulence eddies. The reduction is still noticeable in the high-frequency range (small-scale eddies), which would suggest that the small-scale sweep events are absorbed by the cavity array. However, in the low-frequency range, the reduction in turbulent energy is most likely a result of the bursting process being broken apart due to the reduction in the coherent structures.

The results in Fig. 14 show that downstream of cavity arrays 2 and 3 the energy spectra decrease across the frequency range above 200 Hz when $Re_\theta = 1195$. There is a slight increase, however, across the frequency below this point. Cavity array 1 on the other hand appears to have no effect on the energy spectra. This is to be expected as it is consistent with results shown throughout this paper at this particular Reynolds number. When investigating $Re_\theta = 3771$ the results in Fig. 15 show a similar trend as shown throughout this paper at this particular Reynolds number. Once again the low-frequency energy spectrum is reduced by the largest amount, where cavity array 1 and 2 are able to provide a greater reduction in comparison to cavity array 3. As discussed earlier, this is to be expected as at the higher Reynolds number the shear layer will break
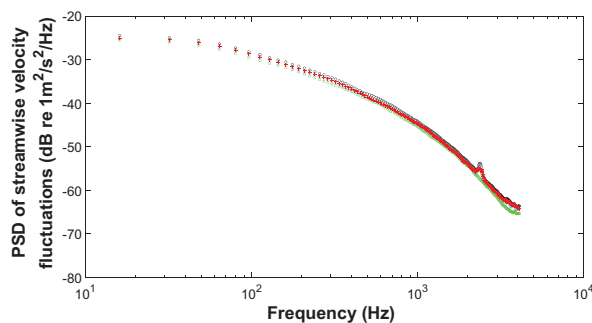

Fig. 14 Average energy spectra at $Re_\theta = 1195$, $y^+ = 100$. *Black circles* no control, *blue triangles* cavity array 1, *green squares* cavity array 2, *plus symbols* cavity array 3

apart while traversing the large orifices found in cavity array 3. Consequently, any turbulence energy reduction is mitigated by the increased turbulence production due to the shear layer breaking apart.

The probability density function (PDF) was also investigated to provide information on the skewness and Kurtosis of the data obtained. Skewness is the measure of symmetry, while Kurtosis is the measure of whether the data are peaked or flat. These profiles are deemed important as they provide a strong indication of whether the near-wall structures have been modified. Figure 16 shows the PDF at $y^+ = 100$ at $Re_\theta = 1927$. The cavity arrays were shown to have little effect on the probability density functions; however, all arrays did achieve a small reduction. Cavity array 1 reduced the skewness and kurtosis by 7.5 and 5.9%, respectively, while the results for cavity array 2 indicate a reduction in skewness and kurtosis by 5.2 and 4%, respectively, and cavity array 3 demonstrated a reduction in skewness and kurtosis by 7 and 6.4%, respectively.

Small reductions were also observed at the other flow speeds investigated. Once again similar trends occurred as discussed throughout this paper, where cavity array 3 was more successful in changing the boundary layer at low

Fig. 13 Average energy spectra at $Re_\theta = 1927$, $y^+ = 100$. *Black circles* no control, *blue triangles* cavity array 1, *green squares* cavity array 2, *plus symbols* cavity array 3
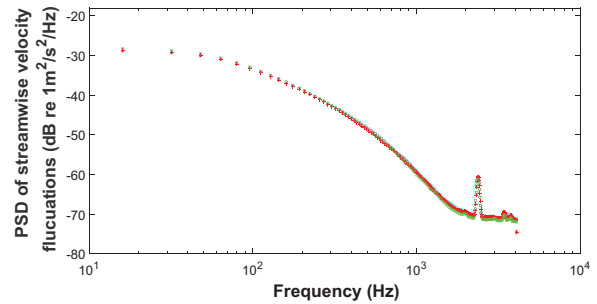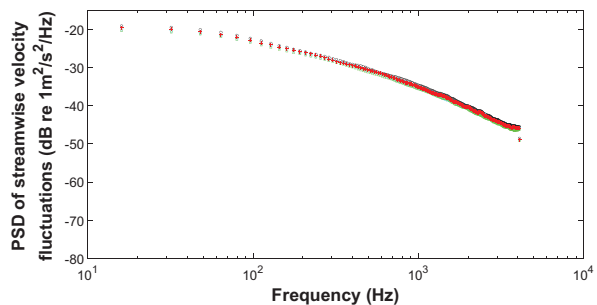

Fig. 15 Average energy spectra at $Re_\theta = 3771$, $y^+ = 100$. *Black circles* no control, *blue triangles* cavity array 1, *green squares* cavity array 2, *plus symbols* cavity array 3
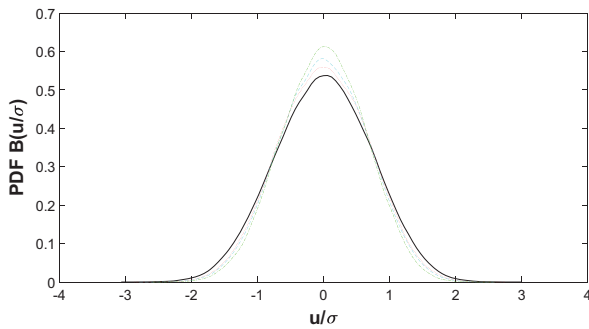
Fig. 16 Probability density function at $Re_\theta = 1927$, $y^+ = 100$. *Black* no control, *blue* cavity array 1, *green* cavity array 2, *red* cavity array 3

Reynolds number, while cavity array 1 had more success at the larger Reynolds number. For $Re_\theta = 1195$ (Fig. 17a) cavity array 3 provided reductions in skewness and kurtosis by 18 and 12%, respectively. Cavity array 1 on the other hand was only able to provide reductions in skewness and kurtosis by 5%, while cavity array 2 provided reductions in skewness and kurtosis by 15 and 11%, respectively. At $Re_\theta = 3771$ (Fig. 17b) cavity array 1 provided reductions in skewness and kurtosis by 17 and 10%, respectively, while cavity array 2 and 3 could only manage reductions by 11.8 and 7.3, and 6.8 and 4%, respectively. These changes in the skewness and kurtosis of the boundary layer are a strong indication that the coherent structures have been modified by the use of the cavity arrays.

7 Discussion

As shown throughout this paper, the use of micro-cavities had a significant effect in reducing the turbulence energy production of the boundary layer. The results from the streamwise measurements indicate a reduction through the turbulence intensity results and based on this a turbulence production reduction occurs; however, as the wall-normal component are not measured and beyond the scope of this paper no values are reported. It was initially hypothesised that the cavities would operate by capturing the sweep events and disrupt the overall bursting process in the boundary layer. At a Reynolds number of $Re_\theta = 1195$, it was shown that cavity array 3 ($d^+ = 40$) was more successful in reducing the turbulence and sweep intensity in the boundary layer than cavity arrays 1 and 2 which had a diameter of $d^+ = 20$ and $d^+ = 30$, respectively. This difference in size was shown to have a significant effect on sweep intensity reduction, as cavity arrays 2 and 3 provided reductions of 7 and 10.5%, respectively, while the effect of cavity array 1 was negligible. This difference is hypothesised to be related to the diameter of the holes in
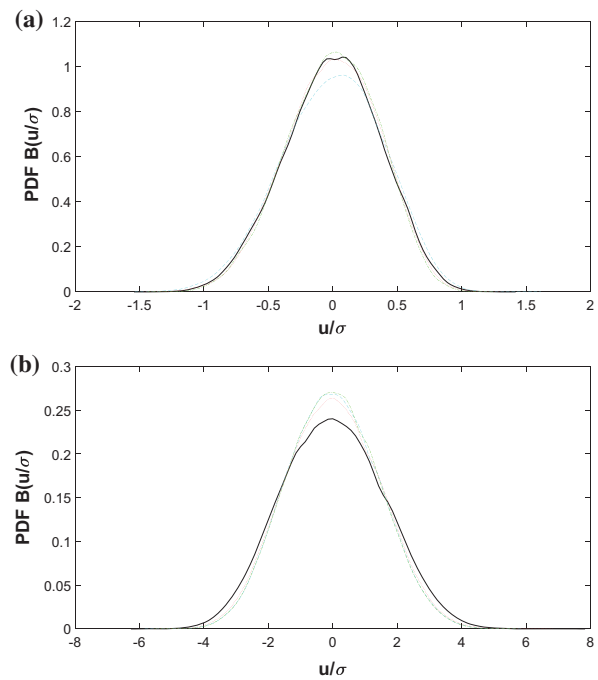

Fig. 17 Probability density function at **a** $Re_\theta = 1195$, $y^+ = 100$, **b** $Re_\theta = 3771$, $y^+ = 100$. *Black* no control, *blue* cavity array 1, *green* cavity array 2, *red* cavity array 3

comparison to the estimated size of the sweep events. By choosing a diameter that is too small, as demonstrated by cavity array 1, the sweep events are restricted in entering the cavity array and consequently no disruption of the bursting phenomenon occurred. With this in mind, however, the cavity array cannot be too large, since when the diameter of the holes becomes too large the shear layer is more prone to break apart and cause an increase in turbulence energy production. This was shown to occur at a Reynolds number of $Re_\theta = 3771$ where cavity arrays 1 ($d^+ = 70$) and 2 ($d^+ = 105$) were more successful in reducing the turbulence and sweep intensity in the boundary layer than for increased diameter of $d^+ = 145$ (cavity array 3). It can be seen that the diameter of cavity array 3 at this particular Reynolds number is excessively large, and the results indicate an enormous reduction in the control of the boundary layer, as opposed to the other Reynolds numbers. The turbulence intensity profile shows a small increase in turbulence energy very close to the wall for cavity array 3. This increase can be associated with a breakdown of the shear layer whilst traversing the large orifice of cavity array 3. The result of this shear layer breaking down causes an increase in the turbulence energy close to wall, whilst a minor reduction is maintained further away in the logarithmic region. However, the boundary layer has still been adversely affected in the near-wall

region, which causes a much smaller value of sweep intensity reduction when comparing the sweep intensity reduction values. Unlike the low Reynolds number results, for $Re_\theta = 3771$ the sweep intensity was reduced by only 2% by cavity array 3, as opposed to cavity arrays 1 and 2 which produced superior values of 10.5 and 9%, respectively.

Collating all the results, Fig. 18 can be used to demonstrate the relationship between orifice diameter and sweep intensity reduction. Figure 18 clearly demonstrates an optimal value of $d^+ \approx 60$ will yield the greatest reduction in the sweep intensity profile. The graph also demonstrates that the other aspects of the hypothesis are supported by the data. When $d^+ < 30$ the orifice of the cavities is too small to allow the sweep events to be entrained into the cavity array and consequently no reduction is achieved. When $d^+ > 105$ the orifice of the cavities becomes too large and therefore the boundary layer breaks apart while traversing the orifice and the consequent break-up of the shear layer causes an increase in turbulence energy. This results in the overall sweep intensity reduction being less than the optimal value. The figure itself does show a couple of outliers and this is expected. The sweep events are chaotic by nature and consequently it is expected that the sweep reduction values will vary somewhat between measurements. This is mitigated as much as possible by taking averaged VITA results.

The outliers in Fig. 18 are also due to the manufacturing quality of the three cavity arrays. As discussed previously in this paper the microscope images of the three cavity arrays revealed small inconsistencies with each of their geometries. Roughness and surface finish in the holes may provide a blockage when sweep events enter each orifice and consequently the sweep reduction will be affected. The two arrays which appear to be affected the most by poor surface finish are cavity arrays 1 and
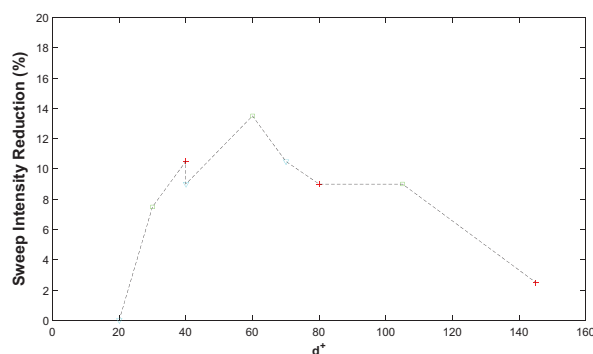
3. The chaotic nature of the sweep events combined with the manufacturing quality of the cavity arrays will affect the overall results.

8 Summary and conclusion

In this study, three plates containing cavity arrays of different geometries were considered, at a variety of Reynolds numbers. The characteristics of the boundary layer were analysed using hot-wire anemometry downstream of each of the cavity arrays, and the results were used to calculate the streamwise boundary layer profile, the properties of the coherent structures, the energy spectrum and the probability density functions.

The results from this study indicated different parameters to consider when implementing the cavity array as a potential technique to control the boundary layer. From the data a cavity orifice diameter equal to or less then $d^+ = 20$ is undesired. Such a small orifice will cause the sweep events to be restricted and no events will be captured by the array. However, if the diameter of the orifice is too large an even more undesirable effect will occur and result in an increase in turbulence energy production in the near-wall region. Consequently, it is recommended that the orifice diameter be below $d^+ = 145$, as values higher than this will cause the shear layer to break apart violently and increase the turbulence production in the near-wall region. The results also showed that the optimal value for maximum turbulence energy and sweep attenuation occurs at $d^+ = 60$.

The conclusions drawn here are based on the results downstream of the three cavity arrays investigated. Future work intends to focus more intently on the optimal diameter of the orifice at which the most reduction can be achieved. Further work also needs to be expanded on analysing the physical mechanism by which the reduction is achieved. This could include velocity measurements below the cavity arrays and microphone measurements within the cavity to provide stronger evidence into what is being captured by the arrays. The results presented here are only the beginning of the development of the knowledge required for this area of work.

Fig. 18 Average VITA sweep event intensity reduction with respect to the orifice diameter at $Y^+ = 100$. *Blue triangles* cavity array 1, *green squares* cavity array 2, *plus symbols* cavity array 3

References

Blackwelder RF, Eckelmann H (1979) Streamwise vortices associated with the bursting phenomenon. J Fluid Mech 94:577–594

Blackwelder RF, Kaplan RE (1976) On the wall structure of the turbulent boundary layer. J Fluid Mech 76(part 1):89–112

Chang K, Constantinescu G, Park SO (2006) Analysis of the flow and mass transfer processes for the incompressible flow past an open

cavity with a laminar and a fully turbulent incoming boundary layer. J Fluid Mech 561:113–145

Choi KS (1987) On physical mechanism of turbulent drag reduction using riblets. Transport Phenomena in Turbulent flows, Hemisphere Publishing Corp, New York, pp 185–198

Choi KS (1989) Near-wall structure of a turbulent boundary layer with riblets. J Fluid Mech 208:417–458

Choi KS, Fujisawa N (1993) Possibility of drag reduction using d-type roughness. Appl Sci Res 50:315–324

Choi KS, Graham M (1998) Drag reduction of turbulent pipe flows by circular-wall oscillation. Phys Fluids 10(1):7–9

Choi KS, Jukes T, Whalley R (2011) Turbulent boundary-layer control with plasma actuators. Philos Trans R Soc A 369:1443–1458

Clauser FH (1954) The turbulent boundary layer. Adv Appl Mech IV:1–51

Corino ER, Brodkey RS (1969) A visual investigation of the wall region in turbulent flow. J Fluid Mech 37(part. 1):1–30

Ghanadi F (2014) Application of a Helmholtz resonator excited by grazing flow for manipulation of a turbulent boundary layer, PhD thesis. School of Mechanical Engineering, University of Adelaide, Australia

Ghanadi F, Arjomandi M, Cazzolato BS, Zander AC (2015) Analysis of the turbulent boundary layer in the vicinity of a self-excited cylindrical Helmholtz resonator. J Turbul 16:705–728

Hooshmand D, Youngs R, Wallace JM (1983) An experimental study of changes in the structure of a turbulent boundary layer due to surface geometry changes. AIAA, Paper 83-0230

Kendall A, Koochesfahani M (2006) A method for estimating wall friction in turbulent boundary layer. In: 25th AIAA aerodynamic measurement technology and ground testing conference. 5–8 June 2006, San Francisco, California, USA

Kim HT, Kline SJ, Reynolds WC (1971) The production of turbulence near a smooth wall in a turbulent boundary layer. J Fluid Mech 50(part. 1):133–160

Lockerby D (2001) Numerical simulation of boundary-layer control using MEMS actuation, PhD thesis. The University of Warwick, England, UK

Maa DY (1998) Potential of microperforated panel absorber. J Acoust Soc Am 104(5):2861–2866

Marusic I, Kunkel GJ (2003) Streamwise turbulence intensity formulation for flat-plate boundary layers. Phys Fluids 15(8):2461–2464

Offen GR, Kline SJ (1975) A proposed model of the bursting process in turbulent boundary layers. J Fluid Mech 70(part. 2):209–228

Orlandi P, Jimenez J (1993) On the generation of turbulent wall friction. Phys Fluids 6:634–641

Patterson GK, Chosnek J, Zakin JL (1977) Turbulence structure in drag reducing polymer solutions. Phys Fluids 20:S89–S99

Robinson SK (1991) Coherent motions in the turbulent boundary layer. Annu Rev Fluid Mech 23:601–639

Sarohia V (1977) Experimental investigation of oscillations in flows over shallow cavities. AIAA J 15(7):984–991

Savins JG, Seyer FA (1977) Drag reduction scale-up criteria. Phys Fluids 20:S78–S84

Schlatter P, Orlu R (2010) Assessment of direct numerical simulation data of turbulent boundary layers. J Fluid Mech 659:116–126

Silvestri A, Ghanadi F, Arjomandi M, Cazzolato BS, Zander AC (2017) The application of different tripping techniques to determine the characteristics of the turbulent boundary layer over a flat plate. ASME J Fluid Eng (submitted)

Smith BL, Glezer A (1998) The formation and evolution of synthetic jets. Phys Fluids 10:2281–2297

Wallace JM, Eckelmann H, Brodkey RS (1972) The wall region in turbulent shear flow. J Fluid Mech 54:39–48

Walsh MJ (1983) Riblets as a viscous drag reduction technique. AIAA Journal 21(4):485–486

Whalley RD (2011) Turbulent boundary-layer control with DBD plasma actuators using spanwise travelling-wave technique, PhD thesis. The University of Nottingham, England, UK

Chapter 5

The effect of orifice length and backing volume on the attenuation of coherent events

5.1 Paper 3: Attenuation of turbulence by the passive control of sweep events in a turbulent boundary layer using micro-cavities

This chapter analyses the flow over an array of applied micro-cavities using hotwire anemometry in a wind tunnel. The sensitivity of the flushed-surface cavity array in reducing the turbulent energy production is investigated by varying the thickness and backing cavity volumes of the array. This is important as the geometry investigated in this chapter determines what happens to the events once captured by the cavity array and is used to support the hypothesis of the previous chapter. In addition, the mechanism behind the observed sweep attenuation is considered. While this mechanism is not definitively identified, significant steps were made in understanding the micro-cavity as a flow control technique, which was previously absent in the previous chapter.

The volume of the backing cavity was shown to be the most important parameter in determining the attenuation of streamwise velocity fluctuations within the logarithmic region of the turbulent boundary layer, where it was found the orifice length of the cavity array had a negligible effect on the performance of the cavity array in controlling the boundary layer.

The results presented in this chapter show that the maximum reduction in turbulence generation was achieved when the backing volume was at its largest, namely 3.1×10^6 times greater than the viscous length scale at $\mathrm{Re}_\theta = 3771$. The reduction in turbulence intensity, sweep intensity and energy spectrum was shown to be 5.6%, 6.3% and 13.4% respectively for this backing cavity volume.

Furthermore, when the cavity volume was reduced to zero, the turbulent boundary layer turbulence statistics were found to be the same as the baseline statistics. Consequently, this chapter illustrates that a greater reduction in turbulence intensity, sweep intensity and energy spectrum can be achieved using a larger backing volume.

Chapter 6 consequently attempts to explain the mechanism of the weakening of the coherent structures in the turbulent boundary layer. In addition the next chapter also aims to determine the maximum backing cavity volume to achieve the largest possible reduction in turbulence generation.

This chapter has been published as:

Silvestri, A, Ghanadi, F, Arjomandi, M, Chin, R, Cazzolato, BS, Zander, AC, 2017,

'Attenuation of turbulence by the passive control of sweep events in a turbulent boundary layer using micro-cavities', Physics of Fluids, vol. 29, pp. 115102*.*

Statement of Authorship

Title of Paper	Attenuation of turbulence by the passive control of sweep events in a turbulent boundary layer using micro-cavities
Publication Status	☑ Published ☐ Accepted for Publication ☐ Submitted for Publication ☐ Unpublished and Unsubmitted w ork w ritten in manuscript style
Publication Details	Silvestri, A, Ghanadi, F, Arjomandi, M, Chin, R, Cazzolato, BS, Zander, AC, 2017, *'Attenuation of turbulence by the passive control of sweep events in a turbulent boundary layer using micro-cavities', Physics of Fluids,* vol. 29, pp. 115102*.

Principal Author

Name of Principal Author (Candidate)	Anton Silvestri		
Contribution to the Paper	Performed data analysis and interpretation, wrote manuscript and acted as corresponding author.		
Overall percentage (%)	70		
Certification:	This paper reports on original research I conducted during the period of my Higher Degree by Research candidature and is not subject to any obligations or contractual agreements with a third party that would constrain its inclusion in this thesis. I am the primary author of this paper.		
Signature		Date	15/06/18

Co-Author Contributions

Name of Co-Author	Farzin Ghanadi		
Contribution to the Paper	Supervised the development of the research and contributed in academic discussion and the review process of submitted manuscripts.		
Signature		Date	15/06/18

Name of Co-Author	Maziar Arjomandi		
Contribution to the Paper	Supervised the development of the research and contributed in academic discussion and the review process of submitted manuscripts.		
Signature		Date	15/06/18

Name of Co-Author	Rey Chin		
Contribution to the Paper	Supervised the development of the research and contributed in academic discussion and the review process of submitted manuscripts.		
Signature		Date	15/06/18

Name of Co-Author	Benjamin Cazzolato		
Contribution to the Paper	Supervised the development of the research and contributed in academic discussion and the review process of submitted manuscripts.		
Signature		Date	15/06/18

Name of Co-Author	Anthony Zander		
Contribution to the Paper	Supervised the development of the research and contributed in academic discussion and the review process of submitted manuscripts.		
Signature		Date	15/06/18

Attenuation of turbulence by the passive control of sweep events in a turbulent boundary layer using micro-cavities

Anton Silvestri,[a] Farzin Ghanadi,[b] Maziar Arjomandi,[c] Rey Chin,[d] Benjamin Cazzolato,[e] and Anthony Zander[f]

School of Mechanical Engineering, University of Adelaide, Adelaide, South Australia 5005, Australia

Cavity arrays have been previously identified to disrupt the sweep events and consequently the bursting cycle in the boundary layer by capturing the structures responsible for the Reynolds stresses. In the present study, the sensitivity of a flushed-surface cavity array in reducing the turbulent energy production has been investigated. Two plates of varying thicknesses and four different backing cavity volumes were considered, at three different Reynolds numbers. The volume of the backing cavity was shown to be the most important characteristic in determining the attenuation of streamwise velocity fluctuations within the logarithmic region of the turbulent boundary layer. However, the results also demonstrated that the orifice length of the cavity array had negligible effect in modifying the reduction of the turbulent energy by the cavity array in this investigation. The results show that the maximum reduction in turbulence generation achieved for this study occurs when the backing volume is 3.1×10^6 times greater than the viscous length scale at $Re_\theta = 3771$. The reduction in turbulence intensity, sweep intensity, and energy spectrum were shown to be 5.6%, 6.3%, and 13.4%, respectively. By decreasing the cavity volume to zero, no change in the turbulent boundary layer turbulence statistics was found. The results suggest a larger reduction in turbulence intensity, sweep intensity, and energy spectrum that can be achieved with a larger backing volume. *Published by AIP Publishing.* https://doi.org/10.1063/1.4995466

NOMENCLATURE

$B(\sigma)$ = probability density function of streamwise velocity
c_f = skin friction coefficient
d = cavity diameter (mm)
k = variable-interval time-averaging (VITA) threshold
K = streamwise wavenumber
λ = streamwise wavelength
Ψ = pre-multiplied energy spectrum
Re_{u_τ} = Reynolds number based on friction velocity
Re_θ = Reynolds number based on momentum thickness
t = time (s)
T_{av} = averaging duration (s)
T_W = window length (s)
TU = turbulence intensity
L = orifice length (mm)
u = streamwise flow velocity (m/s)
u_τ = friction velocity (m/s)
V = backing cavity's volume (m^3)
Var = variance
x = indicates x-direction (streamwise) (m)
y = indicates y-direction (wall-normal direction) (m)
z = indicates z-direction (spanwise) (m)

Symbols

σ = standard deviation
δ = boundary layer thickness (mm)
δ^+ = displacement thickness (mm)
θ = momentum thickness (mm)
ν = kinematic viscosity (m/s^2)

Superscripts

$+$ = denotes viscous time scale $\left(\frac{\nu}{u_\tau^2}\right)$ or viscous length scale $\left(\frac{\nu}{u_\tau}\right)$

I. INTRODUCTION

The coherent structures are a vital part of the boundary layer and therefore skin friction drag. These structures pump high speed fluid toward (sweep) and slow speed fluid away (ejection) from the wall. Ejection events generate approximately 70% of the total stresses in the inner wall region, while sweep events account for the remaining 30% (Offen and Kline, 1975 and Kim *et al.*, 1971) and consequently are deemed to be very important during turbulence generation. These events have been shown to be highly regenerative, and as a result disrupting one of these coherent structures will have a substantial effect on the opposing structure and subsequently the overall skin friction drag value in the boundary layer (Whalley, 2011). Consequently, many have targeted these coherent structures for a reduction in turbulence generation within the turbulent boundary layer. Such studies include, but not limited to, the

[a] anton.silvestri@adelaide.edu.au
[b] farzin.ghanadi@adelaide.edu.au
[c] maziar.arjomandi@adelaide.edu.au
[d] rey.chin@adelaide.edu.au
[e] benjamin.cazzolato@adelaide.edu.au
[f] anthony.zander@adelaide.edu.au

oscillating wall techniques that have been shown to be capable of reducing the skin friction drag by 45% (Choi and Graham, 1998), traveling wave techniques which are capable of reducing the sweep duration and intensity by 35% (Choi *et al.*, 2011), and the synthetic jet recently used by Lockerby (2001), which was shown to be successful in disrupting the sweep and ejection events.

Nevertheless, passive techniques are preferred for real life applications due to their ease of implementation from requiring no external power. One of the most successful passive techniques is the application of streamwise riblets (Walsh, 1983; Choi, 1987; 1989; and García-Mayoral and Jiménez, 2011). Streamwise riblets are small channels along the spanwise direction, aligned in the flow direction, which restrict the streamwise. This technique was shown to be successful in reducing the skin friction drag by 8% (Walsh, 1983). Another passive technique is the flow excited Helmholtz resonator previously studied by Ghanadi *et al.* (2014a; 2014b) to target the coherent structures. The results showed that within the logarithmic region an 11% and 5% reduction in the intensity and duration of the sweep events could be achieved. However, results from Ghanadi (2014b) suggested a possible reduction in the intensity and duration by 5% and 8%, respectively, even when the resonator was not activated by the grazing flow. Choi and Fujisawa (1993) also established an equivalent effect on the boundary layer by using a square cavity. A net drag reduction of 1% could be achieved over the square cavity and lasted for 100 cavity diameters downstream of its leading edge. These findings lead to the possibility of using a cavity array as a possible passive control technique (Blackwelder and Eckelmann, 1979; Corino and Brodkey, 1969; Guo *et al.*, 2010; Orlandi and Jimenez, 1993; and Wallace *et al.*, 1972).

A significant amount of research has been conducted by Silvestri *et al.* (2016; 2017a; and 2017b) to successfully implement a micro-cavity array for passive flow control. This technique was shown to have significant potential for turbulence energy reduction and was found to be an extension to Maa's (1998) work, who previously utilised the idea to absorb sound. Results by Silvestri *et al.* (2017a) showed a successful maximum reduction in the turbulence and sweep intensity by 13% and 14%, respectively. It was hypothesised that the array would capture the sweep events and disrupt the bursting cycle, which is responsible for the shear stress and hence the viscous drag. Boundary layer control using the cavity array will aim to target the component of velocity traveling normal to the wall, but the exact mechanism for the reduction is yet to be found. While the previous article from Silvestri *et al.* (2017a) focused on the external properties of the cavity array, including the array's orifice diameter and spanwise spacing, the internal geometry of the cavity array including the volume and orifice length was not investigated. Early findings suggested the volume underneath of the flushed-surface cavity array is of significant importance, as it alters the overall reduction of sweep and turbulence intensity that the technique was capable of producing (Silvestri *et al.*, 2017b). Consequently, it was hypothesised that the cavity array was capturing sweep events and weakening the structure of each event by dampening the energy of the events by the friction loses through the

cavity array and the large volume of the backing cavity below the array itself. The previous investigation was quite limited and did not provide a reliable scope to confirm this initial finding, while in addition did not investigating the effect of orifice length's effect on the turbulent boundary layer control.

Therefore, the motivation of this research is to provide an insight into the possible cause of the turbulence and sweep intensity using micro-cavities. The present work provides an assessment of the efficacy of micro cavities arrays to reduce the turbulence properties of varying Reynolds numbers (1927 $\leq Re_\theta \leq 3771$) by varying a number of key parameters, including the cavity array orifice length as well as the volume of the backing cavity. The characteristics of the array will be presented and details of the experimental setup will be discussed in Secs. II–VI.

II. EXPERIMENTAL SETUP

Experiments were undertaken at the University of Adelaide in a closed-loop wind tunnel, with a turbulence intensity of 0.5%. The test section used had a square cross section of 0.5 m × 0.5 m and 2 m in length. A 2 m long plate (Fig. 1) was installed in the tunnel such that the plate spanned the whole working section. Due to bluff body separation effects, a super-elliptical edge of a nominal major radius of 114 mm was mounted to the leading edge of the flat plate. In addition, a circulation flap was also mounted to the trailing edge of the plate to minimize any circulation developed over the plate. The walls of the test section were also adjusted as appropriate to result in a zero-pressure gradient for all cases investigated. All boundary layers examined in the study were tripped using a 3 mm rod edge to ensure a fully turbulent boundary layer, as recommended by Silvestri *et al.* (2017c).

Hot-wire anemometry was used to characterize the changes in the structures within the boundary layer due to the cavity array. The hot-wire was located 180 mm downstream from the leading edge of the array being investigated. This location was selected as it was close to the trailing edge of the array where the maximum effect was recorded (Silvestri *et al.*, 2016). The experimental measurements were made with a TSI IFA 300 CTA system, using a single platinum-plated tungsten wire of 5 μm in diameter and 1.25 mm in length. The over-heat ratio was selected to be 1.8, while the operating temperature was 230 °C. This provided sufficient sensitivity as discussed by Silvestri *et al.* (2017a). Each measurement was repeated three times at 20 × 10³ Hz for 15 s to ensure repeatability. This equates a sample interval of 0.83 < Δt^+ < 2.82, which exceeds the minimum time scale for energetic turbulent fluctuations ($t^+ \approx 3$) (Hutchins *et al.*, 2009). Furthermore, the sampling frequency is approximately 100 times the frequency of the bursting events ($f^+ = 0.04$) as defined by Blackwelder and Haritonidis (1983), aliasing was not a problem, as previously discussed by Silvestri *et al.* (2016).

To investigate the geometry of the cavity array's effect on the turbulent boundary layer, two arrays were constructed (Fig. 2). The cavity arrays were aligned with the streamwise direction and were designed for a Reynolds number equal to $Re_\theta = 1.93 \times 10^3$, where $Re_\theta = \frac{u\theta}{\nu}$ (Silvestri *et al.*, 2017a).
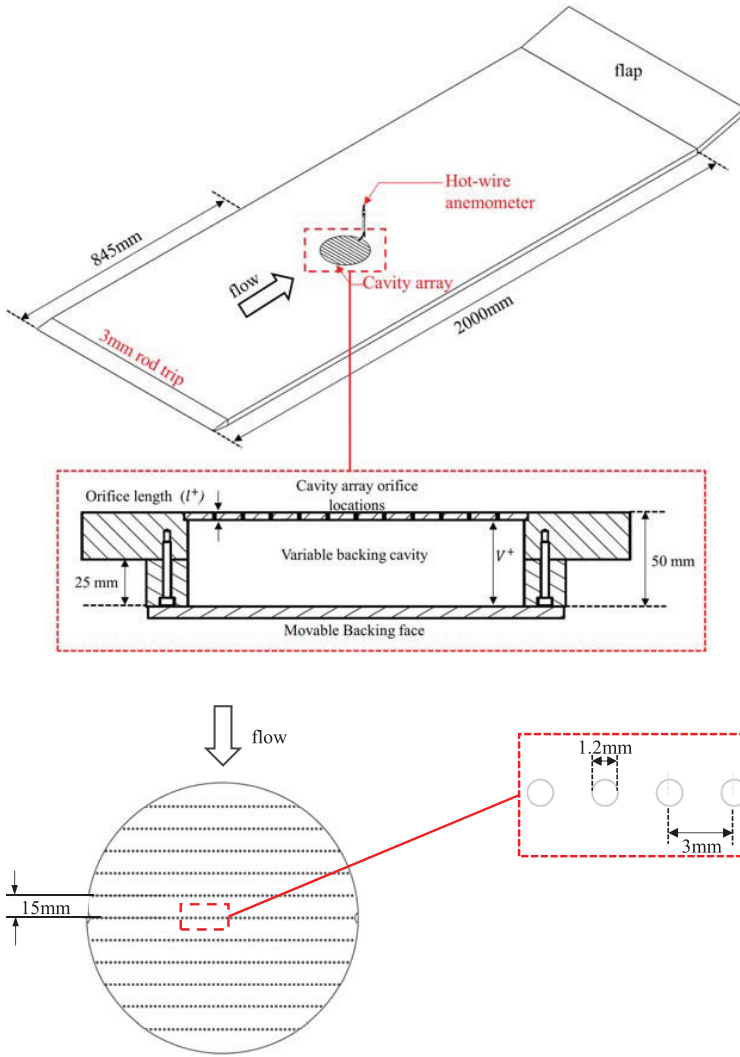
FIG. 1. Schematic of the experimental arrangement.

FIG. 2. Schematic of cavity arrays (Silvestri *et al.*, 2017a).

The dimensions of the array were calculated by the method specified by Lockerby (2001), Silvestri *et al.* (2016), and Silvestri *et al.* (2017a). This resulted in a cavity array with an orifice diameter of 1.2 mm, a streamwise space of 15 mm between each row of cavities, and a spanwise space of 3 mm between each column of cavities. The specific calculations are extensively detailed in Silvestri *et al.* (2017a). Furthermore, the cavity array plates were manufactured with one plate having an orifice length of 4 mm and the other selected to be 2 mm, as detailed in Table I.

For this paper, four different backing cavities were investigated, as detailed in Table I. This was achieved by using backing faces with different geometries to restrict the total volume of the backing cavity. This equated to backing cavity depths of 0 mm, 5 mm, 25 mm, and 50 mm.

To ensure the accuracy of the hotwire anemometry system, a comparison with previously published data has also been included. Figure 3 shows the non-dimensional mean velocity profile at $Re_\theta = 3771$, which has been compared against Marusic and Kunkel (2003), Schlatter and Orlu (2010), and

TABLE I. Summary of cavity volume (V+) and orifice length parameters (l+) used in the investigation.

|	V^+ at Re_θ = 1927	V^+ at Re_θ = 2939	V^+ at Re_θ = 3771	l^+ at Re_θ = 1927	l^+ at Re_θ = 2939	l^+ at Re_θ = 3771
2 mm orifice length	1.4×10^6	1.9×10^6	3.1×10^6	67	81	123
4 mm orifice length	1.4×10^6	1.9×10^6	3.1×10^6	133	162	245
0 mm backing cavity depth	0	0	0	133	162	245
5 mm backing cavity depth	1.4×10^5	1.9×10^5	3.1×10^5	133	162	245
25 mm backing cavity depth	7×10^5	9.6×10^5	1.5×10^6	133	162	245
50 mm backing cavity depth	1.4×10^6	1.9×10^6	3.1×10^6	133	162	245
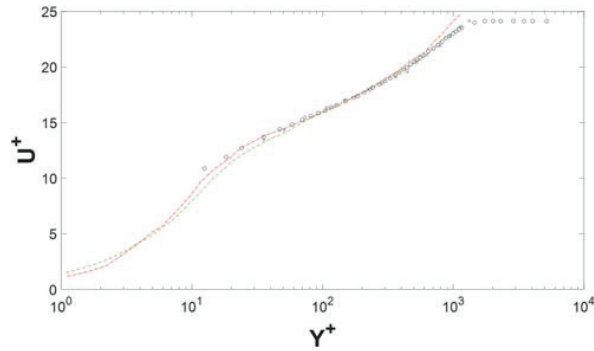
FIG. 3. Error analysis of the mean velocity profile of the boundary layer at $Re_\theta = 3771$. [o(black circles)] Experimental results in this work, [–(green)] Marusic and Kunkel (2003), [-.(red)] Schlatter and Orlu (2010) at $Re_\theta = 4064$, [×(blue)] Ghanadi *et al.* (2015) at $Re_\theta = 3920$.

Ghanadi *et al.* (2015). A maximum error of 9.2%, 7.6%, and 0.5%, respectively, occurs at the points in the viscous sub region. This small discrepancy is deemed negligible as reported by the earlier results of Silvestri *et al.* (2016; 2017a; and 2017b) where a maximum error of 1.5%, 1%, and 0.5% occurs in the logarithmic region.

The velocity measurements were non-dimensionalised for comparison using the viscous length scale $\left(\frac{\nu}{u_\tau}\right)$. The friction velocity (u_τ) was calculated via an iterative process defined by Kendall and Koochesfahani (2006) which used a varying u_τ to curve fit the logarithmic region of the experimental hot-wire data with the log law expression defined by Clauser (1956). The results were shown to provide accurate estimates with a maximum discrepancy of 0.2% (Fig. 4), the details of which can be found in Table II.
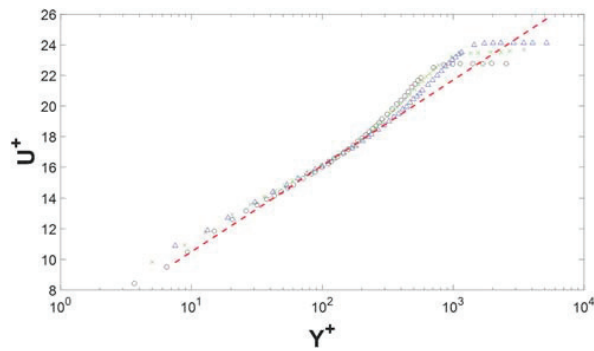
III. EFFECTS OF THE BACKING CAVITY VOLUME AND ORIFICE LENGTH ON THE STREAMWISE VELOCITY AND TURBULENCE INTENSITY PROFILE

Figure 5 shows the streamwise and turbulence intensity profiles downstream of the cavity array and the unaltered turbulent boundary layer for comparison at a Reynolds number of $Re_\theta = 1927$. Changing the depth of the backing cavity appears to have no significant effect on the streamwise mean velocity as demonstrated in Fig. 5(a) for four different cavity depths. This gives the authors confidence in using a curve fit approach to calculate the canonical friction velocity; as it appears, the logarithmic region in streamwise velocity profile is unaffected by the control method. The turbulence intensity figure on the other hand clearly shows a turbulence energy reduction [Fig. 5(b)]. The results show that at a backing cavity volume equal to $V^+ = 1.4 \times 10^6$, the maximum turbulence intensity reduction was equal to 4.2% within the logarithmic region $15 < y^+ < 200$. The volume of the backing cavity was also decreased to $V^+ = 7 \times 10^5$ and $V^+ = 1.4 \times 10^5$, where the turbulence intensity reduction values were shown to decrease to values of 3.6% and 2.7%, respectively. Furthermore, for the case of the backing cavity being removed ($V^+ = 0$), the reduction was shown to be negligible for the turbulence intensity.

The effect that the orifice length of the cavity array has on the turbulent boundary layer was also investigated for lengths of $l^+ = 67$ and $l^+ = 133$. Figure 6 shows the turbulence intensity profile at $Re_\theta = 1927$ and $V^+ = 1.4 \times 10^6$. At this Reynolds number, both arrays ($l^+ = 67$ and $l^+ = 133$) provided a turbulence intensity reduction equal to 4.2%. Unlike the sensitivity to backing cavity volume, the results

FIG. 4. Streamwise boundary layer profile at $Re_\theta = 3771$ [–(red)] log law expression defined by Clauser (1956), [o(black)] experimental results at $Re_\theta = 1927$, [×(green)] experimental results at $Re_\theta = 2939$, [Δ(blue)] experimental results at $Re_\theta = 3771$.

TABLE II. Reynolds number and boundary layer parameters.

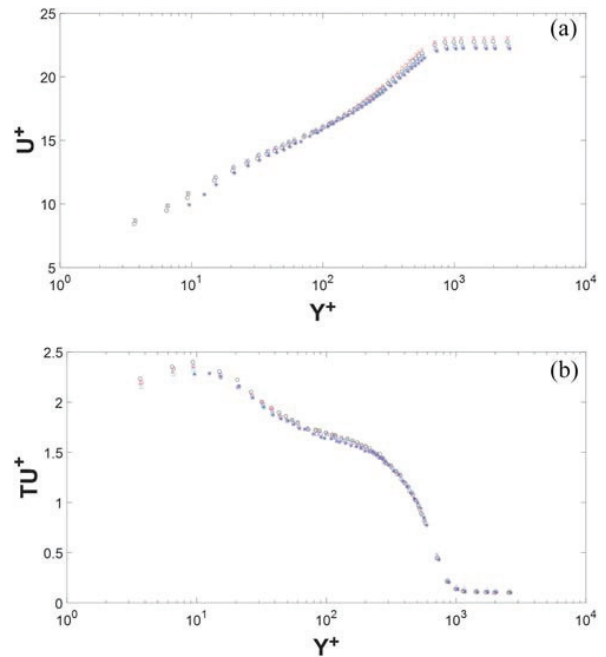|			
$Re_X \left(Re_x = \frac{ux}{\nu}\right)$	5.30×10^5	8.50×10^5	1.18×10^6
$Re_{\delta^+} \left(Re_{\delta^+} = \frac{u\delta^+}{\nu}\right)$	2521	3751	4913
$Re_\theta \left(Re_\theta = \frac{u\theta}{\nu}\right)$	1927	2939	3771
Friction velocity (u_τ)	0.50 m/s	0.61 m/s	0.92 m/s
Viscous length scale $\left(\frac{\nu}{u_\tau}\right)$	3.00×10^{-5} m	2.59×10^{-5} m	1.63×10^{-5} m

FIG. 5. (a) Mean velocity profile at $Re_\theta = 1927$ and $l^+ = 133$, (b) turbulence intensity at $Re_\theta = 1927$. [o(black)] No control, [x(red)] $V^+ = 0$, [Δ(cyan)] $V^+ = 1.4 \times 10^5$, [□(purple)] $V^+ = 7 \times 10^5$, [*(blue)] $V^+ = 1.4 \times 10^6$.
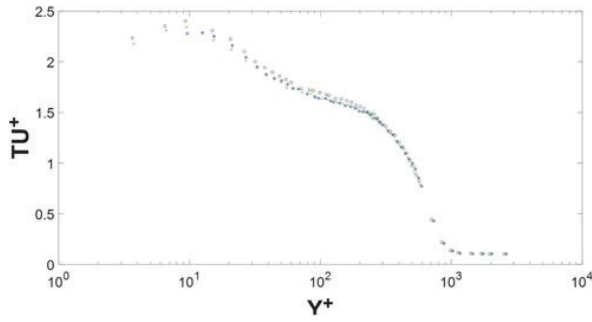
FIG. 6. Turbulence intensity at Re_θ = 1927 and V^+ = 1.4 × 10^6. [o(black)] No control, [+(green)] l^+ = 67, [*(blue)] l^+ = 133.
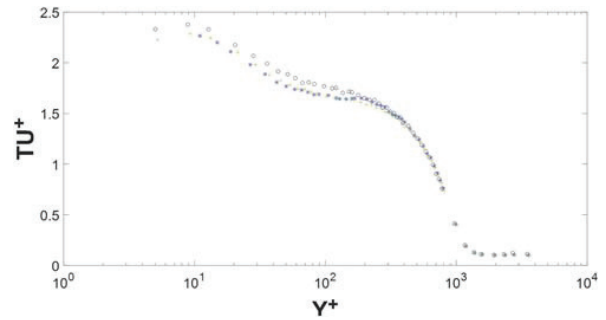

FIG. 8. Turbulence intensity at Re_θ = 2939 and V^+ = 1.9 × 10^6. [o(black)] No control, [+(green)] l^+ = 81, [*(blue)] l^+ = 162.

demonstrated that the orifice length of the cavity array had no impact on the boundary layer turbulence intensity within the range of l^+ investigated.

The turbulence intensity profiles downstream of the cavity array at Re_θ = 2939 show a clear turbulence energy reduction. Figure 7 shows that when the backing cavity was equal to V^+ = 1.9 × 10^6 the maximum turbulence intensity reduction was equal to 6.4% within the logarithmic region 30 < y^+ < 200. The backing cavity provided reduction capabilities of 3.4% and 4% at a backing cavity volume of V^+ = 1.9 × 10^5 and V^+ = 9.6 × 10^5, respectively. Furthermore, similar to the results at Re$_\theta$ = 1927, the backing cavity was removed (V^+ = 0) and the reduction disappeared and no effect was recorded.

Figure 8 shows the turbulence intensity profile at Re_θ = 2939 when investigating the length of the orifice effect on the turbulent energy reduction at V^+ = 1.9 × 10^6. Both arrays (l^+ = 81 and l^+ = 162) provided a turbulence intensity reduction equal to 6.4%.

The turbulence intensity profiles downstream of the investigated cavity array was also obtained at Re_θ = 3771. Figure 9 shows that at a backing cavity volume equal to V^+ = 3.1 × 10^6 the turbulence intensity reduction was equal to 5.6%. When the volume of the backing cavity was decreased to V^+ = 3.1 × 10^5 and V^+ = 1.5 × 10^6, the turbulence intensity reduction value was shown to decrease to values of 3% and 3.2%, respectively. Figure 10 shows the turbulence intensity profile at Re_θ = 3771 when investigating the cavity array orifice length effect on the turbulent energy reduction at V^+ = 3.1 × 10^6. Both
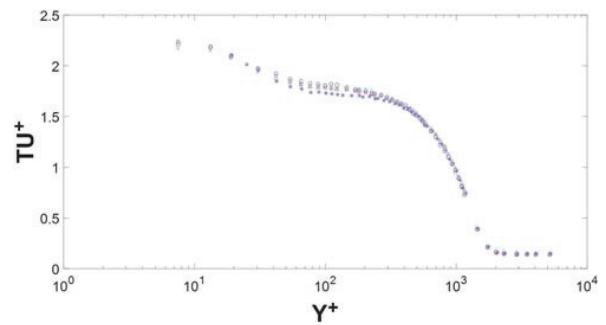

FIG. 9. Turbulence intensity at Re_θ = 3771 and l^+ = 245. [o(black)] No control, [x(red)] V^+ = 0, [Δ(cyan)] V^+ = 3.1 × 10^5, [□(purple)] V^+ = 1.5 × 10^6, [*(blue)] V^+ = 3.1 × 10^6.

arrays (l^+ = 123 and l^+ = 245) provided a turbulence intensity reduction equal to 5.6%. Consequently, the orifice length of the cavity array has negligible effect in modifying the ability of the cavity array to reduce the turbulence intensity of the boundary layer within the range of l^+ investigated, while the volume of the backing cavity has a significant effect on the possible reduction achieved by the passive application of the cavity array.

Sections IV–VI intend to investigate the higher order statistics of the flow, which includes the sweep event structures and the pre-multiplied power energy spectral. The results will consequently analyze the effect of the backing cavity volume and orifice length of the cavity array on controlling the boundary layer.
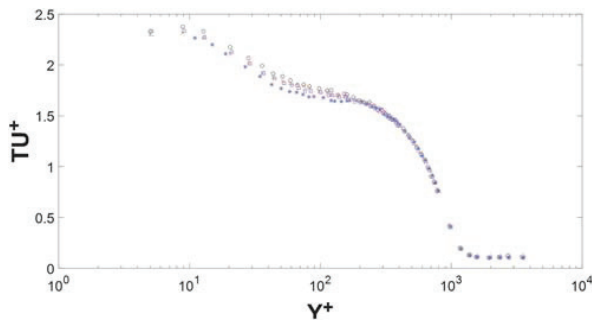

FIG. 7. Turbulence intensity at Re_θ = 2939 and l^+ = 162. [o(black)] No control, [x(red)] V^+ = 0, [Δ(cyan)] V^+ = 1.9 × 10^5, [□(purple)] V^+ = 9.6 × 10^5, [*(blue)] V^+ = 1.9 × 10^6.
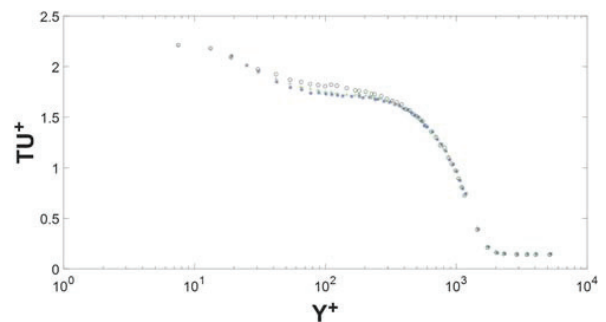
FIG. 10. Turbulence intensity at Re_θ = 3771 and V^+ = 3.1 × 10^6. [o(black)] No control, [+(green)] l^+ = 123, [*(blue)] l^+ = 245.

IV. EFFECTS OF THE CAVITY GEOMETRY ON THE COHERENT STRUCTURES

The variable interval time averaging (VITA) technique, initially applied by Blackwelder and Kaplan (1976), is used to detect the changes in the turbulent boundary layer associated with sweep and injection events. The structures are detected by calculating the VITA of the streamwise velocity fluctuations using the method specified by Silvestri *et al.* (2017a),

$$\hat{u}(t, T_W) = \frac{1}{T_W} \int_{t-T_w/2}^{t+T_w/2} u(s)ds, \tag{1}$$

$$\text{Var}(t, T_W) = \hat{u}^2(t, T_W) - [\hat{u}(t, T_W)]^2, \tag{2}$$

$$Var(t) = \lim_{t \to \infty} \frac{1}{t} \int_0^t u^2(t)dt. \tag{3}$$

If the local variance, $\text{Var}(t, T_W)$ is greater than the variance of the entire signal $k\text{Var}(t)$, a sweep or ejection event is considered to have occurred. The detection function, $D(t)$, which has been previously defined by Whalley (2011) and Silvestri *et al.* (2017a) can be used to differentiate between the coherent structures,

$$D(t) = \begin{cases} 1 & Var(t, T_W) > kVar(t) \quad \frac{du}{dt} > 0 \text{ (sweep event)}, \\ 0 & Var(t, T_W) < kVar(t) \qquad \text{(no event)}, \\ -1 & Var(t, T_W) > kVar(t) \quad \frac{du}{dt} < 0 \text{ (ejection event)}. \end{cases} \tag{4}$$

The averaged VITA events reveal the intensity and duration of the sweep events. Decreased duration or intensity of the events reveals a decrease in the turbulence energy production. A total of 500-1200 ensembles were used in each VITA analysis. All cases investigated performed the analysis at approximately a y^+ value equal to 100, which corresponds to the area of the boundary layer where the maximum turbulence intensity reduction occurred.

A. $Re_\theta = 1927$

The initial results at $Re_\theta = 1927$ show a reduction in the intensity of the sweep events downstream of the cavity array investigated. Figure 11 shows the effect of the varying backing cavity volume on the sweep events. This figure reveals a maximum reduction in sweep intensity by 4.5% when the largest backing cavity volume ($V^+ = 1.4 \times 10^6$) is used. The other backing cavity volumes ($V^+ = 1.4 \times 10^5$ and $V^+ = 7 \times 10^5$)
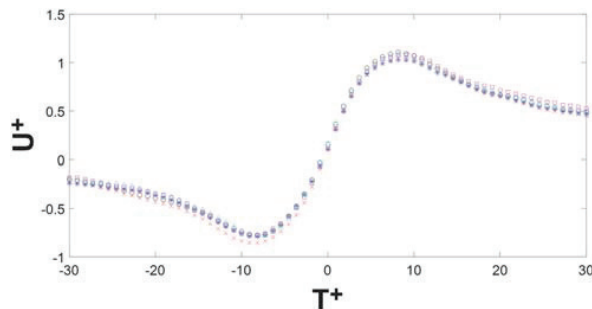
FIG. 12. VITA events at $Re_\theta = 1927$ at $Y^+ = 100$ and $V^+ = 1.4 \times 10^6$. [o(black)] No control, [+(green)] $l^+ = 67$, [*(blue)] $l^+ = 133$.

also reduced the sweep intensity but by a smaller amount of 2.1% and 2.3%, respectively. However, what is even more interesting from this figure is that when the cavity array had no backing cavity volume ($V^+ = 0$) a slight increase in the sweep intensity occurred. This was shown to be approximately 1.2% as indicated in Fig. 11. The duration of $T^+ = 20$, however, is not affected significantly for any of the arrangements investigated.

Figure 12 shows the effect of the cavity array orifice length on the sweep events at $V^+ = 1.4 \times 10^6$. This figure demonstrates a maximum reduction in intensity by 4.5% and 4.2% for $l^+ = 67$ and $l^+ = 133$, respectively, at $Re_\theta = 1927$. This result demonstrates near identical reduction values irrespective of the selected cavity array orifice length. Consequently, similar to the section detailing turbulence intensity, it appears that the orifice length of the cavity array has a negligible effect in modifying the ability of the cavity array to reduce the coherent structures in the boundary layer within the range of l^+ investigated. The duration of $T^+ = 20$ is not affected significantly by any of the arrangements investigated.

B. $Re_\theta = 2937$

When increasing the Reynolds number to $Re_\theta = 2937$, a reduction in the intensity of the sweep events downstream of the cavity array was also recorded. Figure 13 shows the effect of varying the backing cavity volume on the sweep events, with results similar to those found at $Re_\theta = 1927$. A maximum reduction in sweep intensity by 5.2% was achieved when using the largest backing cavity volume ($V^+ = 1.9 \times 10^6$). As

FIG. 11. VITA events at $Re_\theta = 1927$ at $Y^+ = 100$ and $l^+ = 133$. [o(black)] No control, [x(red)] $V^+ = 0$, [Δ(cyan)] $V^+ = 1.4 \times 10^5$, [□(purple)] $V^+ = 7 \times 10^5$, [*(blue)] $V^+ = 1.4 \times 10^6$.

FIG. 13. VITA events at $Re_\theta = 2937$ at $Y^+ = 100$ and $l^+ = 162$. [o(black)] No control, [x(red)] $V^+ = 0$, [Δ(cyan)] $V^+ = 1.9 \times 10^5$, [□(purple)] $V^+ = 9.6 \times 10^5$, [*(blue)] $V^+ = 1.9 \times 10^6$.
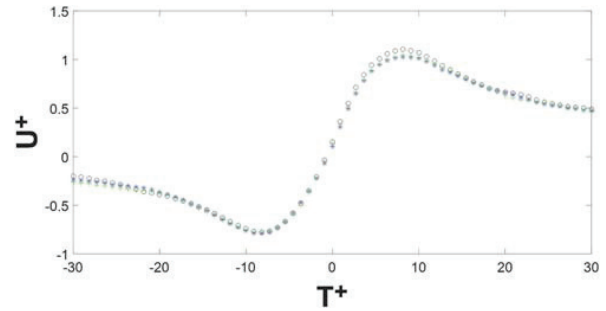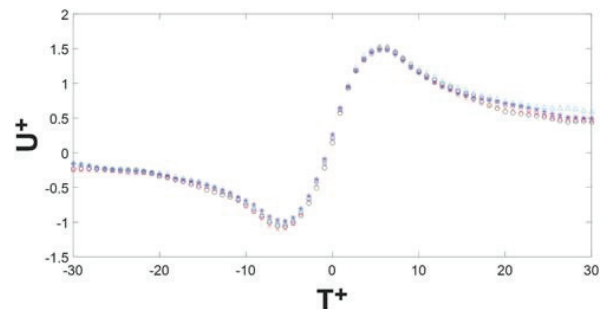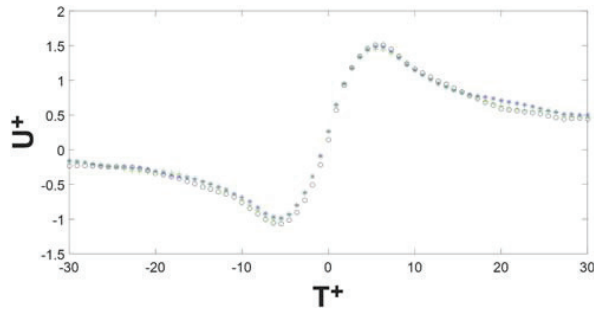
FIG. 14. VITA events at Re_θ = 2937 at Y^+ = 100 and V^+ = 1.9×10^6. [o(black)] No control, [+(green)] l^+ = 81, [*(blue)] l^+ = 162.
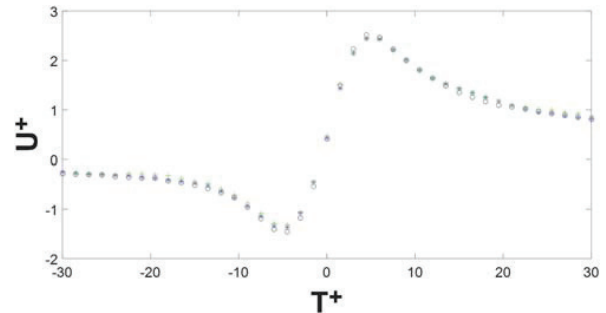

FIG. 16. VITA events at Re_θ = 3771 at Y^+ = 100 and V^+ = 3.1×10^6. [o(black)] No control, [+(green)] l^+ = 123, [*(blue)] l^+ = 245.

observed at Re_θ = 1927, a reduction in the sweep intensity of 1.7% and 2.9% was observed with the smaller backing cavity volumes ($V^+ = 1.9 \times 10^5$ and $V^+ = 9.6 \times 10^5$), respectively. Furthermore, when the cavity array had no backing cavity volume ($V^+ = 0$), a slight increase in the sweep intensity occurred once again. This was shown to be approximately 1.7% as indicated in Fig. 13.

Figure 14 shows the effect of the cavity array orifice length on the sweep events at Re_θ = 2937 and $V^+ = 1.9 \times 10^6$. This figure demonstrates a maximum reduction in intensity by 5.7% and 5.2% for l^+ = 81 and l^+ = 162, respectively. This result demonstrates near identical reduction values irrespective of the selected cavity array orifice length. This was also seen at Re_θ = 1927 and throughout Sec. III and validates that the orifice length of the cavity array has negligible effect in modifying the ability of the cavity array to reduce the coherent structures in the boundary layer within the range of l^+ investigated.

C. Re_θ = 3771

At a Reynolds number of Re_θ = 3771, a reduction in the intensity of the sweep events downstream of the cavity array was also recorded. Figure 15 shows the effect of the varying backing cavity volume on the sweep events, where a maximum reduction in sweep intensity by 5.7% was achieved when using the largest backing cavity volume ($V^+ = 3.1 \times 10^6$). The other backing cavity volumes ($V^+ = 3.1 \times 10^5$ and $V^+ = 1.5 \times 10^6$) were also shown to be capable of reducing the sweep intensity by 3.6% and 4%, respectively. Furthermore, at $V^+ = 0$ (the
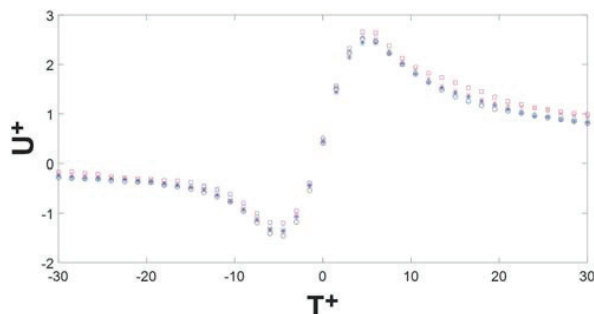
backing cavity was removed), the reduction was shown to be approximately 1.7%.

Figure 16 shows the effect of the cavity array orifice length on the sweep events at Re_θ = 3771 and $V^+ = 3.1 \times 10^6$. This figure demonstrates a maximum reduction in intensity by 6.3% and 5.7% for l^+ = 123 and l^+ = 245, respectively. This result demonstrates near identical reduction values irrespective of the selected cavity array orifice length.

V. EFFECTS OF THE CAVITY GEOMETRY ON THE ENERGY SPECTRA OF THE BOUNDARY LAYER

The average pre-multiplied energy spectrums of multiple velocity histories at the three different Reynolds numbers have also been investigated. The streamwise pre-multiplied energy spectra are defined as $\Psi_x = \frac{K_x u}{u_\tau^2}$ (where K_x is the streamwise wavenumber). The locations have all been selected to be below $y^+ = 200$, where the buffer and logarithmic regions are located and consequently a significant proportion of the turbulent energy production (Kline *et al.*, 1967). From Fig. 17, it can be seen that a significant reduction is occurring in the lower to mid-wavelength values $\lambda_x < 1200$ at Re_θ = 1927, which are commonly associated with the small-scale eddies. At $V^+ = 1.4 \times 10^6$, the largest reduction occurs, where the average value achieved is approximately 8.3%. The other backing cavity volumes ($V^+ = 1.4 \times 10^5$ and $V^+ = 7 \times 10^5$) show a diminished reduction, reducing the energy spectrum by a maximum of 3.1% and 5.4%, respectively. When the cavity array had no backing cavity volume ($V^+ = 0$), no

FIG. 15. VITA events at Re_θ = 3771 at Y^+ = 100 and l^+ = 245. [o(black)] No control, [x(red)] $V^+ = 0$, [Δ(cyan)] $V^+ = 3.1 \times 10^5$, [□(purple)] $V^+ = 1.5 \times 10^6$, [*(blue)] $V^+ = 3.1 \times 10^6$.

FIG. 17. Average pre-multiplied energy spectra at Re_θ = 1927 and l^+ = 133. (black) No control, (red) $V^+ = 0$, (cyan) $V^+ = 1.4 \times 10^5$, (purple) $V^+ = 7 \times 10^5$, (blue) $V^+ = 1.4 \times 10^6$.

FIG. 18. Average pre-multiplied energy spectra at $Re_\theta = 1927$ and $V^+ = 1.4 \times 10^6$. (black) No control, (green) $Th^+ = 67$, (blue) $Th^+ = 133$.

change in the energy spectrum could be observed, demonstrating a similar effect as shown throughout this paper with 1% increase.

Figure 18 plots the orifice length's effect on the turbulent energy reduction at $V^+ = 1.4 \times 10^6$. The results demonstrate near identical reduction values irrespective of the selected cavity array orifice length, where an average reduction of 6.7% and 8.3% for $l^+ = 67$ and $l^+ = 133$ is observed, respectively.

Figure 19 shows the energy spectrum at $Re_\theta = 2937$, where it can be seen once again that a significant reduction is occurring at the low and mid-range wavelength values, associated with the small coherent structures. At $V^+ = 1.9 \times 10^6$, the largest backing cavity for this Reynolds number, the largest reduction occurs, where the maximum value achieved is approximately 13.4%. The other backing cavity volumes ($V^+ = 1.9 \times 10^5$ and $V^+ = 9.6 \times 10^5$) show a diminished reduction, reducing the energy spectrum by a maximum of 5.4% and 7.3%, respectively. With no backing cavity volume ($V^+ = 0$), negligible change in the energy spectrum could be observed, demonstrating a similar effect as the other Reynolds number investigated ($Re_\theta = 1927$). Figure 20 also shows the effect of the cavity array orifice length on the turbulent energy reduction at $V^+ = 1.9 \times 10^6$. Figure 20 demonstrates near identical reduction values irrespective of the selected cavity array orifice length. This figure demonstrates a maximum reduction of 13.2% and 13.4% for $l^+ = 81$ and $l^+ = 162$, respectively.

Figure 21 shows the energy spectrum at $Re_\theta = 3771$, where it can be seen that a significant reduction is occurring

FIG. 20. Average pre-multiplied energy spectra at $Re_\theta = 2937$ and $V^+ = 1.9 \times 10^6$. (black) No control, (green) $Th^+ = 81$, (blue) $Th^+ = 162$.

FIG. 21. Average pre-multiplied energy spectra at $Re_\theta = 3771$ and $l^+ = 245$. (black) No control, (red) $V^+ = 0$, (cyan) $V^+ = 3.1 \times 10^5$, (purple) $V^+ = 1.5 \times 10^6$, (blue) $V^+ = 3.1 \times 10^6$.

in the low and mid-range wavelength values once again. At $V^+ = 3.1 \times 10^6$, the largest backing cavity for this Reynolds number, the largest reduction occurs, where the maximum value achieved is approximately 13.4%. For the other backing cavity volumes ($V^+ = 3.1 \times 10^5$ and $V^+ = 1.5 \times 10^6$), the energy spectrum is shown to be reduced by a maximum 5.4% and 7.3%, respectively. With no backing cavity volume ($V^+ = 0$), negligible change in the energy spectrum could be observed, demonstrating a similar effect as the other Reynolds number investigated ($Re_\theta = 1927$ and $Re_\theta = 2937$). Figure 22 shows the effect of the cavity array orifice length on the turbulent energy reduction at $V^+ = 3.1 \times 10^6$, which demonstrates similar reduction values irrespective of the selected
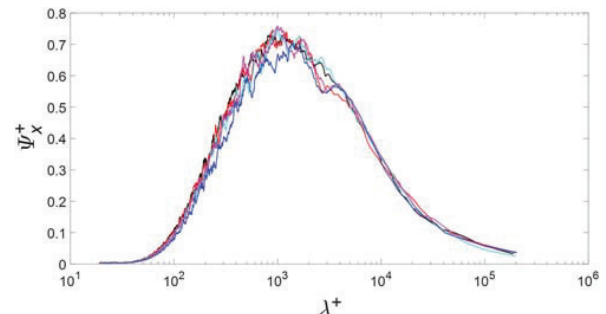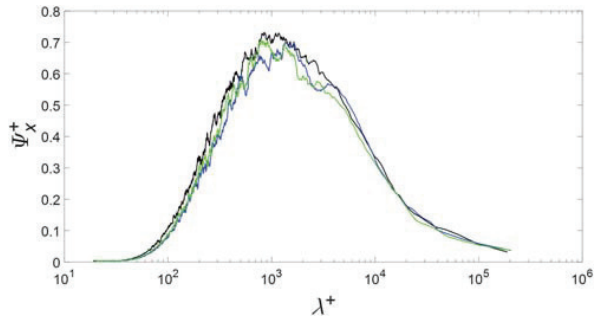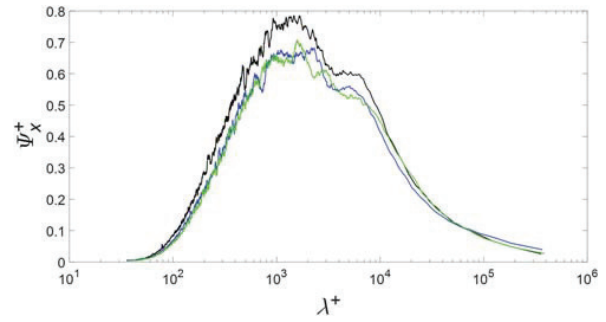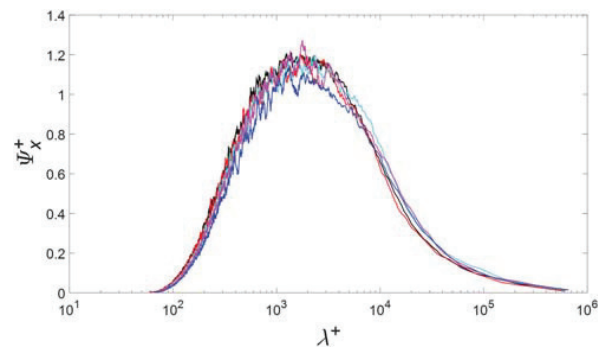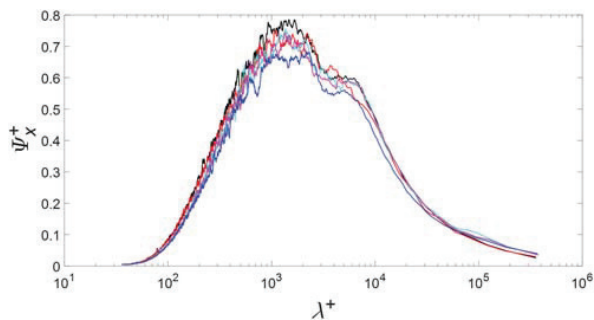

FIG. 19. Average pre-multiplied energy spectra at $Re_\theta = 2937$ and $l^+ = 162$. (black) No control, (red) $V^+ = 0$, (cyan) $V^+ = 1.9 \times 10^5$, (purple) $V^+ = 9.6 \times 10^5$, (blue) $V^+ = 1.9 \times 10^6$.
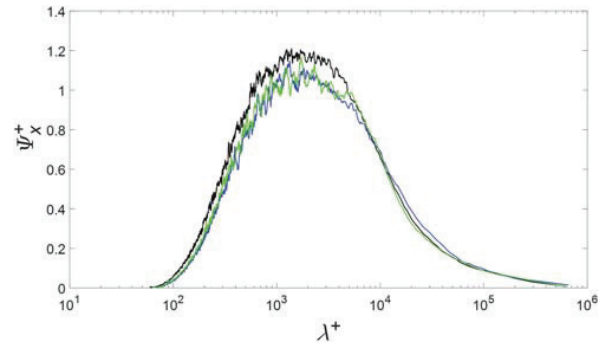

FIG. 22. Average pre-multiplied energy spectra at $Re_\theta = 3771$ and $V^+ = 3.1 \times 10^6$. (black) No control, (green) $Th^+ = 123$, (blue) $Th^+ = 245$.

cavity array orifice length. A maximum reduction of 13.2% and 13.4% for $l^+ = 123$ and $l^+ = 245$, respectively, are achieved.

The results throughout this section show a significant trend between the two Reynolds numbers. As mentioned previously, the reduction is predominantly in the low and mid-range wavelengths (small-scale structures). However, at the higher wavelengths, an increase is noticed between the no control and control cases. This result suggests that the cavity array redistributes the energy from the smaller scale structures into the larger sized structures associated with the high wavelengths. However, as the coherent structures are responsible for the shear stresses in the near wall region, the passive cavity array results in a net turbulent energy reduction at the locations discussed above.

VI. DISCUSSION

Micro-cavities have been shown to have a significant effect in modifying the coherent structures located in the turbulent boundary layer. The reduction in the sweep events causes the turbulence intensity to decrease, as the structures are more violent at the smaller scales and hence reducing the energy at this scale, results in a reduction in turbulence intensity. It was initially hypothesised that the cavities would reduce the turbulent structures in the boundary layer by capturing the sweep events and disrupting the bursting process in the boundary layer. An attempt was then made in this paper to determine what happened to the sweep events when they were captured. The initial hypothesis from the authors suggested that the cavity array was weakening the structure of the captured sweep events by dampening the energy of the events through the friction loses in the cavity array and the large volume of the backing cavity below the array itself (Silvestri *et al.*, 2017b). It is shown that at each Reynolds number studied, no reduction in turbulence intensity, sweep intensity, and the energy spectrum was observed when the backing cavity was absent. Furthermore, the reduction in sweep intensity was shown to increase as the volume of the backing cavity approached $V^+ = \infty$, as demonstrated in Fig. 23. This result suggests that the losses for a very short length cavity are negligible. Therefore,

without the backing cavity, the passive cavity array is not able to control the coherent structures in the boundary layer. The impedance of the passive micro-cavities would be so high without a backing cavity that there would be effectively no flow and hence no losses through the system. The reduction is consequently shown to increase as the volume of the backing cavity is increased due to the fact that the impedance of the system would also decrease causing the flow to be more effective at being drawn into the cavity array. This finding is also supported by the results of the cavity array orifice length on the reduction achieved by the passive control device. The two arrays with different orifice lengths ($l^+ = 67$ and $l^+ = 133$) had near identical results for turbulence intensity (4.2% reduction), sweep VITA analysis (4.5% and 4.2% reduction), and their corresponding energy spectrum (8.3% reduction). This behavior was observed at the other two Reynolds numbers ($Re_\theta = 2937$ and $Re_\theta = 3771$) demonstrating a pattern suggesting the orifice length of the cavity array has negligible effect in modifying the reduction capabilities of the cavity array. This would once again suggest that the losses for a short cavity are negligible and explain why changing the orifice length of the cavity array had no effect.

However, the authors believe that they have identified another possible mechanism that influences the coherent structures. Once an event enters the cavity array, the energy of the single event is possibly redistributed across all orifices in the cavity array. This mechanism would result in a sweep event being removed from the boundary layer and disrupting the bursting process. However, to maintain a balance of momentum, the energy is redistributed into the boundary layer across all cavities in the array. As the sweep event has such a small amount of energy (small wavelengths), when redistributed across all holes, the resulting ejection of energy back into the boundary layer is negligible and has no detrimental effect on the turbulent energy of the near wall region. This mechanism is also supported by the results obtained in this paper. By having no backing cavity, this redistribution cannot occur. Furthermore, changing the orifice length of the cavity array will have negligible effect on the hypothesis described, which is supported by the results obtained. The orifice length of the cavity array does not influence the capture of the coherent
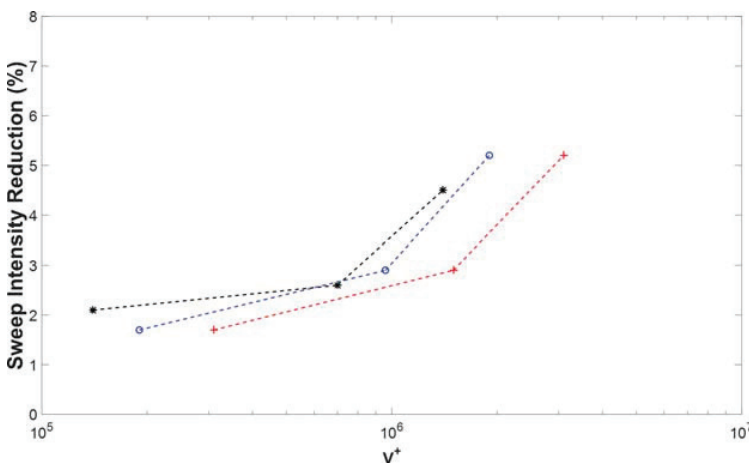

FIG. 23. Average VITA event intensity reduction with respect to the volume of the backing cavity at $Y^+ = 100$. [*(black)] $Re_\theta = 1927$, [o(blue)] $Re_\theta = 2939$, [+(red)] $Re_\theta = 3771$.

structures, which was already identified by Silvestri *et al.* (2017a) as being based on the diameter of the cavities and the streamwise and spanwise spacing.

The results pertaining to the volume of the backing cavity are also viable with the method specified previously. With a smaller backing cavity volume, the authors have identified that the impendence would increase. An increase in impendence would consequently cause the sweep events to have more difficulty in traversing the backing cavity as there is effectively no flow as mentioned previously. As a result, the authors suspect that in the cases of a smaller volume the sweep events are redistributed over a reduced amount of cavities due to the high impedance of the flow. Therefore, the results support a non-linear reduction in turbulence intensity with increasing cavity volume. However, there will likely be an upper limit in the cavity volume to achieve maximum reduction, which was beyond the scope of this paper. Future work endeavours to determine the method in which the reduction in the turbulence energy production occurs as well as determining the upper limit of the cavity volume.

VII. SUMMARY

Two plates of varying orifice length and four different backing cavity volumes were considered, at three different Reynolds numbers. The features of each boundary layer investigated were considered using a hotwire anemometry system located downstream of the arrays investigated. The results were used to evaluate the streamwise and turbulence intensity profile, coherent structures properties, and the pre-multiplied energy spectrum.

The results from this work specified different parameters to consider while implementing the flow control technique. The volume of the backing cavity had significant effect on the turbulent energy in the boundary layer, while the orifice length of the cavity array had negligible effects on altering the control devices sweep attenuation capabilities. The data support a non-linear reduction in turbulence intensity with increasing cavity volume. However, there will likely be an upper limit in the cavity volume to achieve the maximum turbulence energy and sweep attenuation possible, which was not found in this paper.

The conclusions found in this work are based on altering both the backing cavity volume and cavity array orifice length. Future work aims to focus on the results when an infinite backing cavity is present to determine the upper limit of the reduction, as well as analyzing the physical mechanism by which the reduction is achieved and what occurs inside the backing cavity when a coherent structure is captured. This could be accomplished by supplementing the measurements from this investigation with numerical modeling results to quantify the change in the captured structures. The results presented here are only the beginning of the development of the knowledge required for this area of work.

Blackwelder, R. F. and Kaplan, R. E., "On the wall structure of the turbulent boundary layer," J. Fluid Mech. **76**(Part 1), 89–112 (1976).

Blackwelder, R. F. and Eckelmann, H., "Streamwise vortices associated with the bursting phenomenon," J. Fluid Mech. **94**, 577–594 (1979).

Blackwelder, R. F. and Haritonidis, J. H., "Scaling of the bursting frequency in turbulent boundary layers," J. Fluid Mech. **132**, 87–103 (1983).

Choi, K. S., "On physical mechanism of turbulent drag reduction using riblets," in *Transport Phenomena in Turbulent Flows: Theory, Experiment, and Numerical Simulation; Proceedings of the Second International Symposium, Tokyo, Japan, Oct. 1987* (Hemisphere Publishing Corp., New York, USA, 1988), pp. 185–198.

Choi, K. S., "Near-wall structure of a turbulent boundary layer with riblets," J. Fluid Mech. **208**, 417–458 (1989).

Choi, K. S. and Fujisawa, N., "Possibility of drag reduction using d-type roughness," Appl. Sci. Res. **50**, 315–324 (1993).

Choi, K. S. and Graham, M., "Drag reduction of turbulent pipe flows by circular-wall oscillation," Phys. Fluids **10**(1), 7–9 (1998).

Choi, K. S., Jukes, T., and Whalley, R., "Turbulent boundary-layer control with plasma actuators," Philos. Trans. R. Soc., A **369**, 1443–1458 (2011).

Clauser, F. H., "The turbulent boundary layer," Adv. Appl. Mech. **IV**, 1–51 (1956).

Corino, E. R. and Brodkey, R. S., "A visual investigation of the wall region in turbulent flow," J. Fluid Mech. **37**(Part 1), 1–30 (1969).

García-Mayoral, R. and Jiménez, J., "Drag reduction by riblets," Philos. Trans. R. Soc., A **369**(1940), 1412–1427 (2011).

Ghanadi, F., Arjomandi, M., Cazzolato, B. S., and Zander, A. C., "Understanding of the flow behaviour on a Helmholtz resonator excited by grazing flow," Int. J. Comput. Fluid Dyn. **28**(5), 219–231 (2014a).

Ghanadi, F., "Application of a Helmholtz resonator excited by grazing flow for manipulation of a turbulent boundary layer," Ph.D. thesis, School of Mechanical Engineering, University of Adelaide, Australia, 2014b.

Ghanadi, F., Arjomandi, M., Cazzolato, B. S., and Zander, A. C., "Analysis of the turbulent boundary layer in the vicinity of a self-excited cylindrical Helmholtz resonator," J. Turbul. **16**, 705–728 (2015).

Guo, H., Borodulin, V. I., Kachanov, Y. S., Pan, C., Wang, J. J., Lian, Q. X., and Wang, S. F., "Nature of sweep and ejection events in transitional and turbulent boundary layers," J. Turbul. **11**(34), 1–51 (2010).

Hutchins, N., Nickels, T. B., Marusic, I., and Chong, M. S., "Hot-wire spatial resolution issues in wall-bounded turbulence," J. Fluid Mech. **635**, 103–136 (2009).

Kendall, A. and Koochesfahani, M., "A method for estimating wall friction in turbulent boundary layer," in *25th AIAA Aerodynamic Measurement Technology and Ground Testing Conference, 5–8 June* (AIAA, San Francisco, California, USA, 2006).

Kim, H. T., Kline, S. J., and Reynolds, W. C., "The production of turbulence near a smooth wall in a turbulent boundary layer," J. Fluid Mech. **50**(Part 1), 133–160 (1971).

Kline, S. J., Reynolds, W. C., Schraub, F. A., and Runstadler, P. W., "The structure of turbulent boundary layers," J. Fluid Mech. **30**(Part 4), 741–773 (1967).

Lockerby, D., "Numerical simulation of boundary-layer control using MEMS actuation," Ph.D. thesis, The University of Warwick, England, UK, 2001.

Maa, D. Y., "Potential of microperforated panel absorber," J. Acoust. Soc. Am. **104**(5), 2861–2866 (1998).

Marusic, I. and Kunkel, G. J., "Streamwise turbulence intensity formulation for flat-plate boundary layers," Phys. Fluids **15**(8), 2461–2464 (2003).

Offen, G. R. and Kline, S. J., "A proposed model of the bursting process in turbulent boundary layers," J. Fluid Mech. **70**(Part 2), 209–228 (1975).

Orlandi, P. and Jimenez, J., "On the generation of turbulent wall friction," Phys. Fluids **6**, 634–641 (1993).

Schlatter, P. and Orlu, R., "Assessment of direct numerical simulation data of turbulent boundary layers," J. Fluid Mech. **659**, 116–126 (2010).

Silvestri, A., Ghanadi, F., Arjomandi, M., Cazzolato, B. S., and Zander, A. C., "Control of the turbulent boundary layer by the application of a cavity array," in 20th Australasian Fluid Mechanics Conference, Perth, Australia, 5–8 December 2016.

Silvestri, A., Ghanadi, F., Arjomandi, M., Cazzolato, B. S., and Zander, A. C., "Attenuation of sweep events in a turbulent boundary layer using micro-cavities," Exp. Fluids **58**(5), 58 (2017a).

Silvestri, A., Ghanadi, F., Arjomandi, M., Cazzolato, B. S., and Zander, A. C., "The effect of the backing cavity on the control of the turbulent

boundary layer by the application of a cavity array," in 10th International Symposium on Turbulence and Shear Flow Phenomena, Chicago, IL, USA, 6–9 July 2017b.

Silvestri, A., Ghanadi, F., Arjomandi, M., Cazzolato, B. S., and Zander, A. C., "The application of different tripping techniques to determine the characteristics of the turbulent boundary layer over a flat plate," J. Fluid Eng. **140**, 011204 (2017c).

Wallace, J. M., Eckelmann, H., and Brodkey, R. S., "The wall region in turbulent shear flow," J. Fluid Mech. **54**, 39–48 (1972).

Walsh, M. J., "Riblets as a viscous drag reduction technique," AIAA J. **21**(4), 485–486 (1983).

Whalley, R. D., "Turbulent boundary-layer control with DBD plasma actuators using spanwise travelling-wave technique," Ph.D. thesis, The University of Nottingham, England, UK, 2011.

Chapter 6

Mechanism behind the control achieved by

the micro-cavity array

6.1 Paper 4: Mechanism of sweep event attenuation using micro-cavities in a turbulent boundary layer

To further explore the micro-cavity array as a technique to control the turbulent boundary layer an extensive experimental analysis was performed on the backing cavity of the cavity array. The mechanism for the attenuation of captured sweep events was analysed, as well as the non-linear relationship between the volume of the backing cavity and the reduction in sweep intensity found in the previous chapter.

In this chapter a single cavity array was analysed, with two different types of backing cavity. The first group of backing cavities were identical to the models investigated in the previous chapters. This resulted in the orifices in the cavity array sharing a common backing cavity, allowing each orifice to be connected with one another through the backing volume. The second group on the other hand utilised a mesh design which

decoupled the orifices and prevented flow through the orifices interacting via the backing cavity. The results show that the maximum reduction in sweep intensity of 7% was obtained when $Re_\theta = 3771$ and both cases (common backing cavity and individual backing cavities) were capable of producing flow control with very similar behaviour and results.

Furthermore, it was demonstrated that the non-linear relationship between sweep event intensity reduction and cavity volume reached an upper limit in this investigation. The energy spectrum was significantly reduced, by up to 12.5%, in the low and mid-range wavelength values ($\lambda_x^+ < 10^4$), which is commonly associated with the coherent structures.

Consequently this chapter aims to resolve several of the gaps left in previous chapters. More specifically, the mechanism by which the cavity array achieves a reduction of the coherent structures, as well as the backing volume for the optimal attenuation of turbulent structures.

This chapter has been published as:

Silvestri, A, Ghanadi, F, Arjomandi, M, Cazzolato, BS, Zander, AC, Chin, R, 2017, *'Mechanism of sweep event attenuation using micro-cavities in a turbulent boundary layer', Physics of Fluids,* vol. 30, Issue. 4, pp. 055108.

Statement of Authorship

Title of Paper	Mechanism of sweep event attenuation using micro-cavities in a turbulent boundary layer
Publication Status	☑ Published ☐ Accepted for Publication ☐ Submitted for Publication ☐ Unpublished and Unsubmitted work written in manuscript style
Publication Details	Silvestri, A, Ghanadi, F, Arjomandi, M, Cazzolato, BS, Zander, AC, Chin, R, 2017, *'Mechanism of sweep event attenuation using micro-cavities in a turbulent boundary layer', Physics of Fluids,* vol. 30, Issue. 4, pp. 055108.

Principal Author

Name of Principal Author (Candidate)	Anton Silvestri			
Contribution to the Paper	Performed data analysis and interpretation, wrote manuscript and acted as corresponding author.			
Overall percentage (%)	70			
Certification:	This paper reports on original research I conducted during the period of my Higher Degree by Research candidature and is not subject to any obligations or contractual agreements with a third party that would constrain its inclusion in this thesis. I am the primary author of this paper.			
Signature			Date	15/06/18

Co-Author Contributions

Name of Co-Author	Farzin Ghanadi
Contribution to the Paper	Supervised the development of the research and contributed in academic discussion and the review process of submitted manuscripts.
Signature	Date	15/06/18

Name of Co-Author	Maziar Arjomandi
Contribution to the Paper	Supervised the development of the research and contributed in academic discussion and the review process of submitted manuscripts.
Signature	Date	15/06/18

Name of Co-Author	Benjamin Cazzolato
Contribution to the Paper	Supervised the development of the research and contributed in academic discussion and the review process of submitted manuscripts.
Signature	Date	15/06/18

Name of Co-Author	Anthony Zander
Contribution to the Paper	Supervised the development of the research and contributed in academic discussion and the review process of submitted manuscripts.
Signature	Date	15/06/18

Name of Co-Author	Rey Chin
Contribution to the Paper	Supervised the development of the research and contributed in academic discussion and the review process of submitted manuscripts.
Signature	Date	15/06/18

Mechanism of sweep event attenuation using micro-cavities in a turbulent boundary layer

Anton Silvestri,[a)] Farzin Ghanadi,[b)] Maziar Arjomandi,[c)] Benjamin Cazzolato,[d)]
Anthony Zander,[e)] and Rey Chin[f)]
School of Mechanical Engineering, University of Adelaide, Adelaide, South Australia 5005, Australia

Cavity arrays have been identified as a potential passive device to disrupt and capture sweep events, which are responsible for the excess Reynolds stresses in the boundary layer. In the present study, the mechanism of the attenuation of captured sweep events has been analyzed, as well as the non-linear relationship between the volume of the backing cavity and the reduction in sweep intensity. The influence of cavity array on the turbulent boundary layer has been analyzed, with a total of six different backing cavity arrangements with varying volumes. Three of the backing cavities have been used to determine the non-linear relationship between the effectiveness of the cavity array in reducing sweep intensity and the volume of the backing cavity. The other three have been used to determine the mechanism by which the arrays manipulate the captured sweep events. The pre-multiplied energy spectra of multiple velocity histories were significantly reduced, by up to 12.5%, in the low and mid-range wavelength values ($\lambda_x^+ < 10^4$), which is associated with the coherent structures. The results show that the maximum reduction in sweep intensity of approximately 7% may be obtained when $Re_\theta = 3771$. It has been demonstrated that the non-linear relationship between sweep event intensity reduction and cavity volume has reached an upper limit in this investigation. Results from this study have revealed that the cavity array weakens the sweep intensity of the captured sweep events by damping the energy of the events through the friction losses in the cavity array and also in the large volume of the backing cavity. *Published by AIP Publishing.* https://doi.org/10.1063/1.5026130

NOMENCLATURE

d	cavity diameter (mm)
D	backing cavity depth (mm)
k	variable-interval time-averaging (VITA) threshold
K_x	steamwise wavenumber
Re_{u_τ}	Reynolds number based on friction velocity
Re_θ	Reynolds number based on momentum thickness
t	time (s)
T_{av}	averaging duration (s)
T_W	window length (s)
TU	turbulence intensity
L	orifice length (mm)
u	streamwise flow velocity (m/s)
u_τ	friction velocity (m/s)
$\hat{u}$	local mean of the streamwise velocity (m/s)
V	volume of backing cavity (m^3)
Var	variance
x	x-distance (streamwise) (m)
y	y-distance (wall-normal direction) (m)
z	z-distance (spanwise) (m)

Symbols

λ_x	steamwise wavelength (m)
δ^+	displacement thickness (mm)
Ψ	pre-multiplied energy spectrum
ν	kinematic viscosity (m/s^2)

Superscripts

+	viscous time scale $\left(\frac{\nu}{u_\tau^2}\right)$ or viscous length scale $\left(\frac{\nu}{u_\tau}\right)$

I. INTRODUCTION

Skin friction drag is an important problem for many applications found in the world. Such examples include the aerospace industry where the skin friction drag on aircraft is estimated to be approximately 50% of the total drag (Gad-el Hak, 1994; Marec, 2000; and Qin *et al.*, 2017). Consequently, significant research has been undertaken by many to reduce the influence of skin friction drag in turbulent boundary layers through the use of flow control. Two passive mechanisms to control the turbulent boundary layer explored recently are riblets (Walsh, 1983; Choi, 1987; 1989; García-Mayoral and Jiménez, 2011; Greidanus *et al.*, 2015; Benschop and Breugem, 2017; and Kevin *et al.*, 2017) and Helmholtz resonators (Ghanadi *et al.*, 2014a; 2014b; 2015; and Ghanadi, 2015). In the case of riblets, these are aligned in the flow direction and restrict the streamwise structures in the spanwise direction by acting as small fences. This

[a)]anton.silvestri@adelaide.edu.au
[b)]farzin.ghanadi@adelaide.edu.au
[c)]maziar.arjomandi@adelaide.edu.au
[d)]benjamin.cazzolato@adelaide.edu.au
[e)]anthony.zander@adelaide.edu.au
[f)]rey.chin@adelaide.edu.au

technique was shown to be successful in reducing the skin friction drag by 8% (Walsh, 1983). Similar to the synthetic jet, a flow excited Helmholtz resonator was used by Ghanadi *et al.*, 2014a; 2014b; and 2015 to provide a jet of suction and ejection to target the ejection and sweep events, respectively. However, unlike the synthetic jet, the device is completely passive and its driving mechanism is provided by the grazing flow. The Helmholtz resonator targets the coherent structures directly and resulted in a 11% and 5% reduction in the intensity and duration of the targeted structures (Ghanadi *et al.*, 2014a; 2014b; 2015; and Ghanadi, 2015). However, results from the work of Ghanadi *et al.* (2014b) suggested a possible reduction of the intensity and duration by 5% and 8%, respectively, even when the resonator was not activated by the grazing flow leading to the potential of using such a device to achieve sweep attenuation without the need of suction and blowing.

As such, micro-cavities have received significant attention in the past for sound absorption (Maa, 1998) and drag reduction (Choi and Fujisawa, 1993). More recently Silvestri *et al.* (2016; 2017a; 2017b; and 2017d) investigated the effect of micro-cavities on the coherent structures in the turbulent boundary layer. Their technique utilises a cavity array which targets the flow normal to the wall, i.e., the coherent structures (ejection and sweep events) (Robinson, 1991). It has been hypothesised by Silvestri *et al.* (2017a) that targeting these structures can result in the disruption of the bursting cycle responsible for the shear stresses in the near wall region. This is achieved during the inrush of the sweep events toward the wall where the structure is broken up when it enters a single orifice in the cavity array. This results in the next ejection event being delayed as a weakened sweep event is present to push the slower moving fluid away from the wall (ejection event). Silvestri *et al.* (2016; 2017a) have subsequently demonstrated this potential application of the passive micro-arrays in controlling the turbulent boundary layer, where a maximum reduction in the turbulence and sweep intensity by 13% and 14%, respectively, was achieved. Furthermore, Silvestri *et al.* (2017a) also showed the effect of the orifice diameter on the reduction capabilities. It was shown that when the orifice diameter was less than 20 times the viscous length scale, the sweep events were restricted and no events were captured by the array. However at an orifice diameter of 145 times the viscous length scale, separation of the shear layer occurs, causing an increase in the turbulence energy production in the near wall region. It was demonstrated that the optimal orifice diameter to achieve the maximum flow control is 60 times the viscous length scale.

In addition to the work on optimising the external geometry of the cavity array (orifice diameter), significant research has also been conducted on determining the effect of the internal geometry (orifice length and backing cavity volume). It was shown by Silvestri *et al.* (2017d) that the orifice length of the cavity array had a negligible effect on the reduction of the turbulent energy by the cavity array. This was in direct contrast to the backing cavity volume, which improved the flow control capabilities with larger reductions in the turbulence and sweep intensity as well as the energy spectrum when the volume was increased. However one of the biggest limitations from their

study was the limited number of experimental cases to identify the non-linear relationship between increasing cavity volume and sweep intensity reduction. While it was hypothesised that the relationship would plateau and reach an upper limit, no evidence was provided.

Furthermore, Silvestri *et al.* (2017d) focused on determining the physical mechanism that occurs once a sweep event is captured by the cavity array. The authors were able to provide two hypothesises that were supported by the relevant literature. The initial hypothesis from the authors suggests that the cavity array was weakening the structure of the captured sweep events by damping the energy of the events through the friction losses in the orifice and the large volume of the backing cavity installed below the array. The additional hypothesis from the authors also suggests that once a sweep event enters the cavity array, the energy of the single event is redistributed across all orifices in the cavity array. This would result in a sweep event being removed from the boundary layer and disrupting the bursting process.

Therefore, the motivation of this research is to provide the required experimental analysis to review the gaps left unanswered in previous work (Silvestri *et al.*, 2017d). The present work provides a detailed experimental analysis that ultimately determines which hypothesis from previous work accurately defines the mechanism of the cavity array once a sweep event is captured. Furthermore, the non-linear relationship between increasing cavity volume and flow control is further investigated to provide an upper limit in the cavity volume to achieve the maximum possible turbulence energy and sweep attenuation. The characteristics of the array and the details of the experimental setup will be discussed in Secs. II–VI.

II. EXPERIMENTAL SETUP

All experiments were undertaken in a closed-loop wind tunnel located at the University of Adelaide. The wind tunnel has a low turbulence intensity with an average free stream turbulence intensity of 0.5% for all experiments conducted in this study. A flat plate test section was installed in the working section of the wind tunnel, with a width of 0.5 m and a length of 2 m as shown in Fig. 1. The walls of the test section
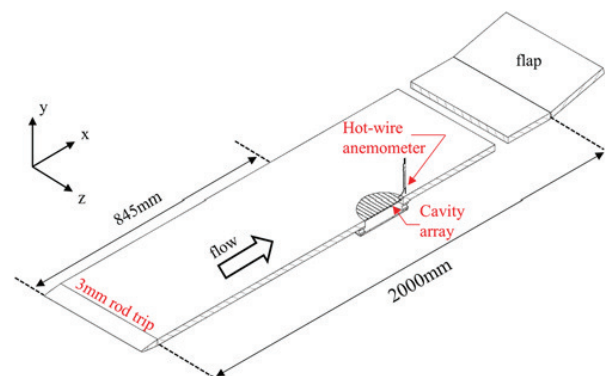

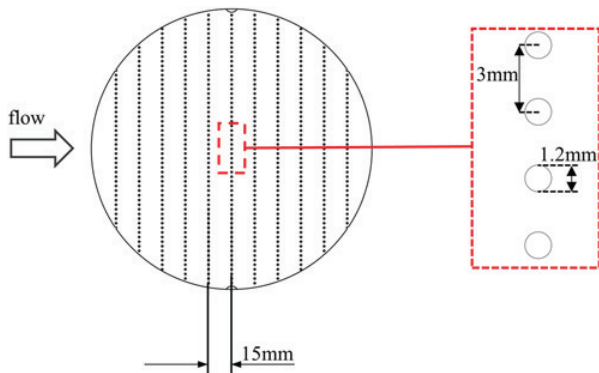FIG. 1. Schematic of the experimental arrangement.

FIG. 2. Schematic of the cavity array.

TABLE I. Summary of the cavity array arrangements used in this investigation.

Case	V^+ at $Re_\theta = 2939$	V^+ at $Re_\theta = 3771$
Cavity array with a common backing cavity		
$D = 25$ mm	2.05×10^6	3×10^6
$D = 50$ mm	3.1×10^6	4.5×10^6
$D = 75$ mm	4.1×10^6	6×10^6
Cavity array with individual backing cavities via use of a mesh		
Case	V^+ at $Re_\theta = 2939$	V^+ at $Re_\theta = 3771$
$D = 25$ mm	2.05×10^6	3×10^6
$D = 50$ mm	3.1×10^6	4.5×10^6
$D = 75$ mm	4.1×10^6	6×10^6

were fixed at the leading edge and adjusted downstream to ensure a zero pressure gradient, while a recirculation flap was installed at the trailing edge of the working section to ensure minimal circulation development over the plate. Furthermore, to minimise any possible flow separation effects due to bluff body separation, a super-elliptical leading edge, with a nominal major radius of 114 mm, was attached to the leading edge. All boundary layers examined in the study were tripped using a 3 mm rod edge to ensure a fully developed turbulent boundary layer, as recommended previously by Silvestri *et al.* (2017c).

A constant temperature hot-wire anemometry (CTA) downstream of the cavity array was used to characterise the changes in the turbulent boundary layer. The hot-wire anemometer was located 180 mm downstream from the leading edge of the array, which itself was located 845 mm downstream from the 3 mm rod used to trip the boundary layer. This location was selected as it was close to the trailing edge of the cavity array where the maximum effect of the cavity array

was recorded (Silvestri *et al.*, 2016). All streamwise velocity measurements were made with a TSI IFA 300 CTA system, using a single platinum-plated tungsten wire of 5 μm in diameter, 1.25 mm in length, and an offset prong of 1.8 mm. The over-heat ratio was selected to be 1.8, while the operating temperature was 230 °C. This resulted in a length-to-diameter ratio of the hot-wire sensor exceeding 200 to minimise attenuation due to end conduction (Ligrani and Bradshaw, 1987). This provided sufficient sensitivity during measurements as discussed by Silvestri *et al.* (2017a). Each measurement was repeated three times at 40×10^3 Hz for 15 s to ensure repeatability. This resulted in a sample interval between $0.42 < \Delta t^+ < 1.41$, which remains below the minimum time scale for energetic turbulent fluctuations ($t^+ \approx 3$) as reported by Hutchins *et al.* (2009).

The cavity array remained the same for all cases investigated, while a variety of backing cavity arrangements were considered. Following the findings and benchmarks of
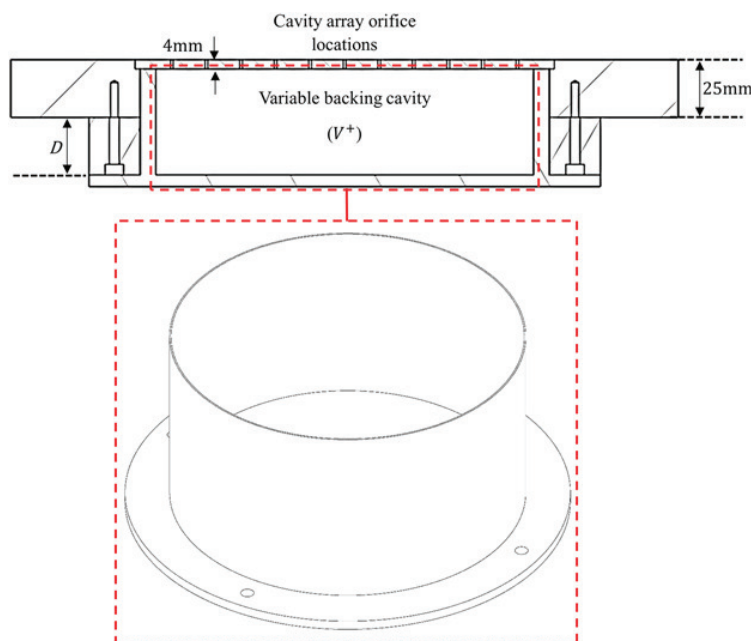

FIG. 3. Schematic of cavity array with a common backing cavity, with isometric view of the backing cavity.
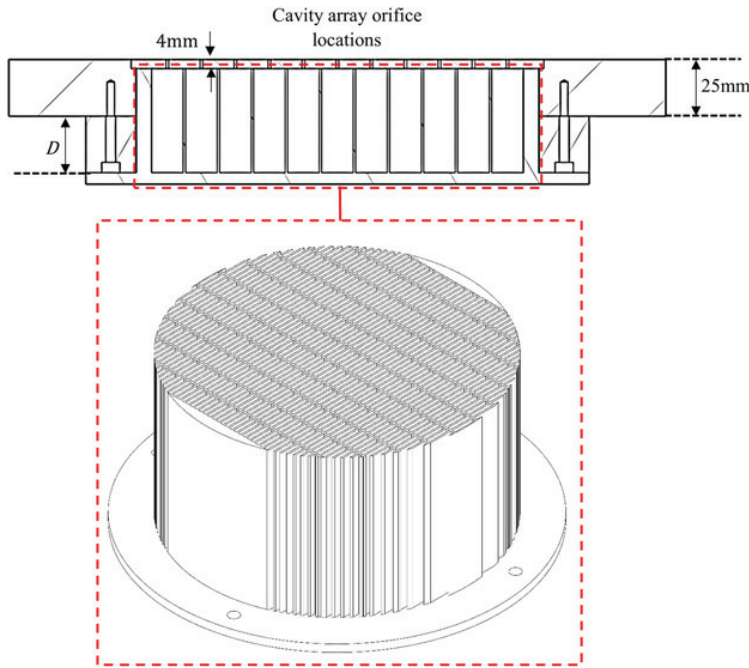
FIG. 4. Schematic of cavity array with individual backing cavities via use of a mesh, with isometric view of the backing mesh.

previous research (Silvestri *et al.*, 2016; 2017a; 2017b; and 2017d) and design guidelines recommended by Lockerby (2001), the cavity array was manufactured to the specifications outlined in Fig. 2. This resulted in a cavity array with an orifice diameter of 1.2 mm ($d^+ \approx 60$), a streamwise spacing of 15 mm ($x^+ \approx 750$) between each row of cavities, and a spanwise spacing of 3 mm ($z^+ \approx 150$). These viscous length scales correspond to the most optimal boundary layer control as previously discussed by Silvestri *et al.* (2017a).

Two groups of backing cavities at three different depths were investigated as shown in Table I.

The first group of backing cavities are near identical to the previous models investigated by Silvestri *et al.* (2017d), as shown in Fig. 3. The orifices in the cavity array share a common backing cavity allowing each orifice to communicate with one another through the backing volume. The second group of the investigated backing cavity arrangements utilises

a mesh design (Fig. 4) to prohibit the flow being captured by each individual cavity to interact. This design converts the previously common backing volume into an uncoupled backing cavity, which allows each individual orifice to have its own individual backing volume (Fig. 4). The first group of arrays, which are utilising a common backing cavity, are being used to determine the non-linear relationship between sweep intensity reduction and backing cavity volume. The second group of arrays, utilising an uncoupled backing cavity will be ultimately used to determine which hypothesis from previous work (Silvestri *et al.*, 2017b; 2017d) accurately defines the mechanism of the cavity array once a sweep event has been captured.

All streamwise velocity measurements throughout this investigation were non-dimensionalised using the viscous length scale $\left(\frac{\nu}{u_\tau}\right)$ and friction velocity (u_τ). This was achieved by applying an initial estimation of the friction velocity (u_τ)
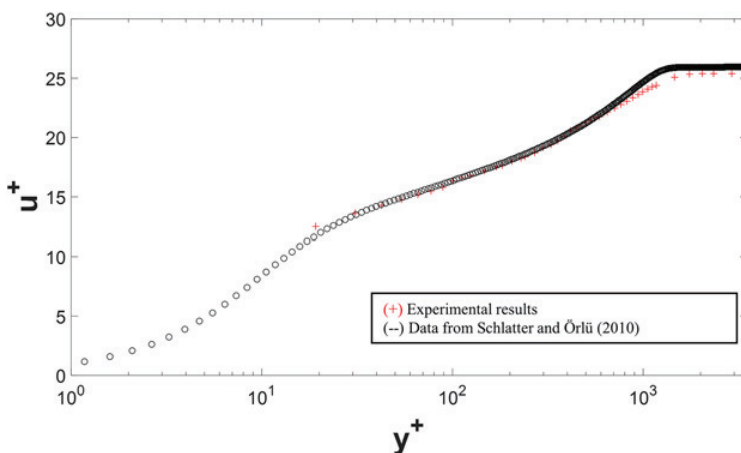

FIG. 5. Mean velocity profile of the boundary layer at $Re_\theta = 3771$. (+ [red]) Experimental flat plate results in this work, (o [black]) data from Schlatter and Örlü (2010) at $Re_\theta = 4064$.

of the turbulent boundary layer. An iterative process defined by Kendall and Koochesfahani (2006) and applied by Ghanadi *et al.* (2014a; 2014b) and Silvestri *et al.* (2017a; 2017c; and 2017d) was used to estimate the friction velocity. The process uses a varying u_τ to curve fit the logarithmic region of the experimental hot-wire data with the Clauser (1954) log law. To validate the iterative process, the experimental data have been compared to previously published data by Schlatter and Örlü (2010). Figure 5 shows the non-dimensional mean velocity profile at $Re_\theta = 3771$, which has been compared against the work of Schlatter and Örlü (2010). As shown in Fig. 5, the measured boundary layer matches the previously published data very closely (maximum streamwise velocity error in the logarithmic region by less than 1%). The experimental data from the work of Schlatter and Örlü (2010) deviate slightly from the experimental results from this investigation, which is associated with the difference in Reynolds numbers.

III. STREAMWISE VELOCITY AND TURBULENCE INTENSITY PROFILE

The streamwise velocity and turbulence intensity profiles of the turbulent boundary layer were measured downstream of the cavity array and the unaltered turbulent boundary layer. This has been included to give confidence in utilising the Clauser (1954) log law curve fit approach to estimate the friction velocity and viscous length scale for both the unaltered boundary layer and the boundary layer with control. Figure 6 shows the streamwise velocity profile at the Reynolds number $Re_\theta = 2939$, where the velocity profiles of each investigated case collapse upon each other. As the boundary layers investigated (with and without control) are not significantly different, it can be assumed that the logarithmic region has a relationship with the canonical friction velocity as per a conventional turbulent boundary layer.

While the mean streamwise velocity profile of the boundary layer is unaffected by the cavity array, the turbulence intensity profile is affected. The turbulence intensity is a statistical concept that measures the magnitude of turbulence in the boundary layer. Figures 7 and 8 show the turbulence intensity profiles of the investigated boundary layers at a Reynolds number of $Re_\theta = 2939$ and $Re_\theta = 3771$, respectively. All cavity array arrangements produced a significant reduction of the turbulence intensity in the logarithmic region ($50 < y^+ < 200$) indicating a significant reduction in the velocity fluctuations. This area has been enlarged in both figures to better represent the reduction achieved and the results have been summarised
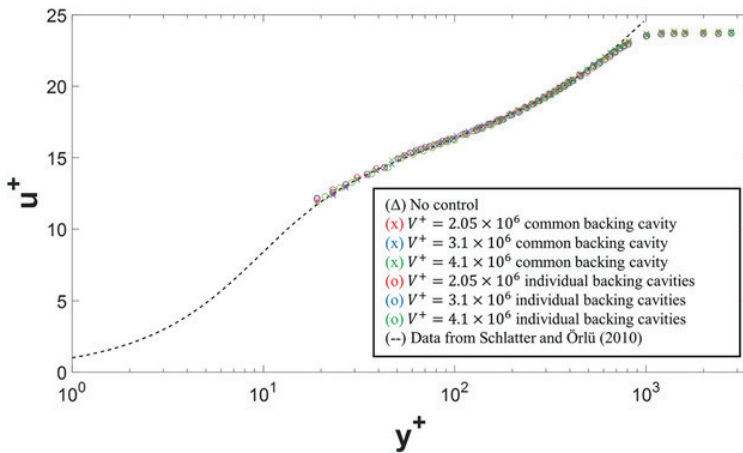
FIG. 6. Streamwise mean velocity profile at $Re_\theta = 2939$ downstream of the array. (Δ [black]) No control, (x [red]) $V^+ = 2.05 \times 10^6$ with common backing cavity (Fig. 3), (x [blue]) $V^+ = 3.1 \times 10^6$ with common backing cavity (Fig. 3), (x [green]) $V^+ = 4.1 \times 10^6$ with common backing cavity (Fig. 3), (o [red]) $V^+ = 2.05 \times 10^6$ with individual backing cavities (Fig. 4), (o [blue]) $V^+ = 3.1 \times 10^6$ with individual backing cavities (Fig. 4), (o [green]) $V^+ = 4.1 \times 10^6$ with individual backing cavities (Fig. 4), (-- [black]) data from Schlatter and Örlü (2010) at $Re_\theta = 3030$.

FIG. 7. Turbulence intensity profile at $Re_\theta = 2939$ downstream of the array. (Δ [black]) No control, (x [red]) $V^+ = 2.05 \times 10^6$ with common backing cavity (Fig. 3), (x [blue]) $V^+ = 3.1 \times 10^6$ with common backing cavity (Fig. 3), (x [green]) $V^+ = 4.1 \times 10^6$ with common backing cavity (Fig. 3), (o [red]) $V^+ = 2.05 \times 10^6$ with individual backing cavities (Fig. 4), (o [blue]) $V^+ = 3.1 \times 10^6$ with individual backing cavities (Fig. 4), (o [green]) $V^+ = 4.1 \times 10^6$ with individual backing cavities (Fig. 4).
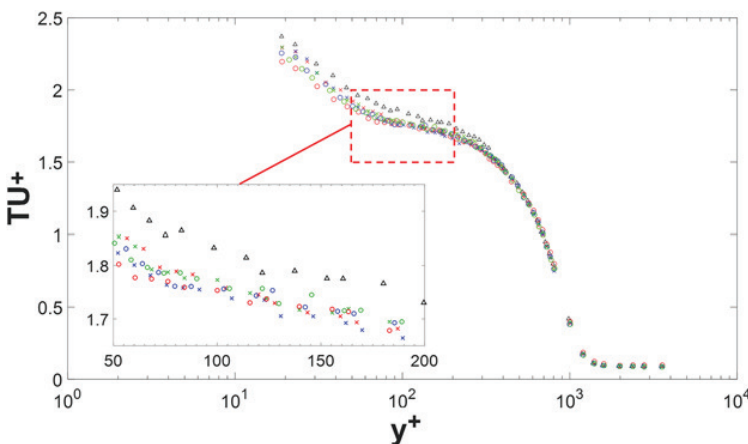
FIG. 8. Turbulence intensity profile at $Re_\theta = 3771$ downstream of the array. (Δ [black]) No control, (x [red]) $V^+ = 3 \times 10^6$ with common backing cavity (Fig. 3), (x [blue]) $V^+ = 4.5 \times 10^6$ with common backing cavity (Fig. 3), (x [green]) $V^+ = 6 \times 10^6$ with common backing cavity (Fig. 3), (o [red]) $V^+ = 3 \times 10^6$ with individual backing cavities (Fig. 4), (o [blue]) $V^+ = 4.5 \times 10^6$ with individual backing cavities (Fig. 4), (o [green]) $V^+ = 6 \times 10^6$ with individual backing cavities (Fig. 4).
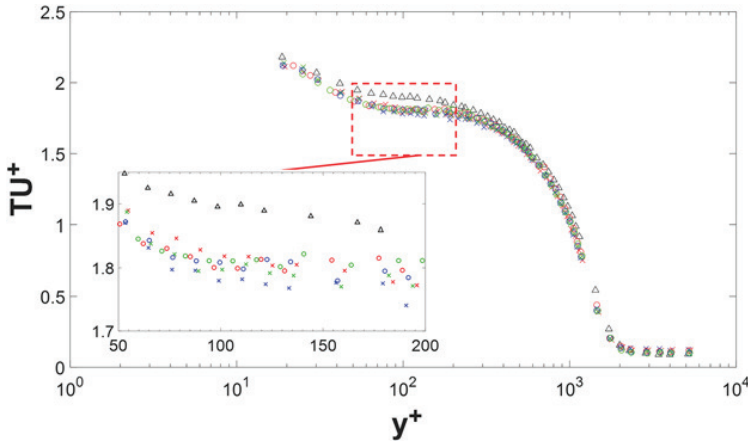
in Table II. At $Re_\theta = 2939$, the minimum and maximum reduction achieved are 4.7% and 7.5%, while at $Re_\theta = 3771$ the minimum and maximum reduction achieved are 4.4% and 7.7%, respectively. While the reduction in turbulence intensity reduction varies, it can be easily seen in Figs. 7 and 8 that the cavity array is able to reduce the turbulence energy when there is no mesh present in the backing cavity (common backing cavity) and when the mesh is installed in the backing cavity (individual backing cavities). While there is no noticeable trend or change in the results, this is believed to be due to the backing volume having significantly less effect on modifying the reduction in turbulence intensity in comparison to the cavity array's other geometric properties (Silvestri *et al.*, 2016; 2017a; 2017b; and 2017d). The cavity array is however successful in controlling the boundary layer irrespective of the individual cavities communicating with one another, suggesting that the cavity array weakens the structure of captured sweep events by damping the energy of the events through the friction loses in the individual cavity and the volume below the array in the backing cavity. To confirm this initial finding, the higher order statistics

of the boundary layer have been investigated, i.e., the magnitude, duration of the coherent structures, and the pre-multiplied energy spectrum.

IV. MAGNITUDE AND DURATION OF THE COHERENT STRUCTURES

The magnitude and duration of the coherent structures has also been considered in this research. To calculate the magnitude and duration of the coherent structures, the variable interval time averaging (VITA) technique, initially applied by Blackwelder and Kaplan (1976), was used to detect and measure the changes in the turbulent boundary layer associated with these structures. The VITA technique has been utilised by many researchers, but not limited to Adrian *et al.* (2000); Choi *et al.* (2011); Whalley (2011); and Ghanadi *et al.* (2015) and more recently by Silvestri *et al.* (2017a; 2017d) to detect events in the boundary layer using the definitions below, $\hat{u}(t, T_W)$ is defined as the local mean of the fluctuating velocity signal and

TABLE II. Summary of the turbulence intensity reduction achieved in this investigation.

	Cavity array with a common backing cavity			
	$Re_\theta = 2939$		$Re_\theta = 3771$	
Case	V^+	Turbulence intensity reduction (%)	V^+	Turbulence intensity reduction (%)
$D = 25$ mm	2.05×10^6	5.5	3×10^6	4.4
$D = 50$ mm	3.1×10^6	7.5	4.5×10^6	7.7
$D = 75$ mm	4.1×10^6	4.7	6×10^6	5.5
	Cavity array with individual backing cavities via use of a mesh			
	$Re_\theta = 2939$		$Re_\theta = 3771$	
Case	V^+	Turbulence intensity reduction (%)	V^+	Turbulence intensity reduction (%)
$D = 25$ mm	2.05×10^6	5.8	3×10^6	5.7
$D = 50$ mm	3.1×10^6	6.3	4.5×10^6	5.8
$D = 75$ mm	4.1×10^6	5.5	6×10^6	5.2

Paper 4: Mechanism of sweep event attenuation using micro-cavities in a turbulent boundary layer
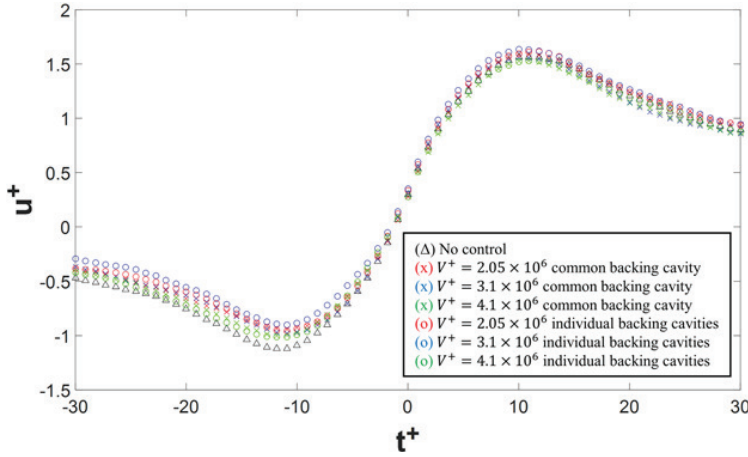
FIG. 9. Sweep VITA events at Re_θ = 2939. (Δ [black]) No control, (x [red]) $V^+ = 2.05 \times 10^6$ with common backing cavity (Fig. 3), (x [blue]) $V^+ = 3.1 \times 10^6$ with common backing cavity (Fig. 3), (x [green]) $V^+ = 4.1 \times 10^6$ with common backing cavity (Fig. 3), (o [red]) $V^+ = 2.05 \times 10^6$ with individual backing cavities (Fig. 4), (o [blue]) $V^+ = 3.1 \times 10^6$ with individual backing cavities (Fig. 4), (o [green]) $V^+ = 4.1 \times 10^6$ with individual backing cavities (Fig. 4).

$$\hat{u}(t, T_W) = \frac{1}{T_W} \int_{t-T_w/2}^{t+T_w/2} u(t)dt, \qquad (1)$$

$$Var(t, T_W) = \hat{u}^2(t, T_W) - [\hat{u}(t, T_W)]^2, \qquad (2)$$

$$Var(t) = \lim_{t\to\infty} \frac{1}{t} \int_0^t u^2(t)dt. \qquad (3)$$

For this research, the authors have continued to use the method specified by Silvestri *et al.* (2017a) and Whalley (2011), using a value of 1.2 for k as per the recommendations of Silvestri *et al.* (2017a) and Whalley (2011). If the local variance, $Var(t, T_W)$, is greater than the variance of the entire signal $kVar(t)$, a sweep or ejection event is considered to have occurred. The detection function, $D(t)$, is defined below as outlined by Whalley (2011) and Silvestri *et al.* (2017a),

$$D(t) = \begin{cases} 1 & Var(t, T_W) > kVar(t), \quad \frac{du}{dt} > 0, \quad \text{sweep event} \\ 0 & Var(t, T_W) > kVar(t), \qquad\qquad \text{no event} \\ -1 & Var(t, T_W) > kVar(t), \quad \frac{du}{dt} < 0, \quad \text{ejection event} \end{cases}. \qquad (4)$$

The averaged VITA events were used to calculate the intensity and duration of the sweep events. Decreased duration or intensity of the events reveals a decrease in the turbulence energy production. Here a total of 500–980 ensembles were used in each VITA analysis dependent on the Reynolds number. All analyses were performed at approximately y^+ = 100, which corresponds to the location of the boundary layer where the maximum turbulence intensity reduction occurs as previously explained by Silvestri *et al.* (2017a).

Applying the VITA analysis to the boundary layer at a Reynolds number of Re_θ = 2939 leads to the results found in Fig. 9. The intensity of the events is calculated based on the peak-to-peak value of the streamwise velocity of the events representing the acceleration of the detected event. A decrease in the sweep intensity coincides with a decrease in the turbulent energy production, which is desired during boundary layer control as it will reduce the shear stresses in the near wall region. Similar to the turbulence intensity results shown in Figs. 7 and 8, all cavity array configurations reduced the intensity of the sweep events (Table III), where a maximum 6.6% reduction was achieved. The reduction achieved is slightly

TABLE III. Summary of the sweep intensity reduction achieved.

	Cavity array with a common backing cavity				
	Re_θ = 2939			Re_θ = 3771	
Case	V^+	Sweep intensity reduction (%)	V^+	Sweep intensity reduction (%)
D = 25 mm	2.05×10^6	5.8	3×10^6	5.8
D = 50 mm	3.1×10^6	6.4	4.5×10^6	6.8
D = 75 mm	4.1×10^6	6.5	6×10^6	7.0

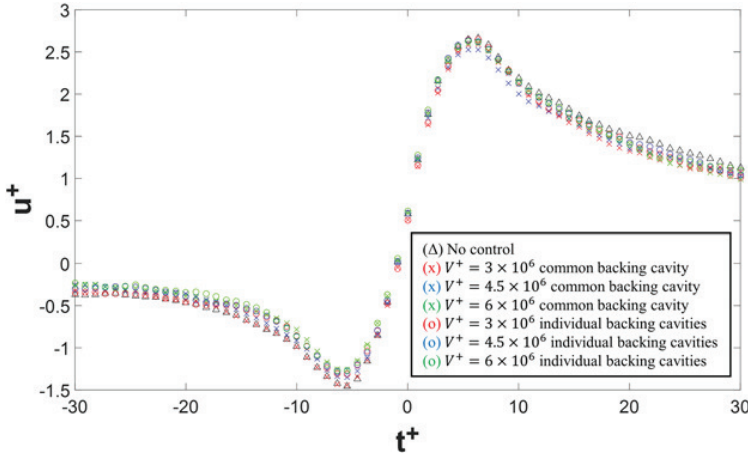|	Cavity array with individual backing cavities via use of a mesh				
	Re_θ = 2939			Re_θ = 3771	
Case	V^+	Sweep intensity reduction (%)	V^+	Sweep intensity reduction (%)
D = 25 mm	2.05×10^6	5.3	3×10^6	5.3
D = 50 mm	3.1×10^6	6.4	4.5×10^6	6.4
D = 75 mm	4.1×10^6	6.4	6×10^6	6.6

FIG. 10. Sweep VITA events at $Re_\theta = 3771$. (Δ [black]) No control, (x [red]) $V^+ = 3 \times 10^6$ with common backing cavity (Fig. 3), (x [blue]) $V^+ = 4.5 \times 10^6$ with common backing cavity (Fig. 3), (x [green]) $V^+ = 6 \times 10^6$ with common backing cavity (Fig. 3), (o [red]) $V^+ = 3 \times 10^6$ with individual backing cavities (Fig. 4), (o [blue]) $V^+ = 4.5 \times 10^6$ with individual backing cavities (Fig. 4), (o [green]) $V^+ = 6 \times 10^6$ with individual backing cavities (Fig. 4).

larger than the previously reported value by Silvestri *et al.* (2017d), which was a maximum reduction of 5.7% at the same Reynolds number and configuration, but at a smaller common backing cavity volume. While the maximum value obtained in this research is higher than the results from the work of Silvestri *et al.* (2017d) (5.7%), the results vary very little between the two largest backing cavity volumes in this paper. At $V^+ = 4.1 \times 10^6$, the sweep intensity reduction is only shown to increase by 0.2% in comparison to the results from $V^+ = 3.1 \times 10^6$. Thus illustrating a plateau of the achieved sweep intensity reduction as the backing cavity volume is increased. Furthermore the cavity array is successful in controlling the boundary layer once again irrespective of the individual cavities communicating with one another. This consequently suggests that the cavity array weakens the structure of captured sweep events by damping the energy of the events through the friction loses in the individual cavity and the volume of below the array in the backing cavity.

The VITA analysis was also applied to the boundary layer at a Reynolds number of $Re_\theta = 3771$, the results of which are shown in Fig. 10 and summarised in Table III. Similar to the results at a $Re_\theta = 2939$, all cavity array configurations demonstrated a reduction in the intensity of the sweep events. For the larger Reynolds number, a maximum sweep

intensity reduction of 7.1% was achieved. This is once again slightly larger than 5.7% reported previously by Silvestri *et al.* (2017d) at the same Reynolds number and configuration, but at a smaller common backing cavity volume. Similar to the previous Reynolds number ($Re_\theta = 2939$), there is strong evidence that the non-linear relationship between backing cavity volume and flow control reaches an upper limit. The two largest backing cavity volumes were once again shown to have a negligible 0.2% difference in the achieved sweep intensity reduction illustrating a limiting value for reduction achieved. Additionally the cavity array was successful in controlling the boundary layer irrespective of the individual cavities communicating with one another (Choi and Graham, 1998).

V. PRE-MULTIPLIED ENERGY SPECTRUM OF THE BOUNDARY LAYER

The average pre-multiplied energy spectra of multiple velocity histories at the different Reynolds numbers have also been investigated. For this investigation, the pre-multiplied energy spectrum is used to show the effect of the cavity array on the energy spectrum at all wavelengths, which is defined as $\Psi_x = \frac{K_x \times FFT(u)}{u_\tau^2}$ (where K_x is the streamwise wavenumber

FIG. 11. Average pre-multiplied energy spectra at $Re_\theta = 2939$. (Solid [black]) No control, (solid [red]) $V^+ = 2.05 \times 10^6$ with common backing cavity (Fig. 3), (solid [blue]) $V^+ = 3.1 \times 10^6$ with common backing cavity (Fig. 3), (solid [green]) $V^+ = 4.1 \times 10^6$ with common backing cavity (Fig. 3), (broken [red]) $V^+ = 2.05 \times 10^6$ with individual backing cavities (Fig. 4), (broken [blue]) $V^+ = 3.1 \times 10^6$ with individual backing cavities (Fig. 4), (broken [green]) $V^+ = 4.1 \times 10^6$ with individual backing cavities (Fig. 4).

TABLE IV. Summary of the reduction in the pre-multiplied energy spectra.

	Cavity array with a common backing cavity				
	$Re_\theta = 2939$		$Re_\theta = 3771$		
Case	V^+	Energy spectrum reduction (%)	V^+	Energy spectrum reduction (%)
$D = 25$ mm	2.05×10^6	8.4	3×10^6	11.1
$D = 50$ mm	3.1×10^6	8.2	4.5×10^6	12.5
$D = 75$ mm	4.1×10^6	8.2	6×10^6	11.9
	Cavity array with individual backing cavities via use of a mesh				
	$Re_\theta = 2939$		$Re_\theta = 3771$		
Case	V^+	Energy spectrum reduction (%)	V^+	Energy spectrum reduction (%)
$D = 25$ mm	2.05×10^6	7.7	3×10^6	10.6
$D = 50$ mm	3.1×10^6	7.6	4.5×10^6	11.2
$D = 75$ mm	4.1×10^6	8.4	6×10^6	11.4

and FFT is the fast Fourier transform). All of the energy spectrum analyses were conducted at a y^+ equal to 100, where the buffer and logarithmic regions are located and hence a significant proportion of the turbulent energy production is located (Kline *et al.*, 1967 and Jimenez, 2013). Figure 11 shows the pre-multiplied energy spectra at a Reynolds number value of $Re_\theta = 2937$, where it can be seen that a significant reduction has occurred in the low and mid-range wavelength values ($\lambda^+ < 10^4$), which is commonly associated with the coherent structures (Bandyopadhyay and Hussain, 1984 and Robinson, 1991), consequently providing further evidence that the cavity array weakens the structure of captured sweep events. A maximum reduction in the energy of 8.4% was achieved in this analysis, which is summarised in Table IV. Similar to the previous results found in this paper, the authors are able to achieve a reduction in the energy spectrum when the backing cavity is shared by all of the orifices and when the backing cavity is uncoupled, illustrating that no communication between each cavity is required for turbulent boundary layer control.

Figure 12 shows the pre-multiplied energy spectra at $Re_\theta = 3771$. Compared to the lower Reynolds number

($Re_\theta = 2939$), a more significant reduction in the energy spectra is observed at the higher Reynolds number ($Re_\theta = 3771$). At a Reynolds number of $Re_\theta = 3771$, a maximum reduction value of 12.5% was achieved as can be seen in Table IV. The cavity array was once again successful in controlling the boundary layer irrespective of the individual cavities communicating with one another strongly supporting the hypothesis detailed in this paper. Furthermore, at the higher Reynolds number a reduction is achieved over a greater range of wavelengths ($\lambda^+ < 10^5$). However, a significant reduction has occurred once again in the low and mid-range wavelength values, which is showing an effect on the coherent structures.

VI. DISCUSSION

A. Determining the mechanism of the cavity array that successfully controls the sweep events and the importance of the backing cavity

Micro-cavities modify the coherent structures found in the near wall region of the boundary layer (Silvestri *et al.*, 2017a).
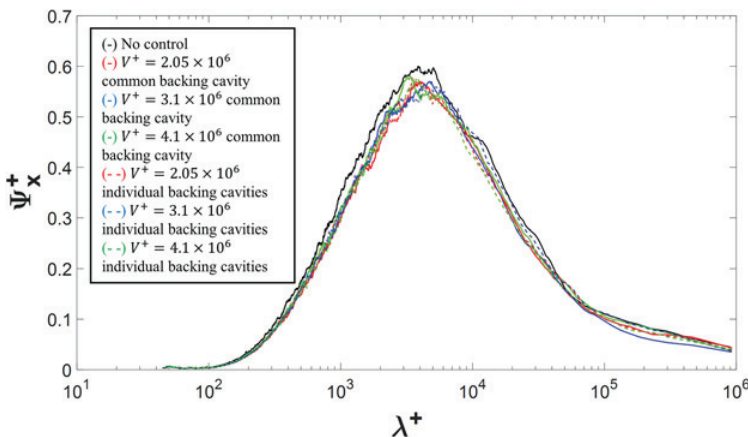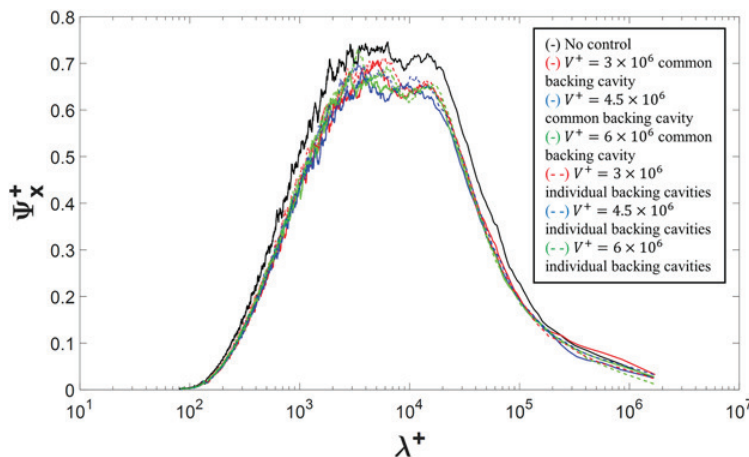

FIG. 12. Average pre-multiplied energy spectra at $Re_\theta = 3771$. (Solid [black]) No control, (solid [red]) $V^+ = 3 \times 10^6$ with common backing cavity (Fig. 3), (solid [blue]) $V^+ = 4.5 \times 10^6$ with common backing cavity (Fig. 3), (solid [green]) $V^+ = 6 \times 10^6$ with common backing cavity (Fig. 3), (broken [red]) $V^+ = 3 \times 10^6$ with individual backing cavities (Fig. 4), (broken [blue]) $V^+ = 4.5 \times 10^6$ with individual backing cavities (Fig. 4), (broken [green]) $V^+ = 6 \times 10^6$ with individual backing cavities (Fig. 4).

FIG. 13. Average VITA intensity reduction with respect to the volume of the backing cavity at $y^+ = 100$. (o– [blue]) $Re_\theta = 2939$ from the work of Silvestri *et al.* (2017d), (o- [blue]) $Re_\theta = 2939$ from the present study, (+-- [red]) $Re_\theta = 3771$ from the work of Silvestri *et al.* (2017d), (+- [red]) $Re_\theta = 3771$ from the present study.
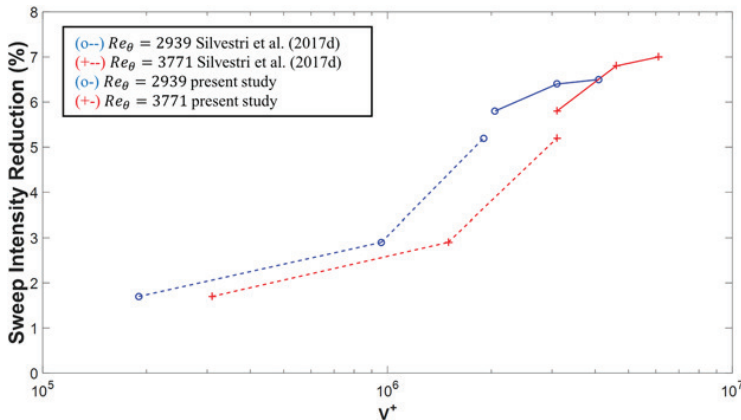
It had previously been hypothesised that the cavities would target the sweep events by capturing the structures to achieve the goal of disrupting the bursting process. The results from this evaluation and previous work (Silvestri *et al.*, 2017b; 2017d) strongly suggest that the cavity array weakens the structure of the captured sweep events by damping the energy of the events through the friction losses in the neck of the orifice and the large volume of the backing cavity below the array itself. As shown throughout this paper, the two groups of backing cavities (common backing cavity and individual backing cavities) were capable of producing a significant reduction on the turbulent boundary layer statistics. The case which shared a common backing cavity allowed all of the individual orifices to be connected from the backing cavity. This design has been shown in the past to be successful in controlling the boundary layer, which made it difficult in determining the mechanism of reduction. Consequently the other cases investigated in this analysis implemented a mesh design in the backing cavity to ensure that all the orifices were not connected to one another, creating a series of individual backing cavities for each orifice.

From the results, both cases (common backing cavity and individual backing cavities) were capable of producing flow control with very similar behaviour and results. This demonstrated that the reduction process occurs irrespective of the cavities being connected. Therefore the hypothesis made previously by the authors (Silvestri *et al.*, 2017b; 2017d) suggesting that the energy of the captured event is redistributed across all orifices in the cavity array is invalid. Flow control is therefore associated with a weakening of the structure of the captured sweep events by damping the energy of the events as discussed. The results throughout this investigation also consistently show that the cases without the mesh and consequently a shared backing cavity are generating a greater reduction in the turbulence properties investigated (turbulence intensity, sweep intensity and energy spectrum) compared to the cases where individual backing cavities are used via a mesh. While initially this might suggest that the mesh affects the mechanism of boundary layer control, the authors do not believe this to be the case. When the mesh is inserted into the backing cavity, a small reduction in the backing cavity volume occurs ($\approx 18\%$ reduction). This would consequently result in

the slightly different values between the cases where a common backing cavity is used and when individual backing cavities are applied.

B. Establishment of the non-linear relationship between cavity backing volume and sweep event control

Furthermore an additional aim of this research was to better understand the non-linear relationship between increasing the cavity volume and the reduction in the sweep events, which is depicted in Fig. 13. The previous work by Silvestri *et al.* (2017d) suggested an upper limit in the obtainable sweep intensity reduction, which was however not found in this paper. While the initial data by Silvestri *et al.* (2017d) did not examine a large enough range to confirm this hypothesis, additional configurations in this research has been used to show the relationship. The reduction values achieved in this research continued to increase (maximum reduction of 7.1%) beyond the values reported by Silvestri *et al.* (2017d) (5.7% reduction in sweep intensity). While the maximum value is higher than the previously recorded value (5.7%), the reduction achieved varies very little between the two largest backing cavity volumes in this paper at both Reynolds numbers. The two largest backing cavity volumes at each Reynolds number were shown to have a negligible 0.2% difference in the achieved sweep intensity reduction illustrating a plateau of the reduction achieved.

VII. SUMMARY AND CONCLUSION

Micro-cavities have been shown to have a significant effect in modifying the coherent structures found in turbulent boundary layers and targeting these structures results in the disruption of the bursting cycle, which is responsible for the shear stresses in the near wall region. However, despite quantitative measurements showing a reduction in turbulence intensity, sweep intensity, and energy spectra, the exact mechanism for the reduction was unknown. For this investigation, a single plate cavity array has been analyzed with a variety of different backing cavities with different volumes and arrangements. Hot-wire anemometry

downstream of the investigated arrays has been used to measure the boundary layer, where the results were then used to evaluate the streamwise velocity and turbulence intensity profile, coherent structures, and the pre-multiplied energy spectrum.

The results from this work aimed to resolve the gaps left in previous studies relating to the application of the passive cavity array as a potential flow control device. From this research, it has been shown that the cavity array weakens the structure of the captured sweep events by damping the energy of the events through the friction losses in the neck of each orifice and the high dissipation of energy from the large volume of the backing cavity below the array. In addition, the true relationship between the backing cavity's volume and sweep intensity reduction was investigated. This was shown to be a non-linear relationship with an upper limit and plateau at larger backing cavity volumes.

The conclusions found in this work are based on altering the volume and geometry of the backing cavity. The findings of this paper are shown to be a significant step forward in the future of controlling the turbulent boundary layer. A clear understanding of the cavity arrays ability to capture the sweep structures and diminish the impact of subsequent coherent structures has been established allowing for future work to visualise the flow of the boundary layer over and into the cavity array. Future studies endeavour to complete this task using numerical modeling or experimental flow visualisation techniques. In addition, hot film sensors and cross probes will be used in future research to calculate the shear stresses directly providing evidence to support the cavity array as a potential skin friction drag reduction technique. While continual research is required to optimise this revolutionary passive control technique, the significance of the results in this research will help develop the knowledge for this area in the future.

Adrian, R. J., Meinhart, C. D., and Tomkins, C. D., "Vortex organization in the outer region of the turbulent boundary layer," J. Fluid Mech. **422**, 1–54 (2000).

Bandyopadhyay, P. R. and Hussain, A. K. M. F., "The coupling between scales in shear flows," Phys. Fluids **27**(9), 2221–2228 (1984).

Benschop, H. O. G. and Breugem, W. P., "Drag reduction by herringbone riblet texture in direct numerical simulations of turbulent channel flow," J. Turbul. **18**(8), 717–759 (2017).

Blackwelder, R. F. and Kaplan, R. E., "On the wall structure of the turbulent boundary layer," J. Fluid Mech. **76**(1), 89–112 (1976).

Choi, K. S., "On physical mechanism of turbulent drag reduction using riblets," in *Transport Phenomena in Turbulent Flows* (Hemisphere Publishing Corp., New York, USA, 1987), pp. 185–198.

Choi, K. S., "Near-wall structure of a turbulent boundary layer with riblets," J. Fluid Mech. **208**, 417–458 (1989).

Choi, K. S. and Fujisawa, N., "Possibility of drag reduction using d-type roughness," Appl. Sci. Res. **50**, 315–324 (1993).

Choi, K. S. and Graham, M., "Drag reduction of turbulent pipe flows by circular-wall oscillation," Phys. Fluids **10**(1), 7–9 (1998).

Choi, K. S., Jukes, T., and Whalley, R., "Turbulent boundary-layer control with plasma actuators," Philos. Trans. R. Soc., A **369**, 1443–1458 (2011).

Clauser, F. H., "The turbulent boundary layer," Adv. Appl. Mech. **4**, 1–51 (1954).

Gad-el Hak, M., "Interactive control of turbulent boundary layers—A futuristic overview," AIAA J. **32**(9), 1753–1765 (1994).

García-Mayoral, R. and Jiménez, J., "Drag reduction by riblets," Philos. Trans. R. Soc., A **369**(1940), 1412–1427 (2011).

Ghanadi, F., "Application of a Helmholtz resonator excited by grazing flow for manipulation of a turbulent boundary layer," Ph.D. thesis, School of Mechanical Engineering, University of Adelaide, Australia, 2015.

Ghanadi, F., Arjomandi, M., Cazzolato, B. S., and Zander, A. C., "Understanding of the flow behaviour on a Helmholtz resonator excited by grazing flow," Int. J. Comput. Fluid Dyn. **28**(5), 219–231 (2014a).

Ghanadi, F., Arjomandi, M., Cazzolato, B. S., and Zander, A. C., "Interaction of a flow-excited Helmholtz resonator with a grazing turbulent boundary layer," Exp. Therm. Fluid Sci. **58**, 80–92 (2014b).

Ghanadi, F., Arjomandi, M., Cazzolato, B. S., and Zander, A. C., "Analysis of the turbulent boundary layer in the vicinity of a self-excited cylindrical Helmholtz resonator," J. Turbul. **16**, 705–728 (2015).

Greidanus, A. J., Delfos, R., Tokgoz, S., and Westerweel, J., "Turbulent Taylor–Couette flow over riblets: Drag reduction and the effect of bulk fluid rotation," Exp. Fluids **56**, 107 (2015).

Hutchins, N., Nickels, T. B., Marusic, I., and Chong, M. S., "Hot-wire spatial resolution issues in wall-bounded turbulence," J. Fluid Mech. **635**, 103 (2009).

Jimenez, J., "Near-wall turbulence," Phys. Fluids **25**, 101302 (2013).

Kendall, A. and Koochesfahani, M., "A method for estimating wall friction in turbulent boundary layer," in *25th AIAA Aerodynamic Measurement Technology and Ground Testing Conference, 5–8 June 2006, San Francisco, California, USA* (AIAA, 2006).

Kevin, K., Monty, J. P., Bai, H. L., Pathikonda, G., Nugroho, B., Barros, J. M., Christensen, K. T., and Hutchins, N., "Cross-stream stereoscopic particle image velocimetry of a modified turbulent boundary layer over directional surface pattern," J. Fluid Mech. **813**, 412–435 (2017).

Kline, S. J., Reynolds, W. C., Schraub, F. A., and Runstadler, P. W., "The structure of turbulent boundary layers," J. Fluid Mech. **30**(4), 741–773 (1967).

Ligrani, O. M. and Bradshaw, P., "Spatial resolution and measurement of turbulence in the viscous sublayer using subminiature hot-wire probes," Exp. Fluids **5**(6), 407–417 (1987).

Lockerby, D., "Numerical simulation of boundary-layer control using MEMS actuation," Ph.D. thesis, The University of Warwick, England, UK, 2001.

Maa, D. Y., "Potential of microperforated panel absorber," J. Acoust. Soc. Am. **104**(5), 2861–2866 (1998).

Marec, J., "Drag reduction: A major task for research," in European Drag Reduction Conference, Potsdam, Germany, 19–21 June 2000.

Qin, S., Chu, N., Yao, Y., Liu, J., Huang, B., and Wu, D., "Stream-wise distribution of skin-friction drag reduction on a flat plate with bubble injection," Phys. Fluids **29**(3), 037103 (2017).

Robinson, S. K., "Coherent motions in the turbulent boundary layer," Annu. Rev. Fluid Mech. **23**, 601–639 (1991).

Schlatter, P. and Örlü, R., "Assessment of direct numerical simulation data of turbulent boundary layers," J. Fluid Mech. **659**, 116–126 (2010).

Silvestri, A., Ghanadi, F., Arjomandi, M., Cazzolato, B. S., and Zander, A. C., "Control of the turbulent boundary layer by the application of a cavity array," in 20th Australasian Fluid Mechanics Conference, Perth, Australia, 5–8 December 2016.

Silvestri, A., Ghanadi, F., Arjomandi, M., Cazzolato, B. S., and Zander, A. C., "Attenuation of sweep events in a turbulent boundary layer using micro-cavities," Exp. Fluids **58**(5), 58 (2017a).

Silvestri, A., Ghanadi, F., Arjomandi, M., Cazzolato, B. S., and Zander, A. C., "The effect of the backing cavity on the control of the turbulent boundary layer by the application of a cavity array," in 10th International Symposium on Turbulence and Shear Flow Phenomena, Chicago, IL, USA, 6–9 July 2017b.

Silvestri, A., Ghanadi, F., Arjomandi, M., Cazzolato, B. S., and Zander, A. C., "The application of different tripping techniques to determine the characteristics of the turbulent boundary layer over a flat plate," J. Fluids Eng. **140**(1), 011204 (2017c).

Silvestri, A., Ghanadi, F., Arjomandi, M., Chin, R., Cazzolato, B. S., and Zander, A. C., "Attenuation of turbulence by the passive control of sweep events in a turbulent boundary layer using micro-cavities," Phys. Fluids **29**, 115102 (2017d).

Walsh, M. J., "Riblets as a viscous drag reduction technique," AIAA J. **21**(4), 485–486 (1983).

Whalley, R. D., "Turbulent boundary-layer control with DBD plasma actuators using spanwise travelling-wave technique," Ph.D. thesis, The University of Nottingham, England, UK, 2011.

Chapter 7

Conclusion and Future Work

In this research micro-cavities have been shown to significantly modify the coherent structures found in turbulent boundary layers. This finding was supported through extensive experimental measurements which focused on the influencing parameters and mechanism by which the cavity array was able to achieve attenuation of the coherent structures. The significant contributions made by this thesis include the analysis of boundary layer transition from laminar to turbulent and how tripping effects the development length. The results demonstrated that to produce a natural turbulent boundary layer using a 2D protuberance, the height of the trip must be less than the undisturbed boundary layer thickness. In addition the effect that a cavity array has on the structure of a turbulent boundary layer has been investigated. The results showed that when the orifice diameter is equal to a value of 60 times the viscous length scale a maximum reduction in the turbulence and sweep intensities of 13% and 14% could be achieved, respectively. Additionally the effect internal (orifice diameter spanwise and streamwise spacing) and external geometry (orifice length and backing cavity volume) of the cavity array on the flow has been identified. The volume of the backing cavity was shown to be the most important parameter in determining the attenuation of streamwise

velocity fluctuations within the logarithmic region of the turbulent boundary layer, while the orifice length of the cavity array was found to have a negligible effect on the impact the cavity array has on the boundary layer. This work culminated in developing an understanding of the mechanism in which the cavity array controls the boundary layer structures. The following chapter summarises the specific conclusions and outcomes of each chapter, and outlines the achievements of this thesis. It concludes with recommendations for future work.

7.1   Characteristics of the turbulent boundary layer

To gain an understanding of the boundary layer and ensure transition into turbulence a thorough analysis of different tripping techniques used to induce a naturally fully developed turbulent boundary layer was investigated. In addition a detailed evaluation was conducted to measure the effect of induced turbulence on the sweep events and other high order statistics of the boundary layer.

The tripping techniques investigated included circular rods, steps and different types of sandpaper. Hot-wire anemometry was used to measure the velocity over a flat plate in a wind tunnel at a variety of locations and Reynolds numbers. The results demonstrated that to produce a natural turbulent boundary layer using a 2D protuberance, the height of the trip must be less than the undisturbed boundary layer thickness. Using such a trip was shown to reduce the development length of the turbulent boundary layer by approximately 50%, which held true for all Reynolds numbers investigated ($Re_x = 1.2 \times 10^5 / Re_x = 1.5 \times 10^6$).

The statistics of the boundary layer were measured to determine the degree to which the investigated boundary layer approximated a naturally turbulent boundary layer. These

statistics included the streamwise velocity profile, turbulence intensity, sweep intensity/duration, power spectral density (PSD) of the velocity fluctuations and the probability density function (PDF) of the data. A number of the investigated boundary layer trips either adversely affected the boundary layer statistics, illustrating an increased turbulence energy production or had no effect at all resulting in no change in the development length of the turbulent boundary layer. The only technique which was shown to have a beneficial effect was a circular rod with a diameter less than the undisturbed boundary layer thickness. The circular rod (d=3mm) was successful in reducing the development length of the boundary layer by 50% whilst maintaining boundary layer statistics similar to a naturally induced turbulent boundary layer. Larger trips were shown to cause a large regeneration region far away from the trip. This resulted in elevated levels of turbulence (turbulence intensity, sweep intensity and pre-multiplied energy spectrum) and was thus avoided when performing experiments requiring a natural turbulent boundary layer. Consequently all subsequent investigations in this thesis utilised the circular rod (d=3mm) to ensure a fully developed turbulent boundary layer during testing.

7.2 Effect on the boundary layer by the cavity array

This study investigated the capability of micro-cavities to control the boundary layer. Experimental measurements of the flow over an array of micro-cavities were analysed and the results showed the cavity array was able to significantly reduce the structures in the turbulent boundary layer. The statistics used to quantify the effect of the cavity array on the boundary layer included the streamwise velocity profile, turbulence intensity,

sweep intensity/duration, power spectral density (PSD) of the velocity fluctuations and the probability density function (PDF) of the data.

The turbulence and sweep intensity were shown to be reduced significantly for certain combinations of micro-cavity geometric parameters. Although the values of reduction was shown to be sensitive to the cavity array parameters, the maximum effect was shown to be a 13% and 14% reduction in the turbulence and sweep intensity respectively. Both statistics are very important when investigating boundary layer control, as a reduction in turbulence intensity shows a reduction in the magnitude of turbulence and velocity fluctuations, while a reduction in sweep intensity shows a decrease in the production of turbulent energy.

In addition, the power spectral density (PSD) and the probability density function (PDF) of the velocity fluctuations were also investigated. The maximum PSD reduction was shown to be 13.4% in the low and mid-range wavelength region ($\lambda_x^+ < 10^4$), which is commonly associated with the coherent structures investigated. The skewness (measure of symmetry) and the kurtosis (measure of peaked or flat data) of the PDF also revealed significant information on the effect the cavity array had on the boundary layer. The cavity arrays demonstrated a maximum reduction in skewness and kurtosis by 18% and 12%, respectively. These changes in the skewness and kurtosis of the boundary layer are a strong indication that the coherent structures have been modified by the use of the cavity arrays.

7.3   Impact of the distribution and sizing of the orifices

Once it was clearly established that cavity arrays could manipulate the sweep events in the boundary layer, the sensitivity of the geometry of the array was investigated. This included the diameter of each orifice in the cavity array, as well as the spanwise and streamwise spacing of each orifice in the array. The results showed that when the orifice diameter is equal to a value of 60 times the viscous length scale a maximum reduction in the turbulence and sweep intensities of 13% and 14%, respectively, could be achieved.

The results also demonstrated that for a cavity orifice diameter less than 20 times the viscous length scale, the sweep events were not captured by the array. Further, if the diameter of the orifice exceeds 145 times the viscous length scale, separation of the shear layer occurs, causing a smaller value of reduction in the turbulence and sweep intensities. The streamwise and spanwise spacing of the micro-cavities were shown to have no significant impact on the reduction capabilities of the cavity array.

7.4   Effect of orifice length and backing volume on sweep attenuation

The sensitivity of the internal geometry of the cavity array arranged flush with the surface was also considered in this thesis. The thickness of the orifice and the volume of the backing cavity were investigated using hotwire anemometry in a wind tunnel at a variety of Reynolds numbers ($1927 < Re_\theta < 3771$).

The volume of the backing cavity was shown to be the most important characteristic in determining the attenuation of streamwise velocity fluctuations within the logarithmic region of the turbulent boundary layer, while the orifice length of the cavity array has negligible effect on the resulting boundary layer. The results showed a maximum

reduction in turbulence generation corresponding to reductions in the average turbulence intensity, peak sweep intensity and average energy spectrum by 7.7%, 7% and 12.5% at the largest backing cavity volume investigated ($V^+ = 6 \times 20^6$).

The non-linear relationship between reduction of sweep event intensity and cavity volume was shown to reach an upper limit, where the energy spectrum was significantly reduced, by 12.5%, in the low and mid-range wavelength region ($\lambda_x^+ < 10^4$) commonly associated with the coherent structures.

7.5   Mechanism by which the micro-cavities achieve boundary layer control

The mechanism responsible for the attenuation of sweep events was also investigated. A single cavity array was analysed, with two different types of backing cavity. The first group of backing cavities shared a common backing cavity volume allowing the exchange of mass and momentum between each orifice via the backing volume. The second group utilised a cellular design to prohibit the captured flow interacting by isolating each orifice to its individual backing cavity. The results show that both cases (common backing cavity and individual backing cavities) were capable of producing flow control with very similar behaviour and results.

The initial hypotheses prior to undertaking these experiments suggested:

1) The cavity array was weakening the structure of the captured sweep events by damping the energy of the events through the friction losses in the orifice and in the large volume of the backing cavity installed below the array.

2) When the captured sweep event enters the cavity array, the mass and energy of the single event is redistributed across all orifices in the cavity array, resulting in

the sweep event being removed from the boundary layer and disrupting the

bursting process.

The results strongly suggested, however, that the cavity array weakened the structure of

the captured sweep events by damping the energy of the events through the friction

losses in the neck of the orifice and also in the large volume of the backing cavity below

the array itself, as the two groups of backing cavities (common backing cavity and

individual backing cavities) were both capable of producing a significant reduction in the

turbulent boundary layer statistics. This demonstrated that the reduction process occurs

irrespective of the orifices being connected and that hypothesis 2), which thus suggested

the energy of the captured event is redistributed across all orifices in the cavity array,

must be invalid.

In summary, the main outcomes of this research *with respect to the objectives of the

thesis* are as follows:

- *Characterise the turbulent boundary layer and investigate how the cavity

  manipulates the boundary layer.* This was achieved by first developing a fully

  transitioned turbulent boundary layer using an artificial tripping techniques. The

  statistics of the boundary layer were measured to determine if the investigated

  boundary layer approximated a naturally turbulent boundary layer. These statistics

  included the streamwise velocity profile, turbulence intensity, sweep

  intensity/duration, power spectral density (PSD) of the velocity fluctuations and the

  probability density function (PDF) of the data. Furthermore experimental

  measurements of the flow over an array of applied micro-cavities were analysed and

  the results showed the cavity array was able to reduce the structures in the turbulent

boundary layer significantly. The maximum effect was shown to be reductions of 13% and 14% in the turbulence and sweep intensity, respectively.

- *Parameterise the configuration and distribution of orifices required to effectively control the boundary layer across the flat plate.* The sensitivity of the performance of the cavity array to its geometry was also investigated. The results showed that when the orifice diameter is equal to a value of 60 times the viscous length scale a maximum reduction in the turbulence and sweep intensities 13% and 14%, respectively, were achieved. Additionally the volume of the backing cavity was shown to be the most important characteristic in determining the attenuation of streamwise velocity fluctuations within the logarithmic region of the turbulent boundary layer, while the orifice length of the cavity array had negligible effect in changing the effect of the cavity array on the boundary layer.

- *Determine the optimal geometric arrangement for the micro-cavities as a boundary layer control device and the method in which the micro-cavities achieve boundary layer control.* The results showed that the maximum reduction in turbulence generation achieved was a reduction in turbulence intensity, sweep intensity and energy spectrum by 7.7%, 7% and 12.5% when the backing cavity volume investigated was at its largest ($V^+ = 6 \times 20^6$). In addition the reduction was shown to occur irrespective of the micro-cavity orifices having a common backing cavity or individual backing cavities. Hence it is suggested that the cavity array weakens the structure of the captured sweep events by damping the energy of the events through the friction losses in the orifice and the large volume of the backing cavity installed below the array.

These outcomes align with the aims of the project stated in the opening chapter, which as can be seen have now all been met.

7.6 Recommendations for future work

While the results in this thesis have shown that micro-cavity arrays can have a significant effect on controlling the turbulent boundary layer on a flat plate, further investigation is warranted. Controlling the turbulent boundary layer is a complex phenomenon and before this technology can be applied to real life applications a considerable amount of additional work is required. This includes undertaking flow visualisation on the cavity array, as well as measuring the true skin friction values over the flat plate. The recommended future work is as follows.

1. Throughout this investigation the free stream turbulence intensity was shown to change slightly between the different experiments conducted. Consequently some results showed greater reduction in the turbulence statistics which was commonly associated with an increased free stream turbulence intensity. As such the level of turbulence reduction achieved is believed to have a relationship with the free stream turbulence intensity. Therefore this forms a gap for this technology, as in real life the free stream turbulence can change during the course of an aircraft flight and the relationship between turbulence reduction and turbulence intensity would need to be identified.

2. While the results were precisely measured using hotwire anemometry, no flow visualisation was conducted in this study. Flow visualisation is beneficial as it allows the entire volume of flow to be analysed as opposed to only a single point as measured by a hotwire. This type of analysis would allow for the detection and

tracking of coherent structures and the resulting change in the structure as they are captured by the array. As such, future studies would need to be consider the use of flow visulisation to identify the effect of the cavity array on the boundary layer. This could be achieved either experimentally using particle image velocimetry (PIV), or numerically using direct numerical simulations (DNS). Use of these two techniques would provide much needed results to develop an increased understanding of the flow in the vicinity of the micro-cavities, in particular at the entrance to the orifice and in the neck of each cavity.

3. This study utilised a single direction hot wire anemometer to measure all of the data presented in this thesis. Consequently no direct measurements of the shear stresses and consequently skin friction values were obtained. Therefore the reductions reported in this thesis are of the turbulence statistics, which, whilst being highly correlated with the shear stresses and skin friction drag, are not able to provide a definitive value of the skin friction drag reduction achieved. This can however be solved by using an X-probe hot wire anemometer which is able to measure the streamwise and spanwise velocity over a flat plate. This was not considered in this work however, as it was beyond the scope of this thesis which aimed to demonstrate a proof of concept.

The completion of the recommend future work would provide significant further advancement of this area of research building on the results presented in this thesis which provide a significant amount of evidence demonstrating the potential of the cavity array as a low cost flow control device to effectively reduce the skin friction drag on flat plates and in aerospace applications.

Appendices

This appendix includes the following conference papers published as:

Silvestri, A, Ghanadi, F, Arjomandi, M, Cazzolato, BS, Zander, AC, 2016, *'Control of the turbulent boundary layer by the application of a cavity array', 20th Australasian Fluid Mechanics Conference*, Perth, Australia, 5-8 December.

Silvestri, A, Ghanadi, F, Arjomandi, M, Cazzolato, BS, Zander, AC, 2017b*, 'The effect of the backing cavity on the control of the turbulent boundary layer by the application of a cavity array', 10th International Symposium on Turbulence and Shear Flow Phenomena*, Chicago, IL, USA, 6-9 July.

Appendix 1: 20th Australasian Fluid Mechanics Conference paper

Statement of Authorship

Title of Paper	Control of the turbulent boundary layer by the application of a cavity array
Publication Status	☑ Published ☐ Accepted for Publication ☐ Submitted for Publication ☐ Unpublished and Unsubmitted work written in manuscript style
Publication Details	Silvestri, A, Ghanadi, F, Arjomandi, M, Cazzolato, BS, Zander, AC, 2016, *'Control of the turbulent boundary layer by the application of a cavity array', 20th Australasian Fluid Mechanics Conference*, Perth, Australia, 5-8 December.

Principal Author

Name of Principal Author (Candidate)	Anton Silvestri		
Contribution to the Paper	Performed data analysis and interpretation, wrote manuscript and acted as corresponding author.		
Overall percentage (%)	70		
Certification:	This paper reports on original research I conducted during the period of my Higher Degree by Research candidature and is not subject to any obligations or contractual agreements with a third party that would constrain its inclusion in this thesis. I am the primary author of this paper.		
Signature		Date	15/06/18

Co-Author Contributions

Name of Co-Author	Farzin Ghanadi
Contribution to the Paper	Supervised the development of the research and contributed in academic discussion and the review process of submitted manuscripts.
Signature	Date 15/06/18

Name of Co-Author	Maziar Arjomandi
Contribution to the Paper	Supervised the development of the research and contributed in academic discussion and the review process of su anuscripts.
Signature	Date 15/06/18

Name of Co-Author	Benjamin Cazzolato
Contribution to the Paper	Supervised the development of the research and contributed in academic discussion and the review process of submitted manuscripts.
Signature	Date 15/06/18

Name of Co-Author	Anthony Zander
Contribution to the Paper	Supervised the development of the research and contributed in academic discussion and the review process of submitted manuscripts.
Signature	Date 15/06/18

Control of the turbulent boundary layer by the application of a cavity array

A. Silvestri, F. Ghanadi, M. Arjomandi, B.S. Cazzolato and A.C. Zander

School of Mechanical Engineering
University of Adelaide, Adelaide, South Australia 5005, Australia

Abstract

The results presented in this paper provide an insight into the effect of a cavity array on the turbulence production within a turbulent boundary layer. In the present study, the turbulent energy production within a fully developed turbulent boundary layer has been reduced using a flushed-surface cavity array underneath a flat plate coupled with an acoustic actuator. The size of the holes in the cavity array were selected to be comparable with the dimensions of the expected coherent structures, based on the friction velocity. Experimental measurements were taken in a wind tunnel at a number of locations along the array in the streamwise direction and at a variety of acoustic frequencies generated by the acoustic actuator. A maximum turbulence intensity and sweep intensity reduction of 11% and 10% respectively occurred at $Re_\theta = 3.771 \times 10^3$ in the logarithmic region of the boundary layer when no drive frequency was provided. From this investigation it has been shown that the drive frequency of the acoustic actuator has no effect on the turbulence reduction by the cavity array. Instead the physical parameters of the array, including the number and diameter of the cavities in the array have a much more significant effect.

Introduction

By reducing the skin friction drag component of viscous drag, the efficiency of all aerospace applications, including aircraft can be improved. A reduction of 5-10% on the fuselage alone resulted in an annual fuel saving of approximately half a billion dollars in the United States during 1989 [1]. This equates to 1.5 billion dollars in today's economy with the increased number of aircrafts. A key focus by the fluid dynamics research community has been to reduce the skin friction drag by controlling the boundary layer, which comprises a significant 48% of the total drag for typical aircraft applications [2]. The most important part of the boundary layer are the coherent structures, which are responsible for the total shear stress in the near wall region. Coherent structures consist of the ejection of low speed fluid from the boundary layer and the inrush of high speed fluid which are known as sweep events [3, 4]. Corino and Brodkey [3] showed that ejection events generated approximately 70% of the total stresses in the near wall region, while the sweep events contributed to the remaining 30%. These two events were shown to be self-replicating and consequently were deemed to be very important during turbulence generation [5, 6]. It is believed a technique which targets this mechanism will cause a more significant reduction in turbulence generation and drag.

One method that will be discussed in this paper is the reduction of the streamwise vortices by producing a local jet at the orifice using an acoustic actuator below the cavity array. This method is very similar to the synthetic jet which has found great success by utilising a diaphragm set in a cavity and driven by a piezo electric element at its resonant frequency. With an open neck and orifice, fluid is drawn in and out of the cavity during the oscillation of the diaphragm. During the outflow cycle vortex rings are generated at

the orifice and travel away from the opening [7]. During the inflow cycle fluid is drawn into the backing cavity below the orifice, which does not affect the vortex ring produced during the next outflow cycle. The design is highly desirable in turbulent flow control due to its self-contained nature with no external fluid source. If timed correctly the ejection process from the acoustically excited cavity array targets fast moving fluid (sweep events), which is moved away from the wall. The inflow stage is used to bring the slow moving fluid (ejection events) closer to the wall. This results in the disruption of both events as research from Lockerby [8] has shown this to be successful.

The passive application of the cavity array to reduce the turbulence generation has also been considered by the authors. By using a cavity with a small orifice the shear layer shall be unaffected crossing the small opening, ensuring the resonance of the Helmholtz mode is not achieved [9, 10]. Consequently only the flow which acts normal to the wall will be affected by the cavity array. In the near wall region the sweep and ejection events act in this direction and consequently this would allow the cavity to be used as a drag reduction method for both higher and lower Reynold's numbers.

The purpose of the present work is to assess the ability of an array of micro-cavities in reducing the turbulent properties of a fully developed boundary layer using either of the two methods discussed above, namely the active and passive applications discussed. In the subsequent sections the characteristics of the cavity array will be discussed and details of the experimental setup will be given. A discussion on the results will be provided and an insight into the capabilities of the cavities' success in reducing the turbulent structures will be provided.

Experimental Procedure

All experiments were performed in a closed-return type wind tunnel located at the University of Adelaide. The tunnel can be operated up to a maximum velocity of 30 m/s with a low level turbulence intensity, fluctuating between 0.4% to 1%. The test section is rectangular with a cross section of $500\text{mm} \times 500\text{mm}$ and 2000mm in length. As shown in Figure 1, a horizontal 2000mm long flat plate was positioned inside the tunnel such that it spanned the whole width of the test section. The finite thickness of the flat plate can lead to bluff body separation effects, therefore to minimize any possible flow separation a super-elliptical leading edge of a nominal major radius of 114mm was attached to the flat plate. A 125mm long circulation flap was also mounted downstream of the plate to minimize any circulation developed over the plate and to ensure that the stagnation point is on the measurement side of the plate. The flap could also be adjusted as appropriate to balance the pressure gradient along the working section. The boundary layer investigated in the study was tripped by a 3mm rod located 140mm downstream of the leading edge as advised by Silvestri et al. [11]. This was done to ensure a fully turbulent boundary layer was achieved for the experimental procedure.
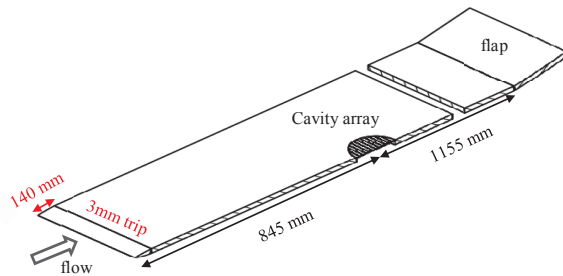
Figure 1: Schematic of the experimental arrangement

This research focuses on the near wall regions, as approximately half of the total turbulence production occurs within this small region [12]. A hot-wire anemometer was used downstream of the boundary layer trip and cavity array to characterize the changes within the boundary layer regions arising from the cavity array located 845mm ($x^+ = 5.13 \times 10^4$) downstream of the leading edge. This length was selected to ensure a fully turbulent boundary layer was developed for the experimental measurements. This was done at four locations ($x^+ = 5.5 \times 10^3$, $x^+ = 8.2 \times 10^3$, $x^+ = 10.9 \times 10^3$, $x^+ = 13.9 \times 10^3$) downstream from the cavity array's leading edge at a single Reynolds numbers and cavity dimension. The streamwise velocity measurements were made with an IFA 300 CTA system, using a single platinum-plated tungsten wire of $5\mu m$ in diameter and 1.25mm in length, which was operated in constant current mode at 0.2mA with an over-heat ratio of 1.8 and an operating temperature around 230°C, which provided sufficient sensitivity to measure the velocity fluctuations with minimum thermal effects. The repeatability of each measurement was also verified 3 times and the data were sampled at 10 kHz for 10 seconds to ensure suitable temporal resolution.

The cavity array (Figure 2) was designed based on the friction velocity value equal to, $u_\tau = 0.5 \, m/s$, a value obtained previously by Silvestri et al. [11] for a Reynolds number approximately equal to, $Re_\theta = 1927$. Using this friction velocity value the spanwise and streamwise spacing and the approximate orifice diameter were calculated based on the method specified by Lockerby [8], which states the orifice diameter to be 40 times the size of the spanwise spacing of the coherent structures. This resulted in a cavity array being designed, utilising 1.2mm diameter holes, with a spanwise spacing of 3mm and a streamwise spacing of 15mm.
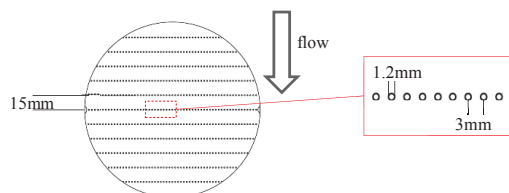

Figure 2: Schematic of the cavity array

This cavity array was tested under multiple conditions, including cases in which the array had an acoustic actuator oscillating at a variety of selected frequencies and as a completely passive control technique. This was done to quantify the turbulence reduction by the active and passive control methods.

Effects of the cavity array on the streamwise and turbulence intensity profiles

When investigating the effect of the cavity array on the turbulent boundary layer a Reynolds number of $Re_\theta = 3771$ was selected. Figure 4 shows the streamwise profile of the boundary layer immediately downstream of the cavity array's leading edge at four locations. The cavity array investigated appears to reduce the thickness of the viscous and logarithmic subregion ($y^+ < 200$), while not changing the overall boundary layer thickness. This can be seen to cause a drag reduction, as with less of the boundary layer consisting of the viscous and logarithmic subregion a reduction in shear stress and skin friction drag will occur.

The array was shown to replicate this for all tested conditons, including the passive array with no excitation and all the experiments conducted with an acoustic actuator coupled at different frequencies. The results indicate that the same amount of reduction was achieved independent on which driving frequency the resonator was set to, including when the array was completely passive and the resonator was not excited.

The reduction of the viscous and logarithmic subregion was also shown to increase downstream of the leading edge. The initial measurement, which was taken at $x^+ = 5.5 * 10^3$ (the midpoint of the cavity array) demonstrated a 4.6% reduction in the viscous and logarithmic subregion in Figure 3(a). This value was shown to increase to 5.3% at $x^+ = 10.9 \times 10^3$ (the end of the cavity array), as shown in Figure 3(b&c). Thus demonstrating the cavity array was responsible for providing the effect on the boundary layer, as the effect was shown to increase once exposed to a larger proportion of the cavity array.

The decrease in the viscous and logarithmic subregion was also shown to continue significantly downstream after the cavity array ended. At a location of $x^+ = 13.9 \times 10^3$ the cavity array was shown to provide a decrease in the subregion by 4.1% (as shown in Figure 3(d)). Thus demonstrating a significant proportion of the boundary layer was changed downstream of the cavity array, showing the effect not to be localised. To illustrate this proposal further the turbulence intensity of the boundary layer was also considered.
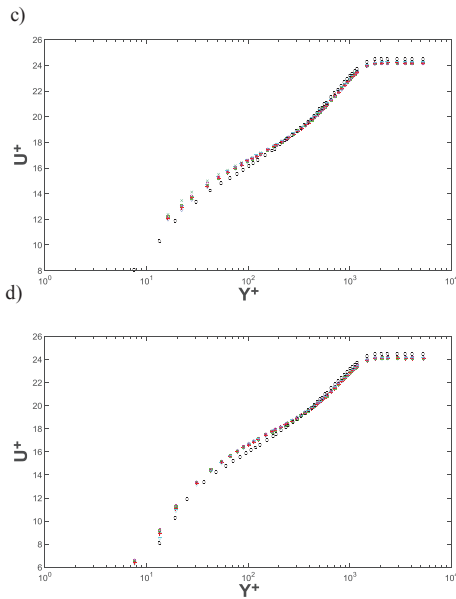
c)

d)
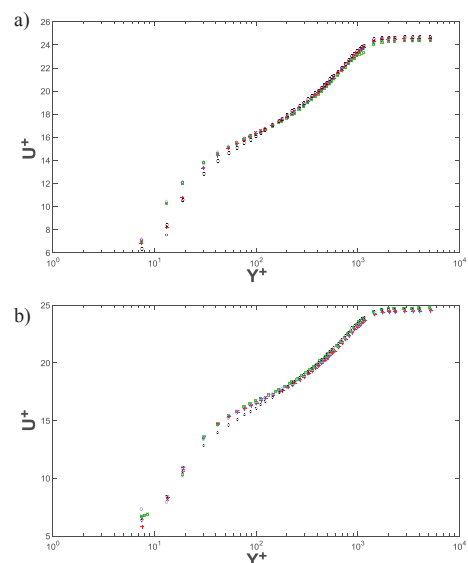
Figure 3: Mean velocity profile at $Re_\theta = 3771$. a) $x^+ = 5.5 \times 10^3$, b) $x^+ = 8.2 \times 10^3$, c) $x^+ = 10.9 \times 10^3$, d) $x^+ = 13.9 \times 10^3$. (o) No control, (▼) cavity array – No excitation, (+) 500Hz excitation, (□) 1000Hz excitation, (◊) 2000Hz excitation, (x) 4000Hz excitation, (*) 8000Hz excitation

The reduction in turbulence intensity is clearly evident in Figure 4 and demonstrates a similar pattern to the results obtained in Figure 3. A turbulence intensity reduction was recorded for all the conditions tested, including the passive array with no excitation and all the experiments conducted with the acoustic actuator driven at different frequencies. The results indicate that the same amount of decrease was achieved independent of the driving frequency, including when the array was completely. This was also observed previously when investigating the mean streamwise profile.

The reduction of the turbulence intensity was also shown to increase the further downstream the measurements were taken. The initial measurement, which was taken at $x^+ = 5.5 \times 10^3$ (the midpoint of the cavity array) demonstrated a 6.6% decrease in the turbulence intensity), as shown in Figure 4(a). This value was shown to increase to 11% at $x^+ = 10.9 \times 10^3$ (the end of the cavity array), as shown in Figure 4(b&c).
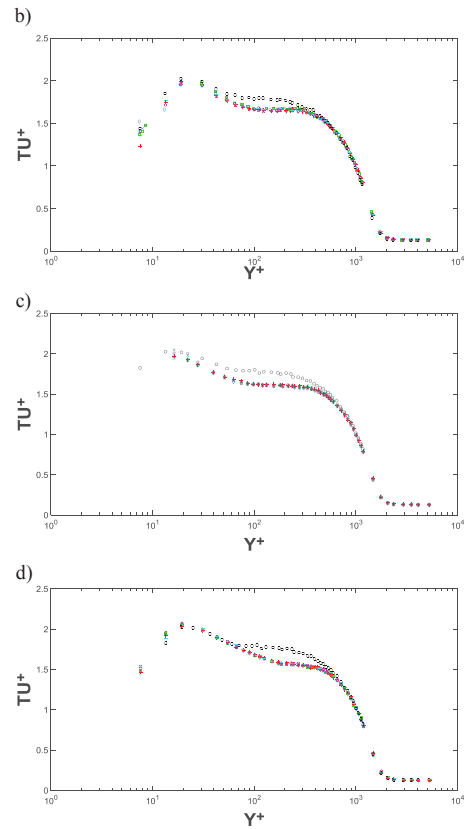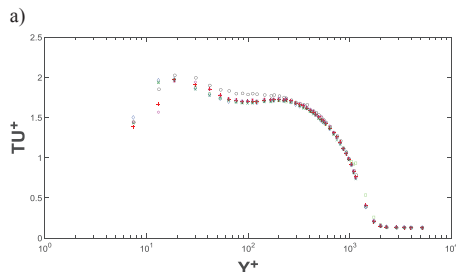
a)

b)

c)

d)

Figure 4: Turbulence intensity profile at $Re_\theta = 3771$. a) $x^+ = 5.5 \times 10^3$, b) $x^+ = 8.2 \times 10^3$, c) $x^+ = 10.9 \times 10^3$, d) $x^+ = 13.9 \times 10^3$. (o) No control, (▼) cavity array – No excitation, (+) 500Hz excitation, (□) 1000Hz excitation, (◊) 2000Hz excitation, (x) 4000Hz excitation, (*) 8000Hz excitation

The decrease in the turbulence intensity was also shown to continue significantly downstream after the cavity array ended. At a location of $x^+ = 13.9 \times 10^3$ the cavity array was shown to provide a decrease in the turbulence intensity in the viscous and logarithmic subregion by 10%, as shown in Figure 4(d). Thus demonstrating a significant proportion of the boundary layer was changed downstream of the cavity array, showing the effect is not localised.

Discussion

The boundary layer was shown to be modified by the cavity array and consequent several important findings were discovered. The most noticeable finding was that the acoustic actuator had no impact on the boundary layer and consequently the driving frequency had no effect on the boundary layer. Therefore the conclusions drawn from this research indicate the reduction achieved from these experiments was due to the passive cavity array. As discussed earlier, one of the methods proposed the cavity array would only impact the coherent structures which act normal to the wall. If this is the case a variable interval time averaging (VITA) technique can be used to detect the changes in the turbulent boundary layer associated with coherent structures. This technique, first applied by Blackwelder and Kaplan [13] for studying the near wall region,

detects the sweep and ejection events where by the velocity rapidly changes. The results at $Re_\theta = 3771$ show a reduction in the intensity and duration of the sweep events. Figure 5 demonstrates a reduction in intensity and duration by 7.6% and 10% respectively at $x^+ = 10.9 \times 10^3$.
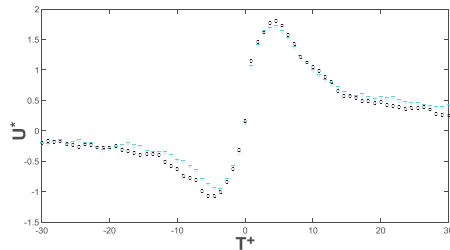

Figure 5: Average VITA sweep events at $Re_\theta = 3771$, $x^+ = 10.9 * 10^3$. (o) No control, (▼) cavity array – No excitation

This reduction is also observed in Figure 6, at a downstream location of $x^+ = 13.9 \times 10^3$, where a sweep intensity reduction of 2.6% was achieved, however the change in duration was insignificant.
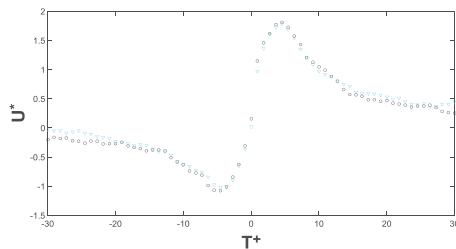

Figure 6: Average VITA sweep events at $Re_\theta = 3771$, $x^+ = 13.9 * 10^3$. (o) No control, (▼) cavity array – No excitation

It was initially hypothesised that the cavities would operate by capturing the sweep events and disrupt the overall bursting process in the boundary layer. This is supported by the VITA results in Figure 5 and Figure 6. These changes in the sweep intensity and duration are strong indicators that the coherent structures have been modified by the use of the cavity arrays as a passive solution. It is believed that the individual cavity offices are too small to allow the shear layer to break apart during the traverse across the orifice. As such resonance of the Helmholtz mode is not observed, which was previously experienced by Ghanandi et al. [9, 10].

Conclusions

The basis of this paper, is the study of micro cavities or perforated plates as a potential control technique in reducing skin friction drag. In this study two mechanisms were considered, with one technique focusing on an active approach and the other as a passive solution. The characteristics of the boundary layer were analysed using hotwire anemometry at four locations; three along the implemented cavity array and one behind, and the results were used to calculate the streamwise boundary layer profile, turbulence intensity and the properties of the coherent structures.

The results from this study indicated the reduction achieved was due to the passive mechanisms suggested. The cavity array was shown to provide substantial reduction to the turbulence intensity, sweep intensity and sweep duration. A maximum reduction in intensity and duration of the sweep events of 7.6% and 10%

respectively was achieved at $x^+ = 10.9 * 10^3$. It is believed this occurred due to the cavity array being small enough to be intrusive to the streamwise boundary layer. Consequently, the flow which acts normal to the wall, commonly associated with coherent structures to be impacted upon by the array. The conclusions drawn here are based on the results along a single cavity array.

References

[1] Zheng, XF, Yan, YY, 2010, *'A Biomimetic Smart Control of Viscous Drag Reduction'*, *Advances in Natural Science,* vol. 3, no. 2, pp. 139-151.

[2] Marec, J, 2000, *'Drag reduction: A major task for research'*, *European Drag Reduction Conference 2000,* Springer Verlag.

[3] Corino, ER, Brodkey, RS, 1969, *'A visual investigation of the wall region in turbulent flow'*, *Journal of Fluid Mechanics*, vol. 37, part. 1, pp. 1-30.

[4] Grass, AJ, 1971, *'Structural features of turbulent flow over smooth and rough boundaries'*, *Journal of Fluid Mechanics,* vol. 50, part. 2, pp. 233-255.

[5] Offen, GR, Kline, SJ, 1975, *'A proposed model of the bursting process in turbulent boundary layers'*, *Journal of Fluid Mechanics*, vol. 70, part. 2, pp. 209-228.

[6] Kim, HT, Kline, SJ, Reynolds, WC, 1971, *'The production of turbulence near a smooth wall in a turbulent boundary layer'*, *Journal of Fluid Mechanics,* vol. 50, part. 1, pp. 133-160.

[7] Smith, BL, Glezer, A, 1998, *'The formation and evolution of synthetic jets'*, *Physics of Fluids,* vol. 10, pp. 2281–2297.

[8] Lockerby, D, 2001, *'Numerical simulation of boundary-layer control using MEMS actuation'*, *Ph.D. Thesis*, The University of Warwick, England, UK.

[9] Ghanadi, F, Arjomandi, M, Cazzolato, BS, Zander, AC, 2014a, *'Understanding of the flow behaviour on a Helmholtz resonator excited by grazing flow'*, *International Journal of Computational Fluid Dynamics,* vol. 28, no. 5, 219–231.

[10] Ghanadi, F, Arjomandi, M, Cazzolato, BS, Zander, AC, 2015, *'Analysis of the turbulent boundary layer in the vicinity of a self-excited cylindrical Helmholtz resonator'*, *Journal of Turbulence,* vol. 16, 705-728.

[11] Silvestri, A, Ghanadi, F, Arjomandi, M, Cazzolato, BS, Zander, AC, 2016, *'The characteristics of the turbulent boundary layer generated by induced transition using different tripping techniques'*, submitted to *Experimental Thermal and Fluid Science.*

[12] Robinson, SK, 1991, *'Coherent motions in the turbulent boundary layer'*, *Annual Review of Fluid Mechanics*, vol. 23, pp. 601-639.

[13] Blackwelder, RF, Kaplan, RE, 1976, '*On the wall structure of the turbulent boundary layer'*, *Journal of Fluid Mechanics,* vol. 76, part 1, pp. 89-112.

Appendix 2: 10th International Symposium on Turbulence and Shear Flow Phenomena paper

Statement of Authorship

Title of Paper	The effect of the backing cavity on the control of the turbulent boundary layer by the application of a cavity array
Publication Status	☑ Published ☐ Accepted for Publication ☐ Submitted for Publication ☐ Unpublished and Unsubmitted work written in manuscript style
Publication Details	Silvestri, A, Ghanadi, F, Arjomandi, M, Cazzolato, BS, Zander, AC, 2017b, *'The effect of the backing cavity on the control of the turbulent boundary layer by the application of a cavity array', 10th International Symposium on Turbulence and Shear Flow Phenomena*, Chicago, IL, USA, 6-9 July.

Principal Author

Name of Principal Author (Candidate)	Anton Silvestri
Contribution to the Paper	Performed data analysis and interpretation, wrote manuscript and acted as corresponding author.
Overall percentage (%)	70
Certification:	This paper reports on original research I conducted during the period of my Higher Degree by Research candidature and is not subject to any obligations or contractual agreements with a third party that would constrain its inclusion in this thesis. I am the primary author of this paper.
Signature	Date 15/06/18

Co-Author Contributions

Name of Co-Author	Farzin Ghanadi		
Contribution to the Paper	Supervised the development of the research and contributed in academic discussion and the review process of submitted manuscripts.		
Signature		Date	15/06/18

Name of Co-Author	Maziar Arjomandi		
Contribution to the Paper	Supervised the development of the research and contributed in academic discussion and the review process of submitted manuscripts.		
Signature		Date	15/06/18

Name of Co-Author	Benjamin Cazzolato		
Contribution to the Paper	Supervised the development of the research and contributed in academic discussion and the review process of submitted manuscripts.		
Signature		Date	15/06/18

Name of Co-Author	Anthony Zander		
Contribution to the Paper	Supervised the development of the research and contributed in academic discussion and the review process of submitted manuscripts.		
Signature		Date	15/06/18

THE EFFECT OF THE BACKING CAVITY ON THE CONTROL OF THE TURBULENT BOUNDARY LAYER BY THE APPLICATION OF A CAVITY ARRAY

Anton Silvestri
anton.silvestri@adelaide.edu.au

Farzin Ghanadi
farzin.ghanadi@adelaide.edu.au

Maziar Arjomandi
maziar.arjomandi@adelaide.edu.au

Benjamin Cazzolato
benjamin.cazzolato@adelaide.edu.au

Anthony Zander
anthony.zander@adelaide.edu.au

School of Mechanical Engineering
University of Adelaide
Adelaide, South Australia, 5005, Australia

ABSTRACT

The streamwise velocity fluctuations within a fully developed turbulent boundary layer has been investigated downstream of a flushed-surface cavity array underneath a flat plate. The size of the holes in the cavity array were selected to be comparable with the dimensions of the expected coherent structures, based on the friction velocity. This study investigates the effect of the backing cavity volume on attenuation of turbulent energy production within the logarithmic region of the turbulent boundary layer. To this end the turbulence intensity profile and sweep attenuation for three different backing cavity volume have been investigated. All measurements were taken in a closed-loop low turbulence wind tunnel at two different free stream velocities. The results show that when the backing cavity's volume is equal to $V^+ = 3 \times 10^3$ the turbulence intensity and sweep intensity are reduced by up to 8% and 7.2% respectively. From this investigation it has been shown that the dampening of sweep events is not solely due to the walls of each individual cavity.

INTRODUCTION

The most important flow structure of a turbulent boundary layer are the coherent structures, which are responsible for the total shear stress in the near wall region. Coherent structures consist of the ejection of low speed fluid from the boundary layer and the inrush of high speed fluid which are known as sweep events (Corino and Brodkey 1969, Guo et al. 2010). These two events were shown to be self-replicating. It was shown that ejection events generated approximately 70% of the total stresses in the near wall region, while the sweep events contributed to the remaining 30 % (Offen and Kline 1975, Kim et al. 1971) and consequently were deemed to be very important during turbulence generation (Offen and Kline 1975, Guo et al. 2010). It is believed a technique which targets the sweep or ejection events specifically will cause a more significant reduction in turbulence generation and drag (Lockerby 2001, Choi et al. 2011, Ghanadi et al. 2014, Silvestri et al. 2016).

One such technique invesitgated is the passive application of the cavity array to reduce the turbulence generation has been considered by the authors (Silvestri et al. 2016, Silvestri et al. 2017a) due to the easy implementation and absence of a power source, which is favourable for aerospace applications. It was observed that by using a cavity with a small orifice diameter ($d^+ < 10$) the shear layer is unaffected crossing the opening, ensuring the resonance of the Helmholtz mode is not achieved (Ghanadi et al. 2015). Consequently only the flow which acts normal to the wall will be affected by the cavity array, as the streamwise profile will be unaffected. In the near-wall region the sweep and ejection events act in this direction and consequently, this will have the potential to use the cavity array as a drag reduction method for both high and low Reynold's numbers. This has been shown previously by Silvestri et al. (2016 & 2017a) to be highly successful in reducing the turbulence intensity and sweep intensity after control was applied where a maximum reduction of 13% and 14% was achieved respecively at a Reynolds number $1.69 \times 10^5 < Re_\theta < 1.18 \times 10^6$.

The events which do enter the cavity array are expected to be dampened by the walls of the cavity and/ or by the large mass of fluid beneath the orifice in the backing cavity. The purpose of the present work is to assess the ability of an array of micro-cavities in reducing the turbulent properties of a fully developed boundary layer and the effect of the backing cavity's volume on its ability. In the subsequent sections the characteristics of the cavity array will be discussed and details of the experimental setup will be given.

1

EXPERIMENTAL PROCEDURE

All experiments were performed in a closed-return type wind tunnel located at the University of Adelaide. The tunnel can be operated up to a maximum velocity of 30 m/s with a low level turbulence intensity, approximately 0.53%. The test section is rectangular with a cross section of 500mm × 500mm an 2000mm in length. As shown in Figure 1, a horizontal 2000mm long flat plate was positioned inside the tunnel such that it spanned the whole width of the test section. The finite thickness of the flat plate can lead to bluff body separation effects, therefore to minimize any possible flow separation a super-elliptical leading edge of a nominal major radius of 114mm was attached to the flat plate. A 125mm long circulation flap was also mounted downstream of the plate to minimize any circulation developed over the plate and to ensure that the stagnation point is on the measurement side of the plate. The walls could also be adjusted as appropriate to balance the pressure gradient along the working section, which was selected to be a zero pressure gradient in this investigation. The boundary layer investigated in the study was tripped by a 3mm rod located 140mm downstream of the leading edge as advised by Silvestri et al. (2017b). This was done to ensure a fully turbulent boundary layer was achieved for the experimental procedure.
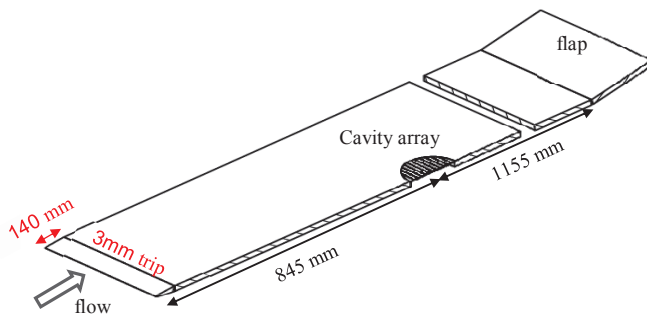

Figure 1: Schematic of the experimental arrangement

A hot-wire anemometer was used downstream of the boundary layer trip and cavity array to characterize the changes within the boundary layer regions arising from the cavity array located $(x^+ = 5.07 \times 10^4)$ downstream of the leading edge. This was done three times with a backing cavity of varying dimensions to monitor the effect the backing cavity had on the boundayr layer. The streamwise velocity measurements were made with a TSI IFA 300 CTA system, using a single TSI platinum-plated tungsten wire of $5\mu m$ in diameter and 1.25mm in length, which was operated with an over-heat ratio of 1.8 and an operating temperature around 230°C, which provided sufficient sensitivity to measure the velocity fluctuations with minimum thermal effects. The repeatability of each measurement was also verified 3 times and the data were sampled at 20 kHz for 15 seconds.

As shown in Figure 2, the cavity array has a varing backing cavity. This was achieved by using backing faces with different geometries to restrict the total volume of the bakcing cavity. The friction velocity value equal to, $u_\tau = 0.5\ m/s$, previously calculated by Silvestri et al. (2017b) was used to design the cavity arrays dimensions. Using this friction velocity value the spanwise and streamwise spacing and the approximate orifice diameter were calculated based

on the method specified by Lockerby (2001), which states that the orifice diameter to be 40 times the viscous length scale and the spanwise spacing to be 100 times the viscous length scale. These approximations were based on the expected size of the coherent strutures in the boundary layer. This resulted in a cavity array comprising 1.2mm diameter holes and a spanwise spacing of 3mm. The cavity array plate was manufactured using a 3D printer with a constant streamwise spacing of 15mm and constant thickness of 4mm as shown in Figure 3. Literature states that the length of coherent structures can be up to 10 times the spanwise spacing (Blackwelder and Eckelmann 1979). Consequently 15mm falls well below this value. In order to investigate the effect of momentum thickness on the turbulence generation within the boundary layer, all measurements have been conducted at two different Reynolds numbers of $Re_\theta = 1927$ and 3771
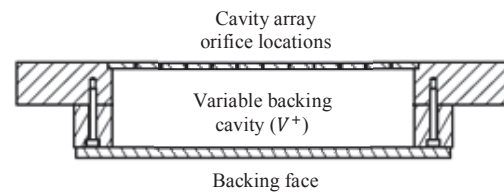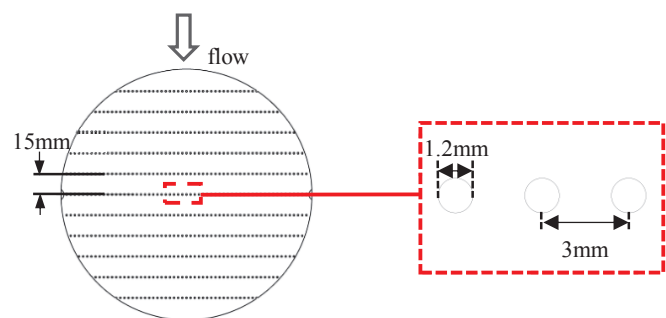

Figure 2: Schematic of the backing cavity

Figure 3: Schematic of the cavity array

EXPERIMENTAL RESULTS

Figure 4 shows the streamwise profile of the boundary layer immediately downstream of the cavity arrays and the corresponding unaltered turbulent boundary layer for comparison. The three backing cavity arrays investigated appear to shift the viscous and logarithmic subregion $(y^+ < 200)$ upwards, while not changing the overall boundary layer thickness. This effect is expected to result in a drag reduction as shown by (Savins and Seyer 1977, Patterson et al. 1977, Hooshmand et al. 1983) where an upward shift of the logarithmic region results in a decreased friction velocity and skin friction coefficient.
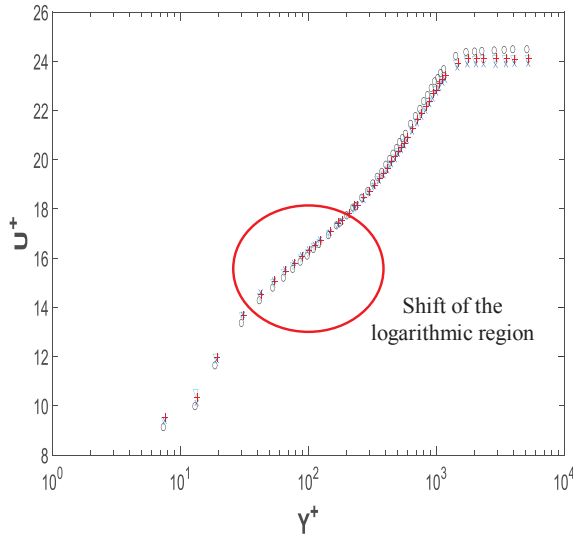
2

Figure 4: Mean velocity profile at $Re_\theta = 3771$. (o) No control, (Δ) $V^+ = 300$, (+) $V^+ = 1500$, (x) $V^+ = 3000$

This reduction is also clearly evident in Figure 5, which shows the turbulence intensity of the same boundary layers investigated. The cavity array is shown to provide a substantial turbulence intensity reduction within the logarithmic region $15 < y^+ < 200$ for all the backing cavities investigated. The largest backing cavity ($V^+ = 3000$) was shown to cause the largest turbulence intensity reduction by 8%. This value was shown to decrease when investigating the other backing cavities, where the values decreased to 3.3% ($V^+ = 300$) and 4.5% ($V^+ = 1500$).
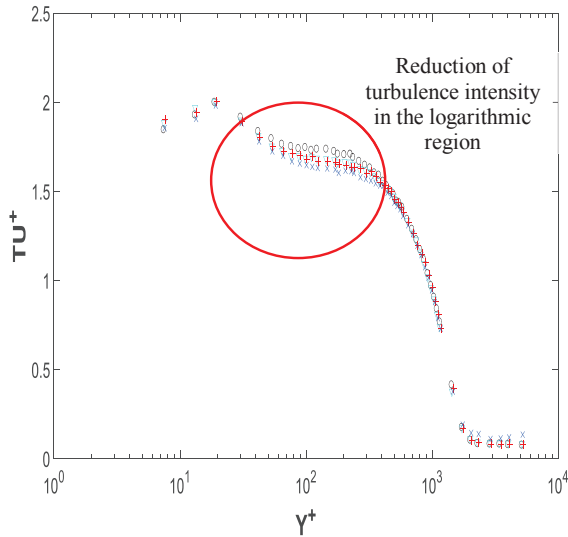

Figure 5: Turbulence intensity profile at $Re_\theta = 3771$. (o) No control, (Δ) $V^+ = 300$, (+) $V^+ = 1500$, (x) $V^+ = 3000$

This efffect is also shown to continue at a lower Reynolds number. Figure 6 shows the effect of the backing cavity on the turbulence intensity at a Reynolds number of

$Re_\theta = 1927$. Similar to the previous figure the largest backing cavity ($V^+ = 3000$) was shown to cause the largest turbulence intensity reduction of 5.6%. As also shown in Figure 6, when the backing cavity volume is reduced by half the turbulence intensity decreases by approximately 3.5% ($V^+ = 1500$). Significant reduction in the backing volume, $V^+ = 300$, results in a turbulence intensity reduction of 2.0%.
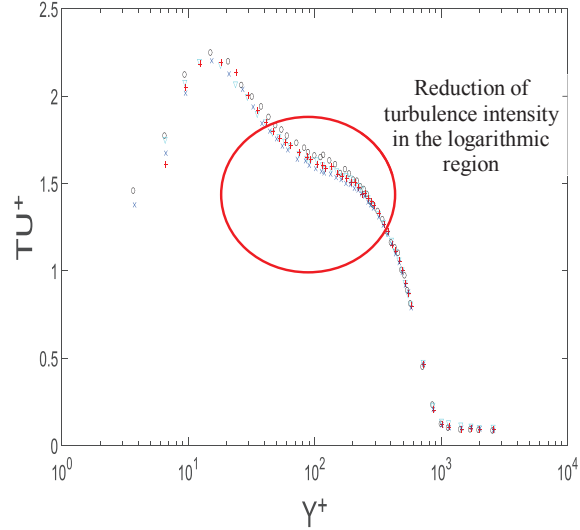

Figure 6: Turbulence intensity profile at $Re_\theta = 1927$. (o) No control, (Δ) $V^+ = 300$, (+) $V^+ = 1500$, (x) $V^+ = 3000$

A variable interval time averaging (VITA) technique has also been used to detect the changes in the turbulent boundary layer associated with coherent structures. The technique was initially applied by Blackwelder and Kaplan (1976) for studying the near wall region and detecting the sweep and ejection events. The VITA analysis for the current boundary layer analysis will focus on the sweep events, since these are the major contributor to turbulent skin friction (Orlandi and Jimenez, 1993). The sweep events are monitored by calculating the VITA of the streamwise velocity fluctuations according to the definition

$$\hat{u}(t, T_W) = \frac{1}{T_W} \int_{t-T_w/2}^{t+T_w/2} u(s) \, ds, \tag{1}$$

The intensity of the events is calculated based on the peak-to-peak value of the streamwise velocity of the events. The duration on the other hand is calculated from the time separation of the peaks in each VITA analysis. Increased duration or intensity of the events reveals an increase in the turbulence energy production. Throughout the investigation a total of 950 ensembles were used in each VITA analysis. This occurred at a $Y^+ = 100$ for all cases investigated.

At $Re_\theta = 3771$ the cavity array was shown to have an effect in reducing the duration and intensity of the sweep events also. Figure 7 shows a maximum reduction in sweep intensity of 7.2% when using a backing cavity of $V^+ =$

3

3000, whilst the reduction that occurs when using the other backing cavities were reduced by only 3.4% ($V^+ = 300$) and 4.4% ($V^+ = 1500$). Sweep duration however was shown to remain unaffected.
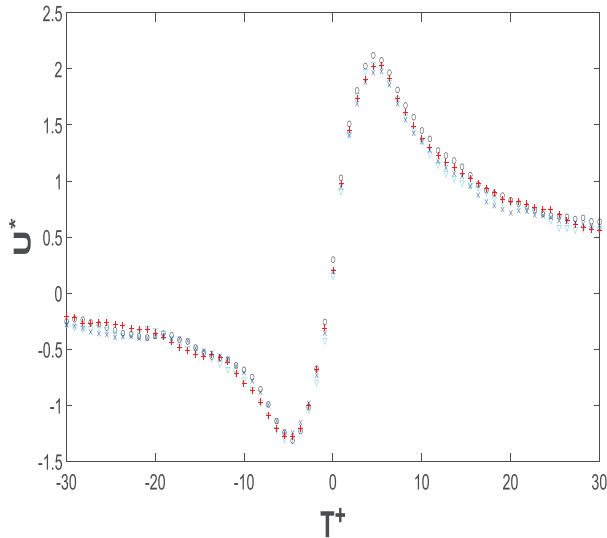

Figure 7: Average VITA sweep events at $Re_\theta = 3771$ at $Y^+ = 100$. (o) No control, (Δ) $V^+ = 300$, (+) $V^+ = 1500$, (x) $V^+ = 3000$

This efffect is also shown to continue at a lower Reynolds number similar to the turbulence intensity. Figure 8 shows the effect of the backing cavity on the sweep intensity at a Reynolds number of $Re_\theta = 1927$. A maximum reduction in sweep intensity of 6.2% was achieved when using a backing cavity of $V^+ = 3000$, whilst the reduction that occurs when using the other backing cavities investigated differ as the intensity was reduced by only 3% ($V^+ = 300$) and 3.1% ($V^+ = 1500$). Sweep duration however was once again shown to remain unaffected by the cavity array at all backing volumes tested.
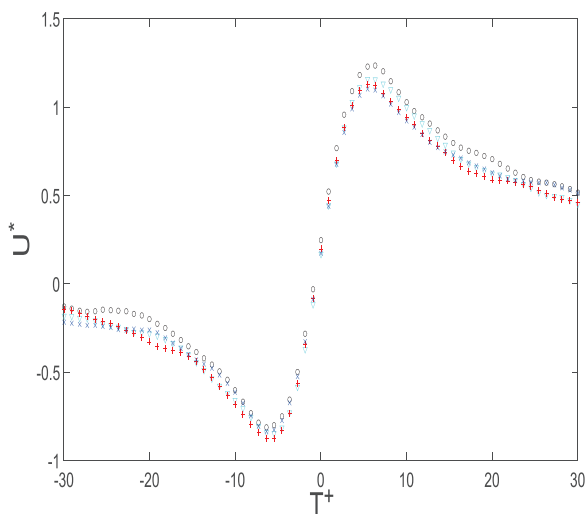

Figure 8: Average VITA sweep events at $Re_\theta = 1927$ at $Y^+ = 100$. (o) No control, (Δ) $V^+ = 300$, (+) $V^+ = 1500$, (x) $V^+ = 3000$

DISCUSSION

It has been hypothesised that the cavities operate by capturing the sweep events and consequently disrupt the overall bursting phenomenon in the boundary layer. It is however unclear what happens to the sweep events as it enters the cavity array. One hypothesis from the authors is that the sweep event's energy is dampened by the cavity array's walls and the backing cavity's volume. This would therefore result in the backing cavity having an effect on the reduction of the turbulent energy production.

However an alternative theory would result in the turbulence energy reduction being independent of the backing cavity's volume. While the cavity array would still form an integral part of passive mechanism, a conservation of energy would occur in the device resulting in no loss of the sweep energy. The corresponding reduction would be a result of a captured sweep event's energy being ejected back into the turbulent boundary layer across all of the cavity array's individual openings. Consequently each event would be redistributed across the large amount of holes resulting in a small, but unnoticeable change in the boundary layer while still retaining the turbulence energy reduction and conservation of momentum from removing a sweep event from the inner wall region of the boundary layer.

While both hypothesises described above appear plausible the results from this work suggest the former hypothesis to be valid. Throughout the work presented a clear trend can be identified where by reducing the backing cavity's volume a reduction in the control of the turbulent boundary layer is visible. This difference is quite significant when comparing the values. At the largest backing cavity volume ($V^+ = 3000$) a significant 7.2% and 6.2% reduction in sweep intensity is achieved at the largest and smallest Reynolds numbers investigated. However at the smallest backing cavity volume ($V^+ = 300$) this value is a reduced to only 3.4% and 3% respectively. As mentioned above if the backing cavity only acted as a channel to link all the cavities together to allow the redistribution of the sweep event's energy then it would be expected that these values are much more similar in value.

4

CONCLUSION

The basis of this paper, is the study of a cavity array as a potential control technique in reducing skin friction drag. In this study the effect of the backing cavity's volume was specifically investigated and two mechanisms were considered. The characteristics of the boundary layer were analysed using hotwire anemometry at a single locations where the results were used to calculate the streamwise boundary layer profile, turbulence intensity and the properties of the coherent structures.

It has been shown that the dampening of sweep events is not solely due to the skin friction loses from the walls of each individual cavity, as the backing cavity volume also has a significant effect on the sweep attenuation values, where a maximum reduction of 7.2% was achieved when the backing cavity's volume was selected to be $V = 5.1 \times 10^{-3}\ m^3$ ($V^+ = 3000$).

The conclusions drawn here are based on the results along a single cavity array. Future work intends to focus more intently on the volume of the backing cavity and if the effect continues for other cavity arrays with different geometries. Furthermore future work will endeavour to analysis the effect of having a backing cavity with zero volume. The results presented here are only the beginning of the development of the knowledge required for this area of work.

REFERENCES

Blackwelder, RF, Eckelmann, H, 1979, *'Streamwise vortices associated with the bursting phenomenon', Journal of Fluid Mechanics,* vol. 94, pp. 577-594.

Blackwelder, RF, Kaplan, RE, 1976, *'On the wall structure of the turbulent boundary layer', Journal of Fluid Mechanics*, vol. 76, part 1, pp. 89-112.

Choi, KS, Jukes, T, Whalley, R, 2011, *'Turbulent boundary-layer control with plasma actuators', Philosophical Transactions of the Royal Society A,* vol. 369, pp. 1443-1458.

Corino, ER, Brodkey, RS, 1969, *'A visual investigation of the wall region in turbulent flow', Journal of Fluid Mechanics*, vol. 37, part. 1, pp. 1-30.

Offen, GR, Kline, SJ, 1975, *'A proposed model of the bursting process in turbulent boundary layers', Journal of Fluid Mechanics*, vol. 70, part. 2, ,pp. 209-228.

Lockerby, D, 2001, *'Numerical simulation of boundary-layer control using MEMS actuation', Ph.D. Thesis*, The University of Warwick, England, UK.

Ghanadi, F, Arjomandi, M, Cazzolato, BS, Zander, AC, 2014, *'Understanding of the flow behaviour on a Helmholtz resonator excited by grazing flow', International Journal of Computational Fluid Dynamics,* vol. 28, no. 5, 219–231

Ghanadi, F, Arjomandi, M, Cazzolato, BS, Zander, AC, 2015, *'Analysis of the turbulent boundary layer in the vicinity of a self-excited cylindrical Helmholtz resonator', Journal of Turbulence,* vol. 16, 705-728.

Guo, H, Borodulin, VI, Kachanov, C, Pan, C, Wang JJ, Lian QX, Wang, SF, 2010, *'Nature of sweep and ejection events in transitional and turbulent boundary layers', Journal of Turbulence,* vol. 11.

Hooshmand, D, Youngs, R, Wallace JM, 1983, *'An experimental study of changes in the structure of a turbulent boundary layer due to surface geometry changes', AIAA*, Paper 83-0230.

Kim, HT, Kline, SJ, Reynolds, WC, 1971, *'The production of turbulence near a smooth wall in a turbulent boundary layer', Journal of Fluid Mechanics,* vol. 50, part. 1, pp. 133-160

Offen, GR, Kline, SJ, 1975, *'A proposed model of the bursting process in turbulent boundary layers'*, *Journal of Fluid Mechanics*, vol. 70, part. 2, pp. 209-228.

Orlandi, P, Jimenez, J, 1993, '*On the generation of turbulent wall friction', Physics of Fluids*, vol. 6, pp. 634–641.

Patterson, GK, Chosnek, J, Zakin JL, 1977, *'Turbulence structure in drag reducing polymer solutions', Physics of Fluids*, vol. 20, pp. S89-S99.

Savins, JG, Seyer, FA, 1977, 'Drag reduction scale-up criteria', Physics of Fluids, vol. 20, pp. S78-S84.

Silvestri, A, Ghanadi, F, Arjomandi, M, Cazzolato, BS, Zander, AC, 2016, '*Control of the turbulent boundary layer by the application of a cavity array', 20th Australasian Fluid Mechanics Conferencce,* Perth, Australia, 5-8 December.

Silvestri, A, Ghanadi, F, Arjomandi, M, Cazzolato, BS, Zander, AC, 2017a, '*Attenuation of sweep events in a turbulent boundary layer using micro-cavities',* submitted to *Experiments in Fluids.*

Silvestri, A, Ghanadi, F, Arjomandi, M, Cazzolato, BS, Zander, AC, 2017b, '*The characteristics of the turbulent boundary layer generated by induced transition using*

5

different tripping techniques', submitted to *Experiments in Fluids.*

Whalley, RD, 2011*, 'Turbulent boundary-layer control with DBD plasma actuators using spanwise travelling-wave technique', PhD Thesis,* The University of Nottingham, England, UK.

6